CHEMISTRY OF THE TERMINAL PNICTOGEN COMPLEXES OF LEAD, TIN AND GERMANIUM

Lisa Ann Marie Harris

DPhil Chemistry

University of Sussex

October 2012

I hereby declare that this thesis has not been and will not be submitted in whole or in part to another University for the award of any other degree.

Signature ……

UNIVERSITY OF SUSSEX

LISA ANN MARIE HARRIS

CHEMISTRY OF THE TERMINAL PNICTOGEN COMPLEXES OF LEAD, TIN AND GERMANIUM

SUMMARY

A series of tin(II) and lead(II) β-diketiminate amides [(BDI)MNRR'] (BDI = [CH{(CH_3)CN-2,6-*i*$Pr_2C_6H_3$}$_2$]; M = Sn, Pb; RR' = *i*Pr_2, H(2,6-*i*Pr_2-C_6H_3), H(2-*i*Pr-C_6H_4), H(C_6H_5)) were synthesised and characterised. The reactivity of [(BDI)MN(*i*Pr)$_2$] and [(BDI)MNH(2,6-*i*Pr_2-C_6H_3)] towards aliphatic electrophiles, heterocumulenes and acids was investigated. The lead systems were found to be more reactive than the tin systems and the amide ligand was found to be more reactive than the anilide ligand. In general, the [(BDI)MNRR'] systems under investigation displayed the expected nucleophilic and basic behaviour. For instance, treatment of [(BDI)SnNH(2,6-*i*Pr_2-C_6H_3)] with methyl triflate resulted in the formation of [(BDI)SnOSO_2CF_3]. However, addition of phenyl isocyanate to [(BDI)MNRR'] (M = Sn, Pb; RR' = *i*Pr_2, H(2,6-*i*Pr_2-C_6H_3)) resulted in the formation of a bis-β-diketiminate complex, [(BDI)M(OC{=NPh}C{=C(Me)CN(H)(Ar)}{C{Me}=CN(Ar)})], a net result of nucleophilic addition to the electrophilic carbon in phenyl isocyanate by the γ-carbon in the BDI backbone. DFT studies were undertaken to rationalise the reactivity.

The reactivity of group 14 metal β-diketiminate phosphide complexes [(BDI)MPR_2] (BDI = [CH{(CH_3)CN-2,6-*i*$Pr_2C_6H_3$}$_2$]; M = Ge, Sn, Pb; R = C_6H_{11}, C_6H_5) towards selenium and

tellurium was examined. For the tin(II) and lead(II) systems, no reactivity was observed upon addition of one or five equivalents of tellurium. In contrast, the germanium(II) systems exhibited unexpected reactivity with selenium and tellurium, where one equivalent of the chalcogen resulted in its insertion into the germanium-phosphorus bond, [(BDI)GeEPR_2] (E = Se, Te), and five equivalents of selenium resulted in a further coordination of a selenium to the phosphorus, [(BDI)GeSeP(Se)R_2]. DFT studies were undertaken in order to rationalise this behaviour. Lastly, the process of aerosol-assisted chemical vapour deposition (AACVD) was undertaken on some of these group 14 metal chalcogenide complexes in order to probe their suitability as a single source precursor (SSP) for thermo-electric materials.

Acknowledgements

First and foremost, I would like to thank my supervisor Robin for the opportunity to complete a DPhil in such an amazing lab with so many wonderful colleagues. Robin's enthusiasm, hard work and brilliance, not to forget her guidance and warmth will always stay with me and has taught me many lessons, both professionally and personally. I feel honoured to have worked with Robin and any pride I feel in my work is a result of Robin's belief in me and my abilities.

I would also like to express my thanks to Martyn and Peter for X-ray crystallography, Iain for help with NMR related issues, Ali for mass-spectroscopy and Qiao for microscopy. I would also like to thank Mick for all the items I was allowed to 'borrow' from the teaching labs.

I must impart a warm thanks to all my wonderful colleagues I had the pleasure to work with over the years for all the great times we shared both inside and outside the lab, especially to Eric, Morgan, Lorenzo, Mat and Luke. To Eric, my friend and colleague, I must express sincere gratitude for all his help and advice over the years and who I have the greatest respect for.

I am grateful to my friends Sarah and Donna who have not only been supportive but kept me sane. To Sarah I would like to thank her for our conversations – your constancy and sunny disposition have always made your company so pleasurable. To Donna I would like to thank her for introducing me to the benefits of running and who I owe my past and any future sub-20 5K times to.

I am extremely grateful to all my family for being so supportive of me over the years. My most sincere gratitude goes towards my mother, Ann, who has put up with my

tantrums and not only bore them well but acted as one of the finest (unpaid) psychiatrists anyone could wish to have. Furthermore, I would also like to thank my cats (past and present) Josie, Susie and Sheba for providing many hours of light hearted moments! Special mention must also be given to my grandfather, Panayiotis, for all his support, assistance and enthusiasm. Without his help I doubt this thesis could have been written. I am also grateful to my uncle Ken (and his partner Theresa) for always being there, from the very beginning to the end, my uncle Nicholas and my brother, Michael.

Table of Contents

List of Figures, Schemes and Tables

List of Abbreviations

AACVD	aerosol assisted chemical vapour deposition
Bbt	bis[bis(trimethylsilyl)methyl]-4-[tris(trimethylsilyl)methyl]phenyl
BDI	β-diketiminate
Calcd	calculated
cm^{-1}	per centimetre
Cp*	pentamethylcyclopentadienyl
CVD	chemical vapour deposition
Cy	cyclohexyl
DFT	density functional theory
dipp	diisopropylphenyl
dippe	1,2-bis(diisopropylphosphino)ethane
dmpe	1,2-bis(dimethylphosphanyl)ethane
DP	degree of pyramidalization
dppe	1,2-bis(diphenylphosphino)ethane
EDS	energy dispersive spectroscopy
Expt	experiment
HOMO	highest occupied molecular orbital
*i*Pr	isopropyl

IR	infrared
kcal mol^{-1}	kilocalorie per mole
kg per litre	kilogram per litre
kJ mol^{-1}	kilojoule per mole
Li^{n}Bu	*n*-butyl lithium
LPCVD	low-pressure chemical vapour deposition
LUMO	lowest unoccupied molecular orbital
Me	methyl
Mes	trismethylphenyl
MOCVD	metal-organic chemical vapour deposition
NMR	nuclear magnetic resonance
PCP	bis(phosphine)
ppm	parts per million
*s*Bu	*sec*-butyl
sccm	standard cubic centimetres per minute
SEM	scanning electron microscopy
SSP	single source precursor
Tbt	tris-(bis(trimethylsilyl)methyl)phenyl
*t*Bu	*tert*-butyl
Tf	triflate

TGA	thermo-gravimetric analysis
THF	tetrahydrofuran
Tip	triisopropylphenyl
Tmeda	N,N,N',N'-tetramethyl-1,2-ethylenediamine
Tp	tris(pyrazolyl)borate
ZPE	zero point energy
% Diff	percentage difference

CHEMISTRY OF THE TERMINAL PNICTOGEN COMPLEXES OF LEAD, TIN AND GERMANIUM

1. Introduction

1.1. History of Ge, Sn and Pb

Most germanium, tin and lead on the earth's surface is naturally found in the form of ores, chiefly germanite (a copper-iron-germanium sulfide composed of only 8% of the element), cassiterite (SnO_2) and galena (PbS).[1] Due to the comparative rarity of germanium ores, germanium, derived from Germania (the Latin name for Germany), was discovered relatively recently compared to tin and lead, by Clemens A. Winkler at Freidberg, Germany, in 1886.[1] However, its existence had been predicted by Mendeleev 15 years prior to its discovery, who had forecast the presence of an element between silicon and tin with an atomic weight of about 71 (it's 72.61) and a density of about 5.5 kg per litre (it's 5.3 kg per litre).

In contrast to germanium, the greater abundance of tin and lead ores, in addition to the ease of conversion of the ores back to metallic tin and lead at low temperatures (in the presence of simple reducing agents), allowed these metals to become some of the first to be utilised by humans.[1] Tin and lead are used to make bronze (up to 30% tin and 3.5% lead), which was first produced in at least the third millennium BC (i.e. the Bronze age) and was used by the peoples of Egypt, Mesopotamia and the Indus valley. Throughout history tin and lead have had a number of applications in many civilisations. From antiquity, bronze was used to make weaponry, tools and works of art. A few famous examples are the 30 metre high statue of the Sun God in the Colossus of Rhodes from the third century BC, the Great Buddha of Kamakura in Japan (made in 1252 AD) and the East Door of the Baptistry of St John in Florence, Italy, from the fifteenth century AD.

Apart from being components of bronze, lead and tin metals have also earned an interesting and prolific history in their own right. For example, tin has been used as tinplate since 320 BC and was a large scale industry during the Middle Ages in Bohemia

and Saxony.[1] By the mid-eighteenth century, tin was used to make an assortment of domestic utensils from plates and tankards to cauldrons and basins. Presently, tin compounds are used for their fungicidal, antimicrobial and insecticide applications.

Lead was extensively used for pipes in Roman times.[1] It is therefore no surprise that the modern chemical name and symbol for lead originates from its Roman meaning, "plumbum", in addition to the modern words "plumbing" and "plumber", in recognition of this metal's use in pipes.[2] Lead was so widely used in Roman society that lead levels in human remains dated from that time are typically 10 – 100 fold higher than 'natural' lead levels found in bones excavated from pre-Roman sites. Most dangerously, lead pans were used to boil down grape juice or sour wine to make sapa, a lead acetate syrup, which was widely used in cooking.[1] This has been used to explain the low birth rate of the Romans and the Empire's population stagnation and eventual decline. The use of lead to sweeten wine endured until the nineteenth century even though its association with outbreaks of 'colic' were acknowledged and it is now known to exacerbate a propensity to gout.[1] In more recent times, lead has been used as a gasoline additive and anti-knocking agent. With the introduction of catalytic converters in the 1970s and the phasing out of leaded gasoline in developed countries, environmental lead levels are in decline, however, lead still has many applications ranging from its use in the automobile industry and building sector to hair gels for men (due to lead acetate's ability to turn grey hair dark brown).[1]

The use of tin and lead in food storage applications have resulted in tragic consequences. Tin pest led to the failure of Scott's expedition to the South Pole in 1912 through disintegration of the tin-soldered joints in cans of paraffin, which resulted in the fuel being leached.[1] Lead poisoning is believed to have caused the crews of John Franklin's ships, who set off to search for the North-West Passage in May 1845, to perish through the leaching of lead from the solder into the food cans.[1] Even though tin and lead have had a long and distinguished history, there is some notoriety associated with their use.

In contrast to the diverse history of lead and tin, the history of germanium is relatively mundane. Germanium has low toxicity and no known biological role, although there have been suggestions that it has an effect on some micro-organisms.[1] Historically, germanium has been used as a semiconductor and was the first element to be used in transistors. Today it is used in special glass for wide-angle camera lenses and for infrared devices. A small proportion of germanium is also used in alloys.

1.2. Recent advances in divalent organotetrylene chemistry

Germanium, tin and lead are the heavier members of group 14 in the periodic table. These elements have 14 electrons in their outer shell, consisting of electrons from the d (nd^{10}), s (ns^2) and p (np^2) orbitals (where n = 3d, 4s and 4p for germanium; 4d, 5s and 5p for tin or 5d, 6s and 6p for lead). In addition, lead has electrons in the $4f^{14}$ orbitals.[3] The electrons in the filled d and f orbitals are low in energy and not reactive. The germanium, tin and lead centres can exist in the 0 oxidation state or can be oxidised to the +2 or +4 oxidation states through the loss of electrons from the p orbitals followed by the s orbital in the valence shell.

The first stable monomeric divalent organogermylene and -stannylene complexes, $[\{(Me_3Si)_2N\}_2Ge]$, $[\{(Me_3Si)_2CH\}_2Ge]$ and $[\{(Me_3Si)_2CH\}_2Sn]$, were synthesised by Lappert et al. between 1974 - 1976.[4,5] In contrast, the first monomeric divalent organoplumbylene derivative, $[Ph_2Pb]$, was successfully generated in 1922 by Krause and Reissaus.[6] This historical context of the divalent metal centre complexes neatly demonstrates the increasing ease in forming monomeric divalent metal centre derivatives travelling down the group due to decreasing thermodynamic gain upon increasing the oxidation state.[3] It is therefore increasingly important, especially when moving from lead to germanium, to stabilise the divalent metal centre either kinetically, through the use of bulky ligands, or thermodynamically, through the use of electron donating ligands. In this Chapter, recent

noteworthy published accounts of ligand systems employed to achieve this aim will be examined, in addition to any interesting structural or chemical properties. Due to the purposes of this study, the examination of those complexes exhibiting M-M bonds and M-TM bonds will be excluded (where M = Ge, Sn or Pb; TM = transition metal) and by-products will not be included. Furthermore, analysis of the reactivity of group 14 metal amide complexes will be omitted from this Chapter due to its greater relevance in Chapter 2, where it will be discussed in depth. Lastly, the conformation of complexes will be shown in Schemes (if known) and only if all the products of that particular reaction mechanism adopt the same conformation.

One of the most popular and versatile ligand systems utilised to stabilise germanium, tin and lead metal centres is the substituted terphenyl ligand, [C_6H_3-2,6-Ar_2]$^-$.[7-15] Multiple variations on the aryl substituents on the terphenyl ligand have been used, including Ar = Mes = 2,4,6-Me_3-C_6H_2; Ar = Trip = 2,4,6-*i*Pr_3-C_6H_2; Ar = dipp = 2,6-*i*Pr_2-C_6H_3.[7-15] Apart from its use in the formation of the heavier analogues of the alkenes and alkynes[14] and forming oligomeric imides,[13,15] the terphenyl ligand has also been used to form a quasi one-coordinate lead cation[7] (**I**) and bis-terphenyl group 14 metal complexes[9] (**II**) (Figure 1). Other terminal ligands coordinated to the terphenyl tetrylene centres have included the alkyl, amide and halide groups.[8,10-12] More recently, a phosphinidene terphenyl ligand has been used to generate group 14 metal centre dimer complexes (**III**) (Figure 1).[13] As shown in Figure 1, variations on the sterics of the aryl substituents of the terphenyl ligand influence the coordination around the group 14 metal centre. For example, the triisopropylaryl substituent was used to stabilise the lead cation **I** because this substituent is more bulky than the aryl group used to stabilise the dimer complexes **III**.

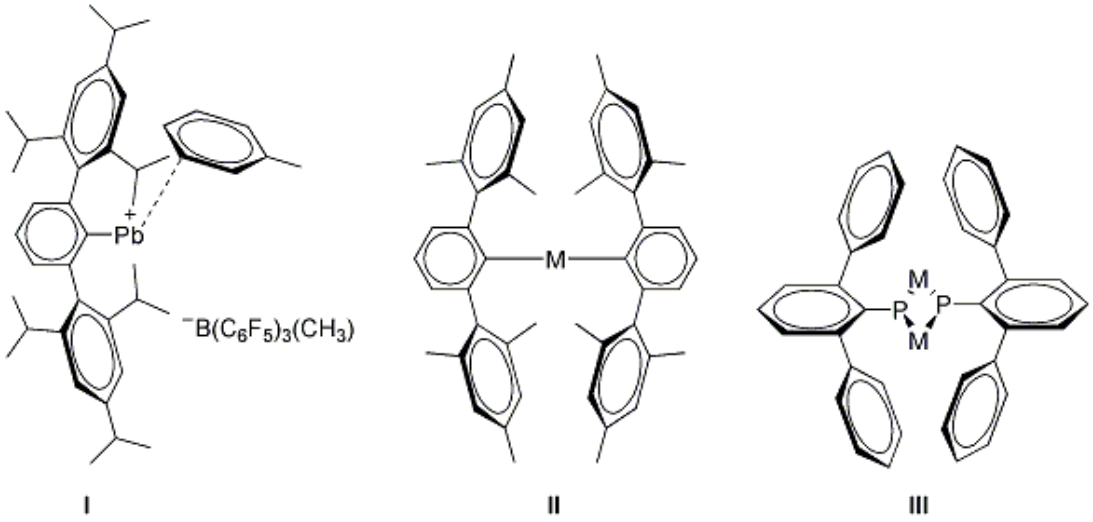

Figure 1 Examples of group 14 metal terphenyl complexes (M = Ge, Sn, Pb).

The five-membered *N*-heterocyclic carbene ligand system, $[\{RNC(R')\}_2C]^-$, has been employed to stabilise group 14 metal centres through the strong donor ability of the carbene. Similar to the terphenyl ligand system, variations to the substituents in the ligand backbone on the nitrogen (where R = dipp, *i*Pr and Mes) and the α-carbons (where R' = H, Me) have been utilised in order to stabilise group 14 metal centres (Figure 2).[16-21]

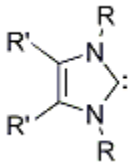

Figure 2 Five-membered *N*-heterocyclic carbene ligand system (R = dipp, *i*Pr, Mes; R' = H, Me).

Work by Weidenbruch et al. identified the presence of two electronic forms of the *N*-heterocyclic carbene plumbylene complex (**IV**) (Figure 3), where the zwitterionic form was found to be dominant due to the nucleophilic character of the carbene.[17] The dominance of the zwitterionic form was hypothesised to be a consequence of the relativistic contraction of electrons in the outer s shell of the metal. Relativistic contraction of the outer s shell, resulting in the absence of back bonding from the metal lone pair to the carbene, has been used to explain the lack of colour for crystals of the *N*-heterocyclic carbene germylene complex and was supported by DFT calculations.[19]

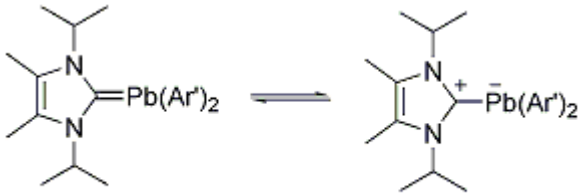

IV

Figure 3 Zwitterionic carbene plumbylene complex (Ar' = 2,6-*i*Pr_2-C_6H_3).

Seven-membered metallacycles incorporating tin and lead centres, [[{$Me_2P(BH_3)$}$(Me_3Si)C${$(SiMe_2)(CH_2)$}]$_2$M] (M = Sn, Pb) (**V**), have been synthesised by Izod et al.[22] The metallacycles were formed upon reaction of [[{$Me_2P(BH_3)$}$(Me_3Si)C${$(SiMe_2)(CH_2)$}]Li$(THF)_3$]$_2$ with one equivalent of [Cp_2M] (eq 1). These cyclic dialkylstannylene and –plumbylenes provide kinetic stabilisation, through the bulk of the ligand, and thermodynamic stabilisation, through the presence of agostic interactions via a B-H···M interaction. DFT studies showed these agostic interactions providing a significant stabilising effect (47.7 kcal mol^{-1} for tin and 42.7 kcal mol^{-1} for lead), thus presenting a new method to stabilise the electron deficient metal centres.

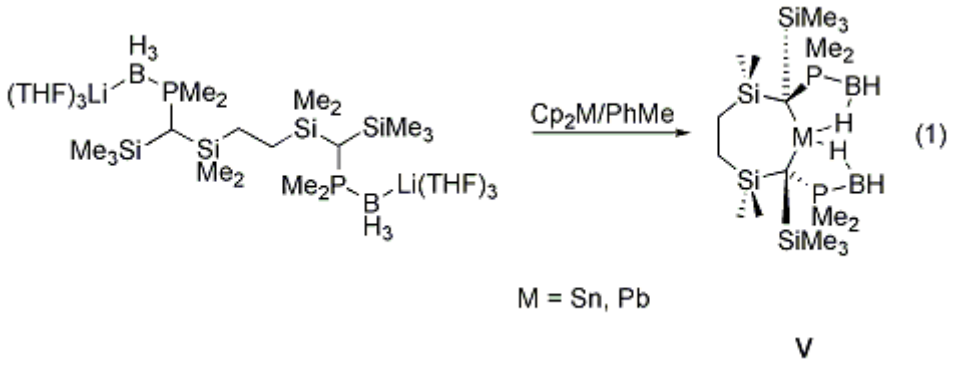

Examples of a range of *N*-heterocyclic tetrylene systems will be reviewed in this Chapter. The reader is also directed to a recent review by Driess et al.[23] The first *N*-heterocyclic tetrylene systems to be examined are the five-membered systems also known as "Arduengo" carbene analogues, [{(R_n)NC(R)}$_2$M] (M = Ge, Sn, Pb). Three general classes can be defined; these are the benzo-fused system (**VI**), the saturated system (**VII**) and the unsaturated system (**VIII**) (Figure 4).

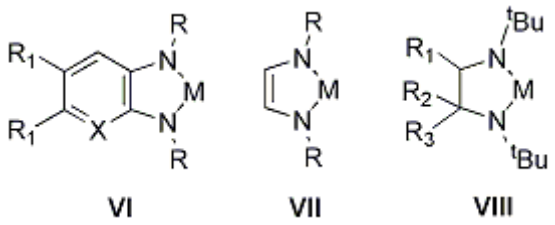

Figure 4 Five-membered *N*-heterocyclic tetrylene ring (M = Ge, Sn, Pb).

Only the synthesis and structural characterisation details of *N*-heterocyclic plumbylene complexes with saturated[24] and benzo-fused groups[21,25] have been reported. In contrast, the germylene[26-32] and stannylene[26,29,33-39] systems have utilised all three species of the five-membered heterocycle ring. Furthermore, two of the benzo-fused

stannylene metallacycles have been linked, forming bis-stannylenes such as the lutidine bridged bis-stannylene (**IX**). These complexes were found to trap tin and lead oxides upon addition of [M{N(TMS)$_2$}$_2$] (M = Sn, Pb) and water, forming a trimetallic complex (**X**) (Scheme 1).[40]

Scheme 1 Lutidine bridged bis-stannylene complex (M = Sn, Pb).

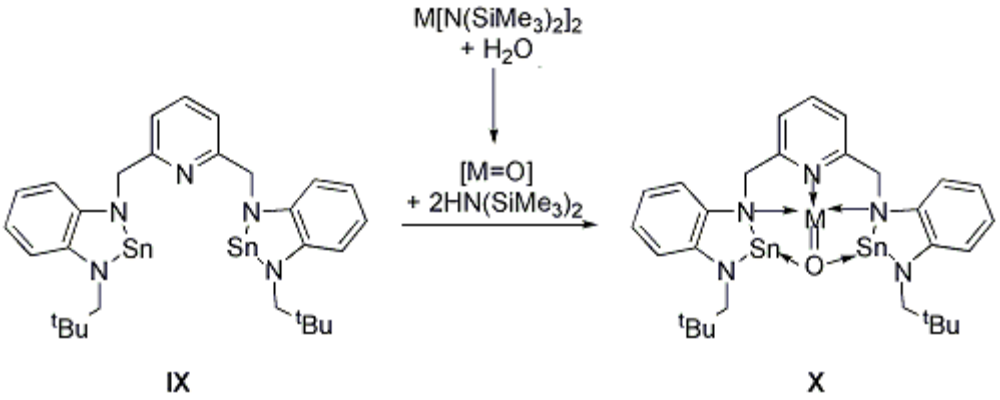

IX X

A new class of group 14 metal phosphide-stabilised 6π dianion complexes, isoelectronic with *N*-heterocyclic "Arduengo" carbene analogues, have been found to stabilise tin centres, [{1,2-(PH$_2$)$_2$C$_6$H$_4$}Sn] (**XI**) (eq 2).[41] The tin phosphide-stabilised 6π dianion complex was formed via dilithiation of [1,2-(PH$_2$)$_2$C$_6$H$_4$] with [Li^{n}Bu], which was then reacted with [Sn(NMe$_2$)$_2$] in the presence of tmeda (acting as a Lewis base donor). Unlike the isoelectronic *N*-heterocyclic carbene analogue, which can employ both electronic and steric stabilisation of low valent group 14 metal centres, this new class of group 14 metal 6π dianion complexes use only electronic stabilisation in the generation of a tin(II) complex **XI**. Electronic stabilisation of the 6π dianion complex was proposed to be enhanced by the formal 6π aromatic system generated because of the largely unhybridised

tin(II) centre, as evidenced by the acute P-Sn-P angle and the relatively short P-Sn single bonds.

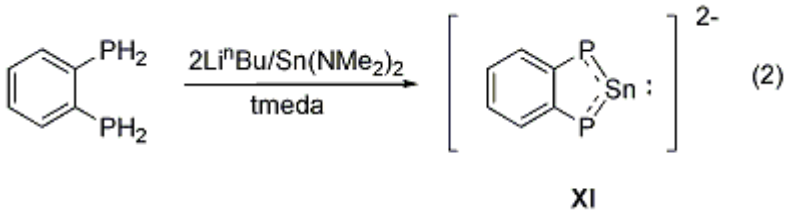

XI

Another five-membered tetrylene ring system which has employed both phosphorus and nitrogen donor ligands are the intramolecularly base-stabilised diphosphagermylene and -stannylene complexes, [{{(Me$_3$Si)$_2$CH}(C$_6$H$_4$-2-NMe$_2$)P}M] (M = Ge, Sn) (**XII**), synthesised by Izod et al.[42] These complexes were generated via the reaction between [GeCl$_2$(1,4-dioxane)] or [SnCl$_2$] and two equivalents of [{{(Me$_3$Si)$_2$CH}(C$_6$H$_4$-2-NMe$_2$)P}M'] (M' = K (Ge) or Li (Sn)) (eq 3). An investigation into the solid-state structure and dynamic behaviour of the five-membered **XII** and six-membered diphosphatetrylenes (**XIII**) was undertaken (Figure 5). The diphosphagermylenes **XII** and **XIII** showed similar structural and dynamic behaviour between the five-membered and six-membered ring systems. In contrast, the five-membered ring diphosphastannylene **XII** displayed significantly different solid-state structural and dynamic behaviour compared to the six-membered ring diphosphastannylene **XIII**. In the instance of the diphosphastannylenes, a weak interaction between the tin centre and nitrogen on the terminal phosphorus-donor ligand in the five-membered ring system result in the terminal amide moiety being directed towards the tin centre. The absence of this interaction in the six-membered system cause the amide moiety to be directed away from the tin centre, this structure is similar to both diphosphagermylene complexes. Furthermore, the dynamic behaviour of the five-membered ring system for the diphosphastannylene was found to be different to

the six-membered ring system for the diphosphastannylene and the diphosphagermylene complexes **XII** and **XIII** at low temperature, whereby a pseudo-trigonal bipyramidal geometry is adopted by the five-membered diphosphastannylene. A later study by Izod et al. removed the dimethylamide group from the ring, resulting in the disruption of the five-membered ring system and creating a sterically demanding phosphide ligand. These tetrylene complexes have three phosphide ligands bridging germanium or tin to lithium (**XIV**) (Figure 5).[43]

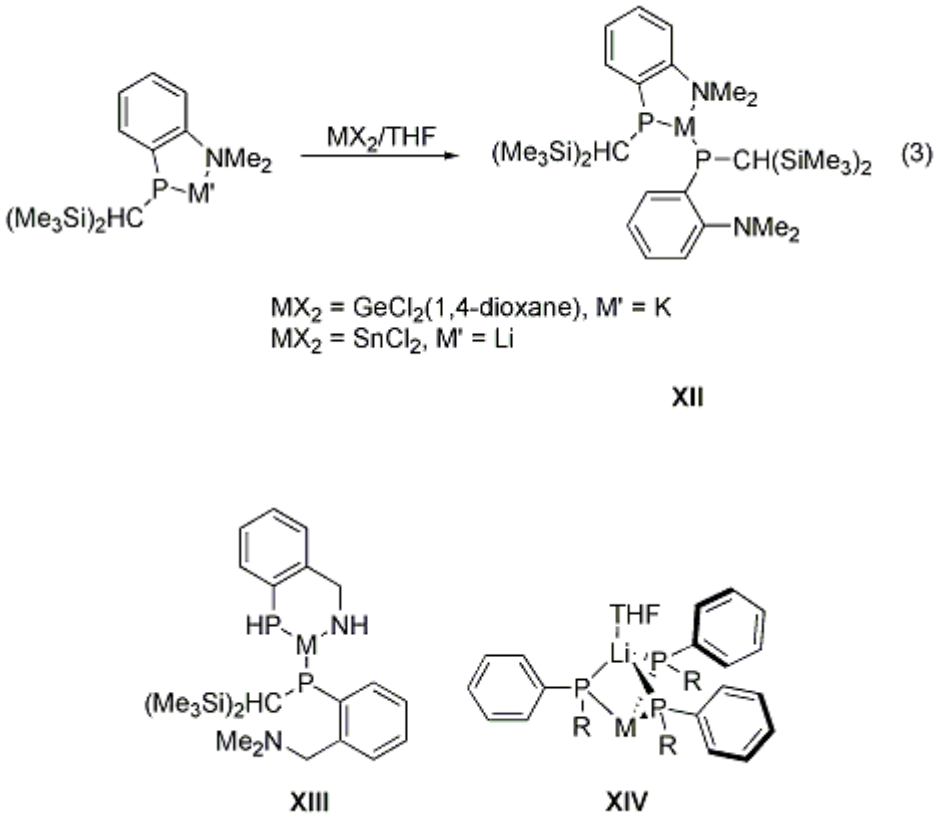

Figure 5 Phosphide-stabilised germanium and tin complexes (M = Ge, Sn; R = $(Me_3Si)_2CH$).

Amidinates and guanidinates, $[(R^1N)_2CR]^-$, can be used to stabilise group 14 metal centres, thus forming *N*-heterocyclic complexes (**XV**) and (**XVI**).[23] The versatility of these

ligands are derived from the choice of substituents on both the nitrogen atoms (R_1) as well as the beta carbon (R_2) in the ligand backbone, so that one or two ligands can be coordinated to the metal centre (Figure 6). The synthesis and characterisation of germanium and tin amidinates and guanidates are more established than the lead.

Germanium and tin have been used to form bis-amidinate germanium[44,45] and tin[46-51] complexes, in addition to amidinate germanium and tin complexes with terminal amides[52] and chlorides[44,53,54] (R group). Amidinate tin alkoxides have also been produced, though no germanium analogues have been reported.[53]

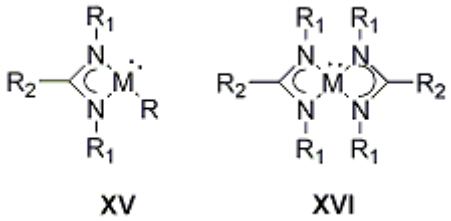

Figure 6 Four-membered *N*-heterocyclic ring (M = Ge, Sn; R = NHR, Cl, OH (Sn)).

The application of *tert*-butylamidinate tin *iso*-propoxide, dimethylamide and bis(trimethylsilyl)amide complexes as potential high activity, single site initiators for the controlled production of *rac*-lactide was investigated by Gibson et al.[53] This study confirmed a hypothesis by Gibson (which arose from a previous study using a β-diketiminate ancillary ligand)[55] whereby the tin centre was found to have a greater influence on tacticity due to the tin's largely unhybridised $5s^2$ lone pair affecting the orientation of the binding monomer relative to the propagating polymer chain. Even though the heterotactic bias is more a result of the tin(II) centre, the ancillary ligand was found to affect the rate of polymerisation. The reactivity of amidinate germanium and tin

amide complexes has been investigated by Richeson et al. and will be discussed at greater length in Chapter 2.

In contrast to the numerous examples of amidinate and guanidate germanium and tin complexes, the lead system has fewer examples, with a bis-amidinate lead complex and amidinate and guanidate lead chloride complexes reported.[56,23] It was found that slow exposure to oxygen to one of the lead guanidate complexes resulted in an oxygen-bridged dimeric lead guanidate, with the oxygen bound to one of the nitrogen substituents' isopropyl carbons (**XVII**) (Figure 7).[56] The mechanism is presumed to be a radical process induced by a diradical oxygen species generated via homolysis of the oxygen bond.

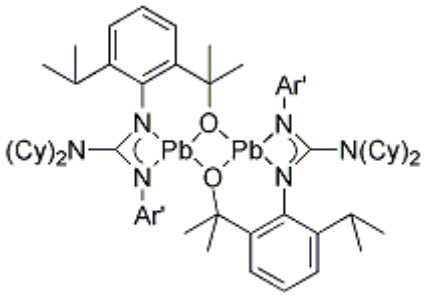

XVII

Figure 7 Oxygen-bridged dimeric lead guanidate complex (Ar' = 2,6-*i*Pr_2-C_6H_3).

The bis(amide)silane ligand, $[(Ar'N)_2SiR_2]^-$, has been used to stabilise group 14 metal centres due to its easily tuneable steric properties, engineered by changes to the substituents on the silyl group and the nitrogen (Ar').[57] Monomeric and dimeric complexes of group 14 metal complexes have been synthesised, with oligomerisation shown to be dependant on the substituents on the silicon. For example, in the bis(amide)silane plumbylene complex, $[\eta^2(N,N)\text{-}R_2Si(dippN)_2Pb:]_n$, a dimer was formed when the beta

substituent is methyl (**XVIII**), whereas a monomer was generated when the beta substituent is a phenyl group (**XIX**) (Figure 8).[58]

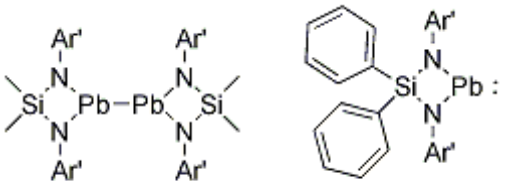

XVIII **XIX**

Figure 8 Examples of monomeric and dimeric bis(amide)silane plumbylene complexes (Ar' = 2,6-*i*Pr_2-C_6H_3).

1.2.1. β-diketiminate

The synthesis of a β-diketimine was published for the first time in 1966.[59] Two years later the use of β-diketiminate as a potential ligand system was realised by Parks and Holm, who used it as an ancillary ligand to generate a series of nickel complexes.[60] Despite this early interest, it has only been in the past two decades in which this ligand system has become ubiquitous in coordination chemistry. The popularity of this ligand is based upon a number of factors, namely its steric and electronic versatility, its (usual) monoanionic nature, especially important when stabilising metal centres in a low oxidation state, and the ease of its large scale synthesis. Firstly, the electronic versatility of this Lewis base ligand, which itself provides thermodynamic stability, can be further fine-tuned through changes to the R^1 - R^5 groups (Scheme 2).

Scheme 2 Some common versions of the (BDI) ligand.

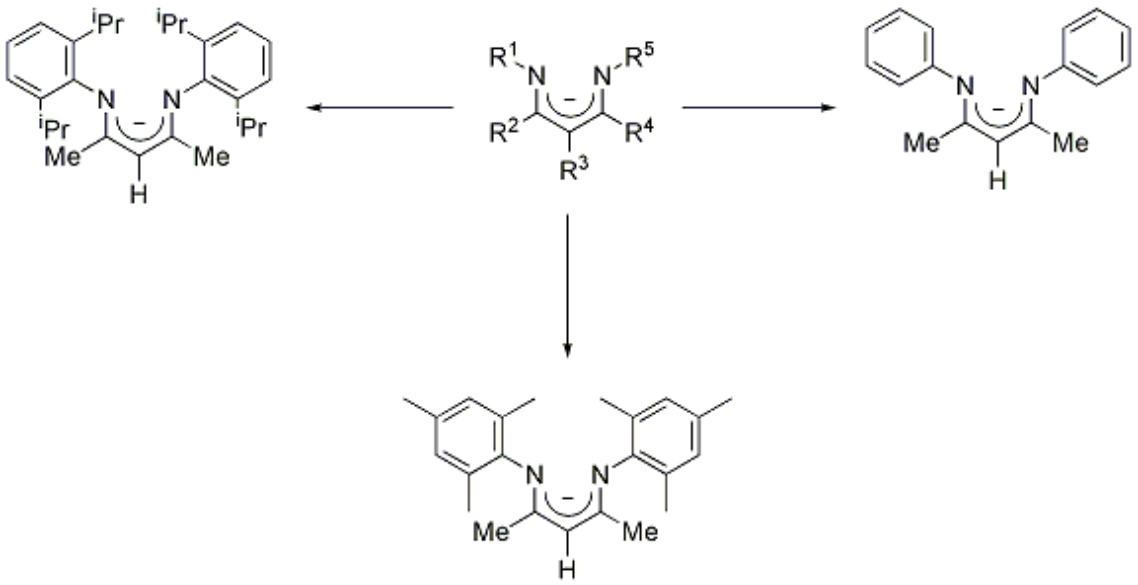

Secondly, the steric bulk of this ligand provides kinetic stabilisation and can be modified through changes to the R^1 and R^5 groups in order to modify the ligand for the requirements of the complex (i.e. the size of the metal centre), the desired oxidation state and the amount of aggregation. The steric versatility of this compound was exemplified by Hill et al., whom by reducing the steric bulk associated with the substituents on the nitrogen in the β-diketiminate, were able to generate a monomeric indium complex ((R^1R^5 = dipp) (**XX**)), a dimeric indium complex ((R^1R^5 = Mes) (**XXI**)) and a linear hexaindium chain complex ((R^1R^5 = 3,5-Me_2-C_6H_3) (**XXII**)) (Figure 9).[61]

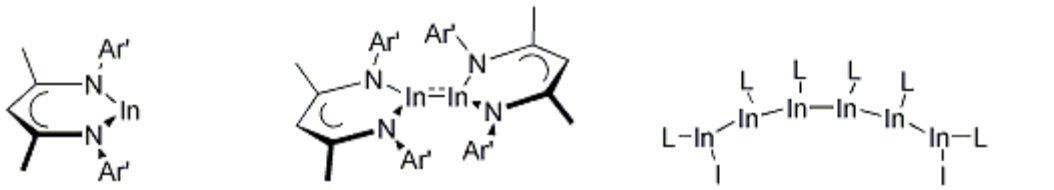

Figure 9 Monomeric, dimeric and oligomeric examples of [(BDI)In] complexes.

As a result of its prolific use, β-diketiminate complexes for virtually all metal centres in the periodic table are known, ranging from the transition and main group metals to the actinides and lanthanides (Figure 10).[62] To highlight a few, a dimeric magnesium(I) complex (**XXIII**) with a Mg-Mg bond was formed by reducing β-diketiminate magnesium iodide with elemental potassium.[63] Reduction of the β-diketiminate aluminium(II) iodide complex, using potassium, produced a β-diketiminate aluminium(I) complex (**XXIV**).[64] In contrast, the β-diketiminate gallium(I) complex **XXIV** was generated via salt metathesis between lithiated β-diketiminate and 'GaI'.[65] Rare low-valent, low coordinate transition metal complexes have also been stabilised via a toluene-bridged inverted-sandwich divanadium(I)[66] and dichromium(I)[67] complex (**XXV**) by reducing the metal chloride with potassium carbide, [KC_8]. The β-diketiminate ligand has also been shown to not only exist in a monoanionic state, but as a dianionic and trianionic ligand. A trinuclear β-diketiminate ytterbium(II/III) complex (**XXVI**), formed via reduction of a bis-β-diketiminate ytterbium complex with ytterbium-napthalene, contained β-diketiminate ligands which were found to reside in the monoanionic and trianionic state.[68] The dianionic bridging β-diketiminate ytterbium(II) complex containing an ytterbium metal centre in a rare +2 oxidation state and low coordinate environment was generated via reduction of a bis-β-diketiminate ytterbium complex with lithium.[68]

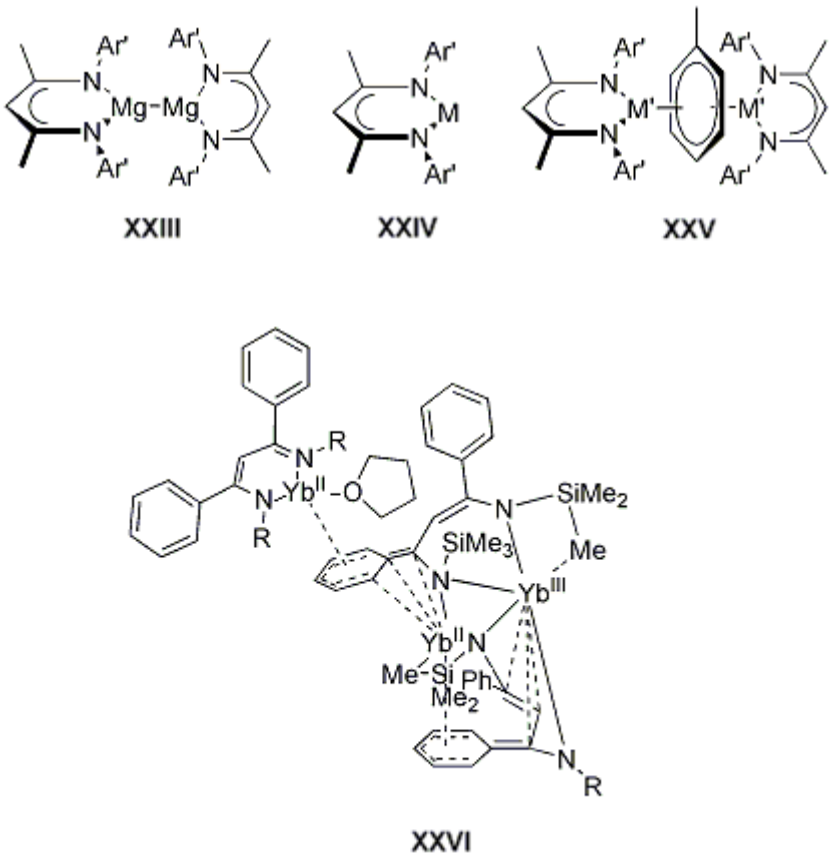

Figure 10 Examples of (BDI) metal complexes (Ar' = 2,6-*i*Pr$_2$-C$_6$H$_3$; M = Al, Ga; M' = V, Cr).

As a result of the steric and electronic versatility of this ligand, depending on modifications to the various R groups on the backbone, different versions of the β-diketiminate ligand have been used by various research groups. The first β-diketiminate divalent germanium and tin complexes were published independently as different versions of the same ligand in 2001 by Barrau (R^1R^5 = phenyl),[69] Dias (R^1R^5 = mesityl)[70] and Roesky and Power (R^1R^5 = 2,6-diisopropylphenyl)[71] (Scheme 2). The first β-diketiminate divalent lead complex was published in 2007 by Fulton and Lappert,[72] using the R^1R^5 = 2,6-diisopropylphenyl substituent. This substituent is the most widely used version of β-diketiminate and will be the version referred to as β-diketiminate from now on (unless otherwise stated to the contrary through the use of superscript to designate the different R^1R^5 groups).

Most β-diketiminate group 14 metal complexes have been created via salt metathesis reactions involving the β-diketiminate group 14 metal halide complexes (**XXVII**). The β-diketiminate group 14 metal complexes that have been generated via this method include the alkoxide and aryloxides (**XXVIII**), alkyls and alkynes (lead) (**XXIX**), amides (**XXX**), azides (**XXXI**), phosphides (**XXXII**) and triflates (**XXXIII**) (Scheme 3).[71,73-82]

Scheme 3 [(BDI)M-Cl] (Ar' = 2,6-*i*Pr_2-C_6H_3; M = Ge, Sn, Pb) salt metathesis reactions.

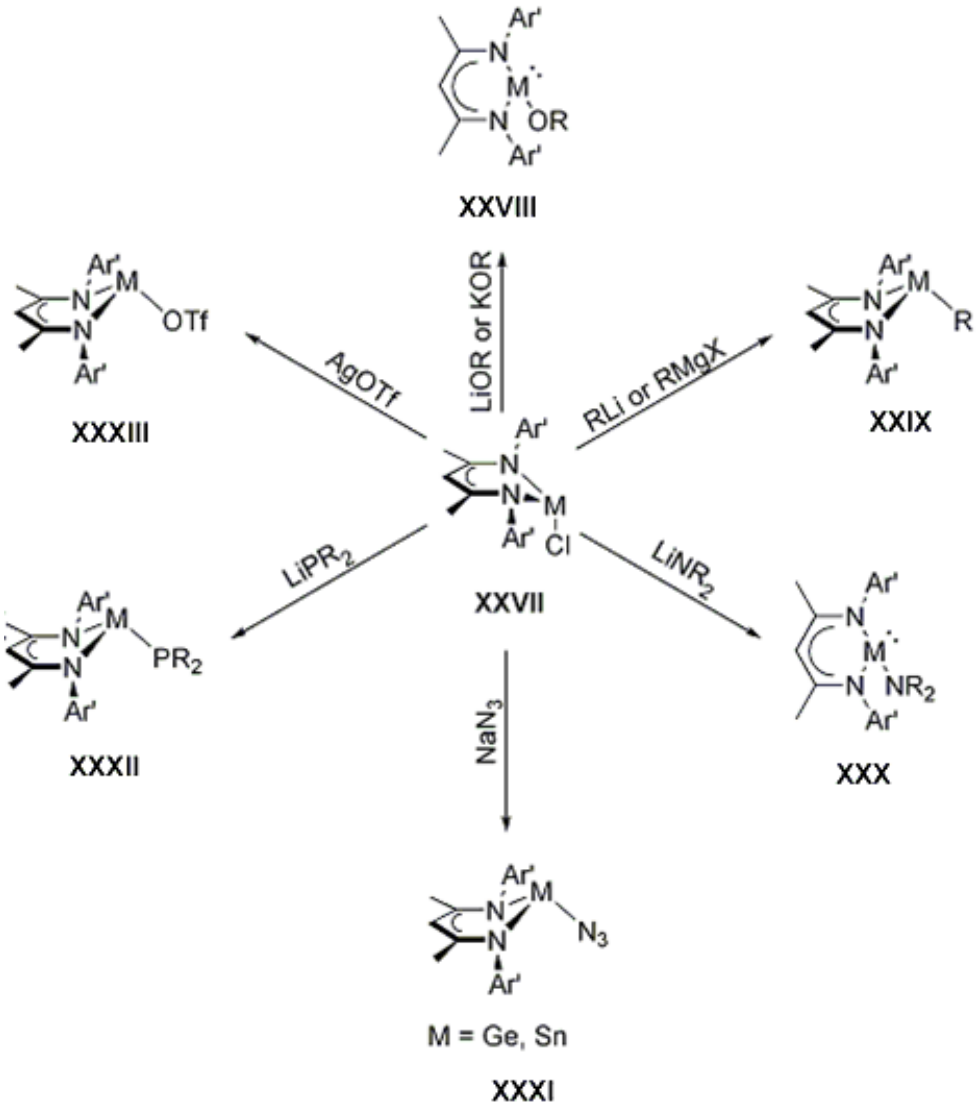

In addition to the salt metathesis reaction used to generate most β-diketiminate group 14 metal complexes, other complexes created via other reaction pathways have been reported (Schemes 4 and 5). In one study, Barrau et al. were able to oxidise the metal centres of the β-diketiminate^{phenyl} germanium and tin chloride complexes (**XXXIV**) using chalcogens (**XXXV**) (Scheme 4).[69] Furthermore, heterocyclizations, which are believed to be a result of an one-electron transfer mechanism, resulted in the β-diketiminate germanium and tin cyclic derivatives (**XXXVI**). Lastly, Barrau et al. were able to extract the chloride, through the use of [Na][BPh_4], forming cationic germanium and tin species (**XXXVII**). The abstraction of chloride with a Lewis acid was also successfully adopted by Fulton et al., forming cationic tin and lead species.[83] In the same study, cationic tin and lead species were also created via methyl group abstraction using a borane.

Scheme 4 Reactivity pattern of [(BDI^{phenyl})M-Cl] (M = Ge, Sn).

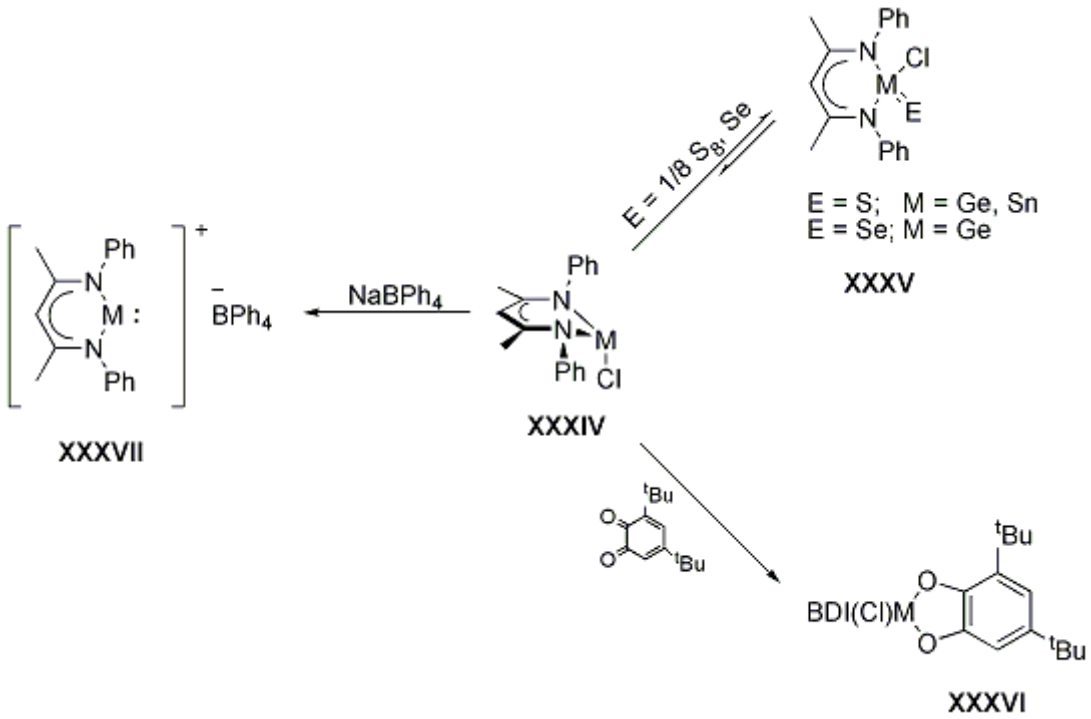

In a study by Roesky et al., attempts to form a tin hydride complex by reacting the β-diketiminate tin chloride complex with the reducing agents [KC_8] and [$LiAlH_4$], afforded a bis-β-diketiminate tin complex (**XXXVIII**) and a known aluminium hydride complex (**XXXIX**), respectively, through reductive dehalogenation (Scheme 5).[71] The germanium and tin hydride complexes (**XL**) were successfully created by Roesky et al. five years later by using [$AlH_3.NMe_3$] as both the reducing agent and hydride source.[84]

Scheme 5 Reactivity pattern of [(BDI)M-Cl] (Ar' = 2,6-*i*Pr_2-C_6H_3; M = Ge, Sn).

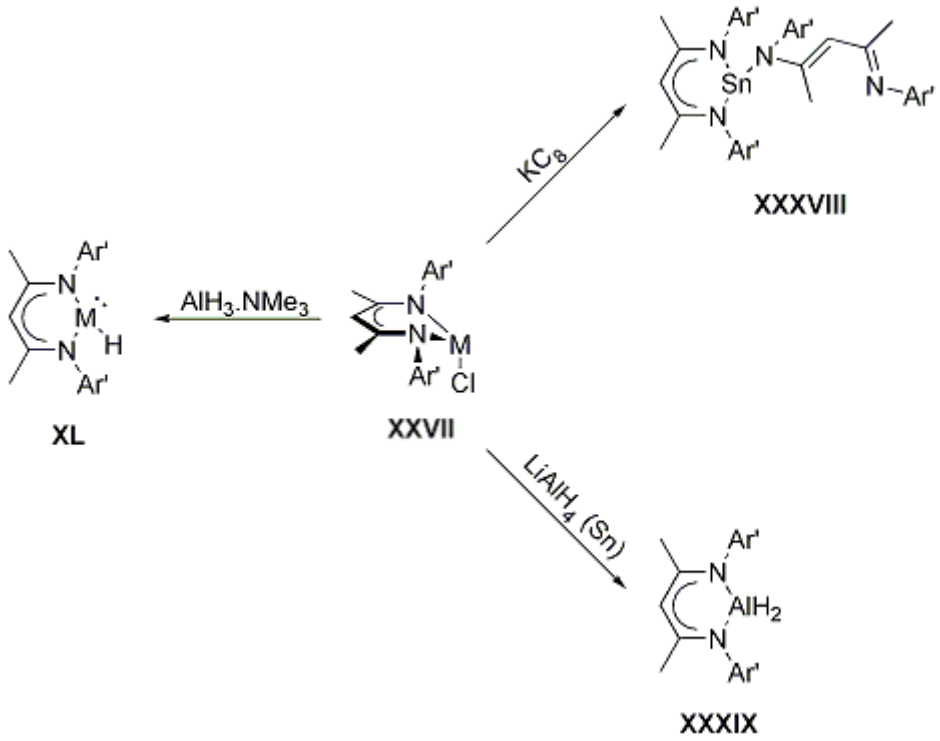

A wide range of β-diketiminate group 14 metal complexes have been generated and the chemistry of some of these complexes examined. Reactivity studies have been performed on group 14 metal alkoxides **XXVIII** (Scheme 6 and 7), amides **XXX** (Chapter 2) and hydrides **XL** (Scheme 8).[55,78,80,82,85-89]

The first reactivity studies performed on the β-diketiminate group 14 metal complexes probed the potential use of β-diketiminate tin *iso*-propoxide **XXVIII** as a well defined initiator for the polymerisation of *rac*-lactide.[73] This study was extended to include the tin dimethylamide complex **XXX** in 2006, which also showed potential as an initiator for well-controlled polymerisation.[55] The electronic properties of the tin(II) centre were found to have greater influence over the polymerisation process relative to the electronic and steric properties of the ancillary ligand compared to other β-diketiminate metal systems. Gibson stated that this mechanism could be more accurately described as, "… a *lone-pair-dominated, chain-end-controlled* process, rather than the *ligand-assisted, chain-end-controlled* process…".[55]

A study by Driess et al. which focused on the reactivity of β-diketiminate lead 2,6-di-*tert*-butylphenoxide **XXVIII** with [LiN($SiMe_3$)$_2$] and [LiP($SiMe_3$)$_2$] yielded the corresponding lead amide **XXX** and lead phosphide **XXXII**, respectively (Scheme 6).[82*1] Furthermore, addition of [*t*Bu_3Si(R)Si=PH] to a lead bis(trimethylsilyl)amide complex **XXX** resulted in the formation of the first lead phosphasilene complex (**XLI**) (Scheme 6). These lead complexes were stated to display potential as initiators for the synthesis of polylactides, similar to the tin complexes investigated by Gibson et al., although subsequent polymerisation studies on these systems were never reported.[55] Driess et al. also reported the re-planarisation of the six-membered C_3N_2Pb ring when the donor ability of the terminal ligand was reduced.[82] Another study by Fulton probed the reactivity of β-diketiminate lead alkoxide complexes **XXVIII** with the heterocumulenes, carbon dioxide and phenyl isocyanate (Scheme 7).[78] This study showed successful carbon dioxide activation by the lead alkoxide complexes resulting in the lead carbonates (**XLII**). The activation reactions by the lead alkoxides were found to be reversible, with the degree of reversibility highly dependent on minor differences to the alkyl groups on the alkoxide

[1]Driess et al. also used lithium bistrimethylsilylphosphide to generate the germanium analogue, using a precursor germanium chloride complex **XXVII**.[81] This study also included the formation of other β-diketiminate germanium phosphides and a triflate.

ligand. In contrast, divergent reactivity was reported during treatment of the lead alkoxides **XXVIII** with phenyl isocyanate. The lead *tert*-butoxide was found to be unreactive, whereas the *iso*-propoxide was shown to undergo insertion into the Pb-O bond such that the nitrogen atom coordinates to the lead centre, resulting in the formulation of a lead carbamate (**XLIII**). The lead alkoxides **XXVIII** were found to exhibit some, albeit contradictory, nucleophilic behaviour towards various electrophiles.

Scheme 6 Reactivity pattern of [(BDI)Pb-OR] (Ar' = 2,6-*i*Pr$_2$-C$_6$H$_3$; R = 2,4,6-*i*Pr$_3$-C$_6$H$_2$) and that of their corresponding products.

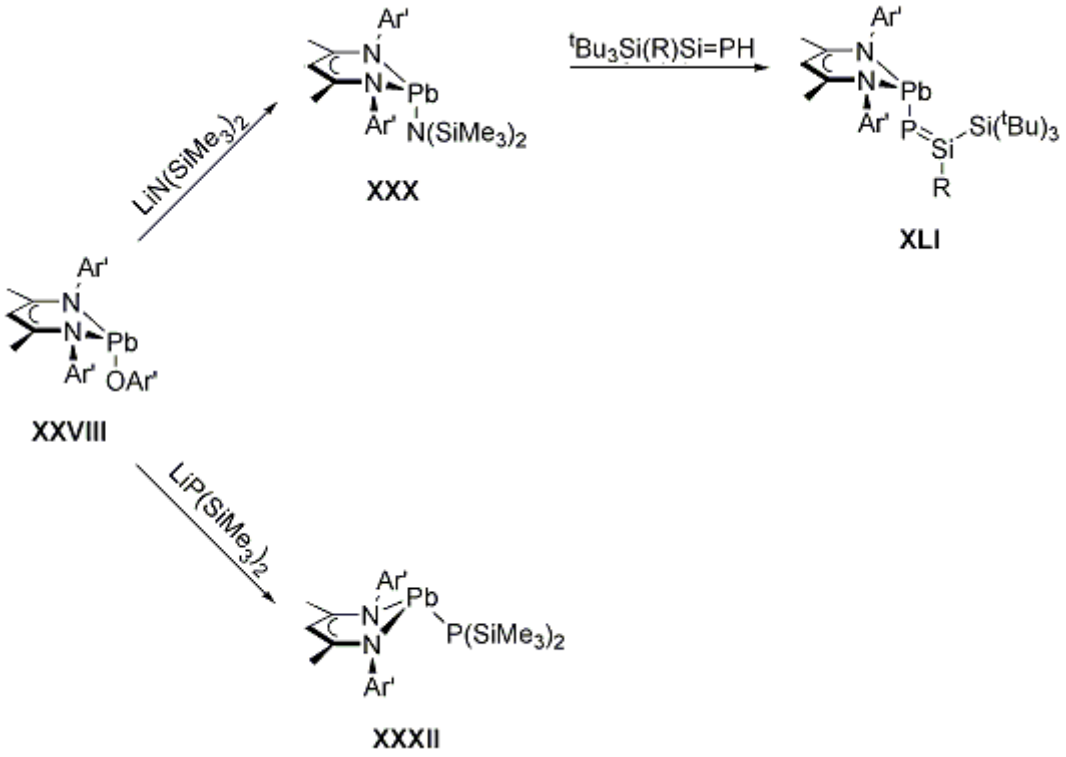

Scheme 7 Reactivity pattern of [(BDI)Pb-OR] (Ar' = 2,6-*i*Pr$_2$-C$_6$H$_3$; R = *i*Pr, *t*Bu, *s*Bu) with heterocumulenes.

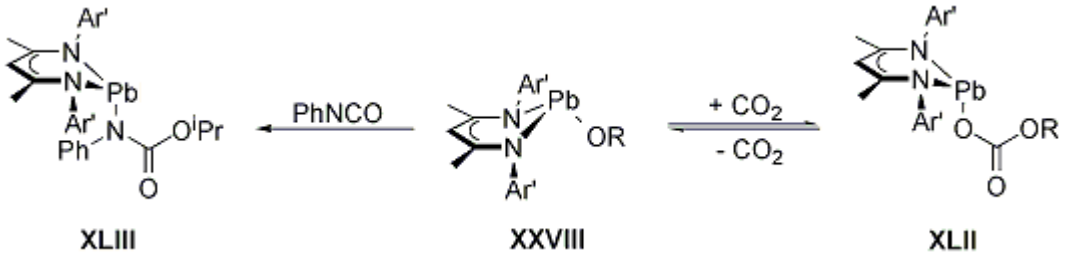

Reactivity studies on the germanium and tin hydride complexes **XL** by Roesky et al. have shown the complexes' abilities to activate small molecules such as alkynes, carbon dioxide, dicyclohexyl carbodiimide and ketones (Scheme 8).[86,90]

Scheme 8 [(BDI)M-H] (Ar' = 2,6-*i*Pr$_2$-C$_6$H$_3$; M = Ge, Sn) reactivity pattern.

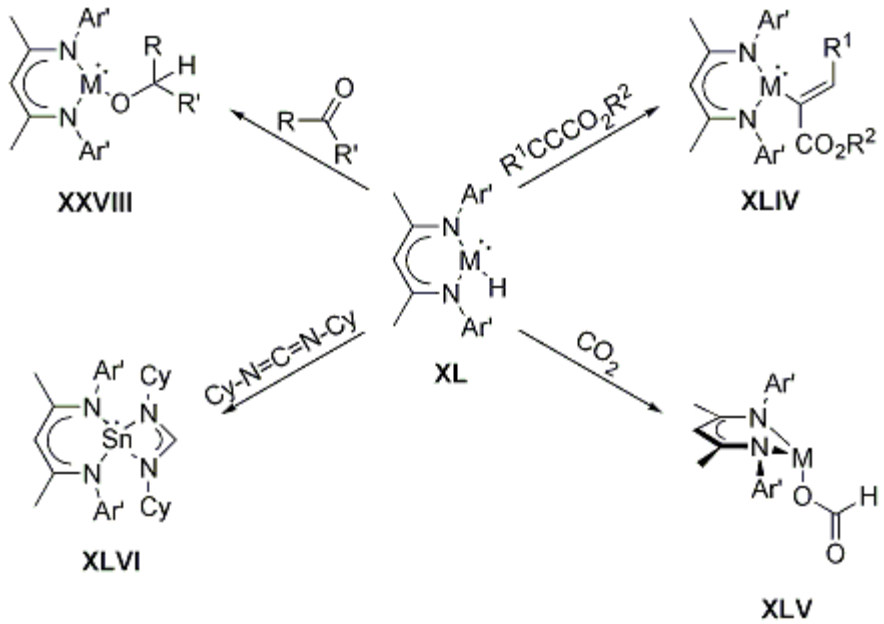

1.2.1.1. Structural studies

X-ray structural data of three-coordinate, divalent β-diketiminate group 14 metal complexes have shown these trigonal pyramidal complexes adopting either an 'endo' or an 'exo' conformation (Figure 11).

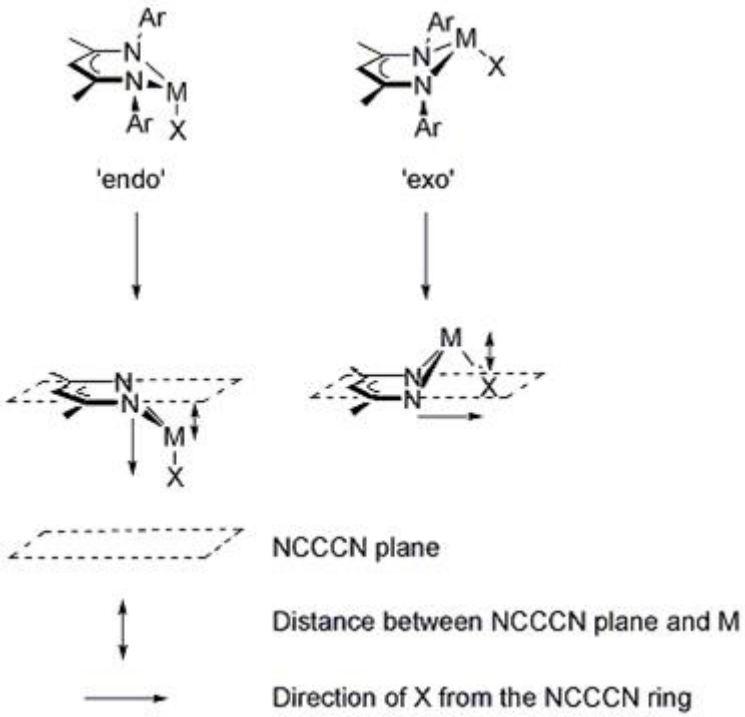

Figure 11 'Endo' and 'exo' conformations adopted by [(BDI)M] (M = Ge, Sn, Pb) complexes in the +2 oxidation state. Aryl groups are omitted from the bottom conformations for clarity.

The 'endo' conformation is characterised by the metal centre (M) and the terminal ligand (X) being positioned on the same side of the NCCCN plane so that X lies in-between the two *N*-aryl groups of the β-diketiminate. In this conformation the M-X bond is also approximately at a 90° angle from the NCCCN plane. The 'exo' conformation is

characterised by the metal centre lying above the NCCCN plane with the terminal ligand directed away from the six-membered ring. This conformation is believed to be adopted only when the 'endo' conformation is not possible on the grounds of steric factors. Analysis of X-ray structural data in Chapters 2 and 3 will include the designation of the conformation adopted by each structurally characterised complex synthesised in this study and arguments to explain these results.

1.2.2. Summary

In summary, recent advances in the synthesis of divalent group 14 metal complexes have been made possible through the development of kinetically and thermodynamically stabilising ancillary ligands. The reactive behaviour of such complexes has been studied and applications for the tin amidinate and β-diketiminate complexes in the polymerisation of *rac*-lactide have been investigated.[53,55,73] In particular, the generation and reactivity of group 14 metal complexes supported by a β-diketiminate ligand have been highlighted due to their relevance to the chemistry reported in subsequent Chapters. Previous research has shown that the terminal ligand on these complexes exhibit mildly nucleophilic behaviour. Recent developments regarding the reactivity of group 14 metal amide complexes (one of the terminal pnictogens whose structural and reactive properties is under investigation in this study) will be expanded upon in Chapter 2, along with the reactivity of late transition metal amide complexes, which are predicted to exhibit similar reactive behaviour. The reactivity of group 14 metal complexes with chalcogens will be discussed in Chapter 3, in addition to recent advances in group 14 metal chalcogenides as single source precursors for chemical vapour deposition.

1.3. Aims

The aim of this research was to probe the chemistry of the terminal pnictogen complexes of lead, tin and germanium in the divalent state. In this study, the divalent state was stabilised via the coordination of a bulky β-diketiminate ancillary ligand (where R^1R^5 = 2,6-diisopropylphenyl). The chemistry of pnictogen complexes involving amide and phosphide ligands was investigated. Firstly, lead and tin amide complexes were synthesised and structurally characterised and then reacted with aliphatic electrophiles, unsaturated electrophiles and carboacids (the products of which were structurally characterised). DFT studies were also performed on the group 14 metal amide complexes in order to enhance our understanding of their reactivity. Secondly, lead, tin and germanium phosphide complexes, already reported in literature, were synthesised and their reactivity examined with one equivalent and an excess of the chalcogens, selenium and tellurium, the products of which were structurally characterised. DFT studies were performed on the germanium dialkyl-chalcogenophosphinites in order to gain further insight into their reactivity. AACVD studies were also performed on the germanium dicyclohexyl-tellurophosphinite complex and other group 14 metal dialkyl-phosphinodichalcogenoates in order to probe their suitability as thermo-electric materials.

2. Group 14 metal amides: synthesis and reactivity studies

2.1. Overview of late transition metal amide chemistry

Relative to their transition metal analogues, the chemistry of group 14 metal terminal amide complexes has not been extensively explored. The chemistry of metal (M) amide complexes is driven by the polarity of the M-N bond. With regards to transition metal analogues, it has been observed that the polarity of the M-N bond increases upon moving from the early and middle transition metal amide complexes to the late transition metals. This is due to differences in back bonding of the nitrogen lone pair on the amide ligand into an empty d orbital on the metal complex. For instance, in early transition metal complexes there are fewer electrons occupying the d orbitals, thus favouring back bonding and reducing the polarity of the M-N bond. In contrast, the low oxidation state of late transition metal amide complexes result in filled dπ orbitals, which causes disruption to ligand-to-metal π-donation. This decrease in electron density delocalisation from the ligand to the metal, relative to the earlier transition metal amide complexes, create an increasingly polarised bond (Figure 12).[91] As a result of this, late transition metal amide complexes are found to display nucleophilic and basic behaviour whereas other transition metal amide complexes (located in the early and middle groups) are found to be relatively inert. Although back bonding is not observed in group 14 metal terminal amide complexes, differences in the electronegativity between the group 14 metal centre and nitrogen in the terminal amide should polarise the bond, resulting in similar nucleophilic and basic behaviour to that of the late transition metal analogues. This Chapter describes the reactivity of group 14 metal terminal amide complexes, however, it begins with an introduction into the reactivity of late transition metal amide complexes, in order to compare our results with such species.

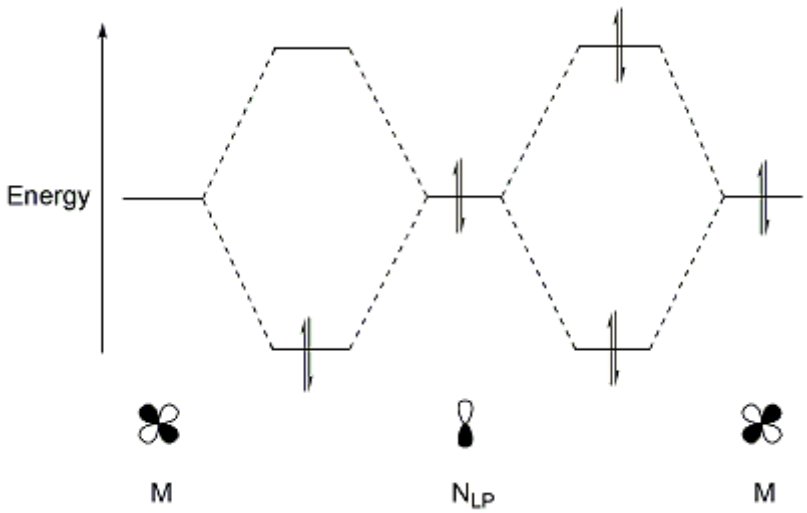

Figure 12 Interaction between a lone pair orbital on the nitrogen (N_{LP}) and empty and filled d orbitals of a transition metal.

2.2. Synthetic procedures

The most popular method employed to synthesise late transition metal amide complexes is the metathesis of a metal chloride or triflate complex with an alkali metal amide. This method was employed to generate a series of chelating bis(phosphine) platinum amides (**XLVIII**), by treating the corresponding platinum chloride complex (**XLVII**) with a lithium amide in THF (eq 4).[92]

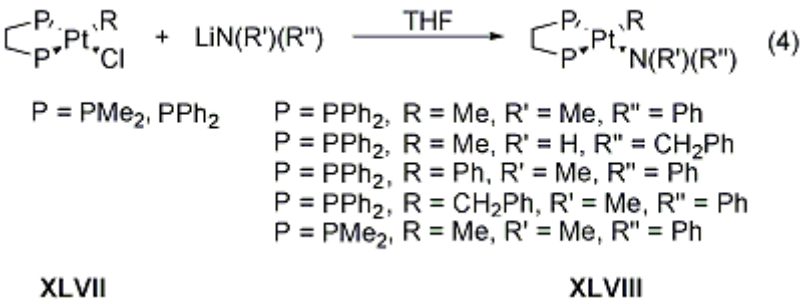

Another method implemented to generate late transition metal amide complexes is the heteroatom exchange method in which one heteroatom group (X) is exchanged with a primary or secondary amine (eq 5). One limitation to this method is the possible reversible nature of these reactions. For instance, the iridium amide complex, [Cp*(PPh_3)Ir(H)(NHR)] (**L**),[93] is in equilibria with the corresponding ethoxide complex (**XXXIX**), from which it was generated. The established equilibrium is dependant upon the M-X and X-H bond dissociation energies, where M-S bonds are generally favoured, followed by M-O bonds and then M-N bonds.[94]

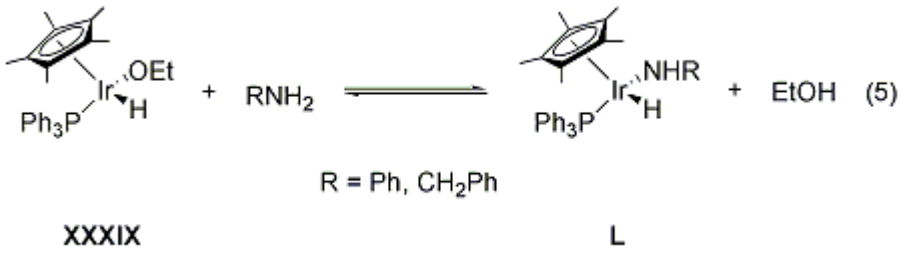

Synthesis of the first late transition metal parent amide complexes (known as parent amide complexes due to the primary amide ligand) presented many challenges. Generally, attempts to yield such compounds resulted in dimeric metal complexes with the parent amide groups bridging two metal centres. The first structurally characterised parent amide complex, [$(dmpe)_2$(H)$RuNH_2$] (**LII**), was reported in 1998.[95] It was synthesised at room temperature from the ruthenium hydride chloride complex, [$(dmpe)_2$(H)RuCl] (**LI**), and $NaNH_2$, in a pressurised ampoule containing a 1:1 mixture of THF and liquid ammonia (eq 6). [Cp*(PMe_3)(Ph)Ir(NH_2)] was also generated using this methodology, however, this complex was reported to be stable only in solution.

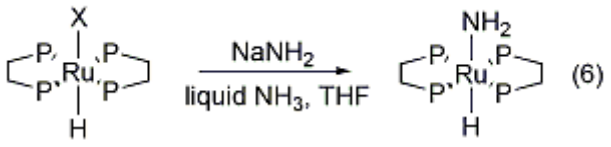

X = OH, Cl P = PMe_2

LI **LII**

Hartwig synthesised the iridium parent amide complex, [(PCP)Ir(H)(NH_2)], by utilising the aromatic pincer ligand PCP (PCP = 1,3-di-*tert*-butylphosphinobenzene).[96] The parent amide complex was not stable at ambient temperatures and spontaneously eliminated ammonia to form the Ir(I) ammonia complex, [(PCP)Ir(NH_3)]. By a slight alteration of the pincer ligand to that possessing an aliphatic backbone (which should increase the electron density at the metal centre), Hartwig was able to achieve the reverse of ammonia elimination and activate ammonia to form [{2,6-(CH_2P-*t*Bu_2)$_2$$C_6H_3$}Ir(H)($NH_2$)] (**LIV**) upon treatment of the Ir(I) propylene complex, [{2,6-(CH_2P-*t*Bu_2)$_2$$C_6H_3$}Ir($C_3H_6$)] (**LIII**), with ammonia at room temperature (eq 7). This complex was also synthesised by dissolving the corresponding iridium hydride chloride complex, [{2,6-(CH_2P-*t*Bu_2)$_2$$C_6H_3$}Ir(H)(Cl)] (**LV**), into ammonia, which was followed by addition of [KN($SiMe_3$)$_2$] to the reaction mixture (eq 8).[96]

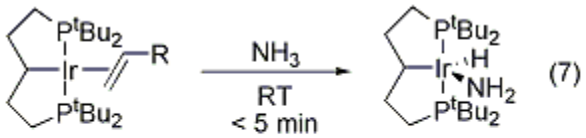

R = CH_3, C_3H_5

LIII **LIV**

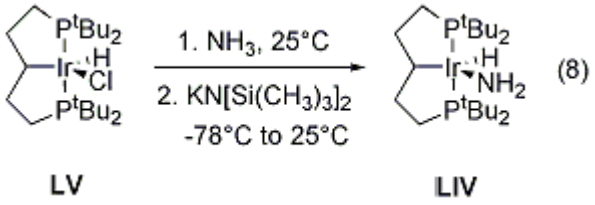

LV **LIV** (8)

2.3. Reactivity studies

The enhanced nucleophilic and basic behaviour of late transition metal amide complexes, caused by the reduction of electron density delocalisation from the amide moiety to the metal centre, has been investigated by examining their reactivity towards a variety of organic electrophiles and acids.

2.3.1. Nucleophilic reactivity with unsaturated organic electrophiles

Unsaturated organic electrophiles, namely heterocumulenes, such as carbon dioxide, carbon disulfide, isocyanates, aldehydes, ketones and nitriles, have all been used to probe the nucleophilicity of the M-N bond. The products of these reactions are generally a result of nucleophilic attack by the amide nitrogen onto an electrophilic carbon centre.

Heterocumulene insertion into the M-N bond was reported for the nickel amide complex, [Ni(Me)(NC_4H_8)(dippe)] (**LVI**).[97] The heterocumulenes found to undergo this insertion were carbon dioxide (**LVII**), phenyl isocyanate (**LVIII**) and phenylthioisocyanate (**LIX**) (Scheme 9).

Scheme 9 Heterocumulene insertion reactivity displayed by [Ni(Me)(NC_4H_8)(dippe)].

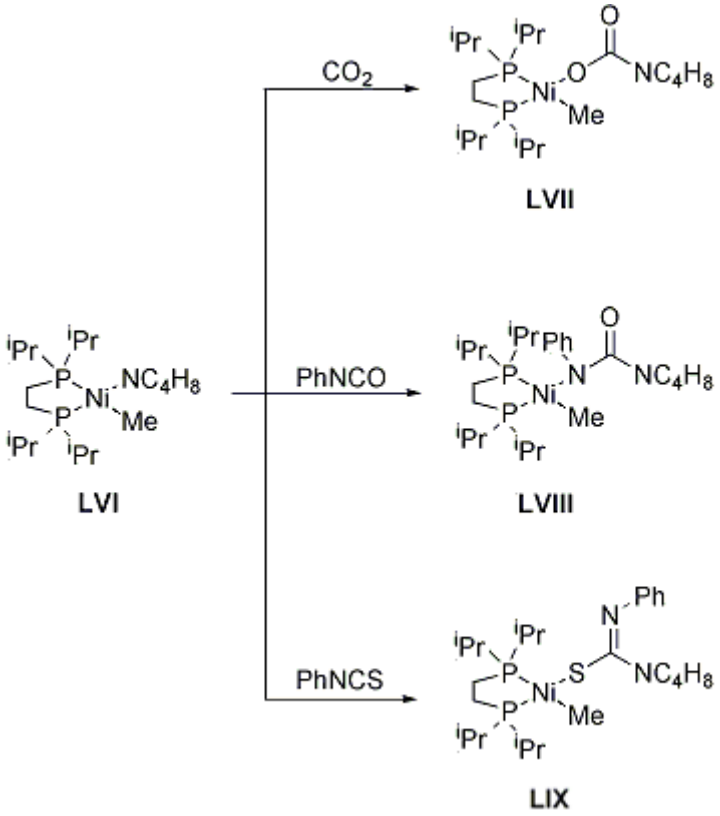

The reactivity of iridium amide complexes **L** with heterocumulenes, including carbon disulfide and methyl isocyanate, resulted in the overall insertion of the heterocumulene into the M-N bond, (**LX**) and (**LXI**) (Scheme 10).[93] Similar reactivity was observed with the related metallacyclic amide complex (**LXII**), in which *tert*-butyl isocyanate inserted into the N-H bond (**LXIII**) (eq 9).[93]

Scheme 10 Heterocumulene insertion in iridium amide complexes (R = Ph, CH_2Ph).

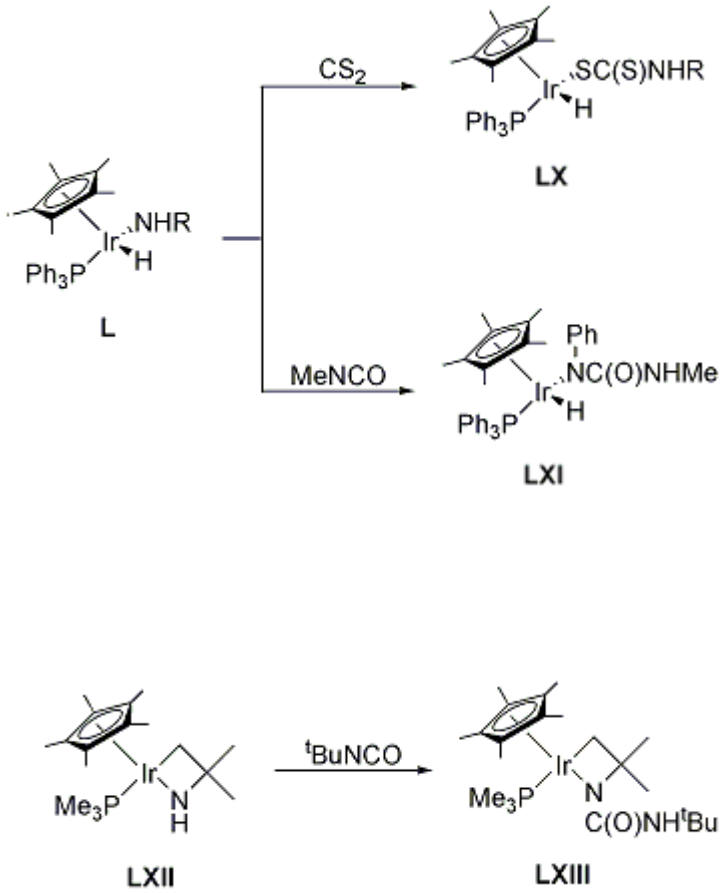

A study probing the reactivity of the ruthenium amide complex, [(PCP)Ru(CO)(PMe_3)(NHPh)] (**LXIV**), was conducted by Gunnoe et al.[98] Interestingly, reactions of the ruthenium amide complex with unsaturated electrophiles, such as benzaldehydes, carbodiimides, isocyanates and nitriles, resulted in the formation of four-membered heterometallacycles (**LXV** – **LXVIII**). These products were proposed to be a result of an intramolecular C-N bond formation between the amide ligand and the unsaturated electrophile, so that the trimethylphosphine moiety is displaced (Scheme 11). The reaction with the carboxamides ([RCONHR], R = Me, Ph) to form the four-membered heterometallacycle (**LXIX**) follows a different pathway as the anilide ligand appears to deprotonate the coordinated amide. This results in the formation of free aniline and an

anionic amidate ligand, which coordinates to the ruthenium centre as a bidentate ligand (Scheme 11).

Scheme 11 Reactivity of [(PCP)Ru(CO)(PMe_3)(NHPh)] (P = tBu$_2$P) with various unsaturated electrophiles.

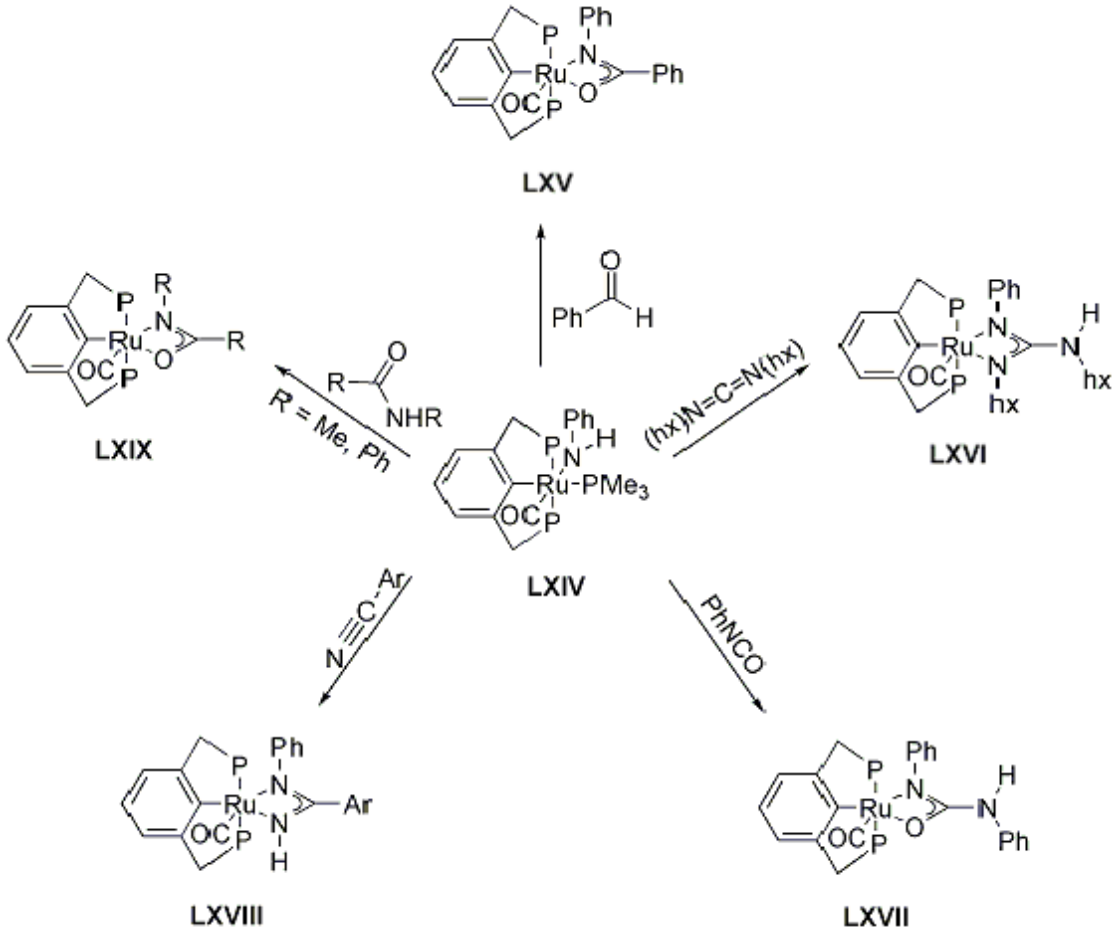

Parent amide complexes generally react with heterocumulenes in a similar manner to that of aryl amide or alkyl amide complexes. For instance, addition of *tert*-butyl isocyanate, isopropyl isocyanate and diisopropylcarbodiimide, resulted in the insertion of the heterocumulene into the N-H bond, (**LXXI**) and (**LXXII**) (Scheme 12).[99]

Scheme 12 Reactivity of [Cp*Ir(PMe_3)(Ph)(NH_2)] with various heterocumulenes (R = *t*Bu, *i*Pr).

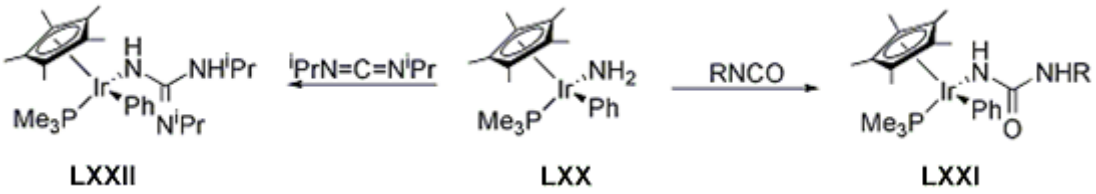

LXXII **LXX** **LXXI**

2.3.2. Reaction with carbon monoxide

Although carbon monoxide possesses an unsaturated carbon centre, it generally is not considered to possess an electrophilic carbon centre due to the formal negative charge on that atom. As such, the reactivity with amide complexes does not proceed via predictable pathways. For instance, reductive elimination was observed upon addition of carbon monoxide, ethylene, isobutyl nitrile and phosphines to the iridium amide hydride, [Cp*IrPPh_3(NHPh)(H)] **L**, resulting in the formation of free aniline and coordination of the electrophile (**LXXIII**) (eq 10).[93] In contrast, addition of carbon monoxide to [(dmpe)$_2$Fe(H)(NH_2)] (**LXXIV**) resulted in the formation of *trans*-[(dmpe)$_2$Fe(H)(NHCHO)] (**LXXV**) (eq 11).[100]

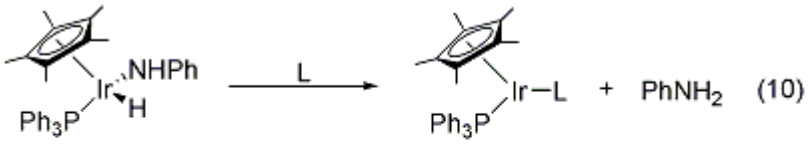

L **LXXIII**

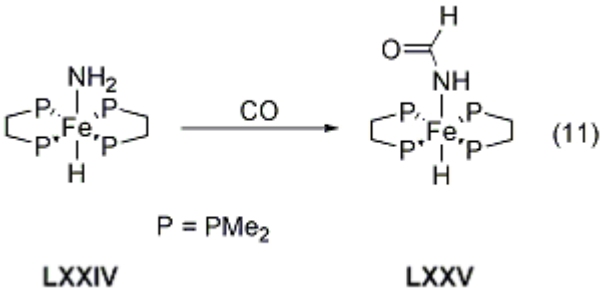

Three mechanisms were proposed to rationalise this reactivity (Scheme 13).[100] The first two pathways involve the coordination of carbon monoxide to the iron centre and displacing one of the coordinated phosphines, forming intermediate B. Migratory insertion of the carbon monoxide into the Fe-N bond of B results in intermediate C. For pathway I, β-hydride elimination ensues, forming iron dihydride complex D, and isocyanic acid, which then inserts into the Fe-H bond and forms F. Support for this mechanism was undermined by deuterium-labelling experiments, where the reaction of $[(dmpe)_2Fe(D)(NH_2)]$ with carbon monoxide resulted in the exclusive formation of *trans*-$[(dmpe)_2Fe(D)(NHCHO)]$.[100] If isocyanic acid had been involved in the reaction than both *trans*-$[(dmpe)_2Fe(D)(NHCHO)]$ and *trans*-$[(dmpe)_2Fe(H)(NHCDO)]$ would have been observed. Furthermore, another reaction involving $[(dmpe)_2Fe(H)(NH_2)]$ and carbon monoxide, in the presence of *cis*-$[(dmpe)_2Fe(D)_2]$, showed no deuterium incorporation into *trans*-$[(dmpe)_2Fe(H)(NHCOH)]$. This showed isocyanic acid was not produced and inserted into the Fe-H/D bond of *cis*-$[(dmpe)_2Fe(H/D)_2]$.[101]

Scheme 13 Proposed mechanisms for the insertion of carbon monoxide into $[(dmpe)_2Fe(H)(NH_2)]$ (P = PMe_2).

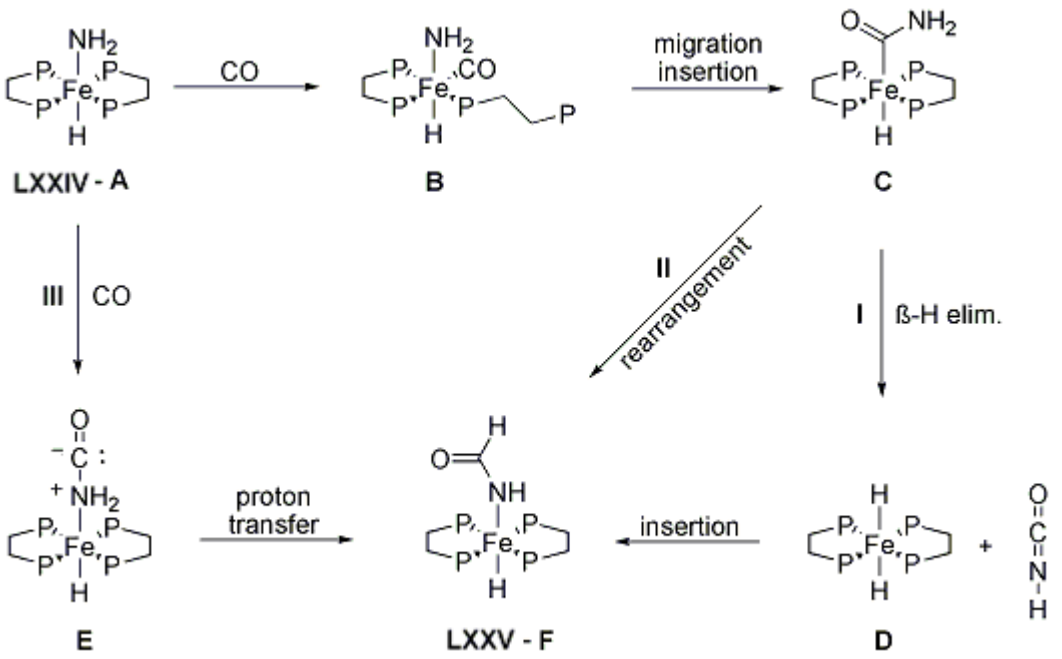

Pathway II involves re-arrangement of complex C to form F. The feasibility of this mechanism was tested by studying whether *trans*-$[(dmpe)_2Fe(H)(CONH_2)]$ is a likely intermediate (Scheme 14).[100] Firstly, *cis*-$[(dmpe)_2Fe(H)_2]$ underwent photolysis, forming $[(dmpe)_2Fe]$. The presence of deuterated formamide (NH_2COD) during photolysis caused the unsaturated iron(0) complex to form *trans*-$[(dmpe)_2Fe(H)(NHCOD)]$ which showed N-H bond activation. No formation of *trans*-$[(dmpe)_2Fe(D)(CONH_2)]$ was observed, which would have been a result of C-H bond activation. This outcome reduces the possibility of the formation of *trans*-$[(dmpe)_2Fe(H)(CONH_2)]$ as an active intermediate.

Scheme 14 Photolysis experiment to test the validity of pathway II (where P = PMe_2).

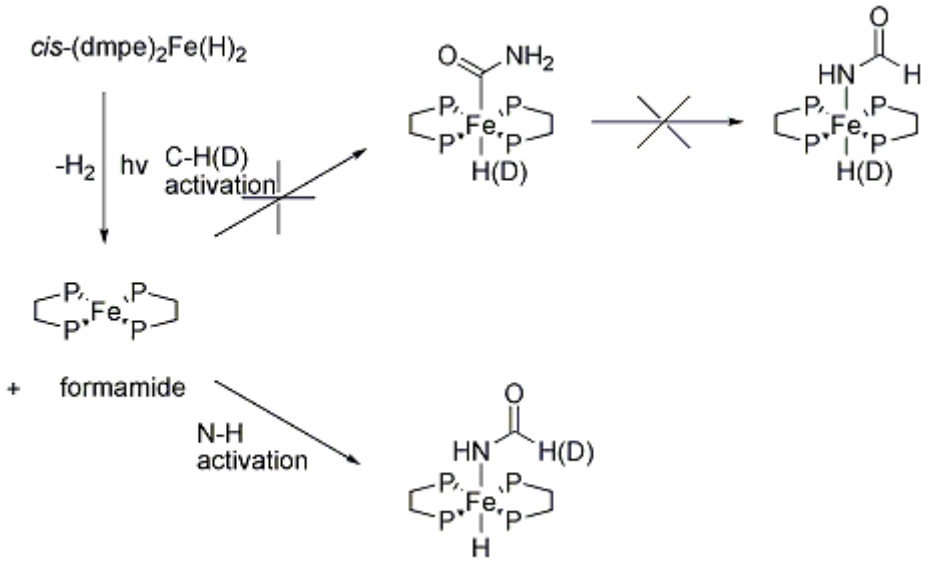

The mechanism favoured by Bergman et al. is that of pathway III (Scheme 13).[100] Unlike I and II, carbon monoxide coordinates to the amide moiety thus forming zwitterionic intermediate, complex E. Proton transfer within the zwitterionic intermediate leads to complex F. This pathway could only occur if the amide is nucleophilic enough to overcome the formal negative charge at the carbon atom of carbon monoxide.

DFT studies by Zhang et al. dispute these mechanisms due to the high energy activation barriers calculated. Based on their studies, a reactant-assisted mechanism was proposed (Scheme 15).[102] This mechanism involves coordination of the carbon monoxide to the amide moiety and the deprotonation of the amide moiety via the nitrogen of the amide group (situated on a second iron amide complex). The second iron amide (protonated) complex would be deprotonated via the abstraction of the proton via the carbon in the bound isocyanic acid group, forming complex F. Based on Zhang's DFT calculations, this mechanism was found to be (theoretically) more thermodynamically and kinetically favoured compared to Bergman's three proposed mechanisms and more

importantly, does not involve nucleophilic addition at the carbon centre of an unactivated carbon monoxide molecule.

Scheme 15 Proposed reactant-assisted mechanism (where P = PMe_2).

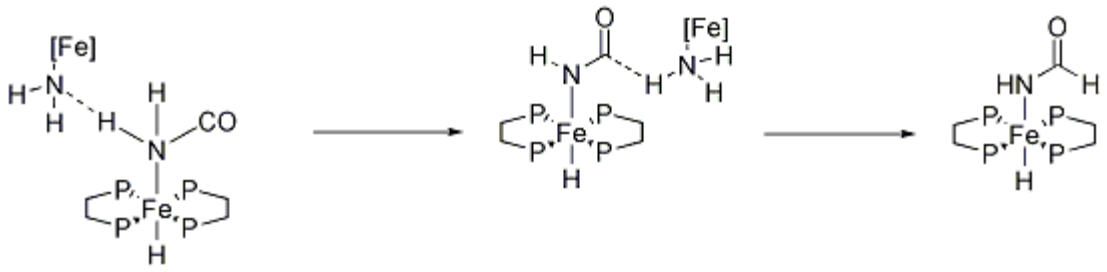

In a related system, addition of carbon monoxide to the iridium amide complex, [Cp*Ir(PMe_3)(Ph)(NH_2)] **LXX**, did not result in the formation of a formamide complex, instead, an iridium fulvene complex (**LXXVI**) was generated.[99] The product is believed to be a result of the displacement of the amide (as an anion) by the carbon monoxide, resulting in the amide deprotonating one of the methyl groups in the Cp* ligand and the generation of a fulvene moiety and free ammonia (Scheme 16). Although the reaction with carbon monoxide led to the eventual formation of multiple products, similar reactivity was observed with 2,6-dimethylphenyl isocyanide (which is isoelectronic to carbon monoxide at the isocyanide carbon atom), forming the isocyanide iridium complex (**LXXVII**).[99]

Scheme 16 Proposed mechanism for the reaction of carbon monoxide or 2,6-dimethylphenyl isocyanide with [Cp*Ir(PMe_3)(Ph)(NH_2)].

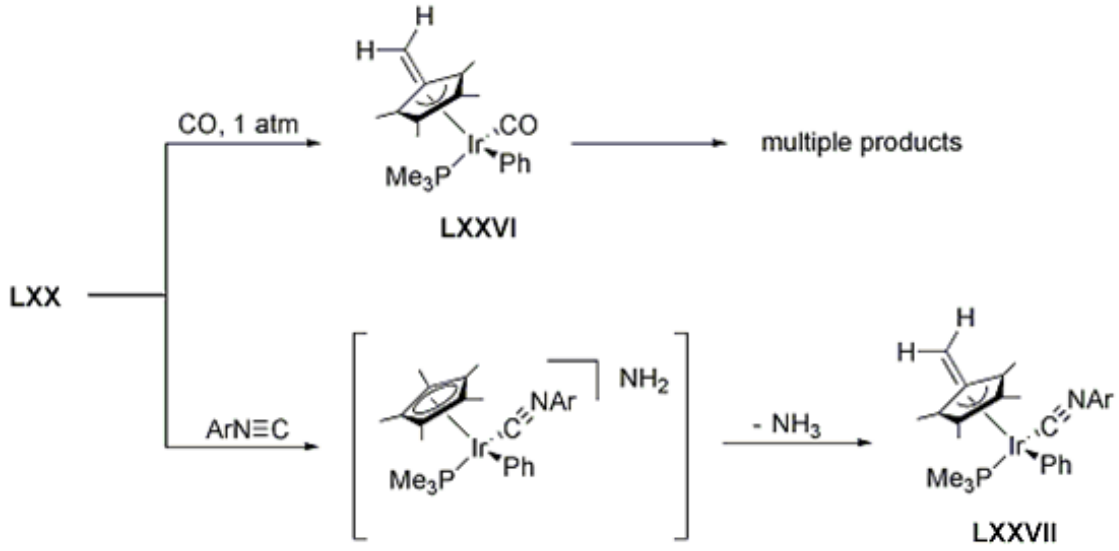

2.3.3. Basic reactivity with weak acids

The exceptional basicity of late transition metal amide complexes has been studied, where even weak acids were found to undergo deprotonation. For example, the ruthenium parent amide complex, [$(dmpe)_2RuH(NH_2)$] **LII**, reacted with weak acids such as phenylacetylene, 1,2-propadiene, propyne, nitriles and cyclobutanone. This resulted in the liberation of ammonia via the protonation of the amide group and (**LXXVIII**) (Scheme 17).[103]

Scheme 17 Basic reactivity of $[(dmpe)_2RuH(NH_2)]$ (P = PMe_2) with weak acids.

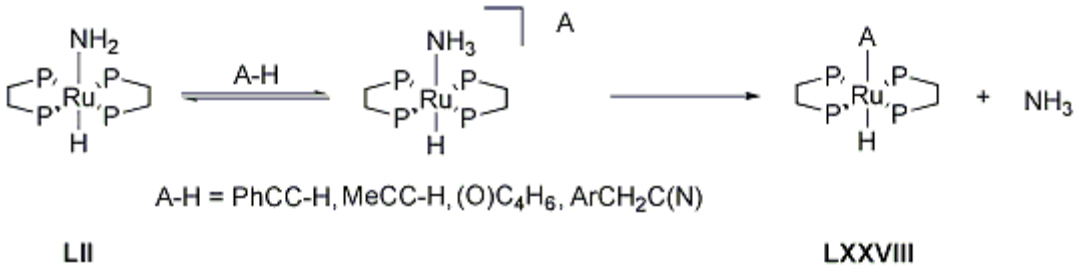

Spectroscopic observance of an intermediate ion pair in equilibrium with the precursor ruthenium complex was reported upon addition of triphenylmethane to the ruthenium amide complex.[103] The use of the sterically bulky acid, fluorene, resulted in the exchange process terminating at ion pair formation. In contrast, when a very weak acid was used, such as toluene, neither the ion pair nor the ammonia-displacement product was observed. Deuterium-transfer experiments were undertaken which proved rapid H/D exchange still occurs. In addition, Ru-N bond dissociation was investigated using $^{15}NH_3$, as a means to observe any ^{15}N incorporation into the ruthenium amide complex. Results showed no observable incorporation of $^{15}NH_3$ into the ruthenium amide complex, so that Ru-N bond dissociation is unlikely for these reactions.

Mechanistic studies undertaken by Gunnoe et al. for the acid-base reaction of the ruthenium complex, $[TpRu(PMe_3)_2NHPh]$ (**LXXIX**), with phenylacetylene, showed that not all acid-base reactions of late transition metal amide complexes proceed via the mechanism outlined in Scheme 17.[104] As demonstrated in Scheme 18, small quantities of the ruthenium triflate complex, $[TpRu(PMe_3)_2OTf]$ (**LXXX**), were shown to act as a catalyst in the formation of the ruthenium phenyl acetylide complex, $[TpRu(PMe_3)_2CCPh]$ (**LXXXI**), resulting in the production of free aniline and the regeneration of the catalyst.

Scheme 18 Proposed mechanism for the acid-base reaction of the ruthenium anilide complex, [TpRu(PMe$_3$)$_2$NHPh], with phenylacetylene.

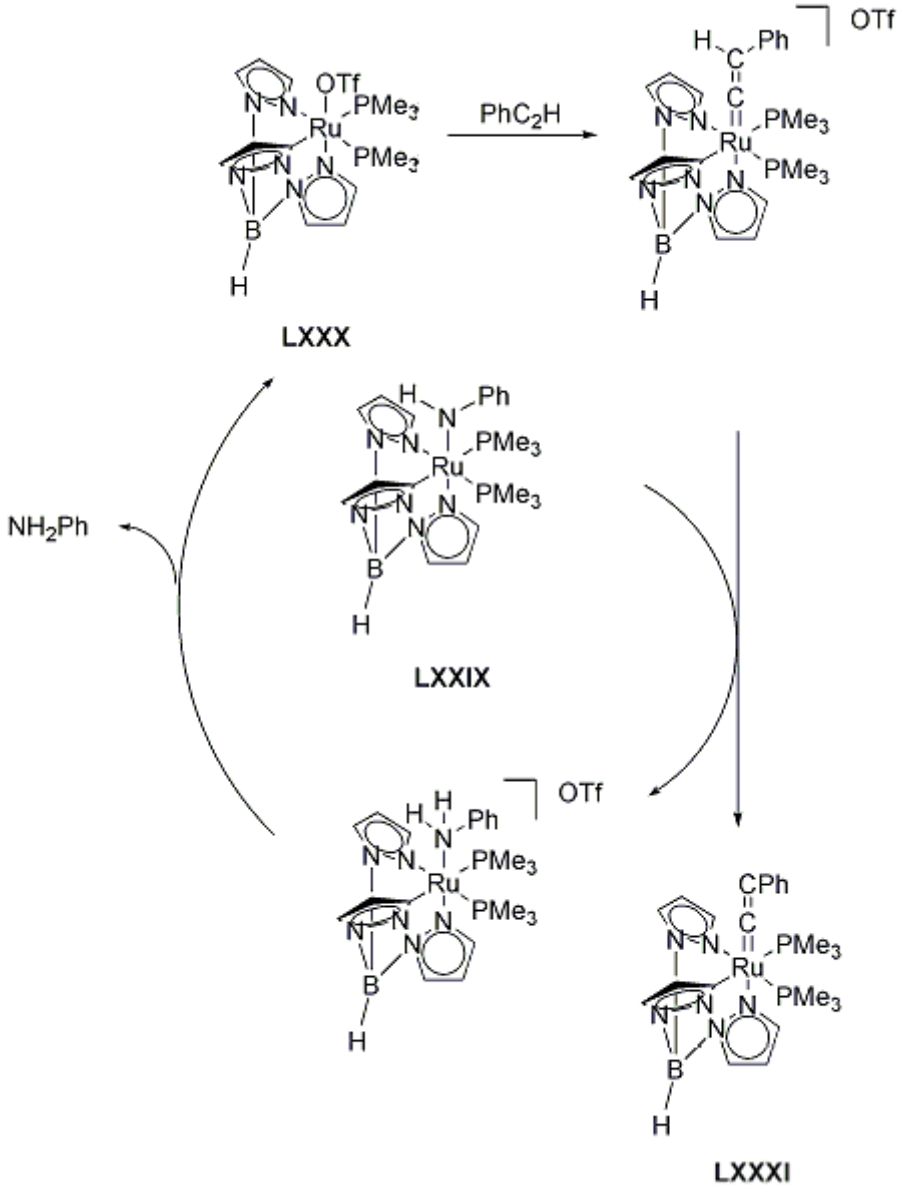

Another result published by Gunnoe et al. involved the addition of 1,4-cyclohexadiene to the ruthenium complex, [TpRu(PMe_3)$_2$NHR] (R = H, *t*Bu) (**LXXXII**), whereby free amine and benzene were generated in addition to a ruthenium hydride complex (**LXXXIII**) (Scheme 19).[104] However, isomerisation of 1,4-cyclohexadiene to an equilibrium mixture of 1,3- and 1,4-cyclohexadiene preceded the formation of benzene. As such, the mechanism was proposed to involve reversible proton transfer to the ruthenium amide complex. This would be followed by elimination of the free amine and the abstraction of hydrogen from the cyclohexadiene anion, thus forming benzene and the ruthenium hydride complex. A similar pathway was also described by Bergman in the reaction between [(dmpe)Ru(H)(NH_2)] and 1,4-cyclohexadiene.[105]

Scheme 19 Proposed mechanism for the acid-base reaction of [TpRu(PMe_3)$_2$NHR] with 1,4-cyclohexadiene (R = H, *t*Bu).

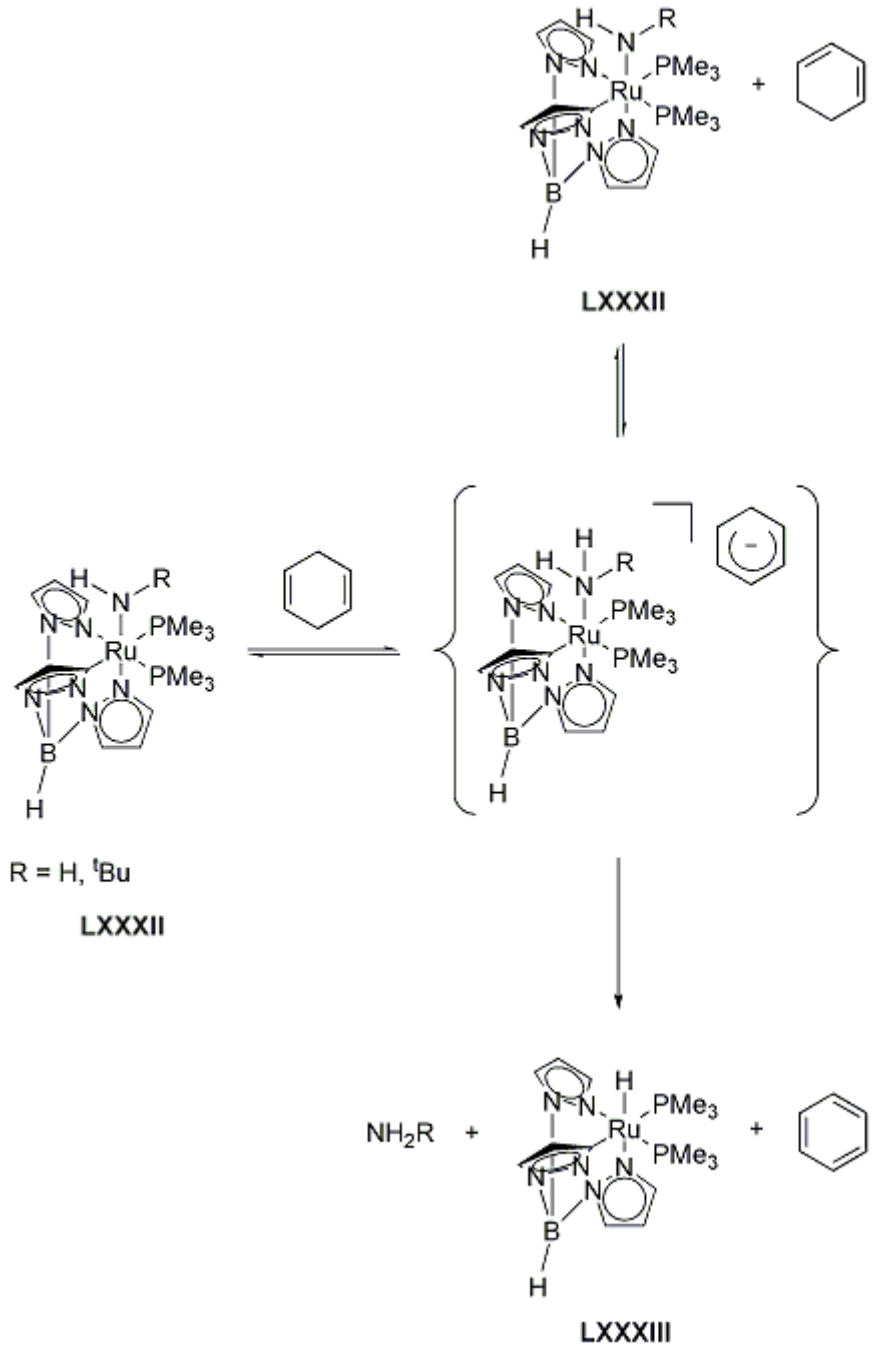

2.4. Overview of group 14 metal amide chemistry

An understanding of the reactivity of group 14 metal amide complexes has been limited by the lack of synthesised complexes. Most literature reports regarding these complexes have tended to focus on their synthesis and characterisation, as described in Chapter 1. Most investigations into the reactivity of group 14 metal amide complexes have focused on complexes supported by amidinate and β-diketiminate ancillary ligands.

2.4.1. Reactivity studies

Reactivity studies on the amidinate germanium(II) and tin(II) trimethylsilylamide species, [{(R'N)$_2$CR}M{N(SiMe$_3$)$_2$}] (M = Ge, Sn; R = Me, *t*Bu; R' = Cy or M = Sn; R = Ph; R' = N(SiMe$_3$)$_2$, N(SiMe$_2$Ph)$_2$), were undertaken with a focus on probing the chalcogenation or dechalcogenation of these complexes through the use of various chalcogen atom sources and chalcogen atom abstractors (Scheme 20).[52,106]

Addition of one equivalent of selenium to amidinate germanium trimethylsilylamide **XV** resulted in oxidative addition of the germanium centre and the generation of a monomeric amidinate germanium selenide complex, [{(CyN)$_2$CR}Ge{N(SiMe$_3$)$_2$}Se] (R = Me, *t*Bu) (**LXXXIV**).[52] In contrast, the analogous reaction with tin did not proceed, which was attributed to resistance to oxidative addition upon descending group 14. However, oxidative addition of the analogous amidinate tin trimethylsilylamide complex with four equivalents of sulfur yielded a tetrasulfide tin complex, [{(CyN)$_2$CR}Sn{N(SiMe$_3$)$_2$}S$_4$] (R = Me, *t*Bu) (**LXXXV**).[106] Upon addition of triphenylphosphine to the tetrasulfide tin complex, abstraction of sulfur atoms from the chelating bidentate sulfide ligand resulted in a dimeric amidinate tin complex with bridging sulfur centres, [({CyNC(R)NCy}Sn{N(SiMe$_3$)$_2$}S)$_2$] (R = Me, *t*Bu) (**LXXXVI**).[106] An alternative route to the same dimeric tin complex involved the addition of a sulfur atom

source (such as styrene or propylene sulfide) to the precursor amidinate tin trimethylsilylamide complex.

Scheme 20 Chalcogenation and dechalcogenation of amidinate germanium(II) and tin(II) trimethylsilylamide complexes (R = Me, *t*Bu).

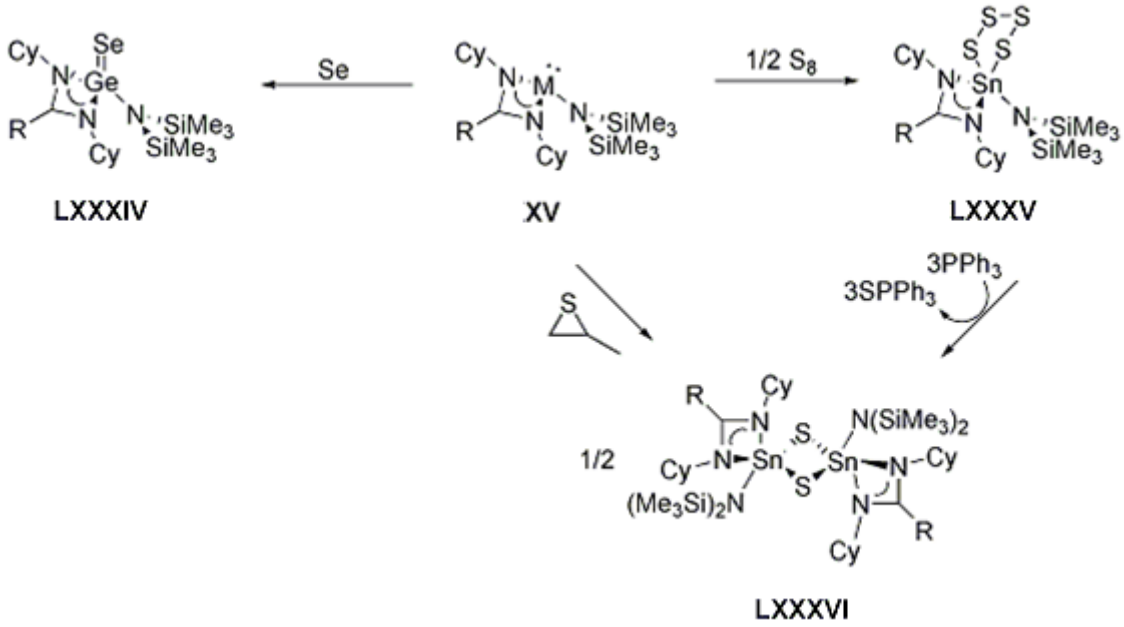

Both amidinate germanium and tin trimethylsilylamide complexes were found to undergo oxidative addition with diphenyldichalcogenides (when the chalcogenide, E = sulfur or selenium), resulting in the insertion of the metal centre into the E-E bond, $[\{(CyN)_2CMe\}M\{N(SiMe_3)_2\}(EPh)_2]$ (M = Ge, Sn; E = S, Se) (**LXXXVII**) and (**LXXXVIII**) (Scheme 21).[107] However, even though the tin product is five-coordinate upon addition of the phenylchalcogenide groups to the metal centre, the germanium product is four-coordinate due to the cleavage of one of the amidinate 'arms' on the metal centre. This is presumably a result of greater steric congestion around the germanium centre due to its smaller size relative to the tin centre. The ligand exchange reaction of selenium with the

four-coordinate germanium complex **LXXXVII** resulted in the elimination of diphenyldiselenide and the formation of the known amidinate germanium selenide complex **LXXXIV**, thus providing a qualitative measure of the relative stabilities between these two complexes.[107]

Scheme 21 Oxidative addition of amidinate germanium(II) and tin(II) trimethylsilylamide complexes with diphenyldichalcogenides and further reactivity (E = S, Se).

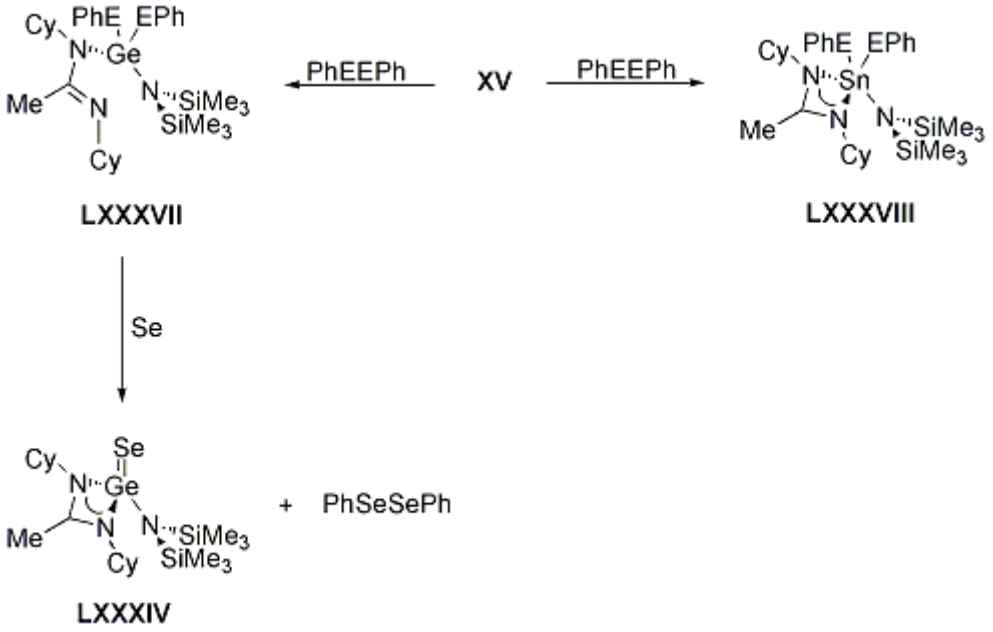

Another study presented the formation of the known tin alkoxide complexes, $[\{(RN)_2CPh\}Sn\{N(SiMe_3)_2\}OC(Ph)_3]$ ($R = N(SiMe_3)_2$, $N(SiMe_2Ph)_2$) (**LXXXIX**), via an alcohol exchange reaction between $[\{(RN)_2CPh\}Sn\{N(SiMe_3)_2\}N(SiMe_3)_2]$ ($R = N(SiMe_3)_2$, $N(SiMe_2Ph)_2$) **XV** and triphenylmethanol (eq 12).[50]

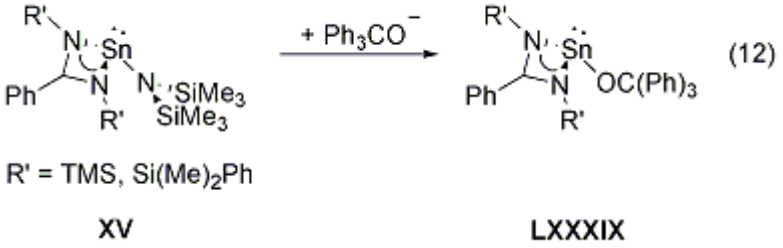

Interest in the reactive properties of β-diketiminate group 14 metal amides, [(BDI)M-NMe_2] (M = Ge, Sn, Pb) **XXX**, has received considerable attention in the past few years with the publication of numerous reactions involving alkynes,[87] fluorinating reagents,[77,89] hydrides,[88] ketones[87,88] and phosphides[82] (Scheme 22). Many of these studies were performed at the same time the research was being undertaken for this thesis.

Scheme 22 [(BDI)M-NMe_2] (Ar' = 2,6-*i*Pr_2-C_6H_3; M = Ge, Sn, Pb) reactivity patterns.

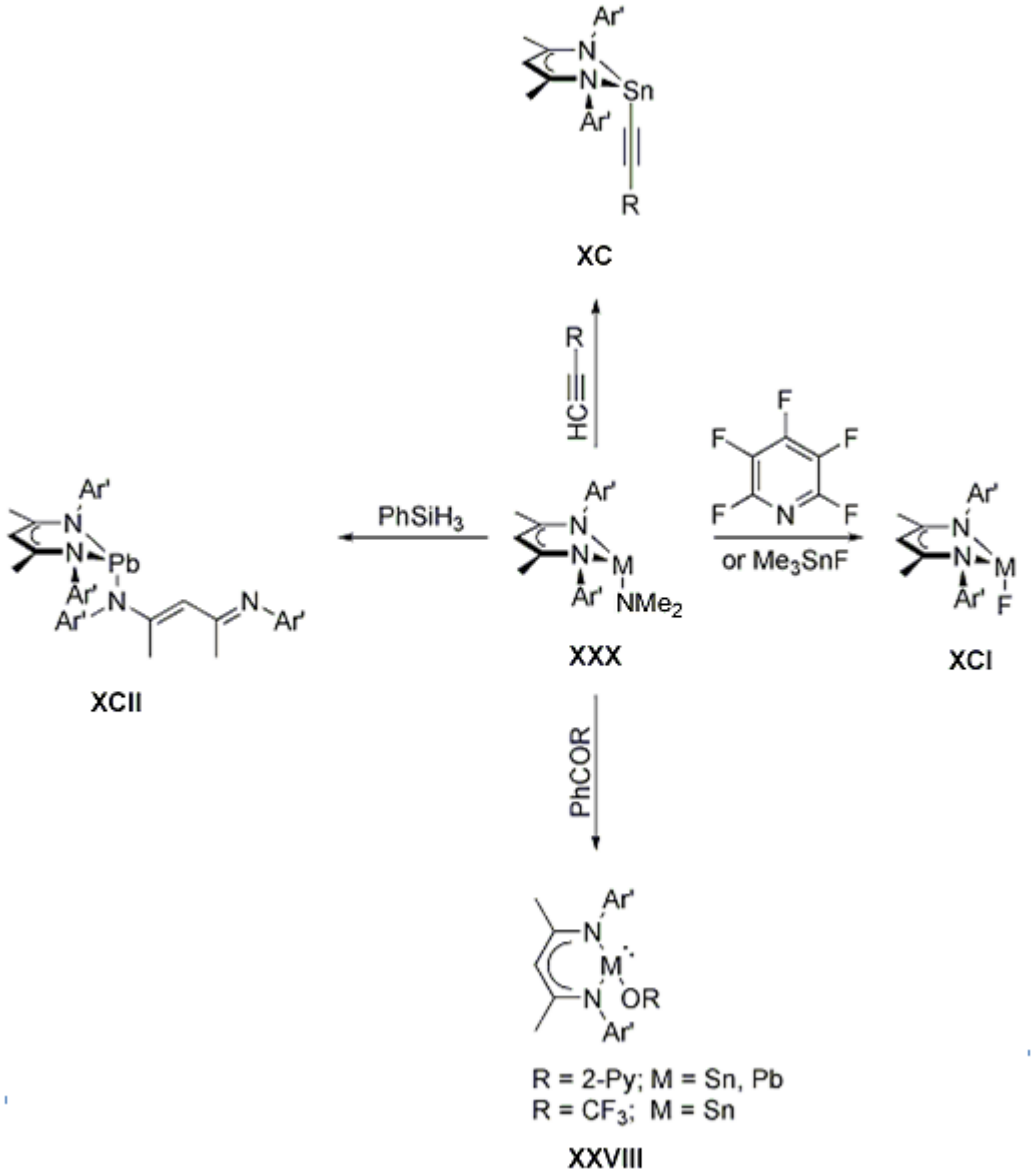

The reaction of the tin amides **XXX** with alkynes resulted in an acid-base reaction, deprotonation of the alkyne and the formation of a β-diketiminate tin alkynyl complex (**XC**).[87] Furthermore, tin and lead amides have been reacted with fluorinating reagents resulting in group 14 metal fluoride complexes (**XCI**).[77,89] Reactivity studies conducted by Roesky et al. into lead and tin dimethylamide showed the insertion of 2-benzoyl pyridine (for tin and lead) and 2,2,2-trifluoroacetophenone (for tin) into the M-N bond (M = Sn, Pb)

resulting in the lead or tin alkoxide **XXVIII**.[87,88] Similar to the outcome of another study published by Roesky et al.,[71] the formation of a bis-β-diketiminate lead complex (**XCII**) was reported as a result of a failed attempt to form a lead hydride, upon addition of phenyl silicon hydride (which was used as a reducing agent).[88]

In conclusion, previous research into the reactivity of late transition metal amide complexes showed these complexes exhibiting exceptional nucleophilic and basic reactivity. This is due to the polarised M-N bond so that reactivity can be observed at the M-N bond with organic electrophiles and weak acids. This reactivity is predicted to parallel that of the group 14 metal amide complexes, assuming that electronegative differences are the primary factor in determining reactivity. In contrast, the reactivity of late transition metal amide complexes should diverge from divalent group 14 metal amide complexes over their contrasting preferences for reductive elimination or oxidative addition. Group 14 metals such as germanium and tin are stable in both the divalent and tetravalent state. This explains why chalcogenation of group 14 metal amide complexes have been relatively well reported. In contrast, reductive elimination of late transition metals is favoured as low oxidation states are preferred. This divergence in chemical behaviour would hence reduce the validity of the comparison when studying the chalcogenation reactions of group 14 metal complexes. As such, Chapter 3 will focus on the chalcogenation reactions of group 14 metal complexes.

Most of the β-diketiminate group 14 metal amide chemistry discussed above was published during the course of this research. Although this was in some ways unfortunate and some reactions reported in this thesis were similar to that which was published, most of the studies undertaken for this thesis focused on the reactivity with simple electrophiles and heterocumulenes as a means of comparing the reactivity of group 14 metal amide complexes with their transition metal analogues. These studies also allow direct

comparison with previous research in the Fulton group on group 14 metal alkoxide complexes (see Chapter 1).

2.5. β-diketiminate Sn(II) and Pb(II) amide and anilide synthesis and characterisation

2.5.1. β-diketiminate stannylene amide and anilide synthesis and characterisation

The β-diketiminate tin(II) chloride, [(BDI)SnCl] **XXVII** (Ar' = 2,6-*i*Pr_2-C_6H_3), was synthesised via a slight modification of known literature procedures.[108] The lithiated β-diketiminate, [(BDI)Li] (**XCIV**), was generated *in situ* through the addition of *n*-butyllithium to an ether solution of [(BDI)H] (**XCIII**). This solution was then added to an ether suspension of $SnCl_2$ and the resulting solution was stirred for 16 hours at room temperature, resulting in the formation of [(BDI)SnCl] **XXVII** (Scheme 23).

Scheme 23 Synthesis of β-diketiminate tin chloride **XXVII** (Ar' = 2,6-*i*Pr_2-C_6H_3).

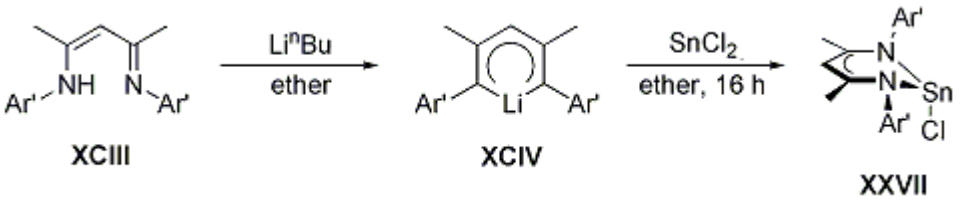

XCIII XCIV XXVII

Subsequent treatment of a toluene solution of the tin chloride complex **XXVII** with lithiated diisopropylamide, suspended in toluene, yielded β-diketiminate tin diisopropylamide, [(BDI)SnN(*i*$Pr)_2$] (**1**) (eq 13).[80]

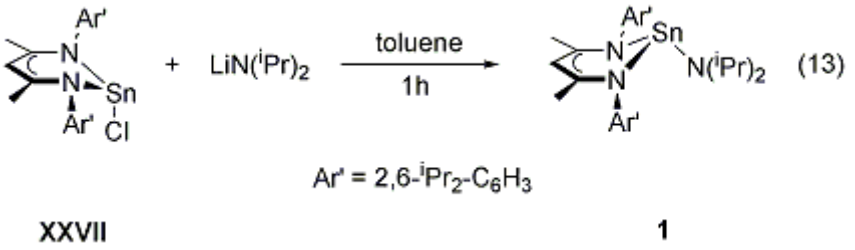

Analysis of the ^{1}H NMR spectrum for the tin diisopropylamide complex **1** shows five doublets and three apparent septets (with a ratio of 2:2:2), relating to the isopropyl groups on the β-diketiminate and amide ligands. Of these isopropyl groups, four doublets and two apparent septets correspond to those groups located on the β-diketiminate. The presence of two apparent septets and four doublets assigned to the isopropyl groups in the β-diketiminate is consistent with a three-coordinate tin centre in a non-planar environment, presumably adopting a pyramidal geometry similar to other divalent, three-coordinate tin complexes. If the β-diketiminate backbone is defined as the carbon and nitrogen atoms generating a metallacycle with Sn (or the NCCCN plane), the *N*-aryl groups on the β-diketiminate ligand are roughly perpendicular to this plane. If the tin centre possesses a planar geometry, all of the isopropyl groups on the *N*-aryl ligand would be chemically equivalent, and the ^{1}H NMR spectrum would contain one apparent septet, with an integration of four protons, and two doublets, each with an integration of twelve protons. But with a pyramidal tin centre, the *N*-aryl isopropyl groups on one side (or 'top') of the NCCCN plane have a different chemical environment to the *N*-aryl isopropyl groups on the opposite side (or 'bottom'). This configuration would give two apparent septets, integrating to two protons each, and four doublets, integrating to six protons each. Unfortunately, the conformation ('endo'/'exo') adopted by this complex can not be deduced from the ^{1}H NMR spectrum. The ^{119}Sn NMR spectrum displays a singlet at -224 ppm, which is lower than [(BDI)SnNMe$_2$] (-172 ppm)[85] and significantly lower than that of [(BDI)Sn{N(SiMe$_3$)$_2$}] (112 ppm)[55] (Table 3). This would be expected due to the greater

electron donating ability of the isopropyl groups on the amide relative to those with trimethylsilyl or methyl groups.[109]

Orange crystals of the tin diisopropylamide complex **1** suitable for X-ray structural analysis were grown overnight from a saturated toluene solution at -27°C (Figure 13). Selected bond lengths and angles are shown in Table 1. The X-ray structural data of the tin diisopropylamide complex **1** shows the three-coordinate tin complex adopting a distorted trigonal pyramidal geometry. The sum of the bond angles around the tin centre is calculated to be 285.1° and the degree of pyramidalization (DP) is equal to 83.2%. DP is a mathematical method of deducing how much the selected centre deviates from an ideal pyramidal geometry. It is calculated by subtracting the sum of the bond angles around the centre in question from 360, and then dividing this value by 0.9. In an idealised pyramidal geometry, the sum of the bond angles would by 270°, resulting in a DP of 100%. For complex **1**, the geometry at the tin centre has a high degree of pyramidalization (sum of the bond angles = 285.1°) and deviates from the perfect pyramidal geometry by 15.1°. The pyramidal metal centre, consistent with DP values, is postulated to be a result of a stereochemically active lone pair that occupies the fourth vertex of the tin centre.[110] As such, a void in the coordination sphere of the tin centre is observed in the solid-state structure. The tin diisopropylamide complex **1** adopts an 'exo' conformation, where the tin centre is displaced from the NCCCN plane (Sn-NCCCN plane) by 1.359 Å and the diisopropylamide ligand points away from the metallacycle. The amide nitrogen centre is displaced from the NCCCN plane (N3-NCCCN plane) by 0.564 Å, which is smaller than other published β-diketiminate tin complexes.[55,85] The sum of the bond angles around the amide nitrogen is 360.0° with a DP of 0, this shows the geometry at the nitrogen centre is not pyramidal but planar. The N2-Sn-N3 bond angle is 104.61(9)°, greater than [(BDI)SnNMe$_2$] (95.59(12)°)[55] and [(BDI)Sn{N(SiMe$_3$)$_2$}] (103.65(14)°).[85] The Sn-N3-C30 bond angle is 127.82(18)°, within the range of the bond angles of [(BDI)SnNMe$_2$] (119.9(4)° and 128.2(3)°). The Sn-N3 bond length is 2.070(2) Å, which is slightly longer

(but within experimental error) of the Sn-N3 bond in the [(BDI)SnNMe$_2$] complex (2.059(4) Å), but shorter than the bond in [(BDI)Sn{N(SiMe$_3$)$_2$}] (2.159(6) Å).

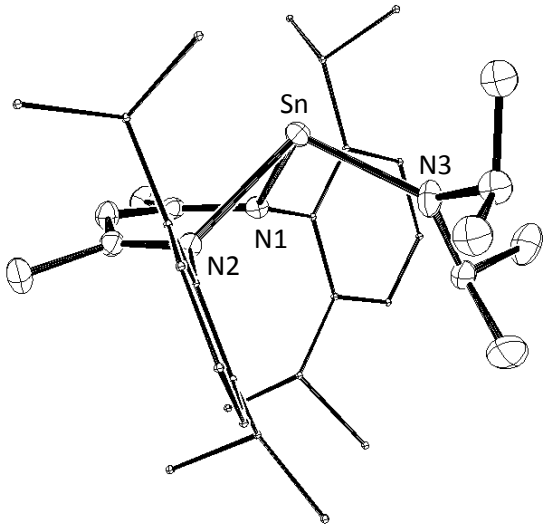

Figure 13 ORTEP diagram of [(BDI)SnN(*i*Pr)$_2$] **1**. Aryl groups are minimised and the hydrogen atoms are omitted for clarity. Thermal ellipsoids are shown at 30%.

Table 1 Selected bond lengths (Å) and angles (°) for [(BDI)SnNRR'] (RR' = iPr$_2$, H(2,6-iPr$_2$-C$_6$H$_3$), H(2-iPr-C$_6$H$_4$)).

[(BDI)SnNRR']			
	[-(iPr$_2$)], **1**	[-H(2,6-iPr$_2$-C$_6$H$_3$)], **2**	[-H(2-iPr-C$_6$H$_4$)], **3**
N3-Sn	2.070(2)	2.1000(17)	2.095(2)
N1-Sn	2.226(2)	2.2143(17)	2.198(2)
N2-Sn	2.290(2)	2.2250(17)	2.205(2)
N3-C30	1.459(4)	1.403(3)	1.396(3)
N3-C33	1.476(4)		
N1-Sn-N2	81.29(8)	83.72(6)	84.36(8)
N1-Sn-N3	99.28(8)	86.08(7)	87.57(9)
N2-Sn-N3	104.61(9)	94.17(7)	90.76(10)
Sn-N3-C30	127.82(18)	131.85(15)	130.38(19)
Sn-N3-C33	117.26(18)		
C30-N3-C33	114.9(2)		
Sum of angles (Sn)	285.1	264.0	262.7
DP (Sn)	83.2	106.7	108.1
Sum of angles (N3)	360.0		
DP (N3)	0.0		
Sn-NCCCN plane	1.359	0.721	0.803
NR$_2$-NCCCN plane	0.564	2.615	2.614

The β-diketiminate tin 2,6-diisopropylanilide complex, [(BDI)Sn(NH{2,6-iPr$_2$-C$_6$H$_3$})] (**2**), was generated by addition of lithiated 2,6-diisopropylanilide (suspended in toluene) to a toluene solution of the tin chloride complex **XXVII** (eq 14).[80]

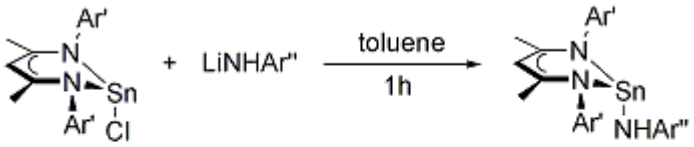

(14)

Ar' = 2,6-$^{i}Pr_2$-C_6H_3

XXVII

Ar'' = 2,6-$^{i}Pr_2$-C_6H_3, **2**
Ar'' = 2-^{i}Pr-C_6H_4, **3**

The ^{1}H NMR spectrum of the tin diisopropylanilide complex **2** shows five doublets, in a 6:12:6:6:6 ratio, and three apparent septets, two of which are overlapping, in a 2:2:2 ratio (Figure 14). The presence of two apparent septets and four doublets, which are assigned to the isopropyl groups in the β-diketiminate, are in line with a three-coordinate tin centre in a non-planar environment, with the same reasoning as stated for the tin diisopropylamide complex **1**. The third septet corresponds to the isopropyl methyl groups on the *N*-aryl ligand bound to tin. The single ^{119}Sn spectroscopy resonance for the tin diisopropylanilide complex **2** is shifted to -745 ppm. This is significantly lower in frequency than other β-diketiminate tin amides (Table 3),[55,85] due to the greater electron donating ability of the substituted aryl group of the anilide.

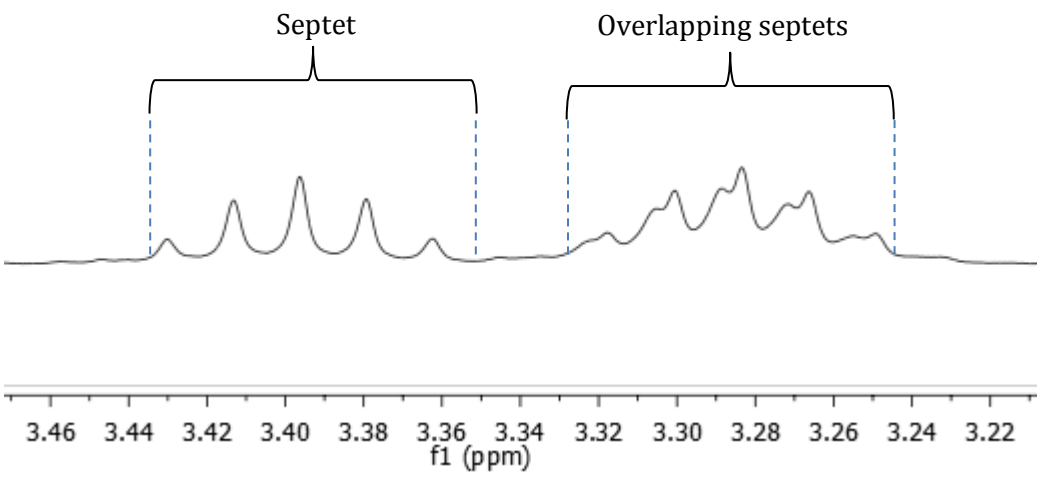

Figure 14 ^{1}H NMR spectrum between 3.47 and 3.21 ppm showing the apparent septets corresponding to three C*H*Me$_2$ environments in [(BDI)Sn(NH{2,6-*i*Pr$_2$-C$_6$H$_3$})] **2**.

Yellow crystals of tin diisopropylanilide complex **2** were grown in a saturated toluene solution at -27°C (Figure 15). X-ray diffraction data from these crystals show the tin diisopropylanilide complex **2** exhibits a distorted trigonal pyramidal geometry at tin with a sum of the bond angles of 264.0° and DP of 106.7%. The geometry, the sum of the bond angles and DP are further evidence supporting the presence of a stereochemically active lone pair for three-coordinate tin amide complexes. The significant differences in the spatial arrangement of the atoms within the distorted trigonal pyramidal geometry, the sum of the bond angles and DP *between* the tin diisopropylamide complex **1** and the tin diisopropylanilide complex **2** could be a result of the different conformations adopted by the complexes. For instance, the isopropyl groups bound to the *N*-amide nitrogen in the tin diisopropylamide complex **1** could potentially interfere with the isopropyl groups on the β-diketiminate ligand such that the complex exhibits an 'exo' conformation. In contrast, the anilide complex **2** has less steric bulk at the *N*-aryl nitrogen as the aryl moiety is planar, thus reducing the space the ligand occupies. This planarity reduces potential steric interaction with the isopropyl groups on β-diketiminate such that the 'endo' conformation can be adopted. Other β-diketiminate tin amides that adopt the 'endo' conformation are

[(BDI)SnNMe$_2$][85] and [(BDI)Sn{{N(SiMe$_3$)$_2$}].[55] The displacement of the tin atom from the NCCCN plane in the tin diisopropylamide complex **1** is larger than the displacement of the tin atom from the NCCCN plane in the tin diisopropylanilide complex **2** at 0.721 Å. In addition, the amide nitrogen is displaced from the NCCCN plane in the tin diisopropylanilide complex **2** by 2.615 Å. The N2-Sn-N3 bond angle is 94.17(7)°, smaller than the N2-Sn-N3 bond angles of tin diisopropylamide **1** (104.61(9)°). The Sn-N3-C30 bond angle is 131.85(15)°, significantly obtuse compared to the idealised bond angles for a pyramidal geometry of 90° (and larger than the corresponding angles in the tin diisopropylamide complex **1** (127.82(18)°)). The Sn-N3 bond length of the tin diisopropylanilide complex **2** is 2.1000(17) Å, this bond length is slightly longer than that of the tin diisopropylamide complex **1**, but shorter than other tin anilide complexes, such as [{(MA-NH)Sn-(μ-HN-MA)$_2$Li.2THF}] (MA = 2-MeO-C$_6$H$_4$) (2.118 Å)[15] and [Sn$_2${N(H)Ar}$_4$] (Ar = 2,6-*i*Pr$_2$-C$_6$H$_3$) (2.117(3) Å and 2.120(4) Å).[111]

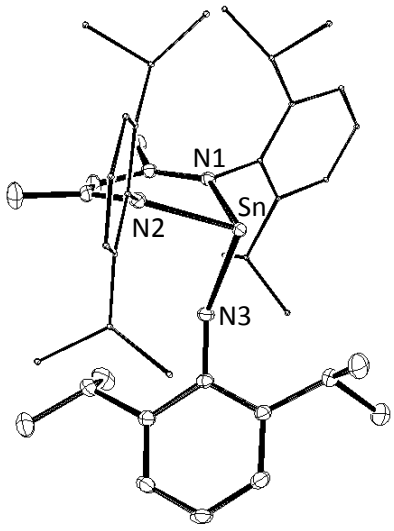

Figure 15 ORTEP diagram of [(BDI)Sn(NH{2,6-*i*Pr$_2$-C$_6$H$_3$})] **2**. Aryl groups situated on the BDI ligand are minimised and the hydrogen atoms are omitted for clarity. Thermal ellipsoids are shown at 30%.

The β-diketiminate tin 2-isopropylanilide complex (**3**) was formed via the addition of a toluene solution of lithiated 2-isopropylanilide to a toluene solution of tin chloride **XXVII** (eq 14).

The ^{1}H NMR spectrum for the tin isopropylanilide complex **3** shows three apparent septets, in a 2:2:1 ratio, and five doublets, in a 6:6:6:6:6 ratio. These resonances correspond to the isopropyl groups in the complex. Two of the three apparent septets (in a 2:2 ratio) and four of the doublets are related to the isopropyl groups on the β-diketiminate ligand, which is consistent with a non-planar environment around the tin atom. The ^{119}Sn spectrum shows a single resonance at -239 ppm, this is significantly higher in frequency than the tin diisopropylanilide complex **2**.

Yellow crystals of the tin isopropylanilide complex **3** suitable for an X-ray diffraction study were grown in a saturated toluene solution at -27°C (Figure 16). X-ray diffraction data show many similarities between the more substituted tin diisopropylanilide complex **2** with the less substituted tin isopropylanilide complex **3**, for instance, both complexes exhibit a pyramidal geometry at tin with similar values for the sum of the bond angles and hence DP. The tin isopropylanilide complex **3** has a value for the sum of the bond angles calculated at 262.7° and a DP of 108.1%, whereas the more substituted tin diisopropylanilide complex **2** has marginally larger values of 264.0° and 106.7% (respectively). Like the tin diisopropylanilide **2**, the less substituted tin isopropylanilide complex **3** adopts an 'endo' conformation. The displacement of the tin atom from the NCCCN plane for the tin isopropylanilide complex **3** is 0.803 Å, which is larger than the tin diisopropylanilide complex **2** (0.721 Å). Furthermore, the tin isopropylanilide complex **3** has a slightly lower displacement of the amide nitrogen atom from the NCCCN plane, at 2.614 Å, relative to the tin diisopropylanilide complex **2** (2.615 Å). The N2-Sn-N3 bond angle is 90.76(10)° (smaller than the tin diisopropylanilide **2** (94.17(7)°)) and the Sn-N3-C30 bond angle is 130.38(19)°, which is slightly smaller than

the tin diisopropylanilide **2** (131.85(15)°). The Sn-N3 bond length is slightly shorter than the tin diisopropylanilide complex **2** at 2.095(2) Å, but within experimental error of each other.

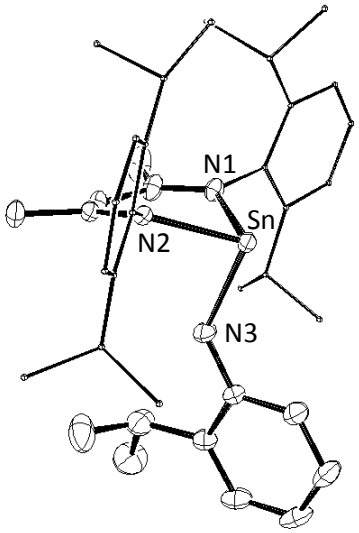

Figure 16 ORTEP diagram of [(BDI)Sn(NH{2-*i*Pr-C_6H_4})] **3**. Aryl groups situated on the BDI ligand are minimised and the hydrogen atoms are omitted for clarity. Thermal ellipsoids are shown at 30%.

2.5.2. β-diketiminate plumbylene amide and anilide synthesis and characterisation

Addition of *n*-butyllithium to a THF solution of [(BDI)H] **XCIII** produced the lithiated β-diketiminate complex, [(BDI)Li] **XCIV**. The $PbCl_2$ was suspended in a THF solution, pipetted into the lithiated β-diketiminate **XCIV** and the solution was stirred in darkness, for 16 hours at room temperature, resulting in the formation of [(BDI)PbCl] **XXVII** (Scheme 24).[72]

Scheme 24 Synthesis of β-diketiminate lead chloride **XXVII** (Ar' = 2,6-*i*Pr_2-C_6H_3).

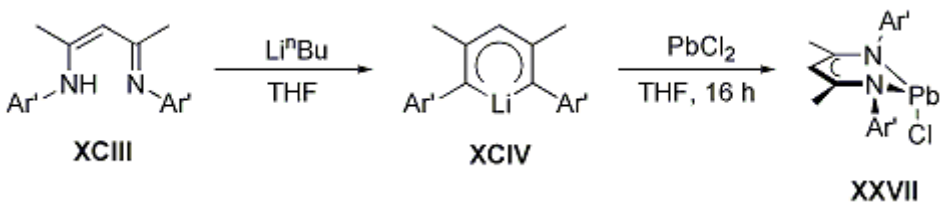

XCIII **XCIV** **XXVII**

Treatment of a toluene solution of the lead chloride complex **XXVII** with lithiated diisopropylamide afforded β-diketiminate lead diisopropylamide, [(BDI)PbN(*i*Pr)$_2$] **4** (eq 15).

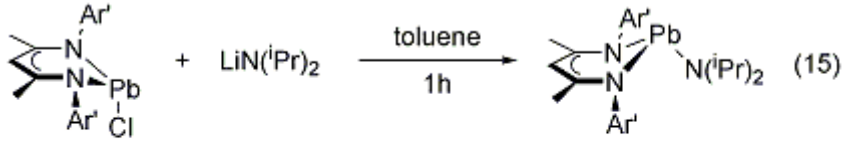

Ar' = 2,6-^{i}Pr$_2$-C_6H_3

XXVII **4**

The ^{1}H NMR spectrum of the lead amide complex **4** shows five doublets, in a 6:6:6:6:12 ratio, and three apparent septets, in a 2:2:2 ratio, corresponding to the isopropyl groups on the β-diketiminate and amide ligands. Of these resonances, four of the doublets and two of the apparent septets are related to the β-diketiminate ligand, and are caused by the chemically inequivalent environments of the isopropyl groups (as discussed for the tin analogue **1**) and are hence consistent with the lead centre being in a non-planar environment. There is a single resonance in the ^{207}Pb NMR spectrum at 2183 ppm, higher in frequency than that of [(BDI)Pb{N(SiMe$_3$)$_2$}] (1824 ppm)[72] and [(BDI)PbNMe$_2$] (1674 ppm),[88] in contrast to the trend observed for the analogous tin complexes (Table 3).

Orange crystals of the lead amide complex **4** suitable for an X-ray diffraction study were grown at -27°C from a saturated toluene solution (Figure 17). Selected bond lengths and angles are shown in Table 2. The lead diisopropylamide complex **4** exhibits a distorted trigonal pyramidal geometry around the three-coordinate lead centre. The lead is displaced from the NCCCN plane by 1.436 Å, which is greater than the analogous tin diisopropylamide complex **1**. The sum of the bond angles around the lead centre is 281.4°, resulting in a DP of 87.3%, these values support the presence of a stereochemically active lone pair. The amide nitrogen atom is displaced from the NCCCN plane by 0.548 Å and the sum of the bond angles and DP around the amide nitrogen are 359.4° and 0.7%, similar to the tin diisopropylamide complex **1**. Overall, the geometry, deviation in planarity of the metal centre from the NCCCN plane, sum of the bond angles and DP are very similar to that of the analogous tin diisopropylamide complex **1**. The N2-Pb-N3 bond angle is 98.93(9)°, larger than the same bond angle in [(BDI)PbNMe$_2$] (94.3(3)°)[88] but smaller than that of [(BDI)Pb{N(SiMe$_3$)$_2$}] (104.91(10)°).[72] The Pb-N3-C30 bond angle in the lead diisopropylamide complex **4** is 115.2(2)°, which is smaller than the analogous angles in [(BDI)PbNMe$_2$] (127.5(8)° and 119.9(10)°). The Pb-N3 bond length is 2.161(3) Å, which is longer than the Pb-N (amide) bond in [(BDI)PbNMe$_2$] (2.155(10) Å) (but within experimental error of each other) and shorter than the Pb-N3 bond in [(BDI)Pb{N(SiMe$_3$)$_2$}] (2.281(3) Å). The same trend was observed for the series of analogous tin complexes (Table 1).

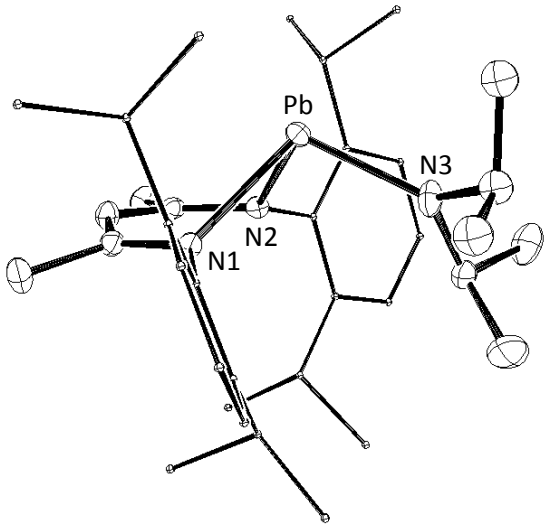

Figure 17 ORTEP diagram of [(BDI)PbN(*i*Pr)$_2$] **4**. Aryl groups are minimised and the hydrogen atoms are omitted for clarity. Thermal ellipsoids are shown at 30%.

Table 2 Selected bond lengths (Å) and angles (°) for [(BDI)PbNRR'] (RR' = *i*Pr$_2$ **4**, H(2,6-*i*Pr$_2$-C$_6$H$_3$) **5**, H(2-*i*Pr-C$_6$H$_4$) **6**, H(C$_6$H$_5$) **7**).

[(BDI)PbNRR']				
	-(*i*Pr$_2$), **4**	-H{2,6-*i*Pr$_2$-C$_6$H$_3$}, **5**	-H{2-*i*Pr-C$_6$H$_4$}, **6**	-NH{C$_6$H$_5$}, **7**
N3-Pb	2.161(3)	2.207(2)	2.202(5)	2.219(3)
N1-Pb	2.392(2)	2.319(2)	2.316(4)	2.340(2)
N2-Pb	2.333(2)	2.328(2)	2.347(4)	2.355(2)
N3-C30	1.477(4)	1.392(3)	1.384(7)	1.376(4)
N3-C33	1.456(4)			
N1-Pb-N2	78.97(8)	81.35(7)	81.00(15)	80.46(8)
N1-Pb-N3	103.44(10)	84.37(8)	83.08(17)	91.64(9)
N2-Pb-N3	98.93(9)	93.35(8)	90.66(18)	89.31(9)
Pb-N3-C30	115.2(2)	130.16(18)	127.1(4)	124.9(2)
Pb-N3-C33	127.2(2)			
C30-N3-C33	116.9(3)			
Sum of angles (Pb)	281.4	259.1	254.7	261.4
DP (Pb)	87.3	112.1	117.0	109.5
Sum of angles (N3)	359.4			
DP (N3)	0.7			
Pb-NCCCN plane	1.436	0.763	0.891	0.357
NR$_2$-NCCCN plane	0.548	2.725	2.714	2.537

Three separate β-diketiminate lead anilide complexes were produced in this study. The first of such complexes was β-diketiminate lead 2,6-diisopropylanilide (**5**). This complex was made through the addition of lithiated 2,6-diisopropylanilide, suspended in toluene, to a toluene solution of the lead chloride **XXVII** (eq 16).

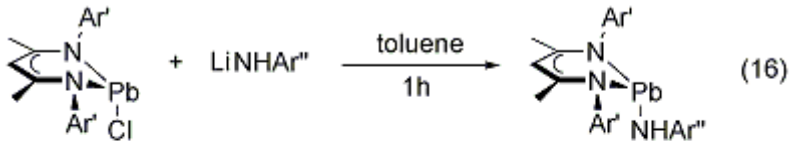

(16)

Ar' = 2,6-$^{i}Pr_2$-C_6H_3

XXVII

Ar'' = 2,6-$^{i}Pr_2$-C_6H_3, **5**
Ar'' = 2-^{i}Pr-C_6H_4, **6**
Ar'' = C_6H_5, **7**

Analysis of the ^{1}H NMR spectrum of the lead diisopropylanilide complex **5** reveals the presence of three apparent septets, in a 2:2:2 ratio, and five doublets, in a 6:12:6:6:6 ratio, which correspond to all the isopropyl groups. The presence of two apparent septets and four doublets, assigned to the isopropyl groups in the β-diketiminate, support the adoption of a non-planar environment at the three-coordinate lead centre. The lead diisopropylanilide complex **5** has a single ^{207}Pb resonance at 1500 ppm. This resonance is in the same range, but at the lower frequency end of the scale, to other β-diketiminate lead amide complexes (Table 3).[72,88]

Yellow crystals of lead diisopropylanilide **5** suitable for X-ray diffraction analysis were successfully grown in a saturated toluene solution at -27°C (Figure 18). A distorted trigonal pyramidal geometry at lead is observed, with the sum of the bond angles calculated to 259.1° and a DP of 112.1%. These values are slightly smaller than the analogous tin diisopropylanilide complex **2**, potentially a result of the relativistic effect. The effect of relativity increases upon descending the periodic table due to the more

positive nuclear charge increasing nuclear attraction (and causing contraction) of the outer s, p and d orbitals, in the order s>p>d. Increasing penetration of the orbitals increases the velocity of the electrons residing in these respective orbitals, leading to a relativistic increase in these electrons' masses and binding energies. As the electrons in the s orbital are more affected than those in the p and d orbitals, the electrons in the s orbital are rendered relatively inert, reducing hybridisation and resulting in a lone pair with greater s character. As stated, this effect is greater for the increasingly heavier elements, hence why the electrons in the s orbital of a lead centre are more affected than those electrons in the s orbital of a tin centre. As such, hybridisation of the outer electrons in lead is comparatively lower, leading to a lone pair with more s character, which is more strongly repelling. This strongly repelling force causes the atoms around the lead centre to be pushed closer together, thus making the bond angles around the lead centre smaller than those of the lighter congeners. The lead atom is displaced from the NCCCN plane by 0.763 Å, which is greater than that of the analogous tin diisopropylanilide complex **2** (0.721 Å). The larger displacement of the lead atom from the NCCCN plane could be caused by the larger atomic radii of the lead(II) atom (1.20 Å)[112] compared to that of the tin(II) atom, at 1.02 Å.[112] The (amide) nitrogen is displaced from the NCCCN plane by 2.725 Å, similar to the analogous tin complex **2** (2.615 Å). The N2-Pb-N3 bond angle is 93.35(8)°, which is smaller than the lead diisopropylamide **4** (98.93(9)°). The Pb-N3-C30 bond angle is 130.16(18)°, similar to the tin diisopropylanilide complex **2** (131.85(2)°). The Pb-N3 bond length is 2.207(2) Å, shorter than the analogous Pb-N bond of the lead diisopropylamide complex **4**, as well as $[Pb_2(NAr)_2]$,[113] but within experimental error of three of the four Pb-N bonds in the $[Pb(NCy)]_2$ complex.[111]

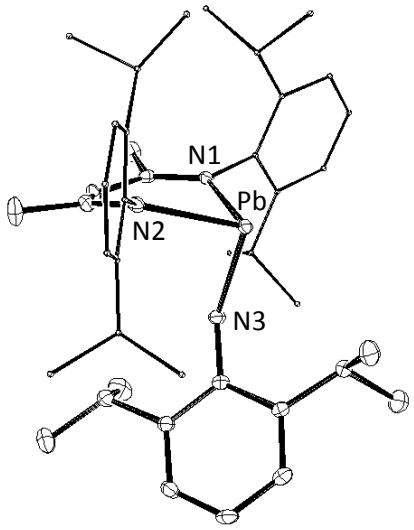

Figure 18 ORTEP diagram of [(BDI)Pb(NH{2,6-*i*Pr$_2$-C$_6$H$_3$})] **5**. Aryl groups situated on the BDI ligand are minimised and the hydrogen atoms are omitted for clarity. Thermal ellipsoids are shown at 30%.

The lead isopropylanilide (**6**) was formed through the addition of lithiated 2-isopropylanilide, suspended in toluene, to a toluene solution of the lead chloride **XXVII** (eq 16).

The ^{1}H NMR spectrum of the lead isopropylanilide complex **6** has three apparent septets, in a 1:2:2 ratio, and five doublets for the isopropyl groups in the complex. Changes to the ratio of the apparent septets, relative to the previously mentioned lead amide complexes **4** and **5**, is a result of the substitution of an isopropyl group to a hydrogen at the 6-position on the anilide so that one isopropyl group is present instead of two. In addition to the apparent septets, four of the doublets relate to the β-diketiminate ligand, thus showing the adoption of a non-planar environment around the metal centre, similar to other β-diketiminate lead amide complexes (**4** and **5**) reported in this thesis and other β-diketiminate lead amide complexes, such as [(BDI)PbNMe$_2$][88] or [(BDI)Pb{N(SiMe$_3$)$_2$}].[72]

The ^{207}Pb spectrum has a resonance at 1379 ppm, which is lower in frequency than that of the lead diisopropylanilide complex **5**.

Yellow crystals of the lead isopropylanilide complex **6** suitable for X-ray diffraction analysis were grown in a saturated toluene solution at -27°C (Figure 19). Similar to other lead amide complexes mentioned, the complex exhibits distorted trigonal pyramidal geometry at lead due to the presence of a stereochemically active lone pair. The sum of the bond angles is 254.7°, resulting in a DP of 117.0%. The lead atom is displaced from the NCCCN plane by 0.891 Å, this is a similar value to the lead diisopropylanilide complex **5** (0.763 Å). The lead isopropylanilide complex **6** adopts an 'endo' conformation similar to previously mentioned tin/lead anilides. The displacement of the amide nitrogen from the NCCCN plane is 2.714 Å, slightly lower than the lead diisopropylanilide **5** (2.725 Å). The N2-Pb-N3 bond angle is 90.66(18)°, which is smaller than the lead diisopropylanilide **5** with an angle of 93.35(8)°. The Pb-N3-C30 bond angle is 127.1(4)°, this is smaller than the more substituted lead diisopropylanilide complex **5** (130.16(18)°). The Pb-N3 bond length for the lead isopropylanilide complex **6** is 2.202(5) Å, which is within experimental error of the Pb-N3 bond length in the lead diisopropylanilide complex **5** (2.207(2) Å).

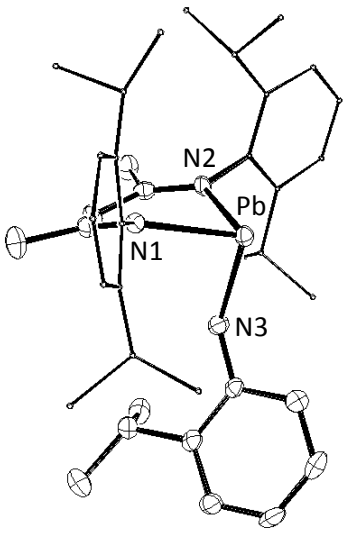

Figure 19 ORTEP diagram of [(BDI)Pb(NH{2-*i*Pr-C_6H_4})] **6**. Aryl groups situated on the BDI ligand are minimised and the hydrogen atoms are omitted for clarity. Thermal ellipsoids are shown at 30%.

The β-diketiminate lead anilide complex (**7**) was formed through the addition of lithiated anilide, suspended in a toluene solution, to a toluene solution of the lead chloride **XXVII** (eq 16). This reaction was performed under near-dark conditions by wrapping the reaction vessel in foil.

Analysis of the ^{1}H NMR spectrum of the lead anilide complex **7** shows similar chemical shifts to that of the previous lead anilide complexes, **5** and **6**. Any differences between spectra are related to the differences in the substituents at the 2- and 6-positions on the anilide ligand. The spectrum shows two apparent septets, in a 2:2 ratio, and four doublets of equal intensity, which indicates a non-planar environment around lead, similar to the lead anilide complexes, **5** and **6**. There is a ^{207}Pb resonance at 1370 ppm, which is lower in frequency than the comparable anilide complexes **5** and **6** (1500 ppm and 1379 ppm, respectively).

A saturated solution of the lead anilide complex **7** formed yellow crystals after storing at -27°C (Figure 20). X-ray diffraction analysis of these crystals show the complex adopting a distorted trigonal pyramidal geometry at lead. The sum of the bond angles is 261.4° with a DP of 109.5%, which is the highest sum of the bond angles and lowest DP at the lead centre relative to all the lead anilide complexes mentioned. There is no obvious trend between the substitution on the anilides and the sum of the bond angles and the DP at the lead centre, suggesting these values are influenced by an interplay of electronic (i.e. electron donating ability of the substituents at the 2- and 6-position) and steric factors (i.e. the greater steric bulk associated with the isopropyl groups relative to the hydrogen groups). The lead atom in the lead anilide complex **7** is displaced from the NCCCN plane by 0.357 Å. The lead anilide complex **7** has no isopropyl groups at the 2- and 6-position, whereas the previous two lead anilide complexes, **5** and **6**, have one or two isopropyl group at these positions, and as a result have similar, higher values for the deviation from planarity of their lead centre suggesting these substitutions are of some importance when considering the extent of deviation from the NCCCN plane. This observation also explains the trend in values for the displacement of the amide nitrogen from the NCCCN plane, where the lead anilide **7** was found to have the lowest displacement value out of all the lead anilides at 2.537 Å. The differences in the steric effects caused by the substituents on the anilide also affect the bond angle around the amide nitrogen (Pb-N3-C30), which is 124.9(2)°, this is the smallest value for all the lead anilide complexes. The bond angle at N2-Pb-N3 is 89.31(9)°, which is lower than the N2-Pb-N3 bond angle of the lead isopropylanilide complex **6** and lower than the diisopropylanilide complex **5**. The bond length for Pb-N3 in the lead anilide complex **7** is 2.219(3) Å, the longest bond length of the lead anilide complexes, including **5** and **6**, but within experimental error for the Pb-N3 bond length in both of these latter complexes.

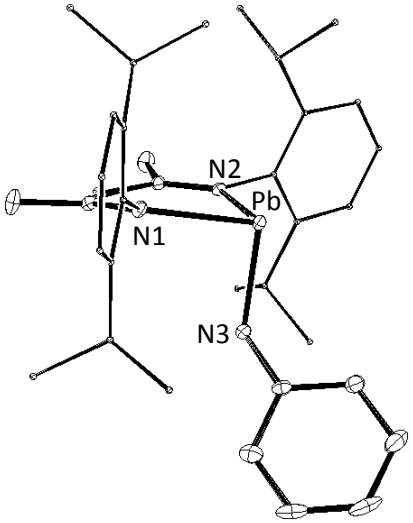

Figure 20 ORTEP diagram of [(BDI)Pb(NH{C_6H_5})] **7**. Aryl groups situated on the BDI ligand are minimised and the hydrogen atoms are omitted for clarity. Thermal ellipsoids are shown at 30%.

Table 3 List of chemical shifts for various complexes of [(BDI)MNRR'] (M = Sn, Pb; RR' = Me_2,[85,88] $(SiMe_3)_2$,[55,76] *i*Pr_2, H(2,6-*i*Pr_2-C_6H_3), H(2-*i*Pr-C_6H_4), H(C_6H_5)) for the ^{119}Sn and ^{207}Pb nuclei.

RR'	^{119}Sn	^{207}Pb
NMe_2	-172	1674
$N(SiMe_3)_2$	112	1824
N(*i*Pr)$_2$	-224	2183
NH(2,6-*i*Pr_2-C_6H_3)	-745	1500
NH(2-*i*Pr-C_6H_4)	-239	1379
NH(C_6H_5)		1370

2.5.3. Summary of stannylene and plumbylene amide complexes

A series of tin and lead amide complexes, [(BDI)MNRR'] (M = Sn and RR' = *i*Pr$_2$ (**1**), H(2,6-*i*Pr$_2$-C$_6$H$_3$) (**2**), H(2-*i*Pr-C$_6$H$_4$) (**3**), or M = Pb and RR' = *i*Pr$_2$ (**4**), H(2,6-*i*Pr$_2$-C$_6$H$_3$) (**5**), H(2-*i*Pr-C$_6$H$_4$) (**6**), H(C$_6$H$_5$) (**7**)), were generated, which are air-sensitive and isolable by crystallisation. All compounds were characterised by multinuclear NMR spectroscopy, IR spectroscopy, elemental analysis and X-ray crystallography. Conclusions drawn from these data show all the complexes adopting a distorted trigonal pyramidal geometry at the metal centre due to the presence of a stereochemically active lone pair occupying the fourth vertex, this influences the sum of the bond angles and therefore the DP. Differences between the tin and lead atoms in analogous complexes have been attributed to the difference in atomic radii between the tin and lead. The 'endo' conformation is observed whenever a ligand can insert in-between the two *N*-aryl groups on the β-diketiminate ligand, however, steric constraints lead to the metal diisopropylamides, **1** and **4**, exhibiting the 'exo' conformation. The conformation influences the sum of the bond angles and DP at the metal centre and the displacement of the metal and amide nitrogen from the NCCCN plane. However, the effect of conformation on the N2-M-N3 and M-N3-C30 bond angles is not conclusive between the 'endo' structures and the one 'exo' structure (Tables 1 and 2). The 'exo' conformation adopted by the tin and lead diisopropylamide complexes, **1** and **4**, have a larger sum of the bond angles and lower DP around the metal centre, as well as larger N2-M-N3 and smaller M-N3-C30 bond angles. There is greater displacement of the metal from the NCCCN plane and lower nitrogen (amide) displacement from the NCCCN plane relative to the tin and lead anilide complexes, **2** to **3** and **5** to **7**, which exhibit an 'endo' conformation. There is a correlation between the displacement of the amide nitrogen from the NCCCN plane and steric bulk on the anilide, with less displacement of the nitrogen upon decreasing steric bulk. There are also smaller bond angles for N2-M-N3 and M-N3-C30 with decreasing steric bulk. There also appears to be some correlation between lower displacement values of the metal centre from the NCCCN plane and

decreasing steric bulk on the anilide. In contrast, there is no clear trend between differences in the steric bulk between the metal anilide complexes and the sum of the bond angles and DP at the metal centre and the M-N bond lengths.

2.6. Reactivity studies on β-diketiminate Sn(II) and Pb(II) amide and anilide complexes

The reactivity of tin and lead amide and anilide complexes towards aliphatic and unsaturated electrophiles and carboacids was investigated in order to compare and contrast their reactivity with transition metal analogues.[94,114]

2.6.1. Reactivity of β-diketiminate stannylene amide and anilide complexes towards aliphatic electrophiles

The nucleophilicity of the tin amide and anilide complexes was investigated using the aliphatic electrophiles, methyl triflate and methyl iodide. These electrophiles led to divergent reactivity when reacted with the tin diisopropylamide **1** and tin diisopropylanilide **2** complexes.

Addition of the stronger electrophile, methyl triflate, to the β-diketiminate tin diisopropylamide **1** resulted in a complex mixture of products at room temperature. In contrast, addition of methyl triflate to β-diketiminate tin 2,6-diisopropylanilide **2** at room temperature resulted in a 100% conversion to the known tin triflate complex, [(BDI)SnOTf] **XXXIII**,[108] after 1 hour, as confirmed by ^{1}H NMR and ^{119}Sn NMR spectroscopy (eq 17).

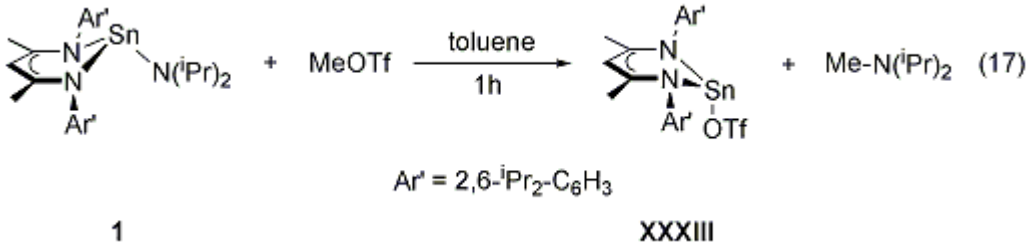

Addition of the weaker electrophile, methyl iodide, to the β-diketiminate tin diisopropylamide **1** afforded a complex mixture of products after 24 hours at room temperature. In contrast, there was no reaction upon the addition of methyl iodide to β-diketiminate tin 2,6-diisopropylanilide **2**, even upon heating to 75°C for several days.

2.6.2. Reactivity of β-diketiminate stannylene amide and anilide towards unsaturated electrophiles

The reactivity of tin diisopropylamide **1** and tin diisopropylanilide **2** was investigated using the unsaturated electrophiles, benzophenone, benzaldehyde, carbon dioxide and phenyl isocyanate.

Addition of benzophenone to both β-diketiminate tin complexes, **1** and **2**, did not result in a reaction, even under forcing conditions. Addition of the more reactive benzaldehyde to either **1** or **2** resulted in a complex mixture of products.

In contrast, β-diketiminate tin diisopropylamide **1** and β-diketiminate tin 2,6-diisopropylanilide **2** reacted upon exposure with 1.30 bar or 1.14 bar (respectively) of carbon dioxide (eq 18). Specifically, addition of carbon dioxide to β-diketiminate tin diisopropylamide **1** yielded the corresponding β-diketiminate tin carbamate (**8**) after 3 days at room temperature (eq 18).[80]

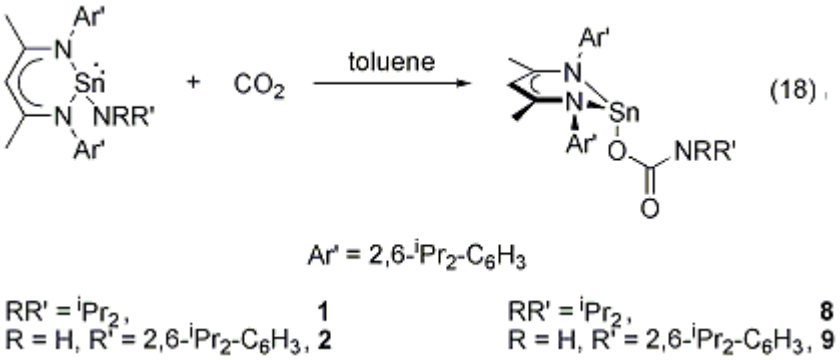

The formation of the tin carbamate complex **8** was confirmed via ^{13}C NMR spectroscopy, where a resonance at 161.8 ppm, indicative of a carbamate carbon, is observed. The ^{119}Sn NMR spectrum has a singlet shifted to a lower frequency (-394 ppm) relative to the initial tin diisopropylamide complex **1** (-224 ppm). The functionality was further confirmed through IR spectroscopy, where new stretches at 1595, 1575 and 1524 cm^{-1} (nujol) are observed. However, conclusive assignment of the IR stretching frequencies is prevented due to overlap of the NCO_2 moiety stretching frequencies with those of the β-diketiminate ligand.

The tin carbamate **8** was successfully crystallised from a saturated toluene solution at -27°C as colourless crystals (Figure 21). Selected bond lengths and angles are reported in Table 4. The tin carbamate complex **8** exhibits a distorted trigonal pyramidal geometry at tin, similar to other β-diketiminate tin complexes. An 'endo' conformation is adopted, where the tin centre is displaced from the NCCCN plane by 0.546 Å. The Sn-O bond is approximately 90° to the NCCCN plane. The sum of the bond angles is 259.6°, the lowest value for all tin complexes under investigation, and the DP is 111.5%. The Sn-O1 bond length is 2.134(6) Å, longer than Gibson's [(BDI)SnO*i*Pr] complex (2.000(5) Å).[73] The Sn···O2 length is 2.839 Å, this value is smaller than the sum of the van der Waals radii for tin and oxygen (3.69 Å),[80] thus suggesting the possibility of an interaction between the tin centre and the oxygen.

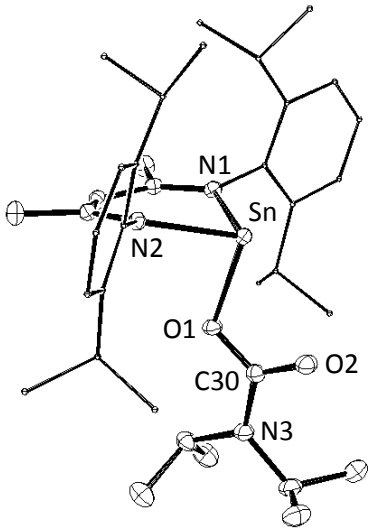

Figure 21 ORTEP diagram of [(BDI)Sn{OC(O)N(*i*Pr$_2$)}] **8**. Aryl groups situated on the BDI ligand are minimised and the hydrogen atoms are omitted for clarity. Thermal ellipsoids are shown at 30%

Table 4 Selected bond lengths (Å) and angles (°) for [(BDI)Sn{OC(O)N(*i*Pr$_2$)}].

[(BDI)Sn{OC(O)N(*i*Pr$_2$)}], **8**			
O1-Sn	2.134(6)	Sn-O1-C30	109.65(15)
O2-Sn	2.839	O1-C30-O2	121.7(2)
N1-Sn	2.205(1)	O1-C30-N3	116.6(2)
N2-Sn	2.201(2)	O2-C30-N3	121.7(2)
O1-C30	1.304(3)	C30-N3-C31	122.02(2)
C30-O2	1.238(3)	C30-N3-C34	120.2(2)
C30-N3	1.366(3)	C31-N3-C34	117.8(2)
N3-C31	1.474(3)	Sum of angles (Sn)	259.6
N3-C34	1.481(3)	DP	111.5
N1-Sn-N2	84.78(7)	Sn-NCCCN plane	0.546
N1-Sn-O1	87.43(7)	O-NCCCN plane	2.514
N2-Sn-O1	87.41(7)		

A toluene solution of the β-diketiminate tin 2,6-diisopropylanilide complex **2** treated with one equivalent of carbon dioxide resulted in the formation of a β-diketiminate tin carbamate complex (**9**) after 4 hours at room temperature (eq 18).

In contrast to 100% conversion, as observed in the formation of **8**, ^{1}H NMR spectroscopy shows only 90% of the tin diisopropylanilide **2** is converted to **9**, with a second minor product, which could be the other isomer of the complex. The ^{13}C NMR spectrum of **9** has a resonance at 161.6 ppm, which is indicative of a carbamate carbon atom. There is a resonance in the ^{119}Sn NMR spectrum at -398 ppm, located at a significantly higher frequency than that of the tin diisopropylanilide precursor complex **2**, but similar to that of the tin carbamate complex **8**. In addition, the IR spectrum shows three stretches at 1554, 1526 and 1517 cm^{-1} (nujol) which correlate to the carbamate

moiety, however, overlap of the NCO_2 moiety stretching frequencies with the β-diketiminate ligand prevent conclusive assignment at other frequencies. Despite repeated attempts, the growth of crystals suitable for X-ray diffraction was unsuccessful.

Addition of phenyl isocyanate to a toluene solution of the β-diketiminate tin 2,6-diisopropylanilide complex **2**, after 4 days at room temperature, afforded the β-diketiminate tin complex (**10**) and an insoluble precipitate (eq 19). The heterocumulene was expected to insert into the Sn-N bond, instead, the isocyanate reacted with the γ-carbon on the β-diketiminate backbone. Complex **10** has a tin centre bound to the oxygen atom (from the phenyl isocyanate species), with the unsaturated carbon centre of phenyl isocyanate bound to the backbone of another protonated β-diketiminate ligand. Treatment of the β-diketiminate tin diisopropylamide complex **1** in toluene solution with phenyl isocyanate also afforded the new β-diketiminate tin phenyl isocyanate complex **10**. DFT calculations to explain this result will be analysed in Chapter 2.7.

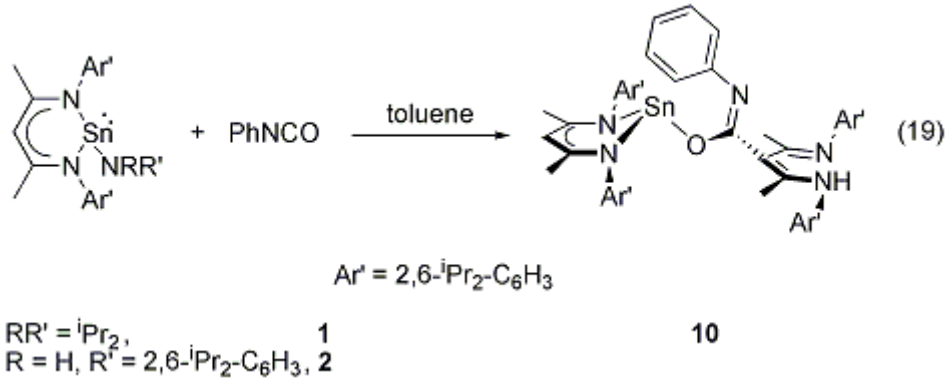

(19)

The presence of the tin phenyl isocyanate complex **10** as the soluble product was confirmed using ^1H NMR spectroscopy, where a resonance is clearly observed at 13.37 ppm, corresponding to the proton bound to the activated β-diketiminate ring. In addition, there are four apparent septets, with a ratio of 2:2:2:2, due to the presence of four

different isopropyl group environments from two β-diketiminate ligands. The presence of an unsaturated carbon centre (O*C*NPh) is detected via ^{13}C NMR spectroscopy through the observance of a resonance at 172.7 ppm. Furthermore, there are resonances corresponding to two β-diketiminate backbones, such as the presence of two carbon resonances at 165.5 ppm and 162.1 ppm, for the β-carbons on the two ligand backbones, two carbon resonances at 23.6 ppm and 19.9 ppm, for the methyl groups attached to the β-carbons on the ligand backbone and the two γ-carbons at 102.2 ppm and 96.3 ppm. The ^{119}Sn NMR spectrum displays a singlet at -373 ppm, significantly higher in frequency than the original tin diisopropylanilide complex **2** (-745 ppm). IR spectroscopy shows three distinct stretches at 2024, 1946 and 1916 cm^{-1} (nujol), corresponding to the isocyanate moiety,[112] thus providing further evidence of the presence of this group.

Crystals of the tin phenyl isocyanate complex **10** suitable for X-ray diffraction studies were grown from a saturated toluene solution at -27°C (Figure 22). Selected bond lengths and angles are reported in Table 5. Complex **10** adopts a distorted trigonal pyramidal geometry at tin and an 'exo' conformation, in contrast to the 'endo' conformation exhibited by the precursor tin diisopropylanilide complex **2**. The tin centre is displaced from the NCCCN plane by 1.136 Å, similar to other complexes exhibiting the 'exo' conformation. The sum of the bond angles is 262.3° and the DP is 108.6%. A long range interaction between Sn and N3 (2.692 Å) is observed. The Sn-O bond length is 2.1063(16) Å, which is shorter than the tin carbamate complex **8** but longer than Gibson's [(BDI)SnO*i*Pr] complex (2.000(5) Å).[73]

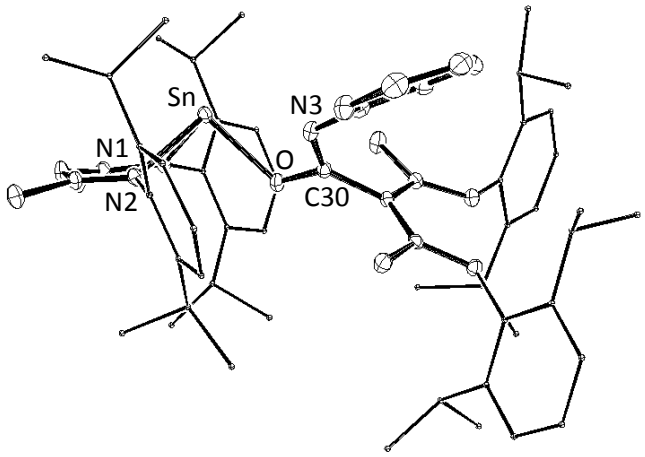

Figure 22 ORTEP diagram of [(BDI)SnOC{N(Ph)}BDI(H)] **10**. Aryl groups situated on the BDI ligand are minimised and the hydrogen atoms are omitted for clarity. Thermal ellipsoids are shown at 30%.

Table 5 Selected bond lengths (Å) and angles (°) for [(BDI)SnOC{N(Ph)}BDI(H)].

[(BDI)SnOC{N(Ph)}BDI(H)], **10**			
O-Sn	2.1063(16)	O-C30-C38	116.8(2)
N1-Sn	2.239(2)	O-C30-N3	116.4(2)
N2-Sn	2.2070(19)	N3-C30-C38	126.8(2)
O-C30	1.316(3)	C30-C38-C37	117.9(2)
C30-N3	1.300(3)	C30-C38-C39	118.3(2)
N1-Sn-N2	81.85(7)	Sum of angles	262.3
N1-Sn-O	82.73(7)	DP	108.6
N2-Sn-O	97.66(7)	Sn-NCCCN plane	1.136
Sn-O-C30	107.25(14)	O-NCCCN plane	0.388

The generation of the new tin phenyl isocyanate complex **10** (instead of the expected Sn-N insertion complex) suggests a different mechanism operates. A plausible mechanism involves nucleophilic attack onto the unsaturated carbon in the phenyl isocyanate by the γ-carbon in the β-diketiminate backbone. Nucleophilic attack at the unsaturated carbon of an electrophile by the γ-carbon on the β-diketiminate backbone is known to have occurred in similar complexes, both within the Fulton group[115] as well as with other systems.[62,116] For instance, Mindiola et al. generated a tripodal diimine-alkoxo complex through nucleophilic attack at the unsaturated carbon in the diphenylketene by the γ-carbon in the β-diketiminate backbone.[116] Furthermore, theoretical and experimental evidence has shown the β-diketiminate displaying non-innocence behaviour, where the frontier π orbitals show the occupied molecular orbital to be redox active so that potential oxidation reactions are possible towards substituents at the 1-, 3- and 5-positions of the ligand.[117] Density functional theory calculations undertaken for this study show activation of the β-diketiminate backbone is energetically comparable to that of the Sn-N (anilide) bond (*vide infra*). Interestingly, this reaction is not general, for instance, addition of *tert*-butyl isocyanate to the β-diketiminate tin 2,6-diisopropylanilide complex **2** did not result in a reaction, even at elevated temperatures.

In an attempt to synthesise a bimetallic complex, the new tin phenyl isocyanate complex **10** was treated with zinc dimethyl and aluminium trimethyl (Scheme 25). Instead of a bimetallic complex, the known β-diketiminate tin methyl complex **XXIX** was formed, in addition to a second product, which is postulated to be a tripodal diimine-alkoxo complex **11**. This complex could be formed due to the oxophilic character of aluminium and zinc centres. However, attempts to isolate the unknown have failed, even after coordinating solvents such as THF and tmeda were utilised to stabilise the complex at room temperature. Mindiola et al. generated a similar tripodal monoanionic ligand, the titanium diimine-alkoxo complex, by reacting a β-diketiminate titanium imide complex with a diphenylketene ($OCCPh_2$) in ether. Attempts to lithiate the non-metallated β-

diketiminate ligand with [Li^{n}Bu] generated a complex mixture of products at room temperature and at -27°C.

Scheme 25 Reactivity of the tin phenyl isocyanate complex **10** with zinc dimethyl and aluminium trimethyl (Ar' = 2,6-*i*Pr$_2$-C$_6$H$_3$; M'Me$_n$ = ZnMe$_2$, AlMe$_3$).

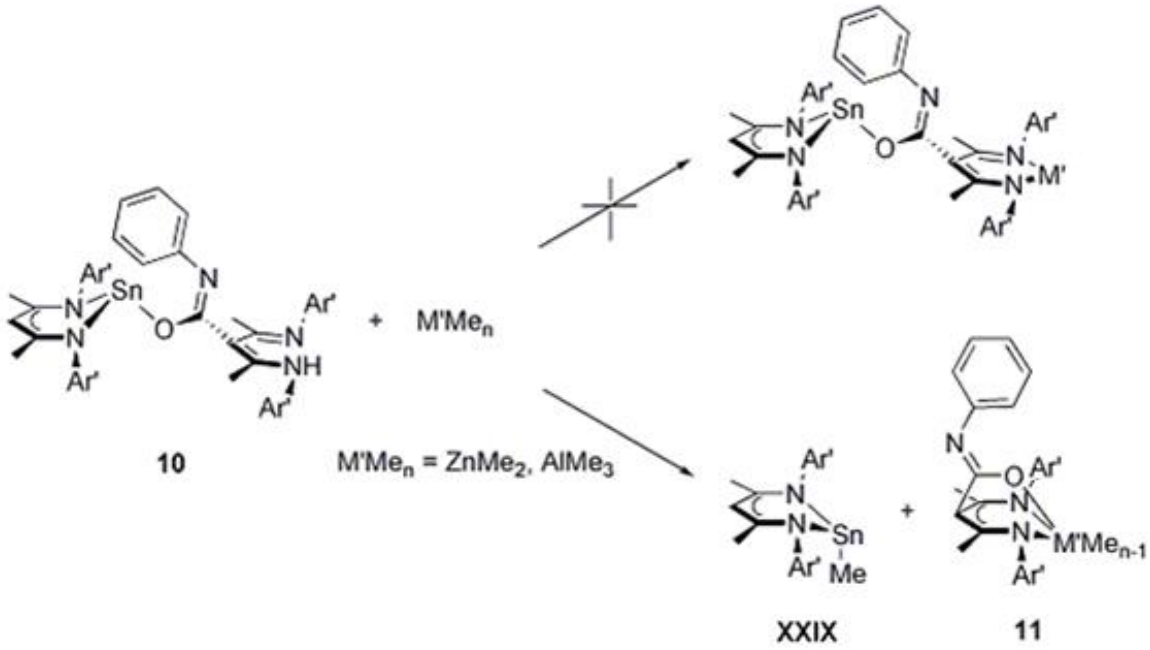

2.6.3. Reactivity of β-diketiminate stannylene amide and anilide towards carboacids

Phenyl acetylene was added to a toluene solution of the β-diketiminate tin diisopropylamide complex **1** and heated to 70°C for 6 days, resulting in the generation of the β-diketiminate tin phenyl acetylide complex (**12**) (eq 20).

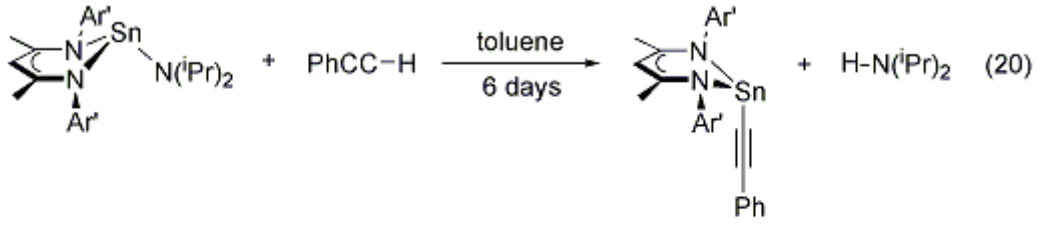

Ar' = 2,6-$^{i}Pr_2$-C_6H_3

1 **12**

The tin phenyl acetylide complex **12** was identified using ^{1}H and ^{13}C NMR spectroscopy. The ^{1}H NMR spectrum shows two apparent septets, in a 2:2 ratio, and four doublets, in a 6:6:6:6 ratio, corresponding to the isopropyl groups in the β-diketiminate ligand. The ^{13}C NMR spectrum reveals a resonance for one of the triply bound carbons (attached to the phenyl ring) in the acetylide moiety at 106.1 ppm, however, the other triply bound carbon coordinated to the tin centre could not be found. The ^{119}Sn NMR spectrum shows a resonance at -206 ppm, which is higher in frequency than Roesky's [(BDI)SnCC(CO_2Et)] complex (-253 ppm).[87] Characterisation utilizing IR spectroscopy provided inconclusive results due to the stretching frequencies of the phenyl acetylide terminal ligand being located either in the fingerprint region (i.e. the aromatic stretching frequencies) or overlapping with the nujol peaks (i.e. the carbon double bond frequency).

Crystals of the tin phenyl acetylide complex **12** suitable for X-ray diffraction studies were grown from a saturated toluene solution at -27°C (Figure 23). Selected bond lengths and angles are reported in Table 6. The tin phenyl acetylide complex exhibits a distorted trigonal pyramidal geometry at tin and an 'endo' conformation. The tin centre is displaced from the NCCCN plane by 0.805 Å, the largest displacement value for all the tin centres adopting the 'endo' conformation. The sum of the bond angles is 267.6° and the DP is 102.7%, the largest value for the former and the smallest value for the latter for all 'endo' structures. The Sn-C16 bond length is 2.196(4) Å and the C16-C17 triple bond

length is 1.190(6) Å. These values are slightly shorter than similar bonds in Roesky's [(BDI)SnCC(CO_2Et)] complex (2.214(2) Å and 1.213(3) Å, respectively).[87] The carbon triple bond length in the isostructural lead complex is longer than the tin complex (at 1.214(5) Å), due to the differences between the metal centres.[79]

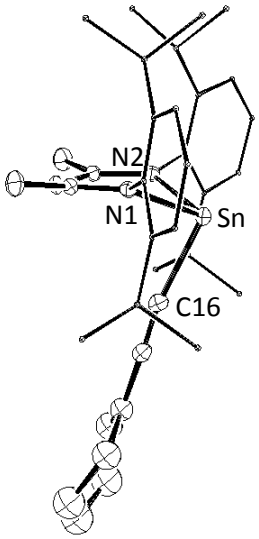

Figure 23 ORTEP diagram of [(BDI)SnCCPh] **12**. Aryl groups situated on the BDI ligand are minimised and the hydrogen atoms are omitted for clarity. Thermal ellipsoids are shown at 30%.

Table 6 Selected bond lengths (Å) and angles (°) for [(BDI)SnCCPh].

[(BDI)SnCCPh], **12**			
C16-Sn	2.196(4)	N2-Sn-C16	90.57(10)
N1-Sn	2.179(2)	Sn-C16-C17	170.7(4)
N2-Sn	2.179(2)	C16-C17-C18	174.2(4)
C16-C17	1.190(6)	Sum of angles	267.6
C17-C18	1.435(6)	DP	102.7
N1-Sn-N2	86.42(12)	Sn-NCCCN plane	0.805
N1-Sn-C16	90.57(10)	C30-NCCCN plane	90.57(10)

Addition of phenyl acetylene to the β-diketiminate tin 2,6-diisopropylanilide complex **2** did not result in a reaction, even after prolonged heating.

In conclusion reactivity studies using aliphatic electrophiles, unsaturated electrophiles and carboacids showed tin diisopropylamide **1** is more reactive than tin diisopropylanilide **2**. Even though reactivity of the tin complexes with the reagents described was predictable in most instances, such as electrophilic attack, heterocumulene insertion (with regards to carbon dioxide) and deprotonation, there was one anomalous result regarding phenyl isocyanate. Reactivity of the tin complexes with phenyl isocyanate yielded an unexpected product, with a mechanism which may involve nucleophilic attack on the carbon (in the phenyl isocyanate) by the γ-carbon in the β-diketiminate backbone instead of by the nitrogen on the terminal ligand. This result will be discussed further when the DFT calculations are described in Chapter 2.7.

2.6.4. Reactivity of β-diketiminate plumbylene amide and anilide complexes with aliphatic electrophiles

Similar to the analogous tin complexes, the nucleophilicity of the lead amide and anilide complexes was investigated using the electrophiles, methyl triflate and methyl iodide (eq 21, 22 and 23).

Addition of methyl triflate to either β-diketiminate lead diisopropylamide **4** or β-diketiminate lead 2,6-diisopropylanilide **5** resulted in the immediate formation of the known [(BDI)PbOTf] **XXXIII**[77] in 100% conversion, at room temperature, as confirmed using ^{1}H NMR and ^{207}Pb NMR spectroscopy (eq 21).

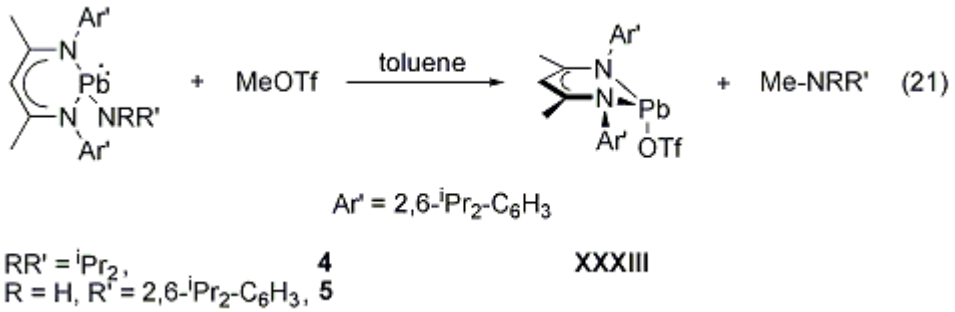

Addition of methyl iodide to the β-diketiminate lead diisopropylamide complex **4** resulted in a 100% conversion to [(BDI)PbI][72] (**XCV**) at room temperature (eq 22). The ^{1}H NMR and ^{207}Pb NMR spectra confirmed the identity of [(BDI)PbI], using published data on this known complex.[72] In contrast, the addition of methyl iodide to a toluene solution of the β-diketiminate lead 2,6-diisopropylanilide complex **5** resulted in no reaction even at 70°C, under normal experimental conditions. However, one test reaction resulted in the isolation of the imide lead dimer **13** (eq 23). Attempts to reproduce this result were unsuccessful and the formation of **13** was attributed to elevated levels of oxygen and/or

water present during the initial test reaction. Unfortunately, synthesis of this molecule via other pathways was unsuccessful.

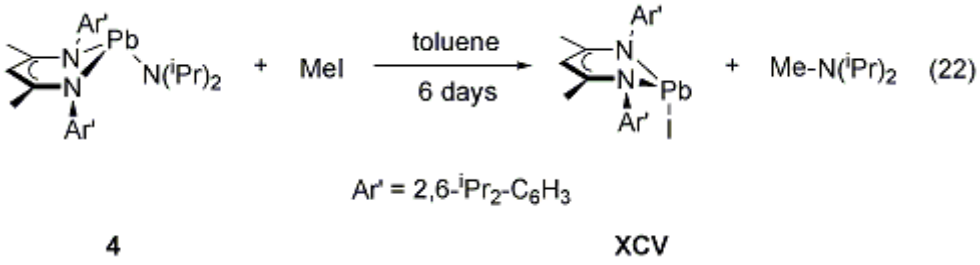

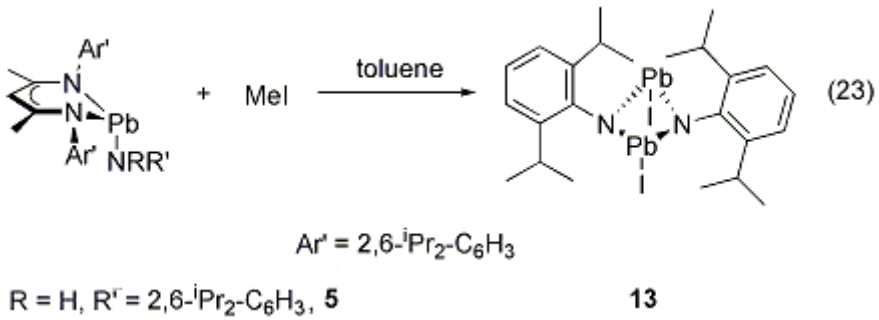

Due to the lack of reproducibility, no spectroscopy characterisation is available, however, crystals of the imide lead dimer complex **13** suitable for X-ray diffraction were grown from a saturated toluene solution at -27°C (Figure 24). Selected bond lengths and angles are reported in Table 7. The two [NH(2,6-*i*Pr_2-C_6H_3)] groups bridge the lead centres in a symmetric fashion, so that the dipp groups are *syn* to each other. The terminal iodide groups bound to the lead centres are also configured *syn* with respect to each other, but are *anti* with respect to the bridging anilides. This shows the conformation adopted is a result of steric effects caused by the bulky dipp substituents. The bridging Pb-N bond distances average 2.396 Å, and range from 2.360(5) Å – 2.427(5) Å, these values are larger than the range and average Pb-N bond distances of Power's [Pb{μ-N(C_6H_3-2,6-(C_6H_2-2,4,6-

$Me_3)_2\}]_2$[113] and Beswick and Wright's $[Pb(NCy)]_4$ cubane.[111] The terminal Pb-I bond lengths average 2.914 Å, and range from 2.9092(4) Å to 2.9187(4) Å.

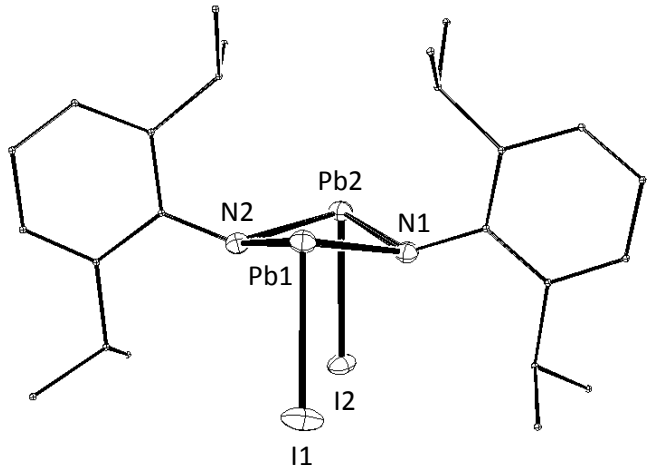

Figure 24 ORTEP diagram of [{PbINH(2,6-*i*Pr_2-C_6H_3)}$_2$] **13**. Aryl groups are minimised and the hydrogen atoms are omitted for clarity. Thermal ellipsoids are shown at 30%.

Table 7 Selected bond lengths (Å) and angles (°) for [{PbINH(2,6-*i*Pr_2-C_6H_3)}$_2$].

[{PbINH(2,6-*i*Pr_2-C_6H_3)}$_2$], **13**			
N1-Pb1	2.427(5)	N1-Pb1-I1	86.47(12)
N2-Pb1	2.420(5)	N2-Pb1-I1	85.75(11)
N1-Pb2	2.374(5)	N1-Pb2-I2	92.38(12)
N2-Pb2	2.360(5)	N2-Pb2-I2	88.08(11)
I1-Pb1	2.9187(4)	I1-Pb1-Pb2	96.637(10)
I2-Pb2	2.9092(4)	I2-Pb2-Pb1	102.303(11)
N1-Pb1-N2	76.08(16)	Pb2-N1-Pb1	99.57(17)
N1-Pb2-N2	78.22(16)	Pb2-N2-Pb1	100.15(17)

2.6.5. Reactivity of β-diketiminate plumbylene amide and anilide with unsaturated electrophiles

The reactivity of lead diisopropylamide **4** and diisopropylanilide **5** with unsaturated electrophiles was examined.

Addition of benzophenone to the β-diketiminate lead diisopropylamide complex **4** did not result in a reaction at room temperature or 40°C. Heating the reaction mixture to 70°C resulted in the decomposition of the complex to a mixture of products including protonated β-diketiminate. A similar lack of reactivity was observed between benzophenone and the β-diketiminate lead 2,6-diisopropylanilide complex **5**. These results are similar to what was observed with the analogous tin systems.

Addition of benzaldehyde to either the β-diketiminate lead diisopropylamide **4** or β-diketiminate lead 2,6-diisopropylanilide **5** complexes resulted in the formation of a complex mixture of products at room temperature. This result is similar to the reactivity observed between benzaldehyde and the analogous tin complexes, **1** and **2**.

When carbon dioxide (one equivalent) was added to an ampoule containing a toluene solution of either the β-diketiminate lead diisopropylamide **4** or β-diketiminate lead 2,6-diisopropylanilide **5** complex, decomposition of both complexes was observed at room temperature. The only identifiable species in both reaction mixtures was the protonated β-diketiminate ligand. This outcome contrasts with a similar reaction involving the analogous tin complexes, **1** and **2**, where the insertion products (the tin carbamate complexes, **8** and **9**) were successfully created. In addition, this decomposition is in sharp contrast to that observed between β-diketiminate lead alkoxide complexes and carbon dioxide.[78]

Phenyl isocyanate was added dropwise to a toluene solution of the β-diketiminate lead diisopropylamide complex **4**, resulting in the formation of a β-diketiminate lead

phenyl isocyanate complex (**14**) after stirring for 24 hours at room temperature in the dark (eq 24). Exposure to light reduced the yield due to conversion of the soluble products into an insoluble yellow precipitate. This result is analogous to the reaction between phenyl isocyanate and the isostructural tin analogue **10** (eq 19). In addition to the major complex **14**, a small amount of protonated β-diketiminate ligand, minor concentrations of unknown complexes and an insoluble yellow precipitate were observed. Complex **14** was also synthesised by treating β-diketiminate lead 2,6-diisopropylanilide complex **5** with phenyl isocyanate, under the same conditions. Although an unidentified side-product is still observed, as well as the insoluble yellow precipitate, no protonated β-diketiminate ligand is found in the ^{1}H NMR spectrum of the crude reaction mixture. It is assumed that the yellow precipitate formed in both reactions is some oligomer of [Pb(NRR')$_2$], these complexes are generally insoluble in hydrocarbons. A few examples of lead and tin dimers and oligomers exist, where large substituents are required to stabilise the low coordination environment and lower the degree of aggregation, these include Power's dimer, [Pb{μ-N(C$_6$H$_3$-2,6-(C$_6$H$_2$-2,4,6-Me$_3$)$_2$}]$_2$,[113] and Beswick and Wright's cubane, [Pb(NCy)]$_4$.[111]

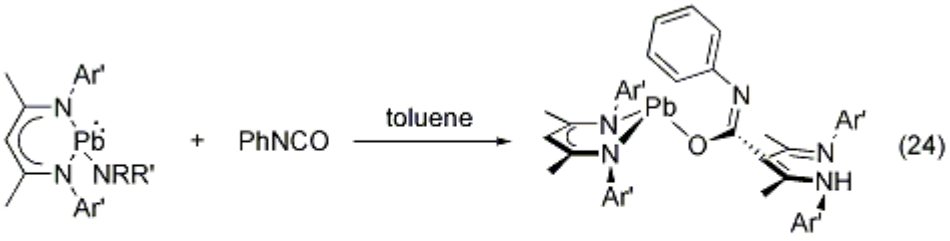

(24)

The ^{1}H NMR spectrum of **14** reveals a resonance at 13.52 ppm belonging to the proton bound to the activated β-diketiminate ring. In addition, there are three apparent septets, with a ratio of 4:2:2, due to the presence of eight isopropyl groups from two β-diketiminate ligands. The loss of the resonance corresponding to the proton bound to the nitrogen in the anilide moiety reflects the elimination of this group from the soluble product. Furthermore, the identical spectra for the main soluble product between the lead diisopropylamide **4** and the diisopropylanilide **5** complexes shows the product is the same and must therefore be devoid of the terminal amide or anilide ligand of the precursor complexes. No clean ^{13}C NMR spectrum could be attained despite repeated efforts. Attempts to obtain clean spectra by using fresh crystals, which were immediately scanned and not exposed to light, failed due to the rapid rate of decomposition of the product. The ^{207}Pb NMR spectrum exhibits a singlet at -981 ppm, significantly lower in frequency than the original lead complexes (2183 ppm and 1500 ppm for **4** and **5**, respectively). IR spectroscopy indicates the presence of the isocyanate moiety through three distinct stretches at 2024, 1946 and 1916 cm^{-1} (nujol). Unfortunately, crystals submitted for X-ray diffraction studies were not suitable for solving the structure.

Similar to the generation of the tin phenyl isocyanate complex **10**, the mechanism for the lead phenyl isocyanate complex **14** is not a standard heterocumulene insertion reaction into an M-X bond (X = N, O, H).[78,86-88] The reaction may involve nucleophilic attack on the phenyl isocyanate carbon by the γ-carbon in the β-diketiminate (as mentioned in detail under Chapter 2.6.2). Even though nucleophilic attack by the γ-carbon position on the β-diketiminate is known, heterocumulene insertion of phenyl isocyanate into the Pb-O bond in [(BDI)PbO*i*Pr] to form [(BDI)PbN(Ph)C(O)O(*i*Pr)] has been reported.[78] In this latter reaction, an *N*-bound carbamate complex is formed (as opposed to an *O*-bound carbamate).

Like the tin phenyl isocyanate complex **10**, reactivity studies conducted on the lead phenyl isocyanate complex **14** focused on the synthesis of a bimetallic complex through the addition of zinc dimethyl and aluminium trimethyl (Scheme 26). Similar to the tin phenyl isocyanate complex **10**, a known β-diketiminate lead methyl complex **XXIX** was formed in addition to an unknown, postulated to be a tripodal diimine-alkoxo complex **11**. Similar attempts to that of the tin complex were employed to isolate the unknown and failed. Treating the lead phenyl isocyanate complex **14** with [Li^{n}Bu], in an attempt to lithiate the protonated β-diketiminate ligand, resulted in a complex mixture of products at room temperature and -27°C.

Scheme 26 Reactivity of the lead phenyl isocyanate complex **14** with zinc dimethyl and aluminium trimethyl (Ar' = 2,6-*i*Pr$_2$-C$_6$H$_3$; M'Me$_n$ = ZnMe$_2$, AlMe$_3$).

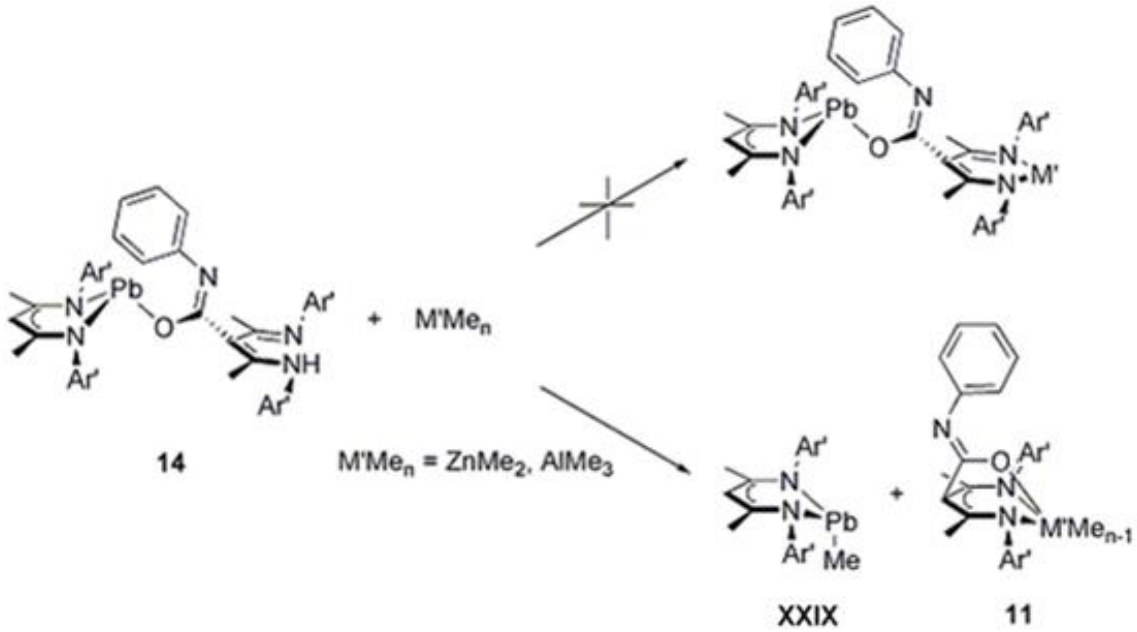

Addition of *tert*-butyl isocyanate to a toluene solution of the β-diketiminate lead 2,6-diisopropylanilide complex **5** resulted in the formation of β-diketiminate lead *tert*-

butyl carbamide (**15**) after 6 hours at room temperature (eq 25). This reactivity is similar to that observed between [(BDI)PbO(*i*Pr)] and phenyl isocyanate.[78]

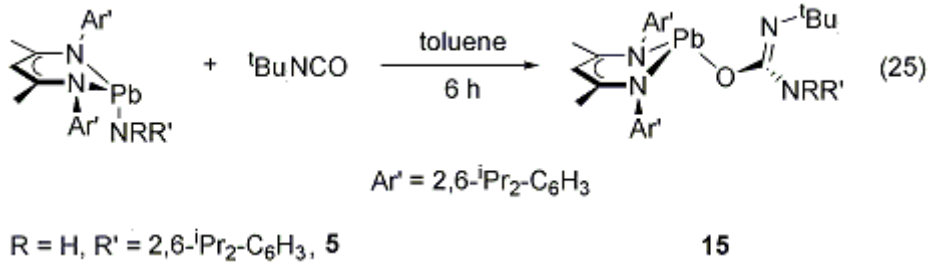

The identity of this complex was confirmed via ^{1}H NMR spectroscopy where three apparent septets are observed, in a 2:2:2 ratio, corresponding to the three different environments of the isopropyl groups in the β-diketiminate ligand and the diisopropylanilide group. The presence of a *tert*-butyl moiety is detected at 0.77 ppm. Further confirmation of the identity of the complex is provided in the ^{13}C NMR spectrum where a resonance at 164.9 ppm corresponds to the carbonyl carbon. In addition, two resonances for the *tert*-butyl moiety are found at 50.3 ppm (*C*Me$_3$) and 30.3 ppm (C*Me$_3$*). The ^{207}Pb NMR spectrum exhibits a singlet at 881 ppm. However, IR spectroscopy does not provide further conclusive results of the insertion product.

Crystals suitable for X-ray diffraction were grown over several days in a saturated toluene solution at -27°C (Figure 25). Data from these crystals show the lead *tert*-butyl carbamide complex **15** adopting a distorted trigonal pyramidal geometry around the metal centre, as well as an 'exo' conformation. The lead centre is displaced from the NCCCN plane by 1.358 Å, similar in value to other complexes adopting the 'exo' conformation. The sum of the bond angles is 260.8° and the DP is 110.2% (this data, in addition to selected bond lengths and angles, are reported in Table 8), significantly different to Fulton's lead carbamate complex, [(BDI)PbN(Ph)C(O)O(*i*Pr)] **XLII** (sum of the

bond angles is 275.3° and the DP is 94%).[78] The differences in these values may be caused by the presence of an interaction between the anilide's nitrogen with the lead centre in the lead *tert*-butyl carbamide complex **15**. The distance between the N4 and Pb atoms is 2.627(6) Å, which is 0.230 Å greater than the N1-Pb bond length of 2.397(7) Å. The O-Pb bond length of 2.249(5) Å is lower than the O-Pb bond length in the lead carbonate complex **XLII** (2.399(13) Å).[78]

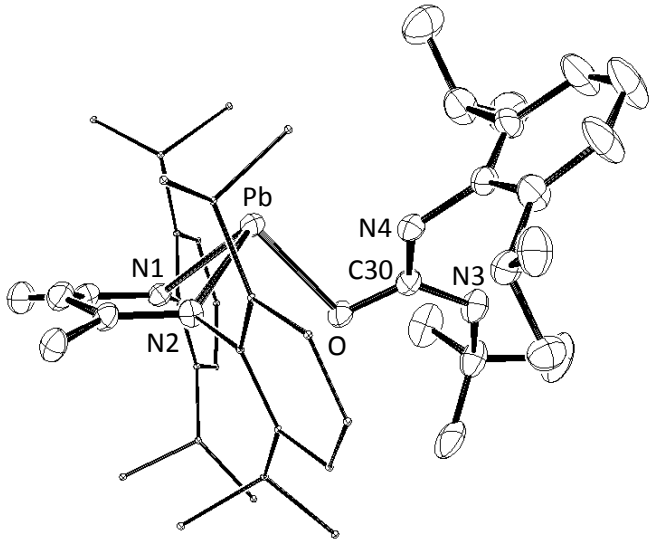

Figure 25 ORTEP diagram of [(BDI)PbOC{N(*t*Bu)}NH(2,6-*i*Pr$_2$-C$_6$H$_3$)] **15**. Aryl groups situated on the BDI ligand are minimised and the hydrogen atoms are omitted for clarity. Thermal ellipsoids are shown at 30%.

Table 8 Selected bond lengths (Å) and angles (°) for [(BDI)PbOC{N(*t*Bu)}NH(2,6-*i*Pr$_2$-C$_6$H$_3$)].

[(BDI)PbOC{N(*t*Bu)}NH(2,6-*i*Pr$_2$-C$_6$H$_3$)], **15**			
O-Pb	2.249(5)	N1-Pb-O	84.5(3)
N1-Pb	2.397(7)	N2-Pb-O	96.8(3)
N2-Pb	2.317(7)	Pb-O-C30	52.2(3)
N3-Pb	2.627(6)	O-C30-N3	177.8(7)
O-C30	1.308(9)	O-C30-N4	69.0(4)
C30-N3	1.376(9)	N3-C30-N4	123.0(7)
C30-N4	1.293(9)	Sum of angles	260.8
N4-C35	1.407(10)	DP	110.2
N3-C31	1.499(12)	Pb-NCCCN plane	1.358
N1-Pb-N2	79.4(3)	O-NCCCN plane	0.112

2.6.6. Reactivity of β-diketiminate plumbylene amide and anilide towards carboacids

Addition of phenyl acetylide to a toluene solution of the β-diketiminate lead diisopropylamide **4** or the β-diketiminate lead 2,6-diisopropylanilide **5** at room temperature resulted in the formation of the known [(BDI)PbCCPh] **XXIX** in 100% conversion, as observed via ^{1}H NMR and ^{207}Pb NMR spectroscopy (eq 26).[79]

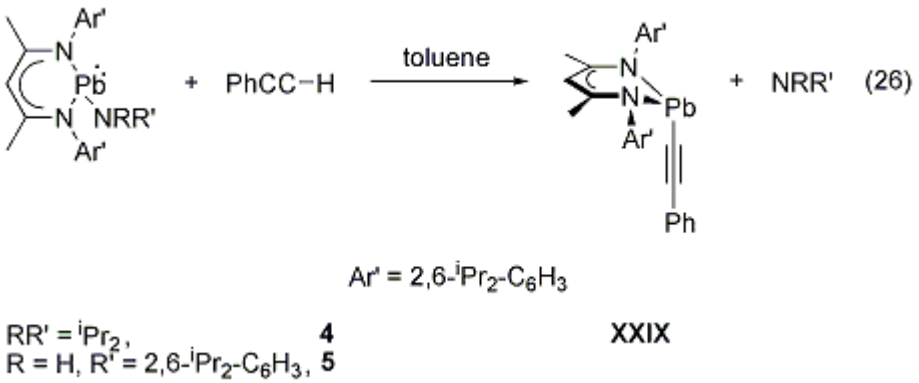

2.6.7. Summary of the reactivity of stannylene and plumbylene amide complexes

In conclusion electrophiles and acids used to probe the reactivity of the lead diisopropylamide **8** and diisopropylanilide **9** complexes show the amide complex is more reactive than the anilide complex, similar to the tin analogues. However, anomalous reactive behaviour was observed when phenyl isocyanate was added to the lead amide complexes (which has already been discussed in detail under Chapter 2.6.2).

The reactivity differences between the analogous lead and tin amide complexes show the lead complexes to be more reactive than their tin counterparts, yet the same general trends in reactive behaviour towards the various reagents are displayed. Larger discrepancies in reactivity are observed between the complexes with different metal centres compared to those with the same metal centre but different terminal ligands, suggesting the identity of the group 14 metal centre affects the reactivity of the complex more than the R group on the terminal nitrogen ligand. This would be expected because lead and tin have different electronegativities (χ) which would have a more profound effect on the polarity of the M-N bond and hence the reactivity of this bond. This explains why the more electronegative Pb atom (χ = 12.7 kJ mol^{-1})[118] displays greater reactivity than the Sn atom (χ = 11.3 kJ mol^{-1}).[118]

2.7. Computational studies on β-diketiminate Sn(II) and Pb(II) amide and anilide complexes

Density functional theory (DFT) studies were executed on the tin and lead amide complexes which underwent reactivity studies (complexes **1**, **2**, **4** and **5**) in order to help understand their reactivity. Geometry optimization calculations were performed on the entire molecule for the tin and lead amide complexes, the level of theory used was B3LYP DFT and Lanl2dz pseudopotentials on tin and lead with 6-31 g* on the other atoms. The calculated structural parameters for the tin and lead amide complexes correlate well with the X-ray crystallography data, with the range of discrepancies between the two data sets calculated to be between approximately -6% to 2% (Table 9).

Table 9 X-ray crystallography data of [(BDI)MNRR'] **1**, **2**, **4** and **5** (M = Sn and RR' = *i*Pr_2 **1**, H(2,6-*i*Pr_2-C_6H_3) **2**; M = Pb and RR' = *i*Pr_2 **4**, H(2,6-*i*Pr_2-C_6H_3) **5**) compared with computed bond distances (Å) and angles (deg) at the B3LYP/Lanl2dz/6-31 g* level of theory.

		[(BDI)SnNRR']		*[(BDI)PbNRR']*	
		1	***2***	***4***	***5***
M-N3	*Expt*	2.07	2.10	2.161	2.207
	Calcd	2.067	2.107	2.152	2.196
	% Diff	**0.14**	**-0.33**	**0.42**	**0.50**
M-N1	*Expt*	2.226	2.214	2.333	2.319
	Calcd	2.265	2.239	2.353	2.322
	% Diff	**-1.75**	**-1.13**	**-0.86**	**-0.13**
M-N2	*Expt*	2.229	2.225	2.392	2.328
	Calcd	2.362	2.254	2.459	2.348
	% Diff	**-5.97**	**-1.30**	**-2.80**	**-0.86**

C1-N1	*Expt*	1.339	1.325	1.338	1.326
	Calcd	1.349	1.336	1.346	1.335
	% Diff	**-0.75**	**-0.83**	**-0.60**	**-0.68**
C3-N2	*Expt*	1.316	1.327	1.312	1.315
	Calcd	1.325	1.337	1.322	1.333
	% Diff	**-0.68**	**-0.75**	**-0.76**	**-1.37**
N1-M-N2	*Expt*	81.30	83.73	78.98	81.36
	Calcd	81.87	85.3	80.26	83.61
	% Diff	**-0.70**	**-1.88**	**-1.62**	**-2.77**
N1-M-N3	*Expt*	99.29	86.09	98.94	84.38
	Calcd	101.13	87.08	101.15	86.62
	% Diff	**-1.85**	**-1.15**	**-2.23**	**-2.65**
N2-M-N3	*Expt*	104.62	94.17	103.44	93.36
	Calcd	107.20	95.14	109.14	95.40
	% Diff	**-2.47**	**-1.03**	**-5.51**	**-2.19**

In order to examine the relative orbital energy on the γ-carbon versus the terminal nitrogen lone pair (to help understand why nucleophilic attack on the phenyl isocyanate happens at the γ-carbon with the amide complexes, **1**, **2**, **4** and **5**) a full natural bond orbital (NBO) analysis was included. The tin diisopropylamide complex **1** has molecular orbitals situated on the nitrogen lone pair at HOMO (-122.78 kcal mol^{-1}), whilst the backbone molecular orbital is situated at HOMO-8 (-149.77 kcal mol^{-1}) (Figure 26). This suggests reactivity centred at the backbone (i.e. electrophilic activation of the γ-carbon in the backbone) is comparable on energetic grounds since the HOMO-8 molecular orbital is marginally lower in energy than the HOMO orbital by 26.99 kcal mol^{-1}. This observation combined with other factors, such as orbital overlap with an antibonding orbital on the heterocumulene, may contribute in determining the reactivity.

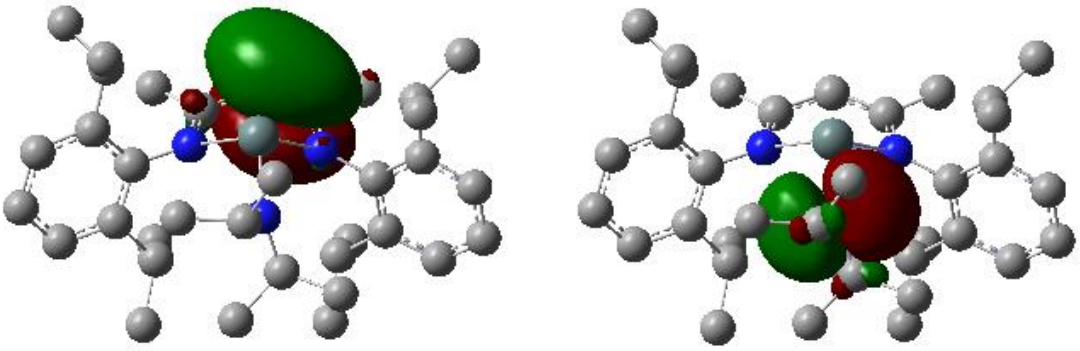

HOMO-8 HOMO

Figure 26 MOs associated with electrophilic activation of the γ-carbon in the backbone (HOMO-8) and heterocumulene insertion into the Sn-N bond (HOMO) for [(BDI)SnN(*i*Pr)$_2$].

The molecular orbital data for the tin diisopropylanilide complex **2** show the complex possessing a molecular orbital at HOMO-10 (-152.86 kcal mol^{-1}) corresponding to reactivity on the backbone, allowing for electrophilic activation of the γ-carbon on the backbone (Figure 27). The molecular orbital corresponding to the nitrogen lone pair is situated at HOMO-11 (-162.29 kcal mol^{-1}) and corresponds to reactivity centred on the Sn-N bond (Figure 27). The energy difference between the two orbitals is significantly small at 9.43 kcal mol^{-1}, thus showing that both pathways are feasible from an energetic view point, therefore other factors must have a role in determining which pathway is favoured. The HOMO is located on part of the aryl group in the diisopropylanilide ligand where no reactivity is observed (Figure 27).

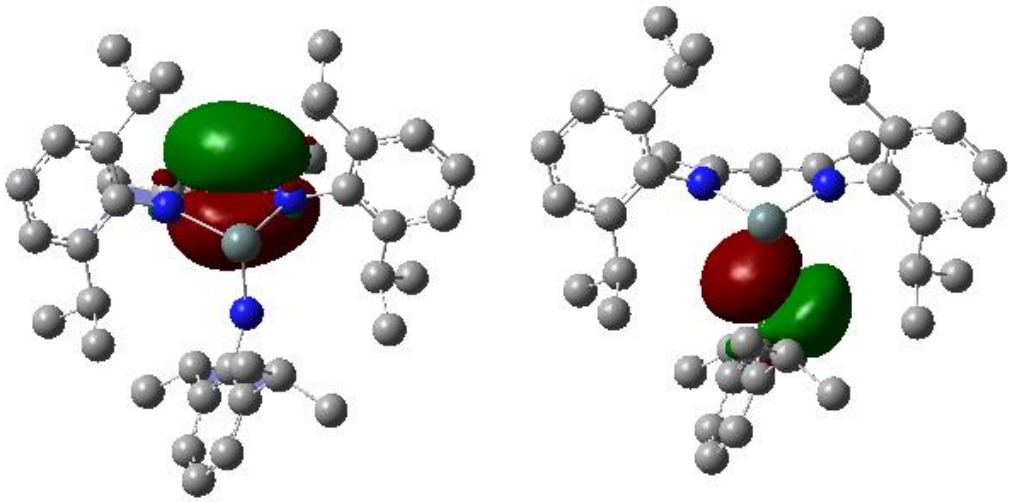

HOMO-10 HOMO-11

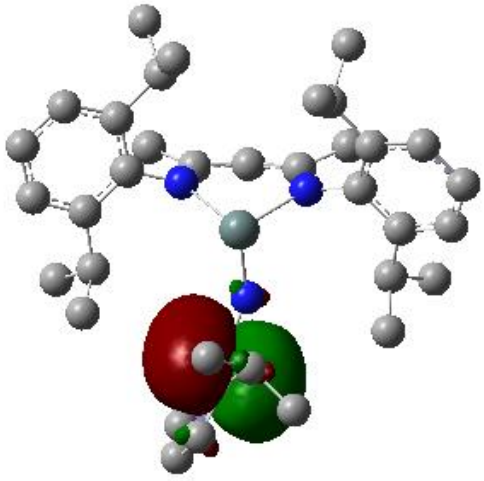

HOMO

Figure 27 MOs associated with electrophilic activation of the γ-carbon in the backbone (HOMO-10), heterocumulene insertion into the Sn-N bond (HOMO-11) and the HOMO for [(BDI)SnNH(2,6-*i*Pr_2-C_6H_3)].

The lead diisopropylamide complex **4** has molecular orbitals for the nitrogen lone pair and the backbone at HOMO-1 (-139.22 kcal mol^{-1}) and HOMO-8 (-147.06 kcal mol^{-1}), respectively (Figure 28). The lone pair molecular orbital is higher in energy than the backbone molecular orbital by 7.84 kcal mol^{-1}. The values of these orbitals are comparable so that reactivity involving electrophilic activation of the γ-carbon in the backbone or heterocumulene insertion into the Pb-N bond are both feasible. In order to ascertain the

favoured pathway based purely on theoretical insight other, unknown factors would also need to be taken into account. The HOMO is found on the nitrogen in the diketiminate backbone where reactivity is not observed (Figure 28).

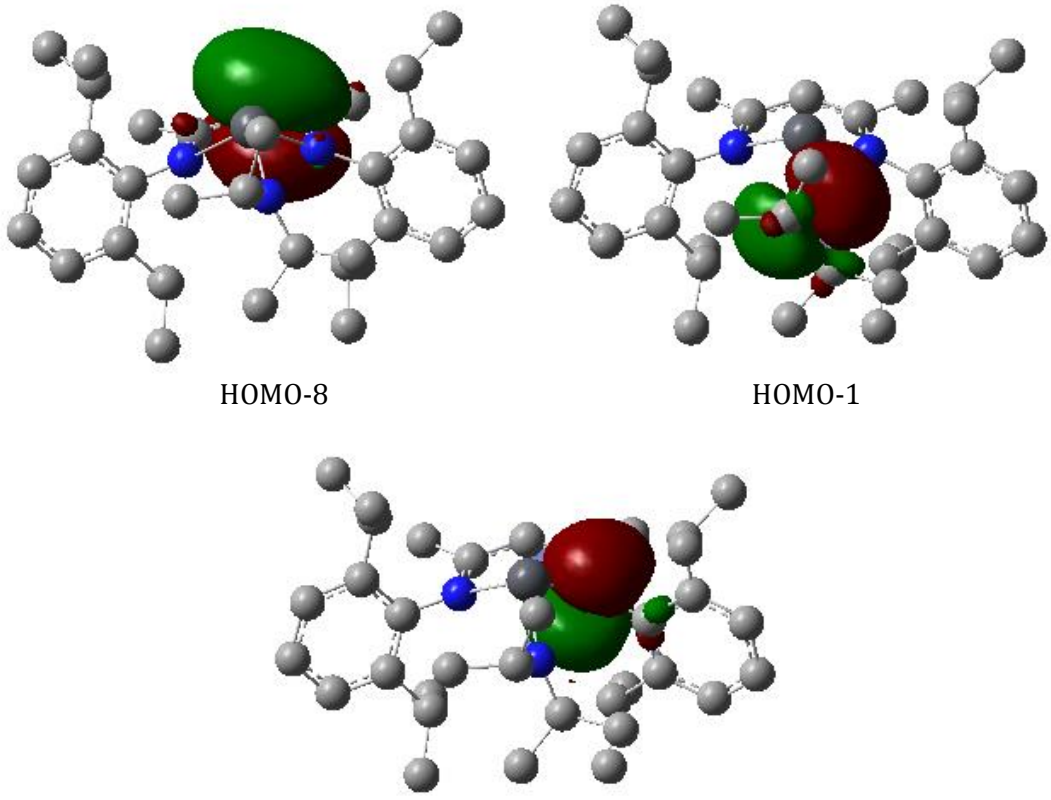

Figure 28 MOs associated with electrophilic activation of the γ-carbon in the backbone (HOMO-8), heterocumulene insertion into the Pb-N bond (HOMO-1) and HOMO for [(BDI)PbN(*i*Pr)$_2$].

The lead diisopropylanilide complex **5** exhibits a molecular orbital where reactivity is centred on the backbone at HOMO-9 (-150.06 kcal mol^{-1}) (Figure 29). This molecular orbital is marginally lower in energy relative to the molecular orbital corresponding to the nitrogen lone pair at HOMO-8 (149.08 kcal mol^{-1}) by 0.98 kcal mol^{-1}

(Figure 29). Similar to complex **2**, the HOMO resides on the aryl group in the diisopropylanilide ligand where no reactivity is observed (Figure 29).

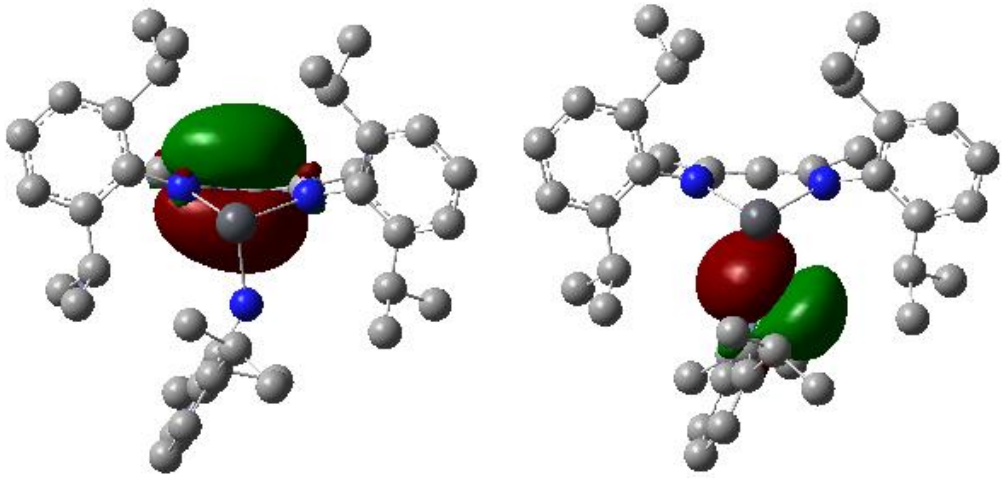

HOMO-9 HOMO-8

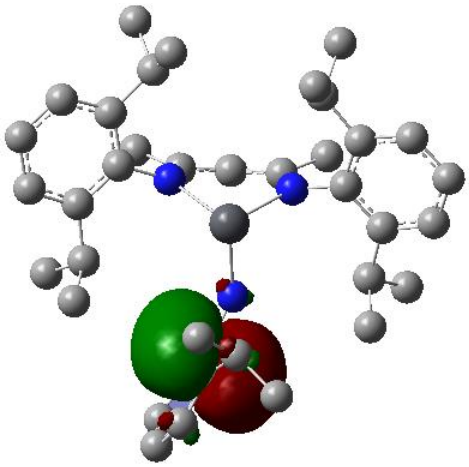

HOMO

Figure 29 MOs associated with electrophilic activation of the γ-carbon in the backbone (HOMO-9), heterocumulene insertion into the Pb-N bond (HOMO-8) and the HOMO for [(BDI)PbNH(2,6-*i*Pr_2-C_6H_3)].

These calculations show the experimental outcome is based on more than purely thermodynamic considerations and may be additionally influenced by kinetic factors. This

may also explain why heterocumulenes are known to undergo electrophilic activation of the γ-carbon at the backbone and heterocumulene insertion (i.e. *tert*-butyl isocyanate and carbon dioxide).

DFT data at the B3LYP/Lanl2dz/6-31 g* level of theory can be used to calculate the hybridisation of the lone pair situated on the metal atom (Table 10). The tin amide complexes, **1** and **2**, have greater hybridisation of the lone pair, with the highest value of hybridisation calculated for the tin diisopropylanilide complex **2** (84.90% s character and 15.10% p character), followed closely by the tin diisopropylamide complex **1** (85.25% s character and 14.75% p character). Relativistic effects (as discussed in the structural data) result in the lead amide complexes displaying less hybridisation, with the lead diisopropylanilide complex **5** calculated to have a lone pair with hybridisation of 91.59% s character and 8.41% p character. The lead diisopropylamide complex **4** displays the least hybridisation with values calculated on the lone pair to be 92.11% s character and 7.89% p character. Furthermore, the sum of the bond angles is larger and DP smaller for the tin amides compared to their lead amide analogues, however, comparisons for these values can not be made between the types of terminal ligands due to the differences in conformation adopted by these complexes.

Table 10 NBO analysis of M(II) (M = Sn, Pb) for compounds **1**, **2**, **4** and **5**.

	Natural electron configuration	Lone pair NBO on M	Lone pair occupancy
[(BDI)SnN(*i*Pr)$_2$] **1**	Sn: 5s(1.72) 5p(1.00)	s(85.25%) p 0.17 (14.75%)	1.96188
[(BDI)SnNH(2,6-*i*Pr$_2$-C$_6$H$_3$)] **2**	Sn: 5s(1.72) 5p(0.96)	s(84.90%) p 0.18 (15.10%)	1.97180
[(BDI)PbN(*i*Pr)$_2$] **4**	Pb: 6s(1.84) 6p(0.87) 7s(0.01)	s(92.11%) p 0.09 (7.89%)	1.97463
[(BDI)PbNH(2,6-*i*Pr$_2$-C$_6$H$_3$)] **5**	Pb: 6s(1.84) 6p(0.83)	s(91.59%) p 0.09 (8.41%)	1.98123

To summarise the findings from the DFT studies, the molecular orbital diagrams for the tin and lead amide complexes, **1**, **2**, **4** and **5**, provide an explanation for the experimental observation for the formation of the metal phenyl isocyanate complexes, **10** and **14**, whereby the energy of the molecular orbitals corresponding to the backbone molecular orbital (understood to be responsible for electrophilic activation of the γ-carbon on the ancillary ligand) and the lone pair (resulting in heterocumulene insertion) are comparable. This outcome suggests that the identity of the resultant product is more likely to be influenced by factors other than purely thermodynamic, such as orbital overlap with an antibonding orbital on the heterocumulene. Lastly, hybridisation of the lone pair is larger for the tin amide complexes over the lead amide complexes due to relativistic effects.

3. Group 14 metal phosphides: reactivity studies

3.1. Recent advances in the multiple bonded chalcogenide complexes of the germanium, tin and lead elements

Due to the attention given on the synthesis of β-diketiminate group 14 metal complexes and their reactivity in Chapters 1 and 2, no further discussion will be dedicated to this topic, with the exception of the chalcogenation of β-diketiminate germanium complexes. The development of the multiple bonded chalcogenide organogermanium, -tin and -lead complexes is of interest within the various chemistry disciplines due to their synthetic and structural properties, as well as potential applications as single source precursors for group 14/16 mixed materials. For example, the synthesis of stable 'heavy ketones,' which possess a double bond between group 14 and 16 elements, may be of potential value in organic chemistry. In addition, the isolation of stable multiple bonds between heavier members of the p-block group are a chemical curiosity in inorganic and physical chemistry due to their violation of the 'classical double bond rule,' where elements with a principal quantum number greater than two, i.e. those elements not in the second row of the periodic table, should not be able to form (p-p)π bonds to themselves or other elements, with greater violation of the rule travelling down the group.[119] A study by Kutzelnigg[119,120] suggests this is caused by the relative strengths of the σ and π bonds. In the lighter group 14 elements, these bond strengths are equivalent so that the formation of π bonds in conjunction with σ bonds is more energetically favourable. In contrast, the heavier group 14 elements possess increasingly stronger σ bonds relative to the increasingly weaker π bonds, hence formation of σ bonds over π bonds is more energetically favourable. For group 16 elements, the formation of σ bonds is favoured over π bond formation. However, preference for σ over π bonds also increases down the group.[121] As a result, the formation of M=E bonds becomes less energetically favourable

upon descending group 14 (M = Ge, Sn or Pb) and when E is from group 16 (E = S, Se or Te). The formation of such M=E bonds therefore requires ligands which enable the kinetic and thermodynamic stabilisation of the M=E bond in order to prevent chalcogenide bridged structures.

In order to generate stable complexes with an M=E bond, investigations into the formation of chalcogenide bridged structures have been undertaken. Questions regarding the thermodynamic drive for dimerisation and the labelling of products either as the i) thermodynamically or ii) kinetically stabilised product, have presented problems surrounding the classification of complexes into one of these two categories.[119,121] Confusion has arisen due to the changes in Gibbs free energy for dimerisation, which drives the thermodynamic stabilisation of a dimerised complex, created by an interplay of other steric and electronic factors which leads to either the thermodynamic or kinetic product.[121] Examples of steric factors which affect the Gibbs free energy are a sterically encumbering ancillary ligand and the size of the chalcogen, which can stabilise the monomeric state by blocking a larger area of the group 14 atom surface, thus hindering dimerisation. Electronic factors, such as the coordination of a base-stabilised ligand, can also stabilise the monomeric state and affect the Gibbs free energy. Based on these considerations, Stahl et al.[121] have argued that *most* monomeric group 14 metal complexes bearing a terminal chalcogenide could be considered thermodynamically stabilised, even those stated to the contrary by their authors. Stahl suggests the criteria for a truly kinetically stabilised product should encompass only those monomeric terminal chalcogenide complexes which dimerise at elevated temperature. The monomeric chalcogenide group 14 metal complexes highlighted in this study will therefore not be labelled as either the thermodynamic or kinetic products due to this confusion.

Whereas research in this area has generally focused on transient M=E bonds (including an extensive number of reviews),[122-136] interest in the stable chalcogenide group

14 metal complexes has grown in the past 15 years. Particular attention has been paid to the chalcogenide germanium complexes, with some of the earliest work in this field concentrated on these complexes. For instance, in 1989, Veith and co-workers isolated and structurally characterised the first chalcogenide germanium complex via oxidative addition of sulfur to the precursor germanium complex, [[η^2-{(μ-*t*BuN)$_2$(SiMeN*t*Bu)$_2$}]Ge], resulting in the multiple bonded germanium sulfide complex, [[η^3-{(μ-*t*BuN)$_2$(SiMeN*t*Bu)$_2$}]GeS] (**XCVI**) (Figure 30).[137]

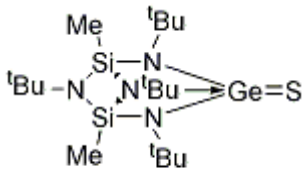

XCVI

Figure 30 Veith's germanium sulfide complex.

This Chapter will focus on the more remarkable stable multiple bonded chalcogenide group 14 metal complexes and their associated synthesise, with particular attention on germanium complexes.

The terphenyl ligand, [C_6H_3-2,6-Ar_2]$^-$, has been used extensively by Tokitoh et al., to synthesise stable multiple bonded chalcogenide complexes of germanium and tin (**C**). A variety of the terphenyl ligands have been examined (Ar = Bbt = C_6H_2-2,6-CH($SiMe_3$)$_2$-4-C($SiMe_3$)$_3$; Ar = Dis = C_6H_2-2,4,6-CH($SiMe_3$)$_2$; Ar = Ditp = C_6H_3-2,6-C_6H_4-2-*i*Pr; Ar = Tbt = C_6H_2-2,4,6-CH($SiMe_3$)$_2$; Ar = Tip = C_6H_2-2,4,6-CH(CH_3)$_2$; Ar = Titp = C_6H_3-2,6-C_6H_4-2,4-*i*Pr).[138-145] Tokitoh et al. have implemented multiple methods in order to generate the chalcogenide complexes including i) cycloreversion of 1,2,4-trichalcogenadimetallolanes (**XCVII**), ii) chalcogenation of the divalent group 14 metal complex (**XCVIII**) or iii)

dechalcogenation of 1,2,3,4-tetrachalcogenametallolanes (**XCIX**) with trivalent phosphorus reagents (Scheme 27). The most popular and successful method applied of the three outlined is iii), followed by ii). It was method iii), the dechalcogenation of 1,2,3,4-tetrachalcogenametallolanes using triphenyl phosphine, implemented by Okazaki et al., that resulted in the formation of the first three-coordinate multiple bonded terminal chalcogenide complexes of tin **C**, with the generation of stable tin-sulfur and tin-selenium double bonded complexes.[146]

Scheme 27 Synthetic routes for the generation of terminal chalcogenide group 14 metal terphenyl complexes (L = C_6H_3-Ar_2; M = Ge, Sn; E = S, Se, Te; R = Ph, Me_2N).

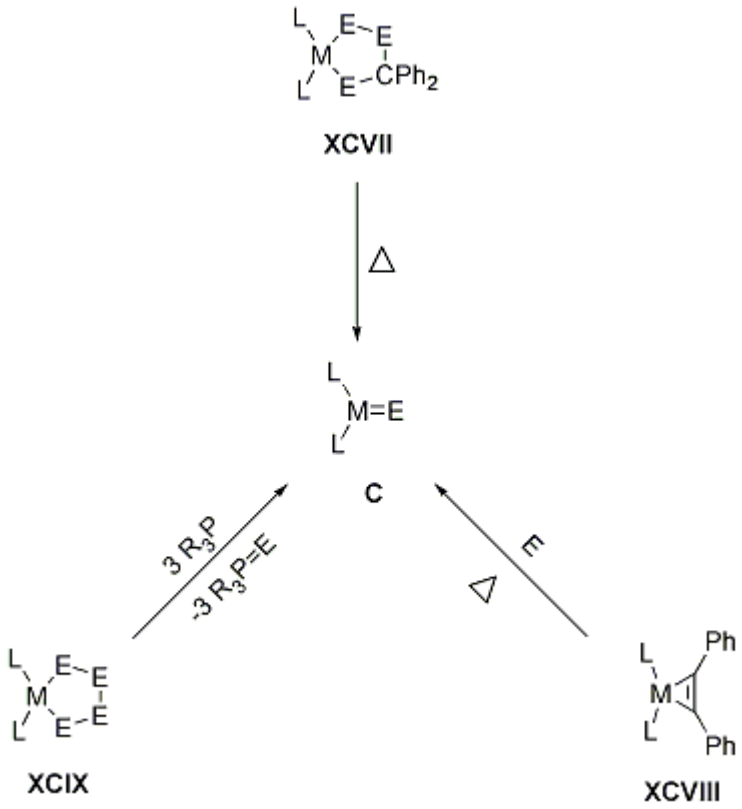

The generation of the only relatively stable multiple bonded chalcogenide complex (**CII**) using sulfur and lead involved the use of the Ar = Tbt and Tip groups and employed

method iii) at low temperature.[147] This allowed the complex to be trapped, as the complex isomerises to [Tbt(TbtS)Pb] (**CIII**) at room temperature via the migration of the Tbt group (Scheme 28). Tokitoh and Okazaki proposed an overall mechanism involving the desulfurisation of the tetrathiaplumbolane using either [Ph_3P] or [$(Me_2N)_3P$], thus forming the plumbanethione **CII**. The plumbanethione undergoes 1,2-aryl migration and these lead complexes dimerise to give an aryl sulfide-bridged organolead heterocycle. Cycloreversion affords **CIII**, for the more crowded plumbylene, whereas cycloreversion of the [TipPbSTip] complex results in an unstable product, so that the complex undergoes dimerisation, followed by 1,2-aryl migration, thus producing the dithiadiplumbetane (**CIV**).

Scheme 28 Generation and reactivity of the terminal sulfide lead terphenyl complex.

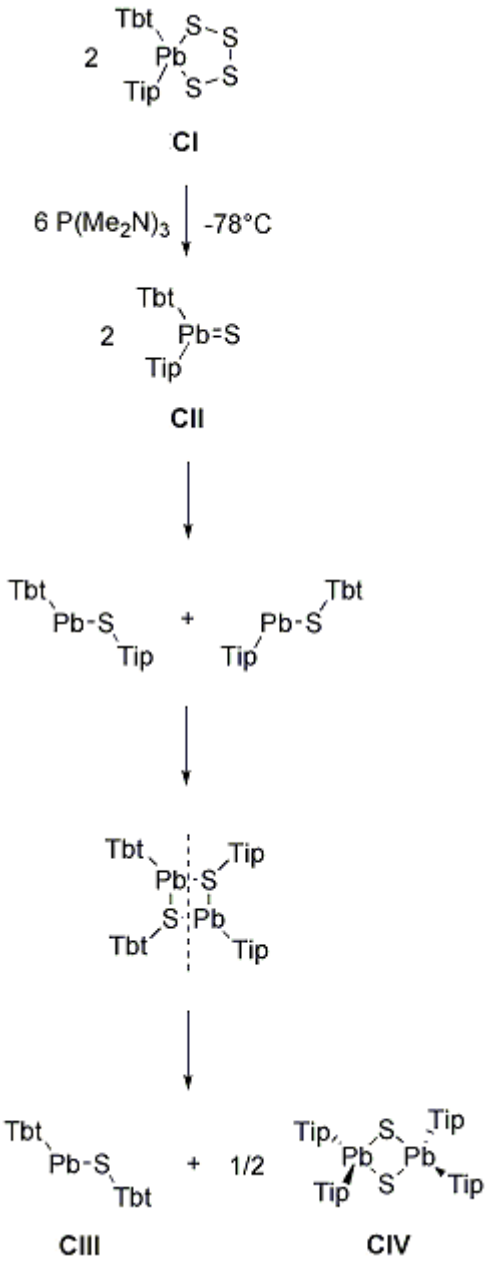

The first multiple bonded tin sulfide and selenide and germanium selenide and telluride complexes were published by Parkin et al., in 1994,[148,149] using the macrocyclic octamethyldibenzotetraaza[14]annulene dianion, $[Li_2(Me_8taa)]$, resulting in $[(\eta^4\text{-}Me_8taa)Ge(E)]$ (E = S, Se, Te) (**CVI**). These tetravalent terminal chalcogenide complexes

were formed via chalcogenation of the divalent group 14 metal complex, [(η⁴-Me₈taa)Ge] (**CV**) (eq 27). This method has been applied in the formation of the tin and lead analogues.

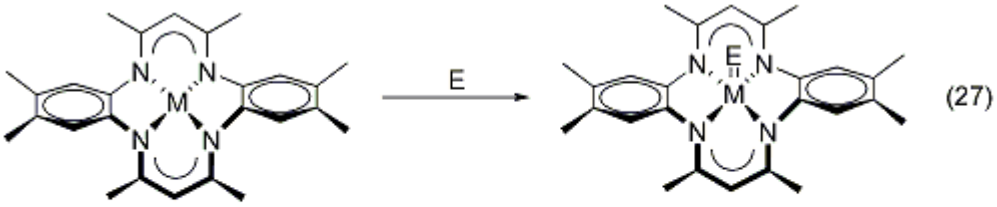

M = Ge, Sn, Pb
E = S, Se, Te

CV **CVI**

The configurations adopted by the [η⁴-Me₈taa] ligand in solid state appear to be dependent on the terminal chalcogenide moiety. The addition of sulfide and selenide groups result in the complex adopting a geometry such that the benzo groups are directed from the macrocyclic N_4 plane towards the [GeE] moiety (Scheme 29). In contrast, the telluride analogue adopts a configuration where the benzo groups are directed away from the [GeTe] moiety (Scheme 29). ^{1}H NMR spectroscopy studies show both isomers for each of the complexes existing in solution. However, reasons for the differences in configurations adopted by each complex outside of the solution were not provided.

Scheme 29 Geometry adopted by the [(η⁴-Me₈taa)Ge(E)] complex. The bridging annulene groups have been omitted for clarity.

E = S, Se

Notable reactivity displayed by the [(η^4-Me_8taa)M] complexes (M = Ge, Sn) **CV** include chalcogen atom transfer reactions (eq 28).[148] For instance, the terminal chalcogenides of sulfur and selenium are able to transfer from the tin to the germanium macrocycle. This is believed to be caused by the stronger Ge=E bonds relative to the Sn=E bonds (the reasons for which have already been discussed in this Chapter). Another interesting observation recorded by Woo et al.[150] which further supports the theory that chalcogen atom transfer is driven by M=E bond strengths, is the reversibility of selenium and sulfur transfer between two tin porphyrin complexes, [(TTP)Sn] (**CVII**) and [(TPP)Sn] (**CVIII**) (eq 29). This was attributed to the equivalent bond strengths of the Sn=E bonds between the two complexes. Furthermore, the rate of atom transfer is faster for the selenium compared to the sulfur, presumably due to the stronger interaction between Sn=S relative to the Sn=Se.

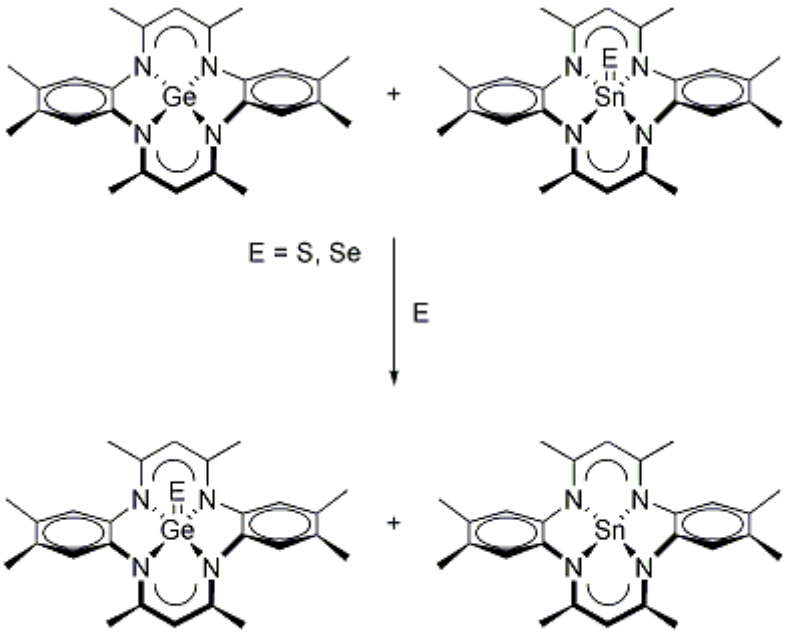

(28)

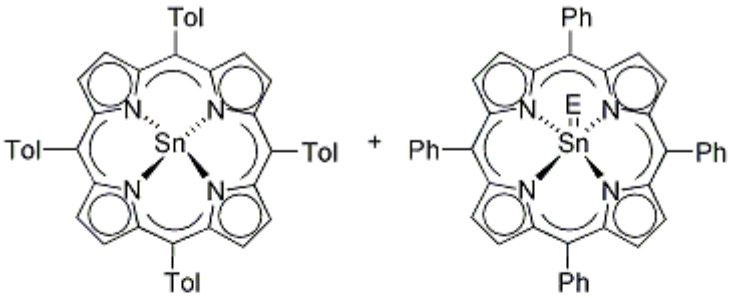

CVII **CVIII**

E = S, Se

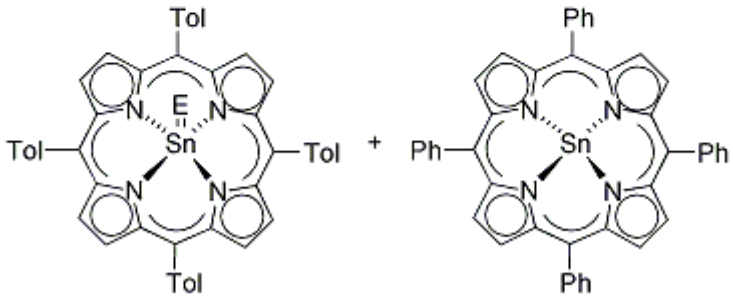

CIX **CX**

(29)

The monomeric dialkyl stannanesulfide, -selenide and -telluride complexes, [{η^2-[(C$_9$H$_6$N)(Me$_3$Si)CH]}$_2$SnE] (E = S, Se, Te) (**CXII**), were synthesised by Leung et al.,[151,152] using 8-(trimethylsilyl)methylquinoline as an *N*-functionalised alkyl ligand (eq 30). The thermal stability of these complexes is attributed to the steric bulk of the substituted quinoline ligand, which stabilises the tin centre through its interaction with the trimethylsilyl-substituted α-carbon and the nitrogen. This series of ligands has been successfully utilised to stabilise monomeric germanium chalcogenide complexes using the chalcogens, sulfur, selenium and tellurium (**CXIV**), via chalcogenation of the divalent group 14 metal diaryl complex (**CXIII**) (eq 31).

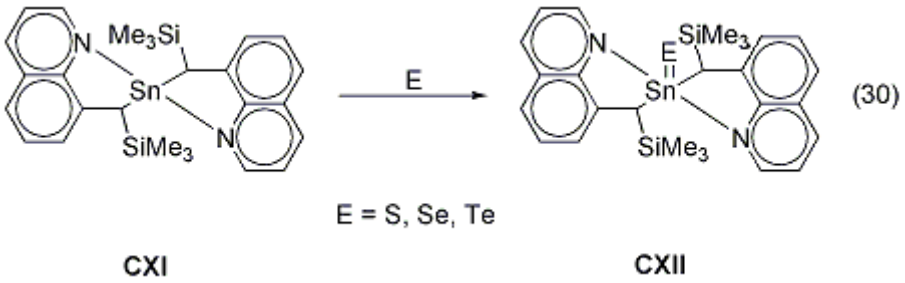

(30)

CXI **CXII**

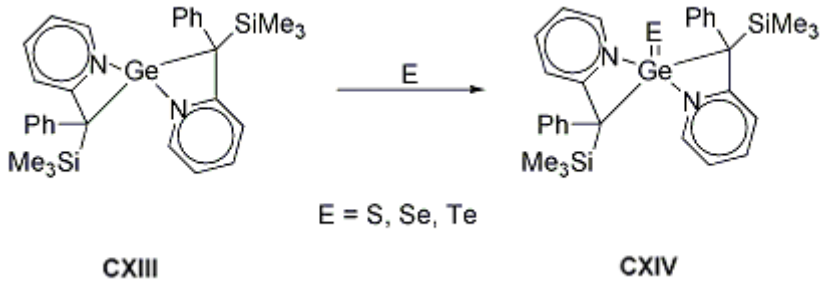

(31)

CXIII **CXIV**

Research by Chivers et al. into imidotin and -germanium cage complexes has yielded the first stannanetelluride complex with a four-coordinate tin centre, [{*t*BuNSn(μ-N*t*Bu)$_2$TeN*t*Bu}(μ$_3$-SnTe)] (**CXV**)[153] (Figure 31). This complex was generated via the treatment of [Li$_2$Te(N*t*Bu)$_3$]$_2$ with [Sn(O$_3$SCF$_3$)$_2$] or [SnCl$_2$], thus forming a tricyclic structure.[154] This discovery led Chivers et al. to study other imidotin and -germanium cage complexes, including those with the first to contain multiple group 14 metal=Se bonds (Sn=Se bonds (**CXVI**) and Ge=Se bonds (**CXVII**)) (Figure 32).[154] Both the germanium and tin complexes were generated via an oxidative addition reaction, whereby selenium powder and the [(MN*t*Bu)$_4$] complex (M = Ge or Sn) were stirred together at elevated temperature. This method was also employed to generate the imidotin complexes with one terminal Sn=E bond (E = Se, Te) (**CXVIII**) (Figure 33).[155]

Figure 31 Chivers' four-coordinate stannanetelluride complex.

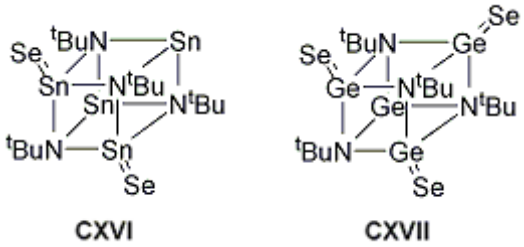

Figure 32 Chivers' imidotin and -germanium cage complexes with multiple group 14 metal=Se bonds.

An interesting result, explored further by Chivers et al.[155] and first investigated by Veith et al.,[156] was the increasing likelihood of dimerisation of complexes of group 14 elements bearing a terminal chalcogenide when travelling up group 16. By isolating and characterising a series of monochalcogenide derivatives (e.g. S, Se or Te) of the seco-cubane tin complexes, $[Sn_3(\mu_2\text{-NH}t\text{Bu})_2\ (\mu_2\text{-NH}t\text{Bu})(\mu_3\text{-N}t\text{Bu})]$, Chivers et al. demonstrated that the sulfide derivative is dimeric (**CXIX**), whilst the telluride is monomeric **CXVIII** (Figure 33). The selenide derivative can exist either as a monomer **CXVIII** or dimer **CXIX**.

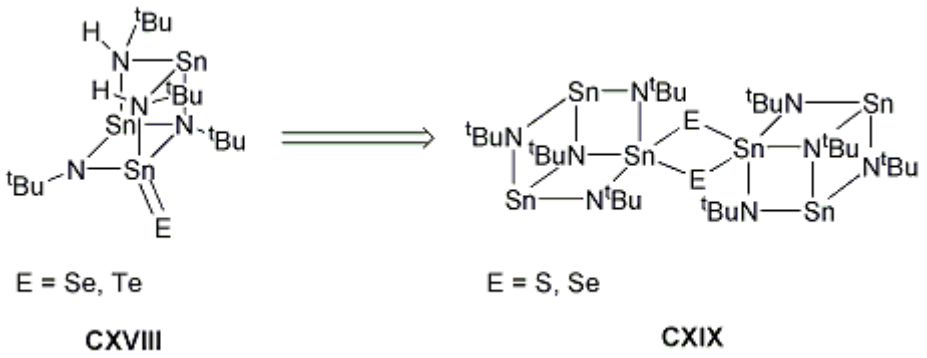

Figure 33 Monochalcogenide derivatives of the seco-cubane tin complexes.

Chalcogenation of the divalent germanium alkyls, chlorides and hydroxides bearing a β-diketiminate ligand (**XXI**, **XXIII**, **CVII**) has been extensively studied by Roesky et al.[144] These reactions have been limited to the use of sulfur and selenium, resulting in the terminal chalcogenide complex (**CXXI**) (eq 32), with no known tellurium analogue reported.

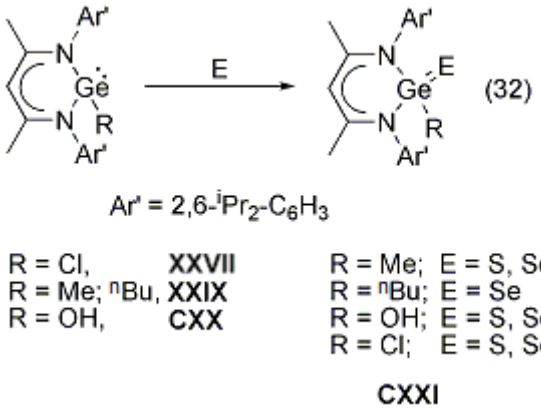

3.1.1. Summary of β-diketiminate group 14 metal phosphide reactivity

Previous work undertaken by Tam in the Fulton group on the synthesis of β-diketiminate group 14 metal dialkyl-chalcogenophosphinites was extended in this study.[115,157] Tam found that addition of one equivalent of selenium to tin or lead dicyclohexylphosphide complexes (**CXXII**) and (**CXXIII**) in a non-polar solvent, such as deuterated benzene or toluene, resulted in the formation of β-diketiminate group 14 metal dicyclohexyl-selenophosphinites (**CXXIV**) and (**CXXV**) (eq 33).

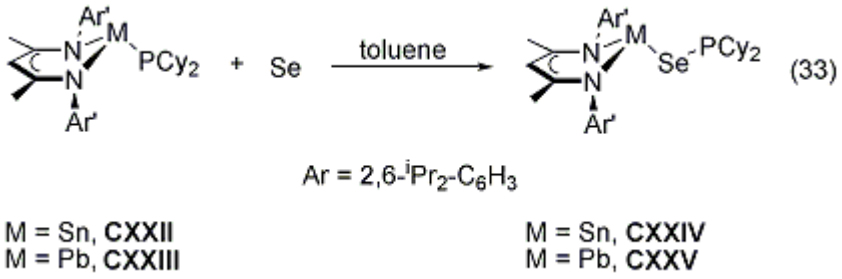

When the germanium dicyclohexylphosphide (**CXXVI**) was treated with excess sulfur in toluene, germanium sulfide (**CXXVII**) was generated (Scheme 30). In contrast, when tin dicyclohexylphosphide **CXXII** was treated with excess sulfur, oxidative addition of the metal centre resulted in the tin sulfide (**CXXVIII**) and a tin dicyclohexyl-phosphinodithioate complex (**CXXIX**) (Scheme 30). The lead dicyclohexylphosphide **CXXIII** exclusively generated the lead dicyclohexyl-phosphinodithioate complex (**CXXX**) under the same experimental conditions (Scheme 30). The difference in products is believed to be a result of the decreasing stability of the +4 oxidation state upon descending the group.

Scheme 30 Reactivity of [(BDI)MPCy$_2$] with excess sulfur (Ar' = 2,6-*i*Pr$_2$-C$_6$H$_3$; M = Ge, Sn, Pb).

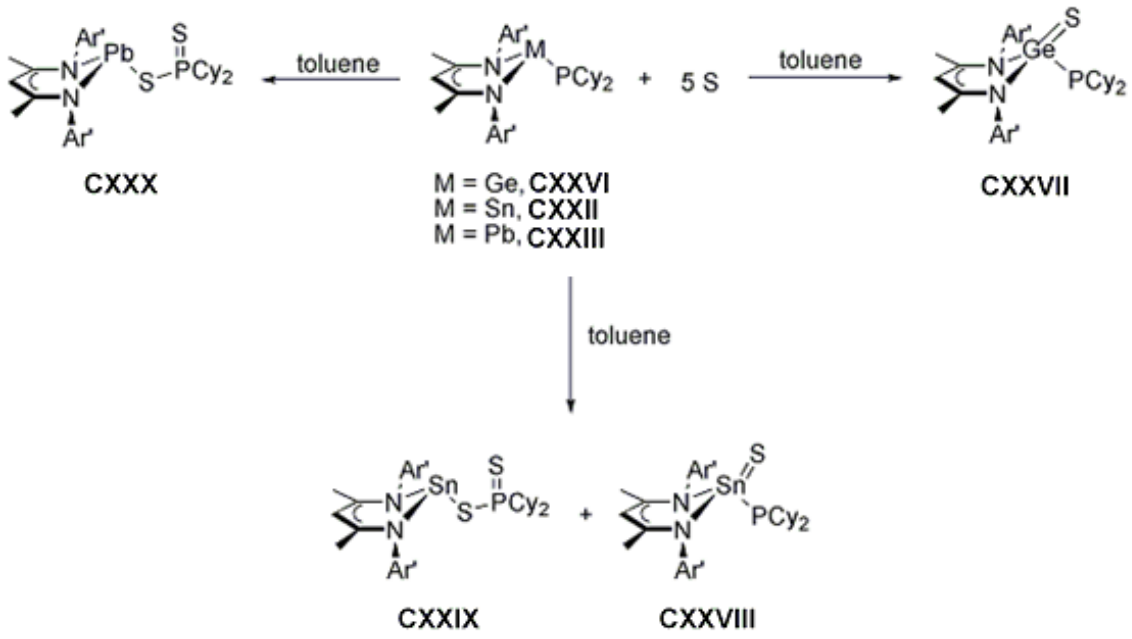

Treatment of the group 14 metal dicyclohexylphosphide complexes **CXXVI**, **CXXII** and **CXXIII** with excess selenium in toluene resulted in the formation of group 14 metal dicyclohexyl-phosphinodiselenoate complexes (**CXXXI**), (**CXXXII**) and (**CXXXIII**) (Scheme 31). Upon crystallisation of germanium dicyclohexyl-phosphinodiselenoate **CXXXI**, a small amount of crystals corresponding to germanium selenide (**CXXXIV**) were also found.

Scheme 31 Reactivity of [(BDI)MPCy$_2$] with excess selenium (Ar' = 2,6-*i*Pr$_2$-C$_6$H$_3$; M = Ge, Sn, Pb).

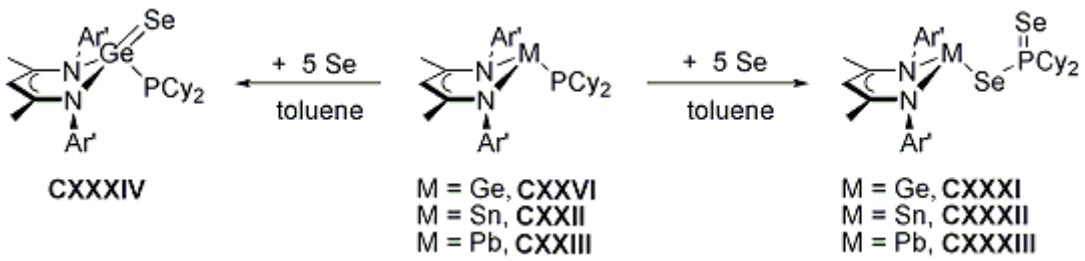

Treatment of the germanium trimethylsilylphosphide complex (**CXXXV**) with excess selenium in toluene produced the germanium selenide (**CXXXVI**), exclusively (Scheme 32). In contrast, treatment of the tin trimethylsilylphosphide complex (**CXXXVII**) with excess selenium in toluene produced the tin trimethylsilylselenide complex (**CXXXVIII**) (Scheme 32).

Scheme 32 Reactivity of [(BDI)MP(SiMe$_3$)$_2$] with excess selenium (Ar' = 2,6-*i*Pr$_2$-C$_6$H$_3$; M = Ge, Sn).

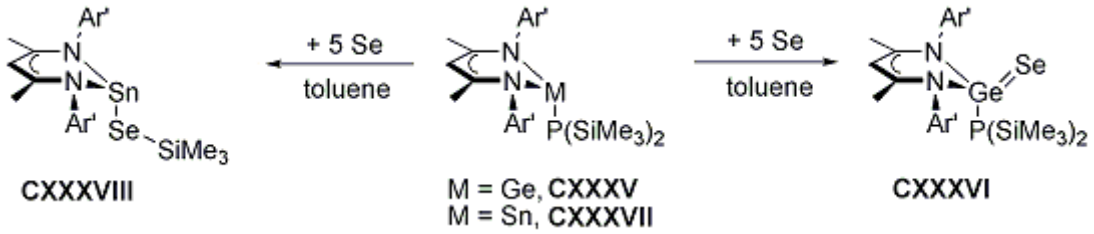

CXXXVIII M = Ge, **CXXXV** M = Sn, **CXXXVII** **CXXXVI**

As the tin dicyclohexylphosphide **CXXII** is believed to react with sulfur and selenium via the same reaction pathway, one equivalent of sulfur was introduced to tin dicyclohexyl-selenophosphinite **CXXIV** in a mixture of 1:1 toluene and pentane, resulting in the formation of tin dicyclohexyl-phosphinoselenothioate (**CXXXIX**) (eq 34).

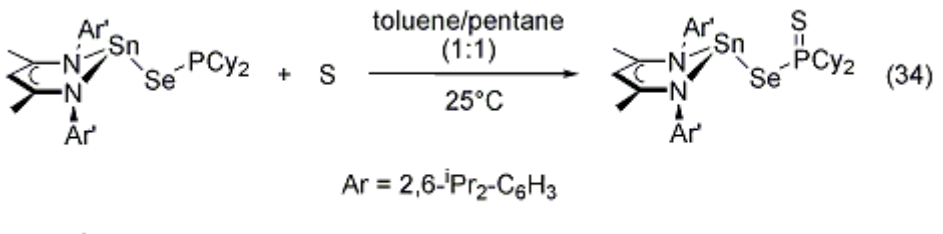

Ar = 2,6-^{i}Pr$_2$-C$_6$H$_3$

CXXXIV **CXXXIX**

3.2. Recent advances in group 14 metal chalcogenides as single source precursors (SSPs) for chemical vapour deposition (CVD)

The application of group 14 metal chalcogenides, namely metal tellurides, as low-band gap semi-conducting materials in solar cells, thermo-electric devices and telecommunications has generated much interest in the synthesis of these materials via chemical vapour deposition (CVD).[158] CVD is a generic name for a number of processes resulting in the deposition of thin solid films.[159] This process involves the transportation of a volatile molecular species into a reactor, where it adsorbs onto the surface of a substrate and reacts, resulting in the deposition of a material as a film. If only one molecular species is involved, the initial complex is called a single source precursor (SSP). The differences between the various CVD techniques are related to the initiation of the molecular species for transportation. Conventional CVD delivers volatile precursors to the reactor via a gas delivery system. The gas delivery system uses a predefined ratio of reactant gas to inert gas to be delivered into the reactor at a specified flow rate. If this involves metal-organic precursors than the method is known as metal-organic chemical vapour deposition (MOCVD). If CVD occurs at low pressure than the method is termed low-pressure chemical vapour deposition (LPCVD). However, if the precursor has low volatility or is thermally unstable than aerosol assisted chemical vapour deposition (AACVD) can be implemented instead. AACVD involves dissolving the precursor in an organic solvent, which is then transported by a carrier gas into a hot zone where it evaporates. This vapour is then transported to the substrate where the precursor adsorbs and reacts on the surface of the substrate. The use of single source precursors (SSPs) for CVD has the advantages that i) the preformed bonds lead to compounds with fewer defects, ii) the conditions of flow and temperature are more simple to control, iii) deposition utilises relatively simple installations, iv) several SSPs are air-stable and therefore easier to handle and characterise and v) they have the potential to reduce the environmental impact of material processing.[160] Due to the aims of this investigation, the synthesis of group 14 metal

chalcogenides in the form of thin films as a semi-conducting material, studies concentrating on the formation of nanocrystals will be excluded, with greater emphasis placed on the deposition of metal tellurides on thin films.

The availability of GeTe films has been limited by the lack of potential volatile, monomeric, thermally stable Ge(II) complexes suitable for CVD. The only GeTe films to be reported are by Chen et al.,[161] who were able to generate a GeTe film using a germanium terminal alkyl telluride complex, [Ge({N(SiMe$_2$CH$_2$CH$_2$Me$_2$Si)}$_2$)(*i*Pr)(Te*i*Pr)] (**CXL**) (Figure 34), as the SSP, using metal-organic chemical vapour deposition (MOCVD).

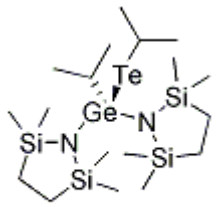

CXL

Figure 34 Germanium terminal alkyl telluride complex used to generate a GeTe film.

The formation of SnE thin films (where E = S and Se), has been reported using numerous SSPs such as tin *o*-xylyl dichalcogenoethers[158] (SnE films), thiosemicarbazone[162] (SnS films) and chelating dithiolate[163] (SnS films) ligand complexes with varying success.[164] The most recent, involving the tin *o*-xylyl diselenoethers, [SnCl$_4$(SeEt$_2$)$_2$] (**CXLI**), and the tin chalcogenoether complex, [SnCl$_4${*o*-C$_6$H$_4$(CH$_2$EMe)$_2$}] (**CXLII**) (Figure 35), by Reid et al.,[158] using low-pressure chemical vapour deposition (LPCVD), also provides a rare example of metal sulfide deposition from C-S bond fission in a thioether complex.

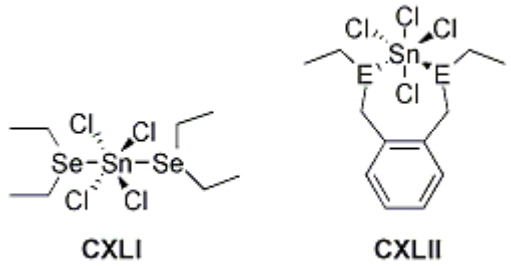

Figure 35 Tin thio- and selenoether complexes (E = S, Se).

The generation of SnTe thin films has also been reported using numerous SSPs, including the bis[bis(trimethylsilyl)methyl]tin chalcogenides (SnSe and SnTe films),[165,166] 2,2,4,4,6,6-hexabenzylcyclotristannatellurane[167] and a homoleptic tin(II) tellurolate incorporating the bulky [$TeSi(SiMe_3)_3$] ligand.[168] Dahmen et al., have reported the most recent compound of this type (in 1999), with the bis[bis(trimethylsilyl)methyl]tin chalcogenides, which were formed via MOCVD.[165,166]

Out of the group 14 metal chalcogenide films, the formation of PbE films (where E = S, Se and Te) are the most widely reported series. O'Brien et al. have published prolifically in this area, utilising complexes such as lead dithiocarbamate,[169,170] dichalcogenoimidodiphoshinate,[169,171] dialkyldiselenophosphinate[172] and xanthate[173] as the SSP complex. A series of lead dichalcogen imidodiphosphinate complexes, [$Pb\{N(PPh_2E)_2\}_2$] (where E = S, Se and Te) (**CXLIII**) (Figure 36),[169,171] have been successfully generated using aerosol assisted chemical vapour deposition (AACVD) (for the telluride complex) and low-pressure metal–organic chemical vapour deposition (LP-MOCVD) for the sulfide and selenide complexes.

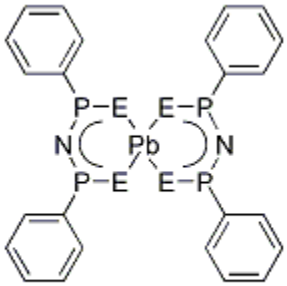

CXLIII

Figure 36 Lead dichalcogen imidodiphosphinate complexes (E = S, Se, Te).

In conclusion, interest in the formation of multiple bonded chalcogenide complexes of the group 14 metals has led to the generation of multiple bonded sulfur, selenium and tellurium moieties to germanium and tin centres, supported by ancillary ligands which thermodynamically and kinetically stabilise the monomeric complex and hence inhibit the tendency of these complexes to form bridged chalcogenide structures. Confusion relating to the labelling of the monomeric complexes as either kinetically or thermodynamically stabilised, due to alterations in Gibbs free energy upon coordination of the ligands, has resulted in the omission of this categorisation in this Chapter. Multiple bonded chalcogenide lead complexes have been restricted to sulfur, due to the increasingly stronger preference for σ bonds over π bonds down groups 14 and 16. Even though these complexes have, as yet, not been utilised as SSPs for chemical vapour deposition processes in order to create group 14 metal-chalcogen materials, there is potential in their application in this respect assuming these complexes are monomeric, volatile and thermally stable at the temperatures these processes take place at. However, modifications to the method can overcome some of these problems. The lack of GeE films (with only one GeTe film reported) and SnTe films provide potential opportunities for the use of these complexes.

3.3. Reactivity studies on β-diketiminate group 14 metal phosphides

3.3.1. β-diketiminate group 14 metal phosphide synthesis

The precursor β-diketiminate tin(II) chloride, [(BDI)SnCl], and lead(II) chloride, [(BDI)PbCl] **XXVII**, were synthesised as stated in Chapter 2.5, via a slight modification of known literature procedures.[108] The β-diketiminate germanium(II) chloride, [(BDI)GeCl] **XXVII**, was synthesised using similar experimental procedure to that of the aforementioned β-diketiminate metal(II) chloride complexes. Firstly, the lithiated β-diketiminate, [(BDI)Li] **XCIV**, was generated *in situ* through the addition of *n*-butyllithium to a THF solution of [(BDI)H] **XCIII**. The solution was then added to a THF solution of [$GeCl_2$.dioxane] and the resulting solution was stirred for 16 hours at room temperature, resulting in the formation of [(BDI)GeCl] **XXVII** (Scheme 33).

Scheme 33 Synthesis of β-diketiminate germanium chloride **XXVII** (Ar' = 2,6-*i*Pr_2-C_6H_3).

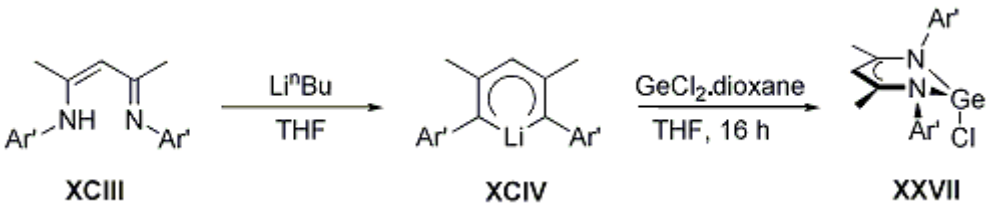

XCIII **XCIV** **XXVII**

A series of β-diketiminate group 14 metal phosphide complexes were thus generated via the treatment of a toluene solution of [(BDI)MCl] **XXVII** (M = Ge, Sn , Pb) with the appropriate lithiated phosphide salt,[115,157,174] affording group 14 metal phosphide complexes [(BDI)MPCy_2] (M = Ge **CXXVI**, Sn **CXXII**, Pb **CXXIII**) and [(BDI)MPPh_2] (M = Ge **CXLIV**, Sn **CXLV**, Pb **CXLVI**) (eq 35).

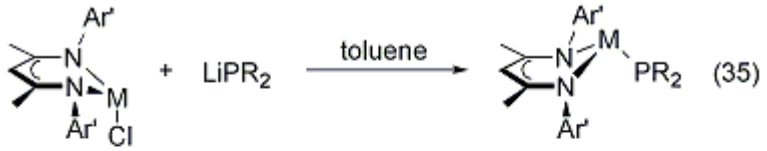

M = Ge, Sn, Pb
R = C_6H_{11}, C_6H_5

Ar' = 2,6-$^{i}Pr_2$-C_6H_3

XXVII

R = C_6H_{11}; M = Ge, **CXXVI**
M = Sn, **CXXII**
M = Pb, **CXXIII**
R = C_6H_5; M = Ge, **CXLIV**
M = Sn, **CXLV**
M = Pb, **CXLVI**

3.3.2. The reactivity of β-diketiminate group 14 metal phosphides with chalcogens

Reactivity studies by Tam investigating the behaviour of group 14 metal phosphide complexes with chalcogens were continued in this study.[115] Prior to this study, Tam examined the reactivity of the tin and lead dicyclohexylphosphide complexes (**CXXII** and **CXXIII**) with one equivalent of selenium, resulting in the formation of the corresponding tin and lead dicyclohexyl-selenophosphinite complexes (**CXXIV** and **CXXV**), as discussed in Chapter 3.1.1.[115] This study expanded upon Tam's results by investigating the reactivity of germanium, tin and lead dicyclohexylphosphide (**CXXVI**, **CXXII** and **CXXIII**, respectively) and diphenylphosphide (**CXLIV**, **CXLV** and **CXLVI**) complexes with one equivalent of chalcogen. In a typical reaction, germanium, tin and lead dicyclohexylphosphide (**CXXVI**, **CXXII** and **CXXIII**) and diphenylphosphide (**CXLIV**, **CXLV** and **CXLVI**) complexes were treated with a chalcogen (one equivalent of selenium or tellurium) in a toluene suspension, at room temperature, and the resulting mixture was stirred until the reaction was complete, as confirmed via ^{1}H NMR spectroscopy. Both the germanium dicylohexylphosphide and diphenylphosphide complexes (**CXXVI** and **CXLIV**) underwent insertion of selenium into the Ge-P bond to form dialkyl-selenophosphinite complexes (**16**) and (**17**) (eq 36). Out of these two germanium phosphide complexes, only

the germanium dicyclohexylphosphide was observed to undergo insertion of the tellurium into the Ge-P bond, forming germanium dicyclohexyl-tellurophosphinite (**18**) (eq 36).

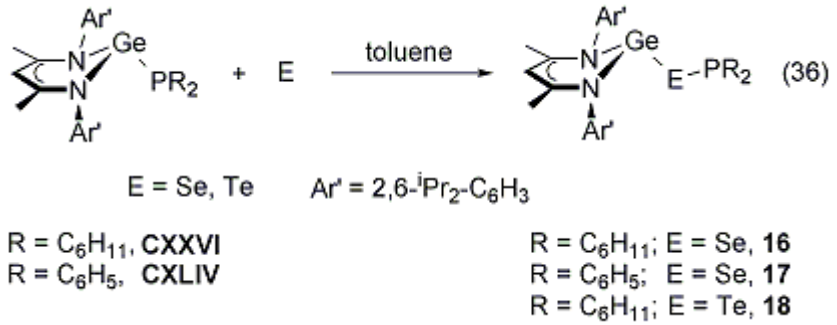

Treatment of the β-diketiminate germanium dicyclohexylphosphide **CXXVI** with one equivalent of selenium yielded the corresponding β-diketiminate germanium dicyclohexyl-selenophosphinite **16** after 24 hours at room temperature (eq 36).

Evidence for the germanium dicyclohexyl-selenophosphinite complex **16** was provided by ^{31}P NMR spectroscopy, with the presence of a new resonance at 41.9 ppm and satellites (198 Hz), caused by the splitting of the phosphinite resonance by the adjacent selenium atom (Figure 37). The magnitude of the coupling is consistent with a P-Se single bond, based on values found in literature.[115,119,175] The chemical shift (41.9 ppm) is significantly higher in frequency than the precursor germanium dicyclohexylphosphide complex **CXXVI** (-14.1 ppm). The ^{77}Se NMR spectrum has a doublet at -19.5 ppm, corresponding to a selenium functional group singly bonded to a phosphorus centre. Similar to the $J_{P\text{-}Se}$ in the ^{31}P NMR spectrum, the selenium-phosphorus coupling constant is 198 Hz. The ^{13}C NMR spectrum reveals resonances corresponding to the methyl group on the β-diketiminate backbone and the *ipso*-carbon in the phosphide's cyclohexyl group which have satellites consistent with coupling to a nearby NMR active nuclei. The magnitude of this coupling is similar to that found in the group 14 metal phosphide

complexes **CXXII**, **CXXIII** and **CXXVI** by Tam et al.[115,157] The coupling has been attributed to through-space scalar coupling of the carbon (methyl or cyclohexyl group) and phosphorus, however, the proximity of the methyl to the phosphorus is longer than that of the selenium and as phosphorus is 100% abundant, a doublet (not satellites) would be observed, therefore, carbon selenium coupling is more plausible. The IR spectra between the germanium dicyclohexyl-selenophosphinite complex **16** and the precursor are too similar to identify any vibrations associated with the Se-P/Ge bond.

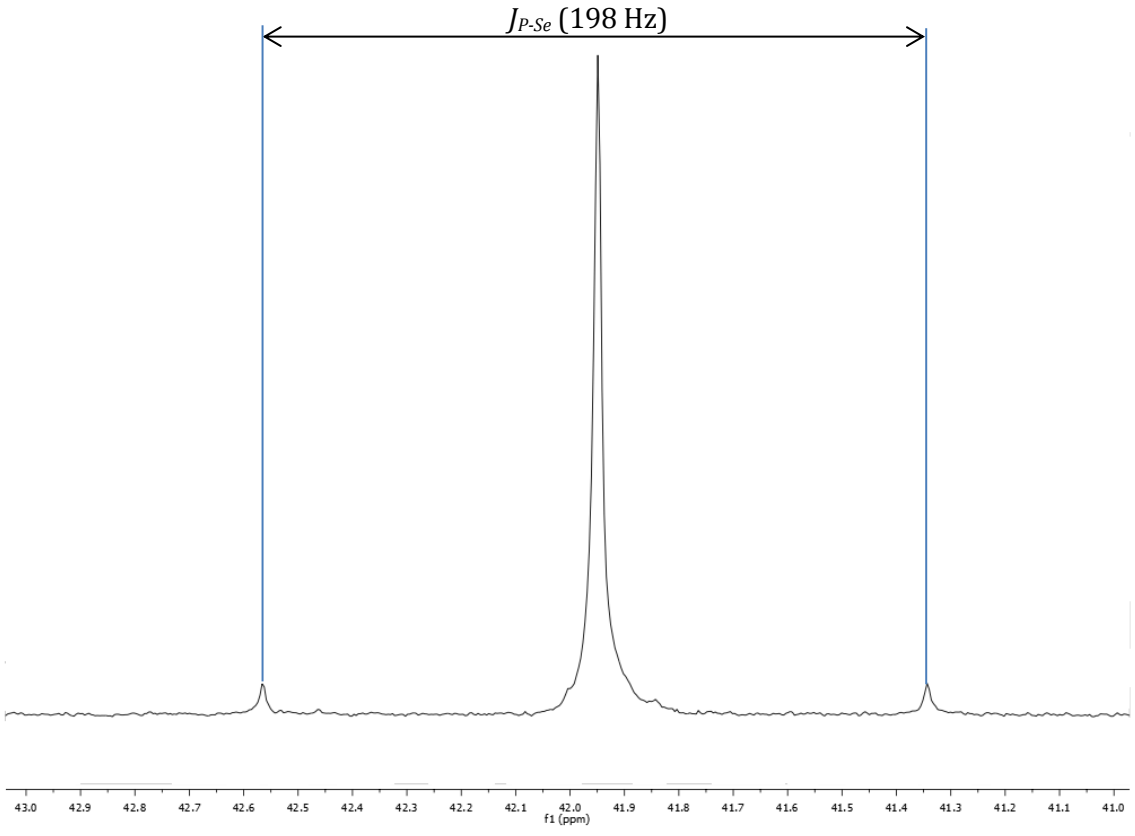

Figure 37 ^{31}P NMR spectrum of [(BDI)GeSePCy$_2$] **16**.

Orange crystals of the germanium dicyclohexyl-selenophosphinite complex **16** suitable for an X-ray diffraction study, were grown from a saturated toluene solution at -27°C (Figure 38). Selected bond lengths and angles are reported in Table 11. Complex **16**

adopts a distorted trigonal pyramidal geometry at germanium and an 'exo' conformation, similar to the precursor germanium dicyclohexylphosphide complex **CXXVI**.[115] The germanium centre is displaced from the NCCCN plane by 0.927 Å, similar to other displacement values reported for other germanium centres in the 'exo' conformation. The sum of the bond angles is 285.7° and DP is 82.6%, in line with the precursor complex **CXXVI** (291.9° and 75.6%).[115] The Ge-Se bond length is 2.4498(5) Å, which is longer than the mean Ge-Se single bond length value (2.384 Å) Parkin et al. reported for a two-coordinate selenium centre.[119] The Se-P bond length is 2.2602(9) Å, this is longer than the Se-P bond in the complex $[(Ph_3Ge)_2\{\mu\text{-Se, Se-P(OEt)}_2\}]$ (2.2190(17) Å).[176] The Ge-Se-P bond angle is 94.07(3)°, which is more acute than $[(Ph_3Ge)_2\{\mu\text{-Se, Se-P(OEt)}_2\}]$ (105.24(5)°).[176]

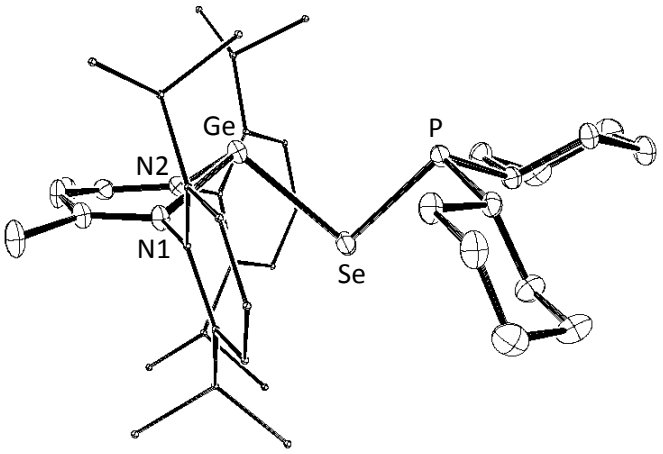

Figure 38 ORTEP diagram of $[(BDI)GeSePCy_2]$ **16**. Aryl groups situated on the BDI ligand are minimised and the hydrogen atoms are omitted for clarity. Thermal ellipsoids are shown at 30%.

Table 11 Selected bond lengths (Å) and angles (°) for [(BDI)GeEPR$_2$] (E = Se when R = Cy, Ph or E = Te when R = Cy).

	[(BDI)GeSePCy$_2$], **16**	[(BDI)GeSePPh$_2$], **17**	[(BDI)GeTePCy$_2$], **18**
N1-Ge	2.027(2)	2.0108(18)	2.019(4)
N2-Ge	2.024(2)	2.0224(19)	2.022(4)
Ge-E	2.4498(5)	2.4490(4)	2.6516(6)
E-P	2.2602(9)	2.2524(7)	2.4705(13)
N1-Ge-N2	88.07(10)	88.20(8)	87.67(15)
N1-Ge-E	100.66(7)	97.17(6)	101.67(12)
N2-Ge-E	96.98(7)	100.54(6)	98.83(12)
Ge-E-P	94.07(3)	90.27(2)	88.12(3)
Sum of angles	285.7	285.9	288.2
DP	82.6	82.3	79.8
Ge-NCCCN plane	0.927	0.986	0.996

The β-diketiminate germanium diphenyl-selenophosphinite complex **17** was generated through the addition of one equivalent of selenium to a toluene solution of β-diketiminate germanium diphenylphosphide **CXLIV** and stirred for 10 days at room temperature (eq 36).

Spectroscopy analysis (^{1}H and ^{31}P NMR spectroscopy), show the presence of two products, where one of the products is the germanium diphenyl-selenophosphinite complex **17** and the other is the decomposition product resulting in a diphenylphosphine dimer **19**. This latter complex increases in concentration over time at the expense of the germanium diphenyl-selenophosphinite complex **17** regardless of restrictions to light exposure and temperature reduction to -27°C. Attempts to exclusively generate complex

17 by reducing the reaction time only resulted in the presence of the unreacted precursor complex **CXLIV**. The two products are observed in the ^{31}P NMR spectrum with the presence of two resonances at 11.1 ppm and -14.9 ppm. The resonance located at the higher frequency (11.1 ppm) is identified as the germanium diphenyl-selenophosphinite complex **17** due to the presence of selenium satellites (219 Hz), consistent with a P-Se single bond.[115,175] The ^{77}Se NMR spectrum reveals a doublet at 136.5 ppm, with a $J_{Se\text{-}P}$ of 217 Hz, consistent with the coupling observed in the ^{31}P NMR spectrum. The chemical shift of the diphenylphosphine dimer **19** in the ^{31}P NMR spectrum is located at the lower frequency (-14.9 ppm) and is similar to the literature value.[177,178] The phosphorus signal of the germanium diphenyl-selenophosphinite complex **17** is much higher in frequency than the precursor germanium diphenylphosphide complex **CXLIV** (-36.0 ppm).[115]

X-ray diffraction studies were undertaken on orange crystals of the germanium diphenyl-selenophosphinite complex **17**, which were grown from a saturated ether solution at -27°C (Figure 39). Selected bond lengths and angles are reported in Table 11. Similar to the precursor germanium diphenylphosphide complex **CXLIV**, the germanium diphenyl-selenophosphinite complex **17** exhibits a distorted trigonal pyramidal geometry at germanium and an 'exo' conformation. Due to the adoption of this conformation, values for the displacement of the germanium centre from the NCCCN plane of 0.986 Å are similar to the germanium dicyclohexyl-selenophosphinite complex **16** (0.927 Å), as is the sum of the bond angles at 285.9° and the DP at 82.3% (the dicyclohexylphosphides values are 285.7° and 82.6%). The Ge-Se bond length is 2.4490(4) Å, which is longer than the mean single bond length value reported by Parkin,[119] but within experimental error of the analogous bond length for the germanium dicyclohexyl-selenophosphinite complex **16** (2.4498(5) Å). Furthermore, the Se-P bond length of the complex **17** is 2.2524(7) Å, which is only slightly shorter than that of the dicyclohexylphosphide derivative (2.2602(9) Å), but longer than [$(Ph_3Ge)_2\{\mu$-Se, Se-P$(OEt)_2\}$] (2.2190(17) Å).[176] The Ge-Se-P bond angle is an acute 90.27(2)°, which is similar to that observed in **16** (94.07(3)°).

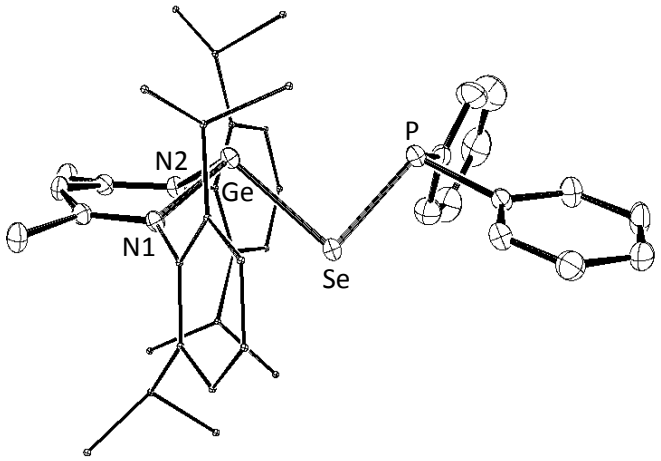

Figure 39 ORTEP diagram of [(BDI)GeSePPh$_2$] **17**. Aryl groups situated on the BDI ligand are minimised and the hydrogen atoms are omitted for clarity. Thermal ellipsoids are shown at 30%.

Spectral data of the diphenylphosphine dimer complex **19** has been published by Neumüller.[178] X-ray diffraction studies undertaken on the crystals of the diphenylphosphine complex **19**, grown in an ether solution at -27°C, confirm the identity of this complex. However, the complex was found to exist in a different space group from that reported in literature. Neumüller reported the diphenylphosphine complex **19** to exist in the P 2_1/n space group,[178] in contrast, this study found the space group to be P 2_1/c (Figure 40).

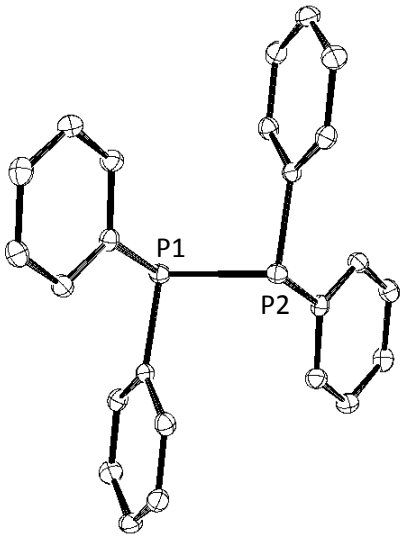

Figure 40 ORTEP diagram of [P_2Ph_4] **19**. The hydrogen atoms are omitted for clarity and thermal ellipsoids are shown at 30%.

The β-diketiminate germanium dicyclohexyl-tellurophosphinite complex **18** was formed upon addition of a toluene suspension of one equivalent of tellurium to a toluene solution of β-diketiminate germanium dicyclohexylphosphide **CXXVI** (eq 36).

Evidence for the β-diketiminate germanium dicyclohexyl-tellurophosphinite complex **18** was obtained through NMR spectroscopy analysis. The ^{31}P NMR spectrum shows a new resonance at 26.1 ppm, this chemical shift is higher in frequency than the precursor germanium dicyclohexylphosphide complex **CXXVI** (-14.1 ppm),[115] but lower in frequency than the germanium dicyclohexyl-selenophosphinite complex **16** (41.9 ppm). The presence of satellites, caused by phosphorus-tellurium coupling, has a magnitude of 407 Hz, which is smaller than the tellurium-phosphorus coupling in [Te{$P(NR_2)_2$}$_2$] (R = Me_2CH) (562 Hz).[175] The ^{125}Te NMR spectrum displays a doublet at -296.8 ppm with a coupling constant of 406 Hz, consistent with the tellurium-phosphorus coupling constant found in the ^{31}P NMR spectrum (Figure 41). Similar to the germanium dicyclohexyl-selenophosphinite complex **16**, coupling in the ^{13}C NMR spectrum corresponding to the

phenyl and methyl groups is observed due to through-space scalar coupling of the carbon to the chalcogen. The IR spectrum does not provide evidence of the germanium dicyclohexyl-tellurophosphinite complex **18** due to the absence of extra vibrations that could correspond to the new product.

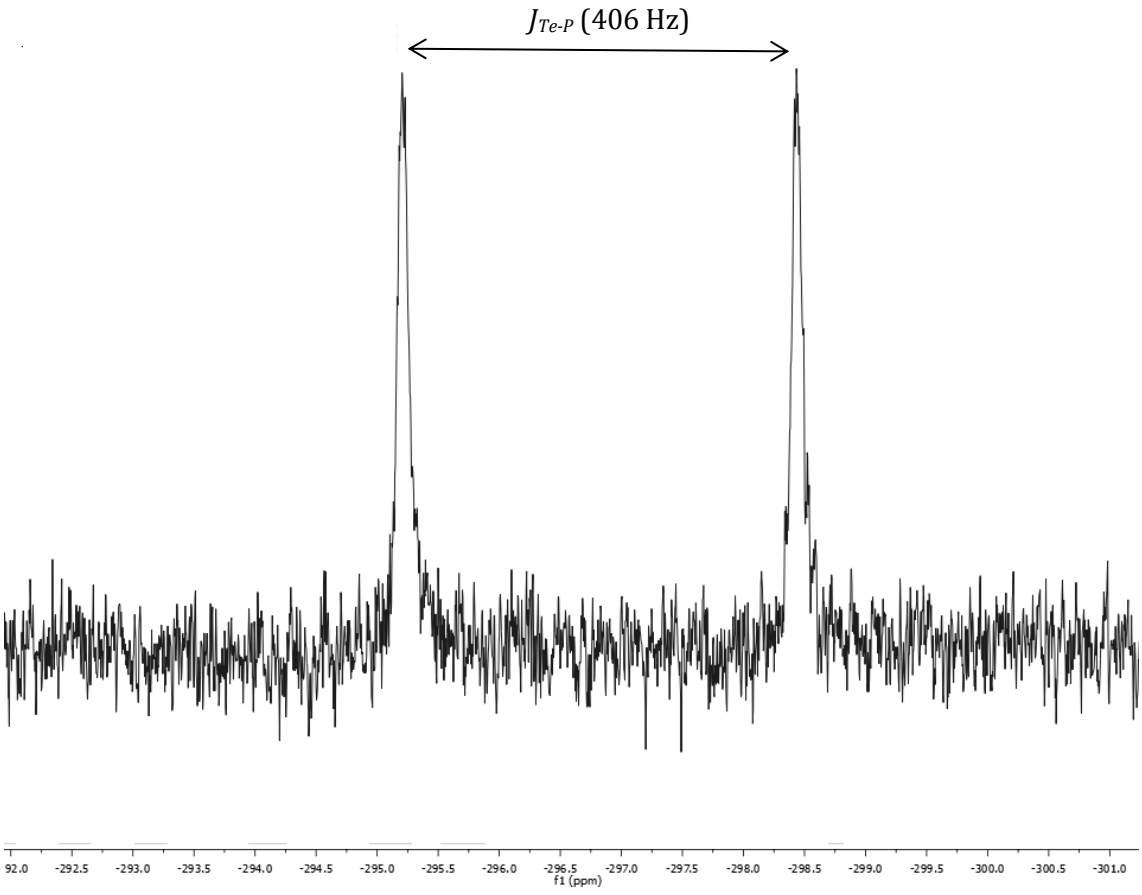

Figure 41 ^{125}Te NMR spectrum of [(BDI)GeTePCy$_2$] **18**.

Red crystals of the germanium dicyclohexyl-tellurophosphinite complex **18** suitable for X-ray diffraction analysis were grown from pentane at -27°C (Figure 42). Selected bond lengths and angles are reported in Table 11. The complex exhibits a distorted trigonal pyramidal geometry around the germanium and an 'exo' conformation, like the other germanium phosphide complexes (**CXXVI** and **CXLIV**)[115] and germanium

selenophosphinite complexes (**16** and **17**). The displacement of the germanium centre from the NCCCN plane, of 0.996 Å, is similar to the aforementioned germanium complexes. Furthermore, the sum of the bond angles is 288.2° and the DP is 79.8%, with similar values to complexes **16** and **17**. The Ge-Te bond length is 2.6516(6) Å, which is longer than the mean single bond length value stated by Parkin et al. at 2.595 Å,[119] whilst the Te-P bond length is 2.4705(13) Å, which is shorter than Niecke's average Te-P bond length (2.568 Å) for [((Me$_2$CHN)$_2$P)$_2$Te].[175] The Ge-Te-P bond angle of 88.12(3)° is slightly more acute than the P-Te-P bond angle in [((Me$_2$CHN)$_2$P)$_2$Te] (94.4(1)°).[175]

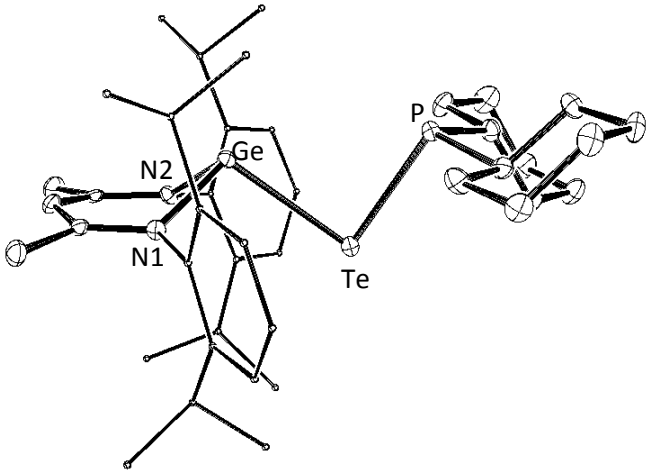

Figure 42 ORTEP diagram of [(BDI)GeTePCy$_2$] **18**. Aryl groups situated on the BDI ligand are minimised and the hydrogen atoms are omitted for clarity. Thermal ellipsoids are shown at 30%.

Addition of one equivalent of tellurium, suspended in toluene, to a toluene solution of the diphenylphosphide complexes, **CXLIV**, **CXLV** and **CXLVI**, or the dicyclohexylphosphide complexes, **CXXII** and **CXXIII**, resulted in no reaction, even at elevated temperature, over a prolonged time period.

Questions arising from this study centre on the chemical behaviour displayed by the precursor metal phosphide complexes with respect to their reactivity with one equivalent of selenium or tellurium. Firstly, previous studies on other group 14 metal complexes with chalcogens show oxidative addition at the metal centre, either creating i) a terminal chalcogenide moiety with a double bond between the metal centre and chalcogenide or ii) two single bonds between the chalcogenide and two metal centres and the formation of a dimer or oligomer (Scheme 34).

Scheme 34 Alternative products of oxidative addition of group 14 metal complexes (L = ligand; M = Ge, Sn, Pb) with chalcogens (E).

The mechanism resulting in the dialkyl-chalcogenophosphinite complexes, **16**, **17** and **18**, is not simple oxidative addition. A mechanism proposed by Tam,[115] based on a proposal by Escudie et al.,[179] involve the chalcogen either coordinating to the germanium centre (Route A) or phosphorus (Route B). Both pathways then form a three-membered heterocycle with the germanium centre and phosphorus, with the chalcogen then inserting into the Ge-P bond, resulting in the overall insertion of the chalcogenide into the Ge-P bond (Scheme 35).

Scheme 35 Proposed mechanism for chalcogen insertion (E = Se, Te) into the Ge-P bond in the germanium phosphide complexes, [(BDI)GePR$_2$] (L = BDI^{dipp}; R = Cy, Ph).

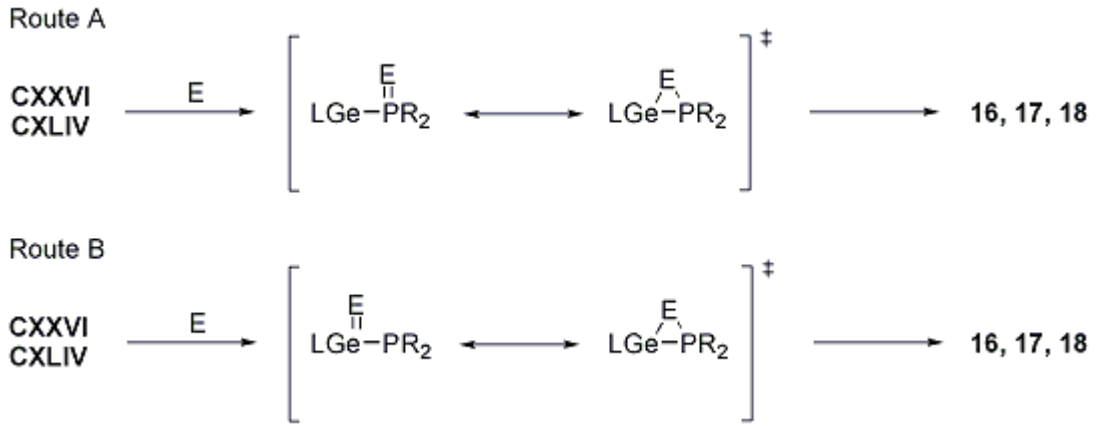

The lack of net oxidative addition at the germanium can be attributed to the relative reactivity of phosphorus vs. germanium, thus generating a separate reaction pathway for the chalcogen in comparison to other systems. For example, oxidative addition at germanium was observed for divalent germanium alkyls, amides, chlorides and hydroxides bearing an ancillary β-diketiminate ligand with sulfur and selenium.[144] This shows oxidative addition of the germanium centre, coordinated to a terminal ligand and a β-diketiminate ligand, by a chalcogen is plausible, however, when that terminal ligand is a phosphide and the chalcogen is selenium or tellurium, this is not always observed. The competing reactivity between the germanium and phosphorus centres was shown by Tam upon addition of excess selenium to germanium phosphide complexes **CXXVI** and **CXXXV**, where the germanium selenide complexes **CXXXIV** and **CXXXVI** were isolated, in addition to the interspersion of crystals of β-diketiminate germanium dicyclohexyl-phosphinodiselenoate **CXXXI** with the latter.[115]

In this study, only one complex, β-diketiminate germanium dicyclohexylphosphide **CXXVI**, reacted with tellurium. This is consistent with the relatively lower reactivity of tellurium compared to the lighter chalcogens. However, the lack of reactivity with the tin

and lead complexes is unexpected as these heavier group 14 complexes have shown more facile reactivity with both sulfur and selenium compared to germanium.[115]

3.3.3. The reactivity of β-diketiminate group 14 metal phosphides with excess chalcogen

The second part of this study involved the addition of five equivalents (an excess) of selenium or tellurium, suspended in toluene, to a toluene solution of a group 14 metal phosphide complex, which was either the germanium, tin or lead dicyclohexylphosphide complex (**CXXVI**, **CXXII** and **CXXIII**) or the diphenylphosphide complex (**CXLIV**, **CXLV** and **CXLVI**). The solution was stirred at room temperature for 24 hours.

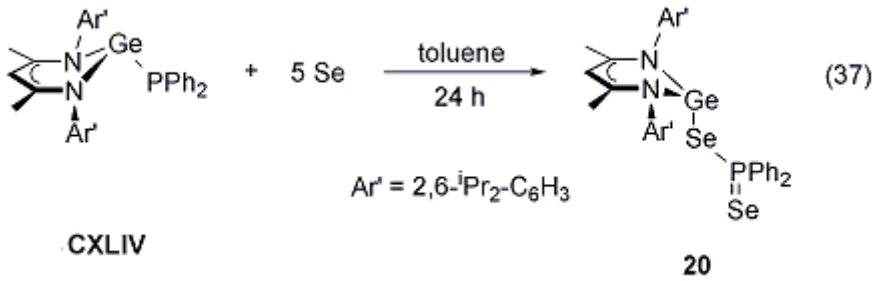

CXLIV **20**

The β-diketiminate germanium diphenyl-phosphinodiselenoate **20** was generated upon addition of five equivalents of selenium, suspended in toluene, to a toluene solution of β-diketiminate germanium diphenylphosphide **CXLIV** (eq 37). The solution was left to stir for 24 hours at room temperature and the complex was purified via crystallisation in ether. In contrast to the previously reported β-diketiminate germanium dicyclohexyl-phosphinodiselenoate complex **CXXXI**, the product was found to be insoluble in non-polar solvents, such as toluene.

Two new compounds, **A** and **B**, were formed from this reaction mixture (Figure 43). Over several days the ratio of the products changed, with the concentration of compound **A** found to increase while the concentration of compound **B** decreased. The ^{31}P NMR spectrum shows both products have phosphorus and selenium, and the satellites are consistent with phosphorus–selenium coupling (Figure 43). The coupling constants are significantly different for both products, where compound **A**, with a chemical shift of 26.3 ppm, is 579 Hz, and compound **B**, with a shift of 19.1 ppm, is 201 Hz. Both resonances are located in a similar range, but significantly higher in frequency than the precursor germanium diphenylphosphide **CXLIV** (-36.0 ppm)[115] or the germanium diphenyl-selenophosphinite **17** (11.1 ppm). This is not only consistent with the presence of selenium in both complexes, but there is more than one selenium atom in each of the products. Compound **A** and **B** have similar phosphorus-selenium coupling constant values to those found by Tam for the germanium dicyclohexyl-phosphinodiselenoate **CXXXI** (551 Hz and 198 Hz).[115] The presence of two different coupling constants recorded for the same complex by Tam, could be caused by the presence of two different complexes (similar to the reaction with the diphenylphosphide complex) even though a single product was isolated, i.e. the germanium dicyclohexyl-phosphinodiselenoate **CXXXI**.[115] Attempts to isolate compounds **A** and **B**, resulted in the isolation of only one compound for X-ray diffraction analysis, the germanium diphenyl-phosphinodiselenoate complex **20**. Failure to isolate pure samples of **A** or **B** prevented conclusive assignment of resonances in the ^{1}H and ^{13}C NMR spectra. Furthermore, the low concentration of crystals used for the representative ^{13}C NMR spectrum prevents conclusive assignment of all the resonances in the spectra or detailed analysis of the origin of the coupling for some of the resonances. However, similar to the germanium dicyclohexyl-selenophosphinite complex **16**, coupling is observed in the ^{13}C NMR spectrum and is consistent with through-space scalar coupling between the phenyl and methyl groups with the selenium.

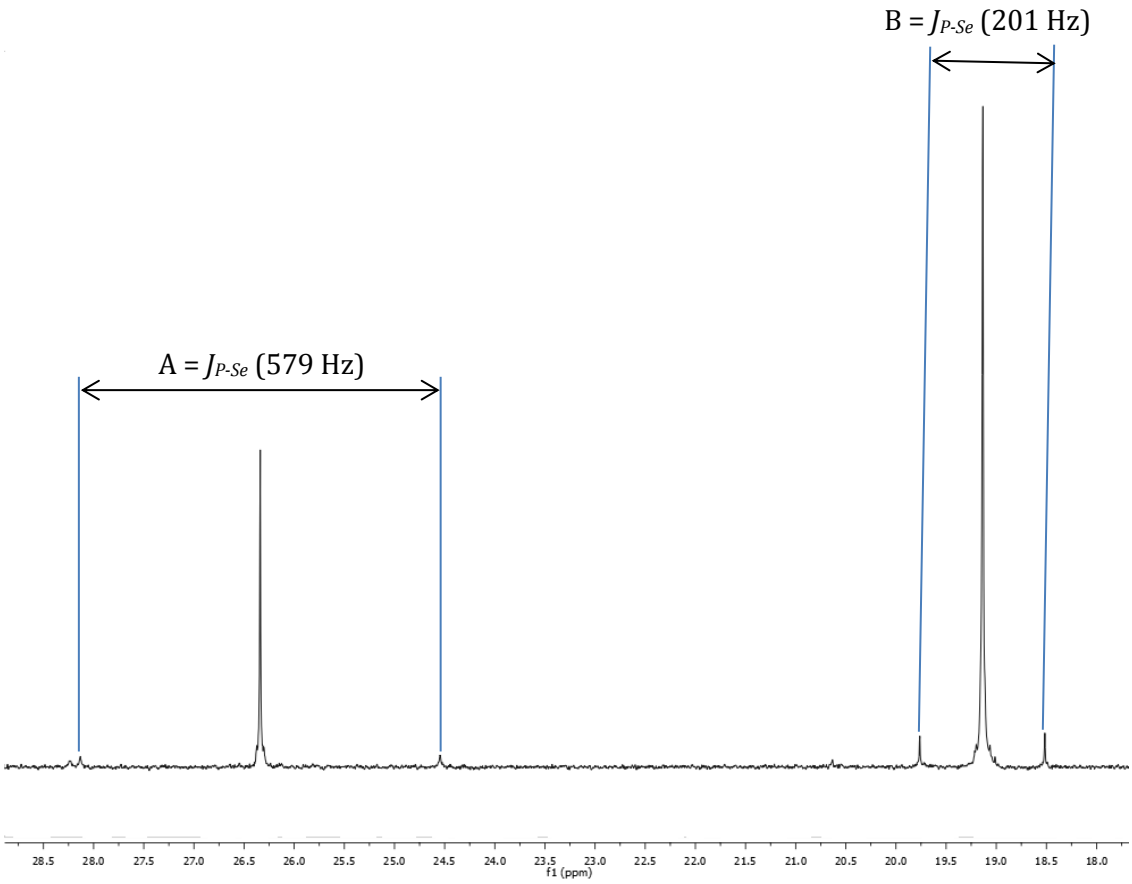

Figure 43 ^{31}P NMR spectrum of **A** and **B**, where **A** or **B** is [(BDI)GeSeP(Se)Ph$_2$] **20**.

X-ray diffraction analysis was performed on yellow crystals of the germanium diphenyl-phosphinodiselenoate complex **20** which were grown in ether at -27°C (selected bond lengths and angles reported in Table 12) (Figure 44). The complex adopts a distorted trigonal pyramidal geometry and an 'endo' conformation, in contrast to the 'exo' conformations adopted by the germanium phosphide complexes (**CXXVI** and **CXLIV**)[115] and the germanium dialky-chalcogenophosphinite complexes (**16** and **17**). The germanium atom is displaced from the NCCCN plane by a significantly low 0.020 Å and the sum of the bond angles is 282.9° with a DP of 85.7%. The Ge-Se1 bond length is 2.5390(5) Å, which is longer than the mean bond length reported by Parkin et al.[119] and the same bonds in the complex [(Ph$_3$Ge)$_2${μ-Se, Se-P(OEt)$_2$}] (2.4050(9) Å)[176] and the germanium dicyclohexyl-phosphinodiselenoate **CXXXI** (2.4613(4) Å).[115] The Se1-P bond length of

2.2209(10) Å is marginally longer, but within experimental error of the Se1-P bond in the germanium dicyclohexyl-phosphinodiselenoate **CXXXI** (2.2208(7) Å)[115] and the complex [$(Ph_3Ge)_2${μ-Se, Se-P$(OEt)_2$}] (2.2190(17) Å).[176] The P-Se2 bond length of 2.1172(10) Å is longer than the corresponding bond in [$(Ph_3Ge)_2${μ-Se, Se-P$(OEt)_2$}] (2.0775(17) Å)[176] and longer than that in the germanium dicyclohexyl-phosphinodiselenoate **CXXXI** (2.1114(7) Å).[115] The Ge-Se-P bond angle of 100.00(3)° is slightly more acute than the germanium dicyclohexyl-phosphinodiselenoate (100.77(2)°). The Se1-P-Se2 bond angle of 115.48(4)° is consistent with germanium dicyclohexyl-phosphinodiselenoate (117.92(3)°).

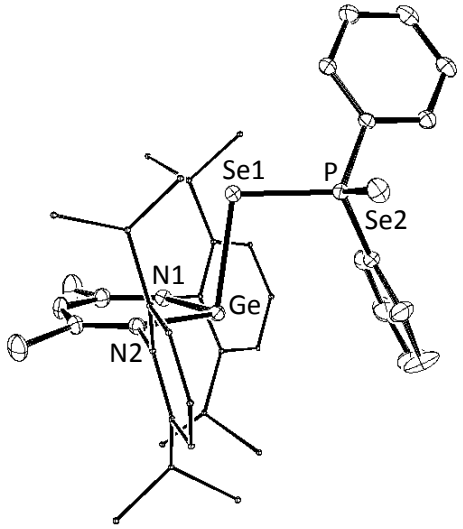

Figure 44 ORTEP diagram of [(BDI)GeSeP(Se)Ph_2] **20**. Aryl groups situated on the BDI ligand are minimised and the hydrogen atoms are omitted for clarity. Thermal ellipsoids are shown at 30%.

Table 12 Selected bond lengths (Å) and angles (°) for [(BDI)GeSeP(Se)Ph_2].

[(BDI)GeSeP(Se)Ph_2], **20**			
N1-Ge	2.004(3)	N2-Ge-Se1	95.75(8)
N2-Ge	2.006(3)	Ge-Se1-P	100.00(3)
Ge-Se1	2.5390(5)	Se1-P-Se2	115.48(4)
Se1-P	2.2209(10)	Sum of angles	282.9
Se2-P	2.1172(10)	DP	85.7
N1-Ge-N2	91.17(11)	Ge-NCCCN plane	0.020
N1-Ge-Se1	95.96(8)		

The relatively planar metallacycle, in contrast to that of **CXXXI**, is consistent with a cationic metal centre. In general, as the terminal ligand becomes more able to bear a negative charge, the group 14 metallacycle becomes relatively planar. This is observed for [(BDI)SnOTf],[71] [(BDI)PbOTf],[79] as well as isolated $[(BDI)Ge]^+$,[180] $[(BDI)Sn]^+$[83] and $[(BDI)Pb]^+$ cations.[83] The $[SeP(Se)Ph_2]$ anion is a selenium derivative of a diphenyl phosphinate, as such, the negative charge can be not only shared over both selenium centres, but also within the two phenyl groups, resulting in a stable anion. In contrast, the alkyl derivative, $[SeP(Se)Cy_2]^-$, is less able to form a stable anion and thus forms a more covalent Ge-Se bond.

Addition of five equivalents of tellurium, in toluene, to a solution of the germanium, tin or lead diphenylphosphide complexes or the tin and lead dicyclohexylphosphide complexes did not result in a reaction, even at elevated temperature, over a prolonged amount of time. These results are consistent with the reactivity displayed by these complexes with one equivalent of the chalcogen, which could be due to the reduction in σ bond energies for M=Te complexes upon descending group 16

(as discussed before for the one equivalent reactions).[181] In contrast, the addition of excess tellurium to a toluene solution of germanium dicyclohexylphosphide **CXXVI** resulted in the germanium dicyclohexyl-tellurophosphinite complex **18**, the same product which is formed when one equivalent of tellurium is added. This could be due to steric congestion around the phosphorus so that only one tellurium is able to coordinate to the phosphorus, due to tellurium's larger radius (2.21 Å)[182] relative to that of selenium's (1.98 Å),[182] however, electronic factors should not be ignored.

The synthesis of the mixed chalcogen system [(BDI)SnSeP(S)Cy_2] **CXXXIX** by Tam[115] provided a precedent for this system and the potential development of mixed chalcogen systems in this study. As a result, one equivalent of selenium was suspended in toluene and added to the germanium dicyclohexyl-tellurophosphinite complex **18** in toluene. In contrast to the reactivity which resulted in the formation of Tam's [(BDI)SnSeP(S)Cy_2] complex,[115] the germanium dicyclohexyl-selenophosphinite complex **16** was generated instead, where the selenium displaced the tellurium from the complex. Similar reactivity has been observed by Parkin et al.,[119] where a terminal chalcogen (E = Se, Te) coordinated to a germanium was displaced by sulfur within the macrocycle complex, [(η^4-Me_8taa)GeE]. This reactivity reflects the relative bond strengths between the Ge-S, Ge-Se and Ge-Te bonds, as bond strengths increase with the lighter chalcogens.

3.3.4. Summary of β-diketiminate group 14 metal phosphides

In summary, reactivity studies were conducted on a series of germanium, tin and lead phosphide complexes, [(BDI)MPR_2], (R = Cy and M = Ge (**CXXVI**), Sn (**CXXII**), Pb (**CXXIII**); R = Ph and M = Ge (**CXLIV**), Sn (**CXLV**), Pb (**CXLVI**)) via the addition of one or five equivalents of the chalcogens, selenium and tellurium. Upon addition of one equivalent of the chalcogens, selenium and tellurium, insertion products [(BDI)GeEPR_2] (E = Se and R = Cy (**16**), Ph (**17**); E = Te and R = Cy (**18**)) were generated. Upon addition of

five equivalents of selenium to the germanium diphenylphosphide complex **CXLIV**, a further selenium is coordinated to the phosphorus, resulting in the formation of germanium diphenyl-phosphinodiselenoate **20**. Similar to the group 14 metal phosphide precursors, the newly synthesised products are air-sensitive, isolable by crystallisation and partially characterised by multinuclear NMR spectroscopy, IR spectroscopy, elemental analysis and X-ray crystallography. Complete characterisation was prevented by time restrictions. The characterisation data shows all complexes adopting a distorted trigonal pyramidal geometry due to a stereochemically active lone pair occupying the fourth vertex, thus affecting the values for the sum of the bond angles and DP. With respect to the germanium dialkyl-chalcogenophosphinite complexes, **16**, **17** and **18**, the X-ray data shows only slight structural differences between the complexes, with slightly larger differences observed between the selenophosphinite complexes, **16** and **17**, and the tellurophosphinite complex, **18**. For example, the sum of the bond angles and DP are very similar between all the germanium phosphinite complexes, ranging between 285.7° and 82.6% (dicyclohexyl-selenophosphinite **16**) to 288.2° and 79.8% (dicyclohexyl-tellurophosphinite **18**). Furthermore, bond lengths are similar, with greater similarity between the selenophosphinite complexes compared to the tellurophosphinite complex, which is due to the difference in the chalcogen. The displacement of the germanium centre from the NCCCN plane displays similar values, however, the dicyclohexyl-selenophosphinite **16** has the smallest displacement value of 0.927 Å relative to the other selenophosphinite **17** and tellurophosphinite **18** complexes (0.986 Å and 0.996 Å, respectively). The chemical shift of the phosphorus in the ^{31}P NMR spectrum of the dicyclohexyl-selenophosphinite complex **16** is higher in frequency than the isostructural germanium dicyclohexyl-tellurophosphinite complex **18**, presumably due to the higher electronegativity of selenium relative to tellurium.

3.4. Computational studies on β-diketiminate Ge(II) phosphide complexes

Density functional theory (DFT) studies were performed on the germanium dialkyl-chalcogenophosphinite complexes, **16**, **17** and **18**. Geometry optimization calculations were undertaken on the entire molecule for the germanium phosphinite complexes, the level of theory used was B3LYP DFT and Lanl2dz pseudopotentials, including a d type polarization function[183] and the effective core potential,[184] on the germanium, phosphorus and chalcogens and 6-31 g* on all other atoms. However, the calculation for the phosphinite **16** consistently crashed before completion so that no results could be obtained. In contrast, the structural parameters which were calculated for the germanium complexes, **17** and **18**, correlate well with the X-ray crystallography data with the range of discrepancies between the two data sets calculated to be between 0.45% and -4.85% (Table 13).

Table 13 X-ray crystallography data of germanium dialkyl-chalcogenophosphinite complexes, **17** and **18**, compared with computed bond distances (Å) and angles (deg) at the B3LYP/Lanl2dz/6-31 g* level of theory (E = Se, Te).

		[(BDI)GeSePPh$_2$], ***17***	*[(BDI)GeTePCy$_2$],* ***18***
Ge-N1	*Expt*	2.011	2.019
	Calcd	2.056	2.074
	% Diff	**-2.24**	**-2.72**
Ge-N2	*Expt*	2.022	2.022
	Calcd	2.092	2.087
	% Diff	**-3.46**	**-3.21**
Ge-E	*Expt*	2.449	2.652

	Calcd	2.511	2.730
	% Diff	**-2.53**	**-2.94**
E-P	*Expt*	2.252	2.471
	Calcd	2.324	2.534
	% Diff	**-3.20**	**-2.55**
Ge···P	*Expt*	3.335	3.564
	Calcd	3.480	3.706
	% Diff	**-4.35**	**-3.98**
C1-N1	*Expt*	1.322	1.323
	Calcd	1.341	1.339
	% Diff	**-1.44**	**-1.21**
C3-N2	*Expt*	1.322	1.337
	Calcd	1.331	1.335
	% Diff	**-0.68**	**0.15**
N1-Ge-N2	*Expt*	88.21	87.67
	Calcd	88.97	88.76
	% Diff	**-0.86**	**-1.24**
N1-Ge-E	*Expt*	97.18	101.67
	Calcd	98.96	101.43
	% Diff	**-1.83**	**0.24**
N2-Ge-E	*Expt*	100.55	98.83
	Calcd	101.56	103.62
	% Diff	**-1.00**	**-4.85**
Ge-E-P	*Expt*	90.27	88.12
	Calcd	91.98	89.45
	% Diff	**-1.89**	**-1.51**

The molecular orbital diagrams were successfully obtained from the checkpoint files for the phosphinites **17** and **18**. As a result of this, discussion of the molecular orbital diagrams and hybridisation will be restricted to the two phosphinites, **17** and **18**. The germanium diphenyl-selenophosphinite complex **17** has a phosphorus lone pair occupying the molecular orbital positioned at HOMO-15 (-197.59 kcal mol^{-1}), whereas the germanium has a lone pair situated at the HOMO-16 molecular orbital (-199.18 kcal mol^{-1}) (Figure 45). The molecular orbitals have an energy difference of 1.59 kcal mol^{-1}, so that oxidative addition at the phosphorus or the germanium centre are energetically comparable.

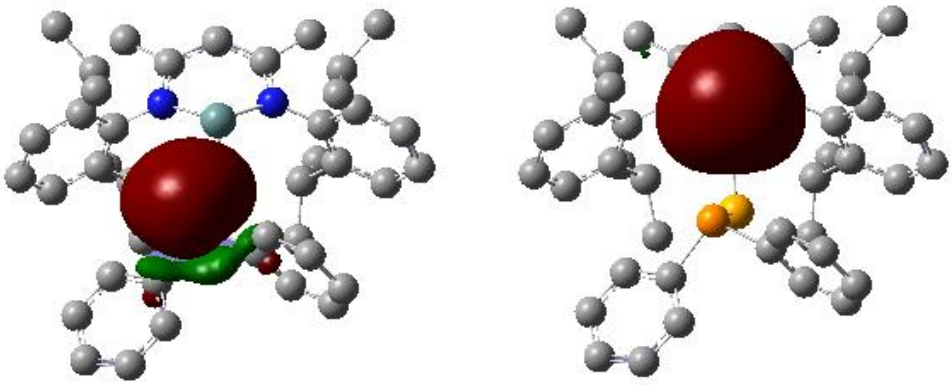

HOMO-15 HOMO-16

Figure 45 MOs associated with the phosphorus lone pair (HOMO-15) and germanium lone pair (HOMO-16) for [(BDI)GeSePPh_2].

The germanium dicyclohexyl-tellurophosphinate complex **18** has a phosphorus lone pair occupying the molecular orbital HOMO-10 (-197.92 kcal mol^{-1}), which is above the molecular orbital corresponding to the germanium lone pair at HOMO-11 (-198.84 kcal mol^{-1}) (Figure 46). The energy difference between the two molecular orbitals is 0.92 kcal mol^{-1}, significantly smaller than the diphenyl-selenophosphinite complex **17**.

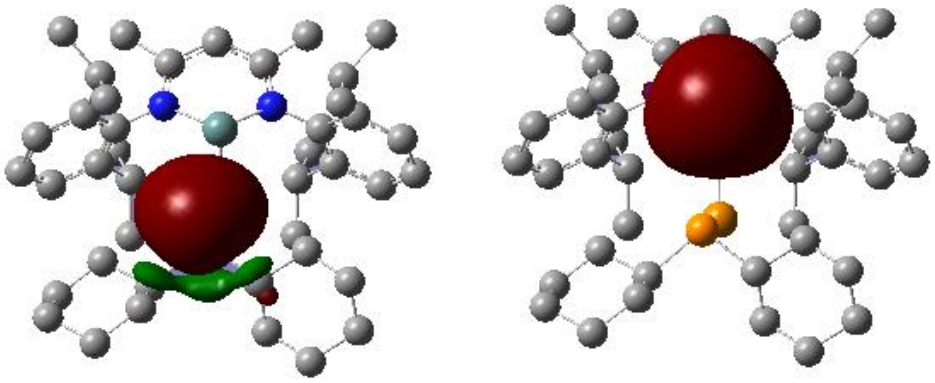

HOMO-10 HOMO-11

Figure 46 MOs associated with the phosphorus lone pair (HOMO-10) and germanium lone pair (HOMO-11) for [(BDI)GeTePCy$_2$].

For both phosphinite complexes the two orbitals are energetically comparable. In addition, space filling models show access to the germanium surface is hindered due to the bulky aryl groups on the β-diketiminate ligand coordinating to the metal centre, which is in contrast to the phosphorus atom where access to the lone pair is less restricted (Figure 47).

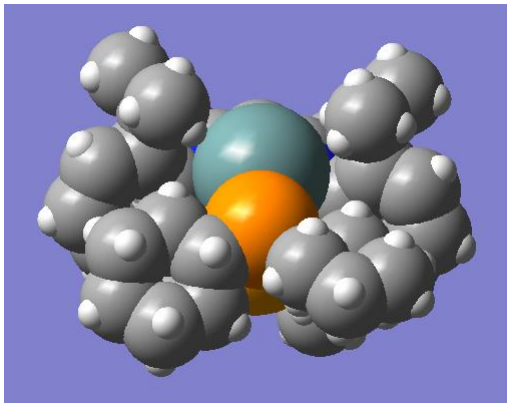

Figure 47 Space filling model for [(BDI)GeSePCy$_2$], using a scale radii of 175%.

Hybridisation of the germanium lone pair is relatively similar between the germanium phosphinite complexes, **17** and **18**, with the largest hybridisation value observed for the germanium diphenyl-selenophosphinite complex **17** (84.15% s, 15.84% p and 0.01% d) and the lowest value observed for the germanium dicyclohexyl-tellurophosphinate complex **18** (84.65% s, 15.34% p and 0.01% d) (Table 14). Both phosphinite complexes possess germanium lone pairs with greater s character participation relative to that of the β-diketiminate germanium chloride **XXI** (81.58% s and 18.42% p).[72]

Table 14 NBO analysis of Ge(II) for compounds **17**, **18** and **20**.

	Natural electron configuration	Lone pair NBO on M	Lone pair occupancy
[(BDI)GeSePPh$_2$] **17**	Ge: 4s(1.73) 4p(1.33) 4d(0.01) 5p(0.01)	s(84.15%) p 0.19 (15.84%) d 0.00 (0.01%)	1.97808
[(BDI)GeTePCy$_2$] **18**	Ge: 4s(1.75) 4p(1.43) 4d(0.01) 5p(0.01)	s(84.65%) p 0.18 (15.34%) d 0.00 (0.01%)	1.96926
[(BDI)GeSeP(Se)Ph$_2$] **20**	Ge: 4s(1.76) 4p(1.24) 4d(0.01) 5p(0.01)	s(86.19%) p 0.16 (13.79%) d 0.00 (0.02%)	1.97279

Calculations were performed on the germanium diphenyl-phosphinodiselenoate complex **20** using DFT. Geometry optimization calculations were performed on the entire

molecule for the germanium phosphinite complexes, the level of theory used was B3LYP DFT and Lanl2dz pseudopotentials, including a d type polarization function[183] and the effective core potential,[184] on the germanium, phosphorus and chalcogens and 6-31 g* on all other atoms (Figure 48). The calculated structural parameters for the complex correlate well with the X-ray crystallography data, with the exception of a possible interaction with Ge···Se, with the differences between the two data sets ranging between 2.78% to -3.84% (excluding the Ge···Se distance) (Table 15).

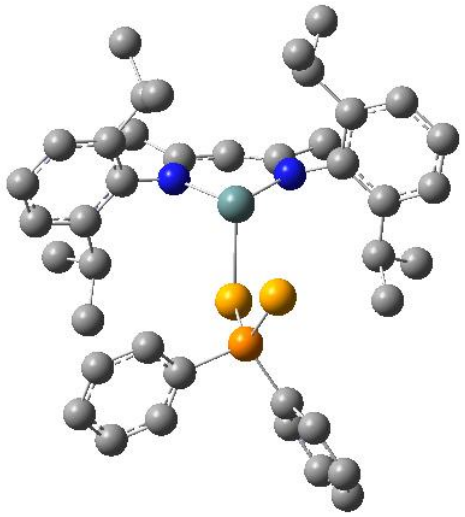

Figure 48 Geometry optimised structure of [(BDI)GeSeP(Se)Ph_2]

Table 15 X-ray crystallography data of the germanium diphenyl-phosphinodiselenoate complex **20** compared with computed bond distances (Å) and angles (deg) at the B3LYP/Lanl2dz/6-31 g* level of theory (E = Se, Te).

*[(BDI)GeSeP(Se)Ph$_2$], **20***					
Ge-N1	*Expt*	2.004	*C3-N2*	*Expt*	1.334
	Calcd	2.049		*Calcd*	1.332
	% Diff	**-2.25**		***% Diff***	**-0.15**
Ge-N2	*Expt*	2.006	*N1-Ge-N2*	*Expt*	91.17
	Calcd	2.083		*Calcd*	90.45
	% Diff	**-3.84**		***% Diff***	**0.79**
Ge-Se1	*Expt*	2.539	*N1-Ge-Se*	*Expt*	95.97
	Calcd	2.605		*Calcd*	97.80
	% Diff	**-2.60**		***% Diff***	**-1.91**
Se1-P	*Expt*	2.221	*N2-Ge-Se*	*Expt*	95.76
	Calcd	2.302		*Calcd*	93.63
	% Diff	**-3.65**		***% Diff***	**2.22**
P-Se2	*Expt*	2.117	*Ge-Se-P*	*Expt*	100.00
	Calcd	2.157		*Calcd*	97.22
	% Diff	**-1.89**		***% Diff***	**2.78**
Ge···Se2	*Expt*	4.921	*Se-P=Se*	*Expt*	115.48
	Calcd	3.737		*Calcd*	116.91
	% Diff	**24.06**		***% Diff***	**-1.24**
C1-N1	*Expt*	1.330			
	Calcd	1.344			
	% Diff	**-1.05**			

The molecular orbital diagrams reveal the molecular orbital of the germanium lone pair pointing towards the selenium atom, thus suggesting a possible interaction between the two atoms, which is consistent with the adoption of the 'endo' conformation by the complex. However, perturbation theory energy analysis shows no significant interaction between a donor germanium lone pair natural bond orbital and an empty acceptor selenium natural bond orbital.[185]

The hybridisation of the germanium lone pair in the germanium diphenyl-phosphinodiselenoate complex **20** (86.19% s, 13.79% p and 0.02% d) is similar, but slightly smaller than that of the germanium diphenyl-selenophosphinite complex **17** (84.15% s, 15.84% p and 0.01% d) (Table 14). The effect of this slight difference in hybridisation values on the sum of the bond angles, DP and bond lengths can not be justified due to the different conformations adopted by the two complexes, which has a more significant effect on the bond lengths, the sum of the bond angles and DP.

3.5. Chemical material studies on β-diketiminate group 14 metal phosphides

All complexes used for the chemical materials studies were generated at the University of Sussex by this author. All chemical material studies were performed either by Dr M. S. Hill at the University of Bath (TGA and AACVD), who generated the films, or Dr Q. Chen at the University of Sussex (SEM and EDS), who analysed the films.

Thermo-gravimetric analysis (TGA) is a method used to monitor the temperatures at which complexes decompose and to identify what the decomposition products are by calculating percentage mass of the new product relative to the precursor. TGA (under a N_2 atmosphere, heated at 5°C min^{-1} with a purge rate of 20 mL min^{-1}) was performed on [(BDI)$GePCy_2$] **CXXVI**,[157] [(BDI)$GeTePCy_2$] **18**, [(BDI)$SnSeP(Se)Cy_2$] **CXXXII**[115] and [(BDI)$PbSeP(Se)Cy_2$] **CXXXIII**[115] to test the suitability of these complexes for AACVD. The

germanium dicyclohexylphosphide complex **CXXVI** was examined to test the propensity of group 14 metal β-diketiminate complexes to undergo controlled thermal decomposition. Failure of this compound to undergo controlled thermolysis would imply that the heavier and more relevant compounds, **18**, **CXXXII** and **CXXXIII**, would also not undergo controlled thermolysis. The other three compounds were examined as potential single source precursors for GeTe, SnSe and PbSe films.

The TGA data for the complexes (Table 16 and Figures 49-52) show the lead dicyclohexyl-phosphinodiselenoate complex **CXXXIII** has a significantly lower decomposition temperature (circa 100°C), and is hence a less stable complex, than the germanium dicyclohexyl-tellurophosphinite complex **18** (207°C), the germanium dicyclohexylphosphide complex **CXXVI** (228°C) or the tin dicyclohexyl-phosphinodiselenoate complexes **CXXXII** (210°C). The tin and lead dicyclohexyl-phosphinodiselenoate complexes show a two-stage decomposition process with an inflection in the profile at circa 200°C. During this first stage, approximately 10% mass is lost for both species. This is consistent with the presence of a molecule of toluene within the crystal matrix, which was found in the unit cell in the X-ray crystallographic data of these molecules.[115] This process is not observed in the germanium dicyclohexyl-tellurophosphinite complex **18** or the germanium dicyclohexylphosphide complex **CXXVI**, both of which exhibit decomposition in a smooth one-step manner. However, these molecules do not crystallise with a solvent molecule in their unit cell.

The presence of only one decomposition step for all complexes (barring the loss of the solvent), reveals that both the β-diketiminate ligand and the cyclohexyl/phenyl group or the phosphide group are lost at similar temperatures. Both germanium complexes, **18** and **CXXVI**, as well as the tin complex **CXXXII** start to lose significant mass around 210 °C, which indicates that the loss of β-diketiminate is commensurate with the loss of the other group. The lead complex **CXXXIII**, starts to decompose soon after the loss of toluene,

indicating that this compound is significantly less stable than the other three. Unfortunately, a positive mass jump was observed in this experiment, indicating that the final data is not reliable and that the experiment should be run again.

The residue from the germanium dicyclohexylphosphide complex **CXXVI** has a mass of 10% of initial material. This is less than the expected 15% based off the mass of the germanium-phosphorus component. A similar margin of difference between the experimental and expected weight per cent is found for the germanium dicyclohexyl-tellurophosphinite complex **18** (residue corresponding to the germanium-telluride moiety has a mass at 20% of initial material, 25% was expected). The experimentally obtained per cent mass of the residues corresponding to the group 14 metal-selenium components for the group 14 metal dialkyl-phosphinodiselenoate complexes have a larger margin of difference with that of the predicted per cent mass, with the tin residue observed to have a per cent mass of 16% (20% is expected) and the lead residue observed to have a per cent mass of 18% (27% is expected, ignoring the mass spike in the middle of the run). These results indicate that all the expected group 14 metal chalcogen products are volatile and that AACVD may be a viable method for generating group 14/16 material using these molecules as single source precursors. Differences between the experimental and theoretical per cent mass for the residues could have been caused by impurities and decomposition of the samples. Attempts were implemented to minimise this error by using crystalline samples of the complexes and transporting the samples in sealed vials, under the inert-atmosphere condition of a glovebox.

Table 16 TGA data for the complexes [(BDI)GePCy$_2$] **CXXVI**,[157] [(BDI)GeTePCy$_2$] **18**, [(BDI)SnSeP(Se)Cy$_2$] **CXXXII**[115] and [(BDI)PbSeP(Se)Cy$_2$] **CXXXIII**.[115]

	Initial mass, mg	Decomposition onset / °C	Decomposition end point / °C	Final % Mass	Expected % Mass
[(BDI)GePCy$_2$]	3.912	228	514	10	15
[(BDI)GeTePCy$_2$]	6.219	207	458	20	25
[(BDI)SnSeP(Se)Cy$_2$]	3.247	210	528	16	20
[(BDI)PbSeP(Se)Cy$_2$]	4.678	Ca. 100	620	18	27

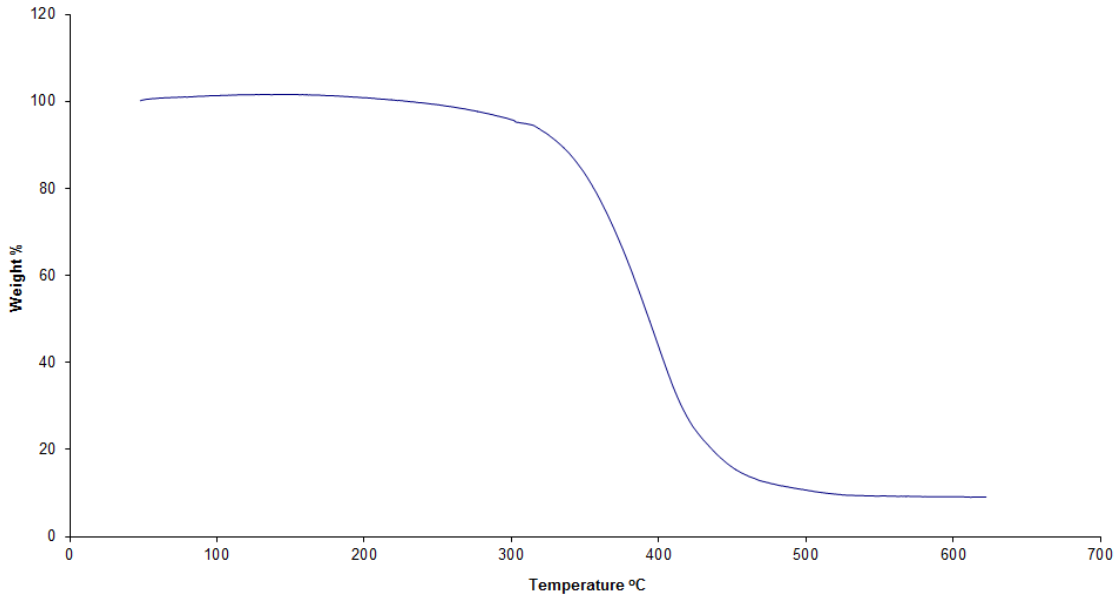

Figure 49 TGA graph [LGePCy$_2$].

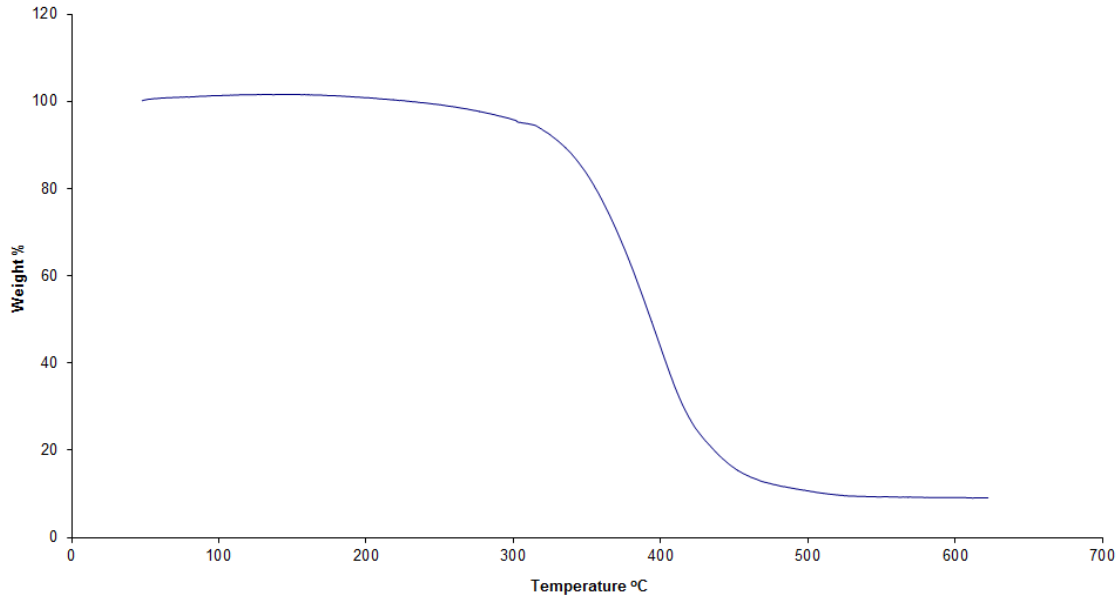

Figure 50 TGA graph [LGeTePCy$_2$].

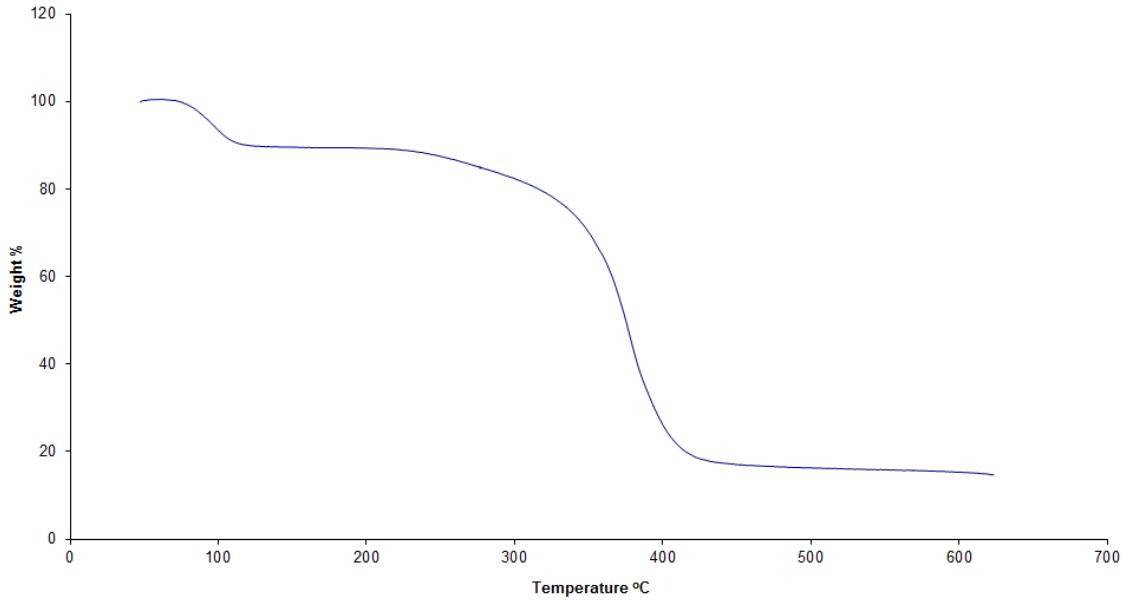

Figure 51 TGA graph [LSnSeP(Se)Cy$_2$].

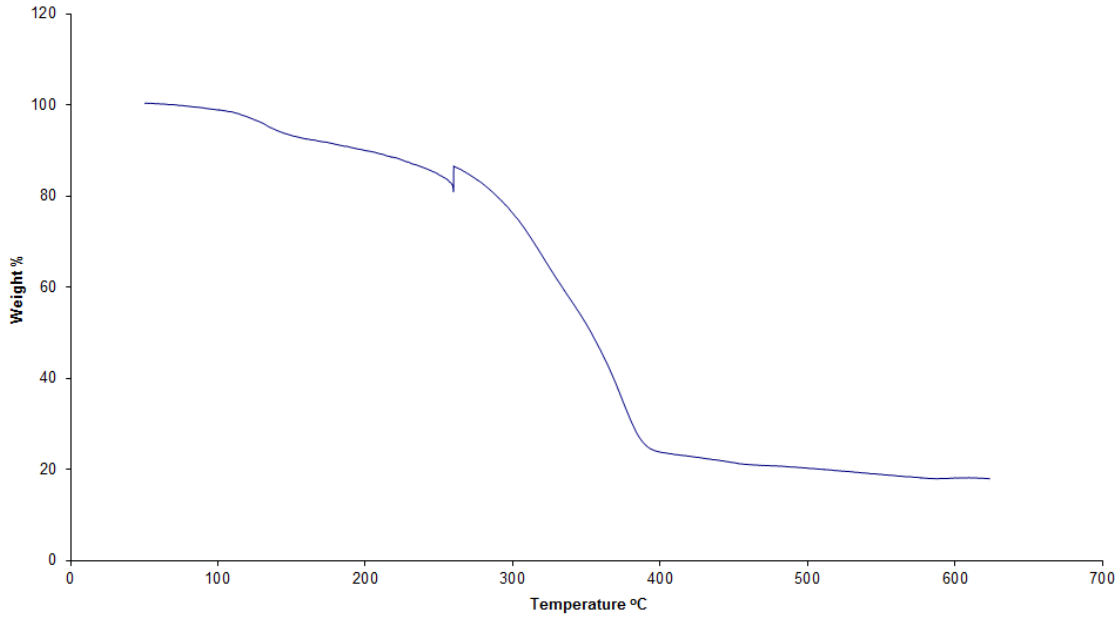

Figure 52 TGA graph [LPbSeP(Se)Cy_2].

AACVD was performed on **CXXXII**, at 198°C, 450°C and 550°C, with an argon carrier gas flow rate of 160 sccm for 1 hour at atmospheric pressure. The reactor was purged with argon for 30 minutes at the stated deposition temperatures prior to deposition of the materials, in order to avoid any *in situ* oxidation. Attempts of AACVD on **18** did not lead to the deposition of material on the glass substrate wafer. Furthermore, AACVD attempts using the lead congener **CXXXIII** did not result in deposition of film onto the glass substrate. Unfortunately, due to time constraints, conditions for the AACVD process could not be varied for these complexes. As such, we do not know whether the lack of film growth was due to some inherent properties of these molecules, or due to inappropriate AACVD conditions.

In contrast, a steel grey film, generated from the decomposed tin dicyclohexyl-phosphinodiselenoate complex, was found to adhere to a Pyrex glass substrate. The product was analysed using SEM (scanning electron microscopy) combined with EDS (energy dispersive spectroscopy). SEM images of the product at growth temperatures

198°C and 450°C (Figure 53 (a) and (b), respectively) show a non-homogenous array of rectangular crystals. Crystals grown at 198°C have an average length of 2 μm, with an average range of diameters between 0.5 to 1 μm. Crystals grown at 450°C have an average length of 2 μm, with an average range of diameters between 1 and 1.5 μm, larger than the crystals grown at 198°C. SEM of **CXXXII** at 550°C (Figure 53 (c)) show a mixture of morphologies of non-homogenous arrays of crystals. Rectangular crystals, similar to the crystals grown at lower temperatures are observed, however, other morphologies of irregular sized crystals are also visible, ranging from larger globular crystals to more indistinct conglomerations of smaller rectangular crystals, which appear to be primitive stages of the globular morphology. All EDS data measured at different temperatures, including 198°C (Figure 54), 450°C (Figure 55) and 550°C (Figure 56), confirm the identity of the film as being composed of tin and selenium, with large traces of silicon (from the glass substrate), thus showing the film sparsely covers the substrate surface. The ratio of Sn:Se at these temperatures are relatively similar (1:1 ratio), with a Sn:Se ratio of 53:47 at 198°C, 53:47 at 450°C and 48:52 at 550°C, showing that annealing at this temperature range does not change the composition (Table 17).

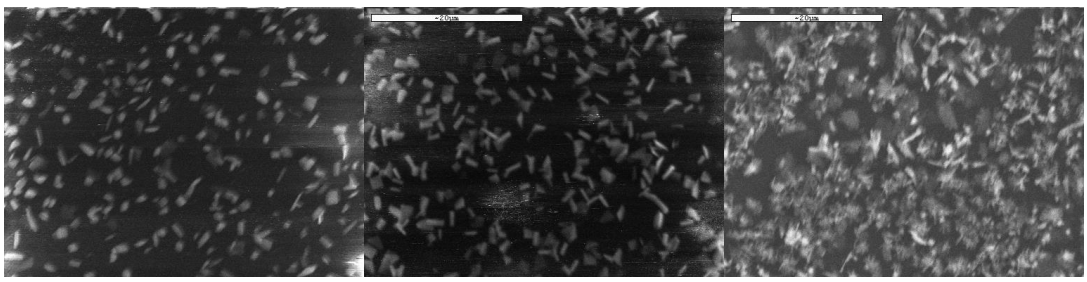

(a) (b) (c)

Figure 53 SEM images of the SnSe films deposited on a glass substrate from the precursor compound **CXXXII** under a magnification of 20 μm at different decomposition temperatures (a) 198°C, (b) 450°C, (c) 550°C.

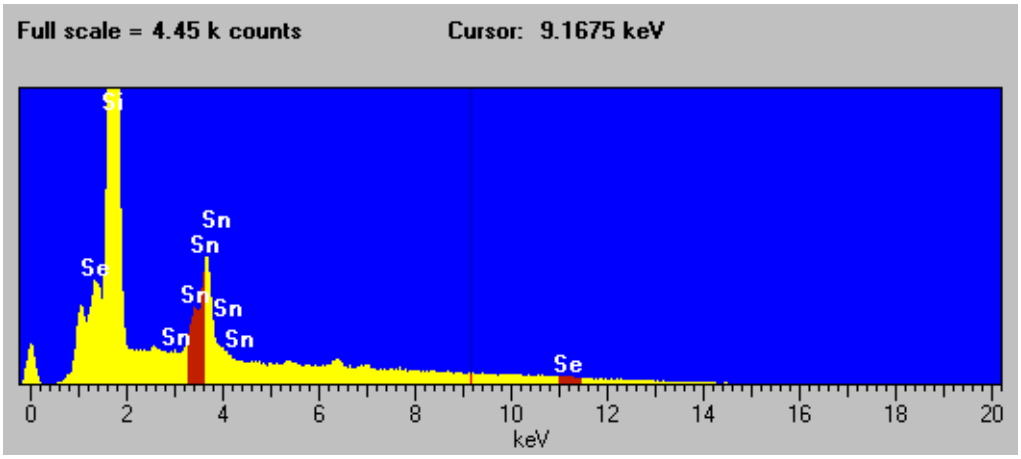

Figure 54 EDS data of the SnSe film from the precursor compound **CXXXII** formed at 198°C (a).

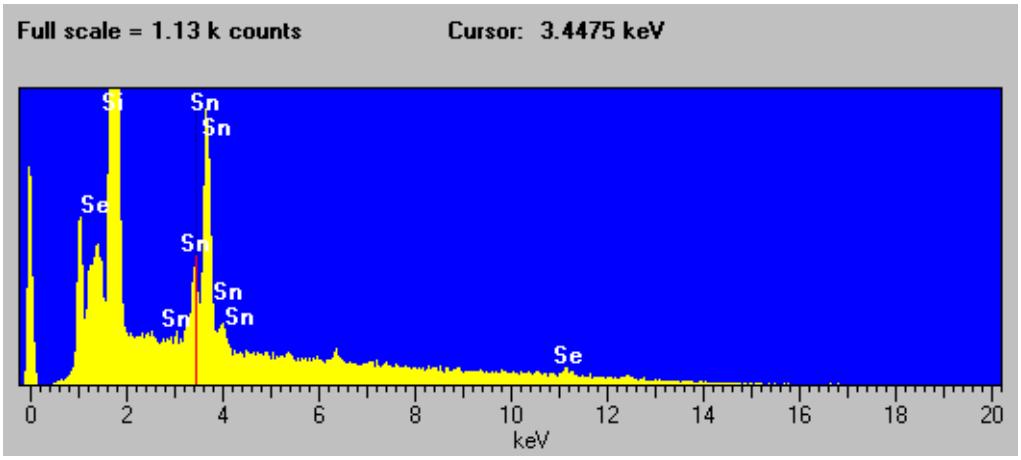

Figure 55 EDS data of the SnSe film from the precursor compound **CXXXII** formed at 450°C (b).

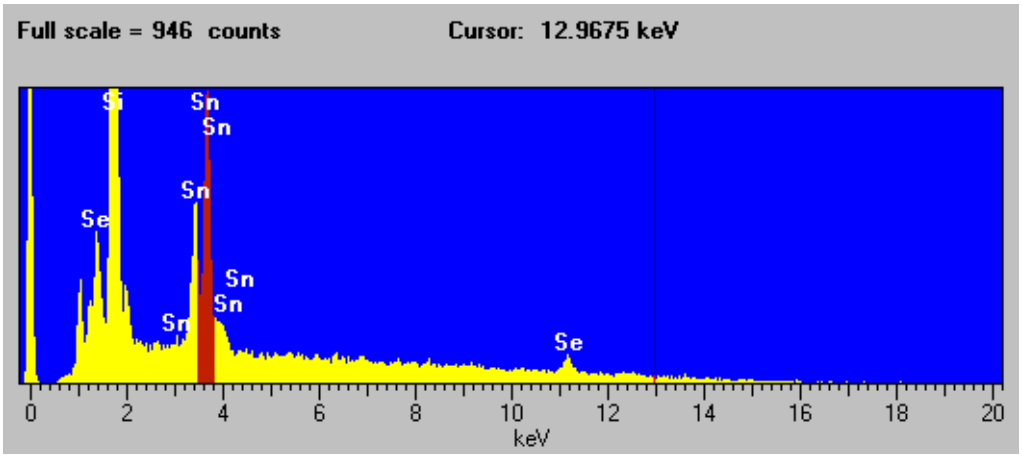

Figure 56 EDS data of the SnSe film from the precursor compound **CXXXII** formed at 550°C (c).

Table 17 EDS data for the elemental composition (%) of AACVD products of compound **CXXXII** at (a) 198°C, (b) 450°C, (c) 550°C (deposited on a glass substrate) and at (d) 450°C, deposited on a silicon wafer.

Element	(a)	(b)	(c)	(d)
Sn	53	53	48	37
Se	47	47	52	63

A further AACVD study using the precursor compound **CXXXII** was performed at 450°C, resulting in the deposition of a steel grey film onto a silicon wafer. The steel grey film was analysed via SEM and EDS. SEM images of the film show crystals are more densely packed onto the substrate surface in an irregular pattern, with crystals predominantly displaying a cubic morphology circa 3µm in length and width, accompanied by long, thin rectangular crystals (Figure 57). EDS analysis confirm the

presence of both tin and selenium in a ratio of 37:63 (Table 17), with large traces of silicon from the substrate detected, thus showing the sparse distribution of the crystals on the substrate surface (Figure 58).

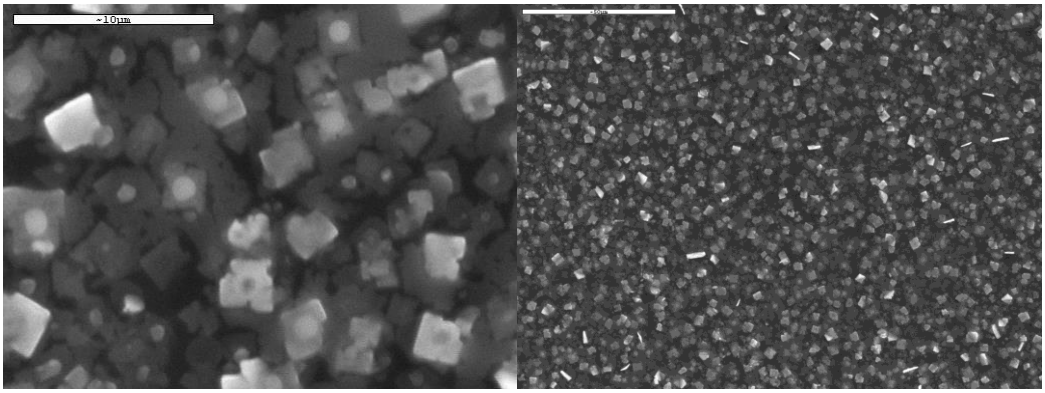

(a) (b)

Figure 57 SEM images of the SnSe films deposited on a silicon wafer from the precursor compound **CXXXII** under different magnifications (a) bar = 10 µm, (b) bar = 50 µm.

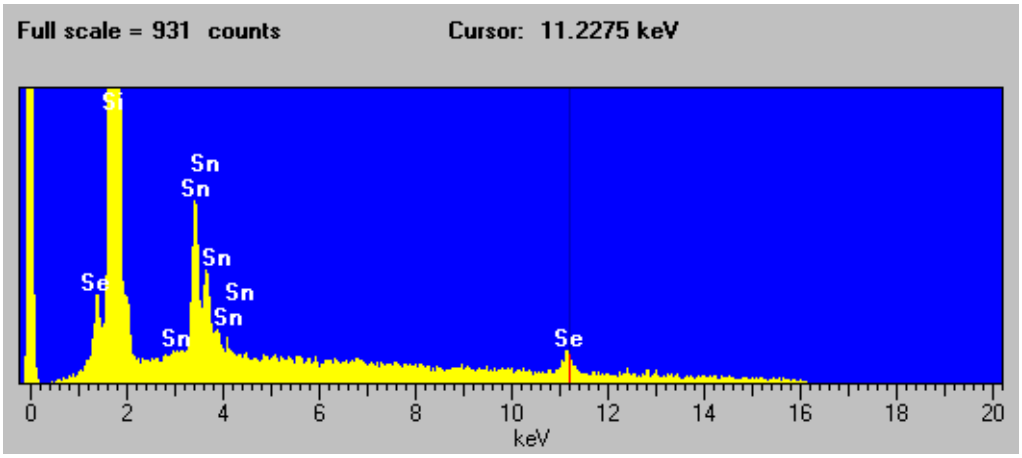

Figure 58 EDS data of the SnSe film from the precursor compound **CXXXII** formed at 450°C.

3.5.1. Summary of AACVD studies

TGA was performed on [(BDI)GePCy$_2$] **CXXVI**,[157] [(BDI)GeTePCy$_2$] **18**, [(BDI)SnSeP(Se)Cy$_2$] **CXXXII**[115] and [(BDI)PbSeP(Se)Cy$_2$] **CXXXIII**[115] in order to test their potential as SSPs for AACVD. TGA data show the germanium dicyclohexyl-tellurophosphinite **18**, tin dicyclohexyl-phosphinodiselenoate **CXXXII** and the lead dicyclohexyl-phosphinodiselenoate **CXXXIII** have potential as SSPs, however preliminary AACVD studies show the germanium dicyclohexyl-tellurophosphinite **18** and lead dicyclohexyl-phosphinodiselenoate **CXXXIII** to be unstable under the stated conditions. In contrast, the tin dicyclohexyl-phosphinodiselenoate complex **CXXXII** was found to produce micromaterials of SnSe films. These films were observed via SEM and EDS and show the sparse distribution of SnSe micromaterials on the substrate surfaces in a non-homogeneous array, with a mixture of morphologies between temperatures and on the same surface. Optimisation of this technique with complexes **CXXXII** and **CXXXIII** were not performed and could be investigated in further studies.

4. Summary of the chemistry of the terminal pnictogen complexes of lead, tin and germanium

In summary, a series of lead(II) and tin(II) β-diketiminate amides and anilides [(BDI)MNRR'] (BDI = [CH{(CH_3)CN-2,6-*i*$Pr_2C_6H_3$}$_2$]; M = Sn and RR' = *i*Pr_2 **1**, H(2,6-*i*Pr_2-C_6H_3) **2**, H(2-*i*Pr-C_6H_4) **3**, or M = Pb and RR' = *i*Pr_2 **4**, H(2,6-*i*Pr_2-C_6H_3) **5**, H(2-*i*Pr-C_6H_4) **6**, H(C_6H_5) **7**) were synthesised via salt metathesis of the group 14 metal chloride precursors and the lithiated amide or anilide. These complexes were found to be air-sensitive and isolable by crystallisation and were characterised by multinuclear NMR spectroscopy, IR spectroscopy, elemental analysis and X-ray crystallography. These complexes adopt a distorted trigonal pyramidal geometry at the metal centre and an 'exo' or 'endo' conformation. The conformation influences the sum of the bond angles, DP at the metal centre and the displacement of the metal and amide nitrogen from the NCCCN plane. Further work to complete the characterisation of [(BDI)PbNH(*i*PrC_6H_4)] **6** via elemental analysis is required in order to complete characterisation for all the lead(II) and tin(II) β-diketiminate amides and anilides.

The reactivity of [(BDI)MN(*i*Pr)$_2$] (M = Sn **1**, Pb **4**) and [(BDI)MNH(2,6-*i*Pr_2-C_6H_3)] (M = Sn **2**, Pb **5**) towards electrophiles and acids was then investigated. The lead analogues are more reactive than their tin analogues and the amide ligand systems are more reactive than the anilide ligand systems. In general, these systems display the predicted nucleophilic and basic reactivity towards the electrophiles and acids examined. However, treatment of these systems with phenyl isocyanate generated a bis-β-diketiminate complex, [(BDI)M(OC{=NPh}C{=C(Me)CN(H)(Ar)}{C{Me}=CN(Ar)})] (M = Sn **10**, Pb **14**), a net result of nucleophilic addition at the γ-carbon to the phenyl isocyanate's electrophilic carbon. DFT studies show comparable energy between the molecular orbitals

corresponding to the backbone molecular orbital, understood to be responsible for electrophilic activation of the γ-carbon on the ancillary ligand, and the amide/anilide-nitrogen lone pair (resulting in heterocumulene insertion). Reactivity studies focusing on the synthesis of bimetallic complexes, by treating the group 14 metal phenyl isocyanate complexes with zinc dimethyl and aluminium trimethyl, yielded the known β-diketiminate metal methyl complexes **XXIX** in addition to an unknown. The unknown is postulated to be a tripodal diimine-alkoxo complex **11**, however, isolation of the unknown was unsuccessful. Further studies to this project would include isolating the unknown and the synthesis of a bimetallic complex from the precursor bis-β-diketiminate complex. Furthermore, complete characterisation of [(BDI)SnOCONH(*i*$Pr_2C_6H_3$)] **9** (X-ray diffraction and elemental analysis), [{(HN-2,6-*i*$Pr_2C_6H_3$)PbI}$_2$] **13** (^{1}H, ^{13}C and ^{207}Pb NMR spectroscopy, IR spectroscopy and elemental analysis) and [(BDI)Pb(OC{=NPh}C{=C(Me)CN(H)(Ar)}{C{Me}=CN(Ar)})] **14** (^{13}C NMR spectroscopy and X-ray diffraction) is needed.

The reactivity of a series of group 14 metal β-diketiminate phosphide complexes [(BDI)MPR_2] (BDI = [CH{(CH_3)CN-2,6-*i*$Pr_2C_6H_3$}$_2$]; R = Cy and M = Ge **CXXVI**, Sn **CXXII**, Pb **CXXIII**; R = Ph and M = Ge **CXLIV**, Sn **CXLV**, Pb **CXLVI**) towards selenium and tellurium was investigated. No reactivity is exhibited upon addition of one or five equivalents of tellurium to the tin(II) or lead(II) systems. In contrast, the germanium(II) systems display reactivity with all studied chalcogens, whereby one equivalent of the chalcogen yielded dialkyl-chalcogenophosphinite complexes [(BDI)GeEPR_2] (E = Se and R = Cy **16**, Ph **17**; E = Te and R = Cy **18**). Furthermore, five equivalents of selenium to the germanium diphenylphosphide **CXLIV** resulted in germanium diphenyl-phosphinodiselenoate **20**. Attempts to form mixed chalcogen systems, similar to Tam's [(BDI)SnSeP(S)Cy_2] **CXXXIX**, by treating germanium dicyclohexyl-tellurophosphinite complex **18** with one equivalent of selenium, resulted in the formation of [(BDI)GeSePCy_2] **16**. Future work would involve completing the characterisation of [(BDI)GeSeP(C_6H_5)$_2$] **17**, which requires IR and ^{13}C

NMR spectroscopy, [(BDI)GeTeP(C_6H_{11})$_2$] **18**, which requires elemental analysis, and [(BDI)Ge(Se)SeP(C_6H_5)$_2$] **20**, which requires IR and ^{77}Se NMR spectroscopy as well as pure ^{1}H and ^{13}C NMR spectra. Even though a ^{125}Te NMR spectrum was obtained for [(BDI)GeTeP(C_6H_{11})$_2$] **18**, repeating this process with a higher concentration of the complex or increasing the number of scans so that tellurium-phosphorus coupling is observed would be desirable.

DFT studies were undertaken to understand the reactivity of germanium dialky-chalcogenophosphinite complexes **17** and **18**, in addition to the germanium diphenyl-phosphinodiselenoate complex **20**. The germanium dialky-chalcogenophosphinite complexes have molecular orbitals for the germanium and phosphorus lone pairs which are energetically comparable, thus favouring oxidative addition at the germanium or phosphorus centre. Furthermore, space filling models for **17** and **18** show restricted access to the germanium surface through steric hindrance. DFT studies on the germanium dicyclohexyl-selenophosphinite **16** were unsuccessful due to repetitive crashing of the calculation, therefore future work would include successful completion of this calculation.

TGA performed on [(BDI)GePCy$_2$] **CXXVI**,[157] [(BDI)GeTePCy$_2$] **18**, [(BDI)SnSeP(Se)Cy$_2$] **CXXXII**[115] and [(BDI)PbSeP(Se)Cy$_2$] **CXXXIII**[115] show all these complexes have potential as SSPs for AACVD. However, preliminary AACVD studies show the germanium dicyclohexyl-tellurophosphinite **18** and lead dicyclohexyl-phosphinodiselenoate **CXXXIII** do not deposit material under the conditions already stated. The tin dicyclohexyl-phosphinodiselenoate complex **CXXXII** is stable under the stated conditions, where micromaterials of SnSe films are produced. SEM and EDS analysis show a non-homogeneous array of crystals, sparsely covering the surface of the substrate, which exhibit a mixture of morphologies on the same surface and between films deposited at different temperatures. Future work would involve making more of complex **CXXXIII** so that further AACVD studies could be undertaken in order to optimise conditions and to

explore the possibility of AACVD on this sample. Further AACVD on complex **CXXXII** by optimising conditions could also be explored so that more desirable deposition can be attained.

5. Experimental

5.1. General considerations

All manipulations were carried out under an atmosphere of dry nitrogen using standard Schlenk techniques or in an inert-atmosphere glovebox. Solvents were dried with sodium, distilled, degassed and stored over 4 Å sieves. The ^{1}H, $^{13}C\{^{1}H\}$, $^{31}P\{^{1}H\}$, $^{77}Se\{^{1}H\}$, $^{125}Te\{^{1}H\}$, $^{119}Sn\{^{1}H\}$ and $^{207}Pb\{^{1}H\}$ NMR spectra were recorded on a Varian 400, 500 or 600 MHz spectrometer. The operating frequencies on the Varian 400 MHz spectrometer for the $^{13}C\{^{1}H\}$, $^{31}P\{^{1}H\}$, $^{77}Se\{^{1}H\}$, $^{125}Te\{^{1}H\}$, $^{119}Sn\{^{1}H\}$ and $^{207}Pb\{^{1}H\}$ nuclei are 100.5 MHz, 161.7 MHz, 76.3 MHz, 104.8 MHz, 150.0 MHz and 83.6 MHz. The operating frequency for the $^{13}C\{^{1}H\}$ nucleus on the Varian 500 MHz spectrometer is 125.7 MHz and the operating frequency for the $^{119}Sn\{^{1}H\}$ and $^{207}Pb\{^{1}H\}$ nuclei on the Varian 600 spectrometer are 223.7 MHz and 125.5 MHz. The Varian 400 and 600 MHz spectrometers were equipped with $X\{^{1}H\}$ broadband-observe probes while the Varian 500 MHz spectrometer was equipped with $^{1}H\{X\}$ inverse broadband-observe probes. The ^{1}H and ^{13}C resonances were externally referenced to TMS, the ^{31}P resonances were externally referenced to 85% [H_3PO_4], the ^{77}Se resonances were externally referenced to [Me_2Se], the ^{125}Te resonance was externally referenced to [Me_2Te], the ^{119}Sn resonances were externally referenced to [Me_4Sn] and the ^{207}Pb resonances were externally referenced to [Me_4Pb]. [LH] (**XCIII**),[186] [LiL] (**XCIV**),[186] [LGeCl],[71] [LSnCl][71] and [LPbCl] (**XXVII**),[72] [LMPCy_2] (**CXII**, **CXXIII**, **CXXVI**)[187] and [LMPPh_2] (**CXLIV**,[174] **CXLV**, **CXLVI**)[187] (M = Ge, Sn, Pb) were prepared according to literature procedures. Reagents were purchased from Acros or Sigma Aldrich or used from existing stocks. All reagents were freshly distilled or crystallised prior to use. Carbon dioxide was used as received (BOC, 100.000%). IR spectra were recorded from Nujol mulls encased between NaCl plates using a Perking-Elmer 1600 FT-IR spectrometer, scanning over the range 4000 to 450 cm^{-1}. Elemental analysis was

performed at London Metropolitan University. Crystals were obtained as outlined in the text. X-ray diffraction data were collected at 173 K on a Nonius Kappa CCD diffractometer, *k*(Mo-Kα) = 0.71073 Å and refined using the *SHELXL-97* software package.[188] Selected bond lengths and angles are given in Tables 1, 2, 4, 5, 6, 7, 8, 11 and 12, with crystallographic data stated in Tables 19-24.

5.2. Computational details

All the calculations were performed using density functional theory (DFT) in the Gaussian 03 program.[189] Geometry optimization for the full complexes of the amides **1**, **2**, **4** and **5**, and the phosphinites and phosphides **16**, **17**, **18** and **20**, were undertaken at the B3LYP level by using a double-ζ basis set (Lanl2dz) for the tin and lead atoms and 6-31 g* for all other atoms in the amide complexes. In addition, a double-ζ basis set (Lanl2dz) and a d type polarization function[183] and the effective core potential were included (Lanl2 ECP)[184] for the germanium, phosphorus and chalcogens in the phosphide and phosphinite complexes, while 6-31 g* was used for all other atoms.

5.3. Synthetic methods

[CH{(CH$_3$)CN-2,6-*i*Pr$_2$C$_6$H$_3$}$_2$SnN(CH{CH$_3$}$_2$)$_2$], 1. A THF solution of lithium diisopropylamide (2M, 219 μL, 0.437 mmol) was added to a solution of β-diketiminate tin chloride, [LSnCl], (0.25 g, 0.44 mmol) in toluene (5 mL), resulting in an immediate colour change to an orange solution, and the mixture was stirred for 1 hour at room temperature. The solution was filtered and the solvent was concentrated under reduced pressure and stored at -27°C for 1 day yielding [Sn(L){N(CH{CH$_3$}$_2$)$_2$}], (0.09 g, 32%) as orange crystals. ^{1}H NMR (C$_6$D$_6$, 293 K): δ 7.14 (d, 2 H, *J* = 1.9 Hz, *m*-H), 7.10 (s, 2 H, *p*-H), 7.07 (d, 2 H, *J* = 2.0 Hz, *m*-H), 4.85 (s, 1 H, middle CH), 3.82 (septet, 2 H, *J* = 6.9 Hz, C*H*Me$_2$), 3.75 (septet, 2 H, *J* =

6.5 Hz, C*H*Me$_2$), 3.25 (septet, 2 H, *J* = 6.7 Hz, C*H*Me$_2$), 1.57 (s, 6 H, NC*Me*), 1.36 (d, 6 H, *J* = 6.7 Hz, CH*Me$_2$*), 1.28 (d, 6 H, *J* = 6.8 Hz, CH*Me$_2$*), 1.19 (d, 6 H, *J* = 6.7 Hz, CH*Me$_2$*), 1.15 (s, 6 H, CH*Me$_2$*), 1.12 (d, 12 H, *J* = 6.8 Hz, CH*Me$_2$*). ^{13}C{^{1}H} NMR (C_6D_6, 293 K): δ 167.1 (N*C*Me), 144.4 (*ipso*-C), 144.2 and 144.2 (*ortho*-C), 126.5 (*para*-C), 124.6 and 124.6 (*meta*-C), 98.8 (middle CH), 51.3, 29.1 and 28.2 (*C*HMe$_2$), 28.0, 26.3, 25.4 and 25.1 (CH*Me$_2$*), 24.9 (NC*Me*), 24.8 (CH*Me$_2$*). ^{119}Sn{^{1}H} NMR (C_6D_6, 293K): δ -224. IR (Nujol, cm^{-1}) 1623 (s), 1552 (s), 1316 (s), 1169 (s), 1100 (s), 934 (s). Anal. calc. for $C_{35}H_{55}N_3Sn$: C, 66.04; H, 8.71; N, 6.60. Found: C, 65.98; H, 8.64; N, 6.52%

[CH{(CH$_3$)CN-2,6-*i*Pr$_2$C$_6$H$_3$}$_2$SnNH(*i*Pr$_2$C$_6$H$_3$)], 2. Lithium 2,6-diisopropylanilide (0.08 g, 0.4 mmol) was added to a solution of β-diketiminate tin chloride, [LSnCl], (0.25 g, 0.44 mmol) in toluene (5 mL) and the mixture was stirred for 1 hour at room temperature. The solution was filtered and the resulting solvent was concentrated under reduced pressure and stored at -27°C for 1 day yielding [Sn(L){NH(*i*Pr$_2$C$_6$H$_3$)], (0.13 g, 41%) as yellow crystals. ^{1}H NMR (C_6D_6, 293 K): δ 7.13-7.07 (m, 8 H, Ar*H*), 6.82 (t, 1 H, *J* = 7.6, *p*-H), 5.59 (s, 1 H, N*H*), 5.00 (s, 1 H, middle CH), 3.44 (septet, 2 H, *J* = 6.8 Hz, C*H*Me$_2$), 3.33 (septet, 4 H, *J* = 6.7 Hz, C*H*Me$_2$), 3.33 (septet, 2 H, *J* = 6.7 Hz, C*H*Me$_2$), 1.65 (s, 6 H, NC*Me*), 1.29 (d, 6 H, *J* = 6.9 Hz, CH*Me$_2$*), 1.25 (d, 12 H, *J* = 6.4 Hz, CH*Me$_2$*), 1.15 (d, 6 H, *J* = 6.8 Hz, CH*Me$_2$*), 1.13 (d, 6 H, *J* = 6.8 Hz, CH*Me$_2$*), 0.95 (d, 6 H, *J* = 6.7 Hz, CH*Me$_2$*). ^{13}C{^{1}H} NMR (C_6D_6, 293 K): δ 164.9 (N*C*Me), 148.0 and 145.5 (*ipso*-C), 143.0, 142.6 and 134.6 (*ortho*-C), 127.3 (*meta*-C), 125.0 (*para*-C), 124.2 and 123.4 (*meta*-C), 116.3 (*para*-C), 97.0 (middle CH), 29.3, 28.8 and 28.6 (*C*HMe$_2$), 26.1, 24.7, 24.7, 24.4 and 24.0 (CH*Me$_2$*), 23.8 (NC*Me*). ^{119}Sn{^{1}H} NMR (C_6D_6, 293 K): δ -745. IR (Nujol, cm^{-1}) 1623 (s), 1589 (s), 1552 (s), 1520 (s), 1283 (s), 1170 (s), 1098 (s), 935 (s), 841 (s), 793 (s), 747(s). Anal. calc. for $C_{41}H_{59}N_3Sn$: C, 69.10; H, 8.35; N, 5.90. Found: C, 69.16; H, 8.50; N, 5.90%

[CH{(CH$_3$)CN-2,6-*i*Pr$_2$C$_6$H$_3$}$_2$SnNH(*i*PrC$_6$H$_4$)], 3. Lithium 2-isopropylanilide (0.06 g, 0.4 mmol) was added to a solution of β-diketiminate tin chloride, [LSnCl], (0.25 g, 0.44 mmol) in toluene (5 mL) and the mixture was stirred for 1 hour at room temperature. The solution was filtered and the resulting solvent was concentrated under reduced pressure and stored at -27°C for 1 day yielding [Sn(L){NH(*i*PrC$_6$H$_4$)], (0.08 g, 29%) as yellow crystals. ^{1}H NMR (C$_6$D$_6$, 293 K): δ 7.20 (d, 1 H, *J* = 7.6 Hz, *m*-H), 7.15-6.94 (m, 8 H, Ar*H*), 6.69 (t, 1 H, *J* = 7.8 Hz, Ar*H*), 5.57 (s, 1 H, N*H*), 4.93 (s, 1 H, middle CH), 3.64 (septet, 2 H, *J* = 6.8 Hz, C*H*Me$_2$), 3.30 (septet, 2 H, *J* = 6.8 Hz, C*H*Me$_2$), 2.99 (septet, 1 H, *J* = 6.8 Hz, C*H*Me$_2$), 1.61 (s, 6 H, NC*Me*), 1.36 (d, 6 H, *J* = 6.8 Hz, CH*Me$_2$*), 1.29 (d, 6 H, *J* = 6.8 Hz, CH*Me$_2$*), 1.16 (d, 6 H, *J* = 6.8 Hz, CH*Me$_2$*), 1.14 (d, 6 H, *J* = 6.8 Hz, CH*Me$_2$*), 1.02 (d, 6 H, *J* = 6.8 Hz, CH*Me$_2$*). ^{13}C{^{1}H} NMR (C$_6$D$_6$, 293 K): δ 165.5 (N*C*Me), 151.2 and 145.5 (*ipso*-C), 142.9, 142.6 and 131.6 (*ortho*-C), 127.2 (*para*- or *meta*-C of Ar), 126.8 and 125.5 (*meta*-C), 125.1, 124.1 and 115.8 (*para*- or *meta*-C of Ar), 115.3 (*meta*-C), 97.2 (middle CH), 29.2, 28.9 and 28.4 (*C*HMe$_2$), 26.9, 24.9, 24.6 and 24.0 (CH*Me$_2$*), 23.8 (NC*Me*), 22.8 (CH*Me$_2$*). ^{119}Sn{^{1}H} NMR (C$_6$D$_6$, 293 K): δ -239. IR (Nujol, cm^{-1}) 1595 (s), 1552 (s), 1525 (s), 1313 (s), 1295 (s), 1263 (s), 1171 (s), 1099 (s), 843 (s), 796 (s), 736 (s), 727 (s), 673(s). Anal. calc. for C$_{38}$H$_{53}$N$_3$Sn: C, 68.06; H, 7.97; N, 6.27. Found: C, 69.19; H, 7.77; N, 6.18%

[CH{(CH$_3$)CN-2,6-*i*Pr$_2$C$_6$H$_3$}$_2$PbN(CH{CH$_3$}$_2$)$_2$], 4. A THF solution of lithium diisopropylamide (2M, 190 μL, 0.379 mmol) was added to a solution of β-diketiminate lead chloride, [LPbCl], (0.25 g, 0.38 mmol) in toluene (5 mL), resulting in an immediate colour change to a red solution, and the mixture was stirred for 1 hour at room temperature. The solution was filtered and the solvent was concentrated under reduced pressure and stored at -27°C yielding [Pb(L){N(CH{CH$_3$}$_2$)$_2$}], (0.04 g, 15%) as orange crystals. ^{1}H NMR (C$_6$D$_6$, 293 K): δ 7.23 (d, 1 H, *J* = 2.5 Hz, Ar*H*), 7.22 (d, 1 H, *J* = 2.5 Hz, Ar*H*), 7.14-7.11 (m, 4 H, Ar*H*), 5.07 (septet, 2 H, *J* = 6.5 Hz, C*H*Me$_2$), 4.81 (s, 1 H, middle CH), 3.86

(septet, 2 H, *J* = 6.8 Hz, C*H*Me$_2$), 3.25 (septet, 2 H, *J* = 6.8 Hz, C*H*Me$_2$), 1.68 (s, 6 H, NC*Me*), 1.42 (d, 6 H, *J* = 6.8 Hz, CH*Me$_2$*), 1.28 (d, 6 H, *J* = 7.00 Hz, CH*Me$_2$*), 1.27 (d, 6 H, *J* = 7.00 Hz, CH*Me$_2$*), 1.21 (d, 6 H, *J* = 6.8 Hz, CH*Me$_2$*), 1.20 (d, 12 H, *J* = 6.5 Hz, CH*Me$_2$*). ^{13}C{^{1}H} NMR (C_6D_6, 293 K): δ 165.2 (N*C*Me), 145.2 (*ipso*-C), 144.3 and 143.2 (*ortho*-C), 126.0 (*para*-C), 124.5 and 124.3 (*meta*-C), 100.2 (middle CH), 53.1, 28.7 and 28.4 (*C*HMe$_2$), 28.0, 26.3, 25.4 and 25.1 (CH*Me$_2$*), 25.1 (NC*Me*), 24.8 (CH*Me$_2$*). ^{207}Pb{^{1}H} NMR (C_6D_6, 293K): δ 2183. IR (Nujol, cm^{-1}) 1623 (s), 1554 (s), 1169 (s), 1105 (s), 933 (s), 790 (s). Anal. calc. for $C_{35}H_{55}N_3Pb$: C, 57.98; H, 7.65; N, 5.80. Found: C, 57.93; H, 7.56; N, 5.70%

[CH{(CH$_3$)CN-2,6-*i*Pr$_2$C$_6$H$_3$}$_2$PbNH(*i*Pr$_2$C$_6$H$_3$)], 5. Lithium 2,6-diisopropylanilide (0.07 g, 0.4 mmol) was added to a solution of β-diketiminate lead chloride, [LPbCl], (0.25 g, 0.38 mmol) in toluene (5 mL) and the mixture was stirred for 1 hour at room temperature. The solution was filtered and the resulting solvent was concentrated under reduced pressure and stored at -27°C yielding [Pb(L){NH(*i*Pr$_2$C$_6$H$_3$)], (0.10 g, 34%) as yellow crystals. ^{1}H NMR (C_6D_6, 293 K): δ 7.18 (d, 2 H, *J* = 7.6 Hz, *m*-H), 7.16-7.08 (m, 6 H, Ar*H*), 6.70 (t, 1 H, *J* = 7.6, *p*-H), 6.19 (s, 1 H, N*H*), 4.90 (s, 1 H, middle CH), 3.48 (septet, 2 H, *J* = 6.7 Hz, C*H*Me$_2$), 3.29 (septet, 2 H, *J* = 6.8 Hz, C*H*Me$_2$), 3.23 (septet, 2 H, *J* = 6.6 Hz, C*H*Me$_2$), 1.71 (s, 6 H, NC*Me*), 1.25 (d, 6 H, *J* = 6.9 Hz, CH*Me$_2$*), 1.23 (d, 12 H, *J* = 6.4 Hz, CH*Me$_2$*), 1.16 (d, 6 H, *J* = 6.8 Hz, CH*Me$_2$*), 1.15 (d, 6 H, *J* = 6.8 Hz, CH*Me$_2$*), 0.99 (d, 6 H, *J* = 6.7 Hz, CH*Me$_2$*). ^{13}C{^{1}H} NMR (C_6D_6, 293 K): δ 164.0 (N*C*Me), 150.4 and 144.8 (*ipso*-C), 143.7, 142.7 and 135.7 (*ortho*-C), 126.7 (*meta*-C), 125.0 (*para*-C), 123.9 and 122.8 (*meta*-C), 116.2 (*para*-C), 100.0 (middle CH), 28.8, 28.3 and 28.2 (*C*HMe$_2$), 26.5, 25.1, 24.7, 24.5 and 24.4 (CH*Me$_2$*), 24.0 (NC*Me*). ^{207}Pb{^{1}H} NMR (C_6D_6, 293K): δ 1500. IR (Nujol, cm^{-1}) 1624 (s), 1589 (s), 1552 (s), 1516 (s), 1252 (s), 1169 (s), 1098 (s), 935 (s), 837 (s), 791 (s), 747 (s). Anal. calc. for $C_{41}H_{59}N_3Pb$: C, 61.47; H, 7.42; N, 5.25. Found: C, 61.46; H, 7.46; N, 5.09%

[CH{(CH$_3$)CN-2,6-*i*Pr$_2$C$_6$H$_3$}$_2$PbNH(*i*PrC$_6$H$_4$)], 6. Lithium 2-isopropylanilide (0.05 g, 0.4 mmol) was added to a solution of β-diketiminate lead chloride, [LPbCl], (0.25 g, 0.38 mmol) in toluene (5 mL) and the mixture was stirred for 1 hour at room temperature. The solution was filtered and the resulting solvent was concentrated under reduced pressure and stored at -27°C for 1 day yielding [Pb(L){NH(*i*PrC$_6$H$_4$)], (0.10 g, 29%) as yellow crystals. ^{1}H NMR (C$_6$D$_6$, 293 K): δ 7.34 (d, 1 H, *J* = 7.2 Hz, *m*-H), 7.11-7.07 (m, 6 H, Ar*H*), 7.06 (t, 1 H, *J* = 7.8 Hz, Ar*H*), 6.70-6.65 (m, 2 H, Ar*H*), 6.47 (s, 1 H, N*H*), 4.83 (s, 1 H, middle CH), 3.63 (septet, 2 H, *J* = 6.6 Hz, C*H*Me$_2$), 3.25 (septet, 2 H, *J* = 6.8 Hz, C*H*Me$_2$), 3.01 (septet, 1 H, *J* = 6.4 Hz, C*H*Me$_2$), 1.68 (s, 6 H, NC*Me*), 1.36 (d, 6 H, *J* = 6.8 Hz, CH*Me$_2$*), 1.26 (d, 6 H, *J* = 6.8 Hz, CH*Me$_2$*), 1.17 (d, 6 H, *J* = 4.8 Hz, CH*Me$_2$*), 1.16 (d, 6 H, *J* = 4.8 Hz, CH*Me$_2$*), 1.05 (d, 6 H, *J* = 6.4 Hz, CH*Me$_2$*). ^{13}C{^{1}H} NMR (C$_6$D$_6$, 293 K): δ 169.8 (N*C*Me), 164.2 and 153.5 (*ipso*-C), 144.9, 143.5, 142.5 and 133.2 (*ortho*-C), 126.6 (*para*- or *meta*-C of Ar), 126.4 and 125.5 (*meta*-C), 125.0, 123.9 and 115.3 (*para*- and *meta*-C of Ar), 114.7 (*meta*-C), 99.8 (middle CH), 28.7, 28.5 and 28.5 (*C*HMe$_2$), 27.0, 25.1, 24.6 and 24.2 (CH*Me$_2$*), 24.1 (NC*Me*), 22.8 (CH*Me$_2$*). ^{207}Pb{^{1}H} NMR (C$_6$D$_6$, 293K): δ 1379. IR (Nujol, cm^{-1}) 1597 (s), 1553 (s), 1519 (s), 1318 (s), 1295 (s), 1171 (s), 1056 (s), 1021 (s), 935 (s), 891 (s), 843 (s), 694 (s).

[CH{(CH$_3$)CN-2,6-*i*Pr$_2$C$_6$H$_3$}$_2$PbNH(C$_6$H$_5$)], 7. Lithium anilide (0.04 g, 0.4 mmol) was added to a solution of β-diketiminate lead chloride, [LPbCl], (0.25 g, 0.38 mmol) in toluene (5 mL) and the mixture was stirred for 1 hour at room temperature, wrapped in foil. The solution was filtered and the resulting solvent was concentrated under reduced pressure and stored at -27°C for 1 day yielding [Pb(L){NH(C$_6$H$_5$)], as yellow crystals. ^{1}H NMR (C$_6$D$_6$, 293 K): δ 7.14-7.07 (m, 8 H, Ar*H*), 6.56 (t, 1 H, *J* = 7.2 Hz, *p*-H), 6.44 (d, 2 H, *J* = 7.6 Hz, Ar*H*), 6.01 (s, 1 H, N*H*), 4.79 (s, 1 H, middle CH), 3.58 (septet, 2 H, *J* = 6.8 Hz, C*H*Me$_2$), 3.21 (septet, 2 H, *J* = 6.8 Hz, C*H*Me$_2$), 1.67 (s, 6 H, NC*Me*), 1.23 (d, 6 H, *J* = 6.8 Hz, CH*Me$_2$*), 1.14 (d, 6 H, *J* = 6.8 Hz, CH*Me$_2$*), 1.14 (d, 6 H, *J* = 6.8 Hz, CH*Me$_2$*), 1.07 (d, 6 H, *J* = 6.8 Hz, CH*Me$_2$*). ^{13}C{^{1}H}

NMR (C_6D_6, 293 K): δ 164.2 (N*C*Me), 156.7 and 145.1 (*ipso*-C), 143.5, 142.5 and 129.3 (*ortho*-C), 126.7 (*para*- or *meta*-C of Ar), 125.1 (*meta*-C), 123.9 and 116.6 (*para*- or *meta*-C of Ar), 114.5 (*meta*-C), 100.3 (middle CH), 28.7 and 28.4 (*C*HMe_2), 26.7, 25.2, 24.6 and 24.4 (CH*Me*$_2$), 24.3 (NC*Me*). ^{207}Pb{^{1}H} NMR (C_6D_6, 293K): δ 1370. IR (Nujol, cm^{-1}) 1589 (s), 1558 (s), 1516 (s), 1169 (s), 1099 (s), 1054 (s), 1020 (s), 988 (s), 933 (s), 863 (s), 818 (s), 791 (s), 749 (s), 723 (s), 696 (s). Anal. calc. for $C_{35}H_{47}N_3Pb$: C, 58.63; H, 6.61; N, 5.86. Found: C, 58.84; H, 6.33; N, 5.79%

[CH{(CH$_3$)CN-2,6-*i*Pr$_2$C$_6$H$_3$}$_2$SnOSO$_2$CF$_3$], XXXIII Methyl triflate (7.9 μL, 0.070 mmol) was added to a solution of β-diketiminate tin diisopropylanilide (0.05 g, 0.07 mmol) in C_6D_6, and the mixture was stirred for 1 hour at room temperature. ^{1}H NMR (C_6D_6, 293 K): δ 7.00–7.14 (m, 6 H, Ar*H*), 5.32 (s, 1 H, middle CH), 3.23–3.37 (septet, 4 H, C*H*Me$_2$), 1.64 (s, 6 H, NC*Me*), 1.22 (d, 12 H, CH*Me*$_2$), 1.16 (d, 12 H, CH*Me*$_2$). Literature ^{1}H NMR (C_6D_6): δ 6.95–7.09 (m, 6 H, Ar*H*), 5.31 (s, 1 H, middle CH), 3.21–3.38 (septet, 4 H, C*H*Me$_2$), 1.62 (s, 6 H, NC*Me*), 1.20 (d, 12 H, CH*Me*$_2$), 1.16 (d, 12 H, CH*Me*$_2$).[71]

[CH{(CH$_3$)CN-2,6-*i*Pr$_2$C$_6$H$_3$}$_2$SnOCON(CH{CH$_3$}$_2$)$_2$], 8. A solution of β-diketiminate tin diisopropylamide (0.25 g, 0.39 mmol) in toluene (5 mL) was loaded into an ampoule. The reaction vessel was connected to a Schlenk line and a cylinder of high purity CO_2. The vessel was immersed in a dry ice/acetone bath, and after three pump/refill cycles, CO_2 was introduced at a pressure of 1.30 bar. The mixture was thawed and then stirred for 3 days at room temperature. The solvent was concentrated under reduced pressure and stored at -27°C yielding [Sn(L)OCON(CH{CH$_3$}$_2$)$_2$], (0.04 g, 14%) as colourless crystals. ^{1}H NMR (C_6D_6, 293 K): δ 7.18-7.13 (s, 4 H, Ar*H*), 7.09 (d, 1 H, *J* = 2.3 Hz, Ar*H*), 7.08 (d, 1 H, *J* = 2.3 Hz, Ar*H*), 5.00 (s, 1 H, middle CH), 3.94 (septet, 2 H, *J* = 6.7 Hz, C*H*Me$_2$), 3.71 (septet, 2 H, *J* = 6.8 Hz, C*H*Me$_2$), 3.18 (septet, 2 H, *J* = 6.8 Hz, C*H*Me$_2$), 1.62 (s, 6 H, NC*Me*), 1.46 (d, 6 H, *J* = 6.7

Hz, CH*Me*$_2$), 1.30 (d, 6 H, *J* = 6.8 Hz, CH*Me*$_2$), 1.21 (d, 12 H, *J* = 6.8 Hz, CH*Me*$_2$), 1.19 (d, 6 H, *J* = 6.9 Hz, CH*Me*$_2$), 1.12 (d, 6 H, *J* = 6.8 Hz, CH*Me*$_2$). $^{13}C\{^1H\}$ NMR (C_6D_6, 293 K): δ 165.3 (N*C*Me), 162.2 (O*C*O), 145.0 (*ipso*-C), 143.3 and 142.6 (*ortho*-C), 127.0 (*para*-C), 124.9 and 124.1 (*meta*-C), 100.2 (middle CH), 45.8, 29.0 and 28.1 (*C*HMe$_2$), 26.7, 25.3, 24.6 and 23.8 (CH*Me*$_2$), 21.6 (NC*Me*). $^{119}Sn\{^1H\}$ NMR (C_6D_6, 293K): δ -394. IR (Nujol, cm^{-1}) 1595 (s), 1575 (s), 1552 (s), 1524 (s), 1337 (s), 1262 (s), 1097 (s), 1050 (s), 1019 (s) 791 (s). Anal. calc. for $C_{36}H_{55}N_3O_2Sn$: C, 63.53; H, 8.15; N, 6.17. Found: C, 63.59; H, 8.26; N, 5.98%

[CH{(CH$_3$)CN-2,6-*i*Pr$_2$C$_6$H$_3$}$_2$SnOCONH(*i*Pr$_2$C$_6$H$_3$)], 9. A solution of β-diketiminate tin diisopropylanilide (0.25 g, 0.35 mmol) in toluene (5 mL) was loaded into an ampoule. The reaction vessel was connected to a Schlenk line and a cylinder of high purity CO_2. The vessel was immersed in a dry ice/acetone bath, and after three pump/refill cycles, CO_2 was introduced at a pressure of 1.14 bar. The mixture was thawed and then stirred for 4 hours at room temperature. ^1H NMR (C_6D_6, 293 K): δ 7.19-7.12 (m, 6 H, Ar*H*), 7.09-7.05 (m, 3 H, Ar*H*), 5.96 (s, 1 H, N*H*), 4.89 (s, 1 H, middle CH), 3.64 (septet, 2 H, *J* = 6.8 Hz, C*H*Me$_2$), 3.33 (septet, 2 H, *J* = 6.8 Hz, C*H*Me$_2$), 3.15 (septet, 2 H, *J* = 6.9 Hz, C*H*Me$_2$), 1.60 (s, 6 H, NC*Me*), 1.35 (d, 6 H, *J* = 6.7 Hz, CH*Me*$_2$), 1.27 (d, 6 H, *J* = 6.8 Hz, CH*Me*$_2$), 1.21 (d, 6 H, *J* = 6.9 Hz, CH*Me*$_2$), 1.14 (d, 12 H, *J* = 6.8 Hz, CH*Me*$_2$), 1.09 (d, 6 H, *J* = 6.8 Hz, CH*Me*$_2$). $^{13}C\{^1H\}$ NMR (C_6D_6, 293 K): δ 165.7 (N*C*Me), 162.0 (O*C*O), 145.7 and 143.0 (*ipso*-C), 142.1, 133.8 and 127.3 (*ortho*-C), 126.9 (*meta*-C), 124.9 (*para*-C), 124.2 and 123.4 (*meta*-C), 115.8 (*para*-C), 99.4 (middle CH), 29.2, 28.8 and 28.3 (*C*HMe$_2$), 26.2, 25.3, 24.8, 24.7 and 24.2 (CH*Me*$_2$), 24.1 (NC*Me*). $^{119}Sn\{^1H\}$ NMR (C_6D_6, 293K): δ -398. IR (Nujol, cm^{-1}) 3413 (s), 1624 (s), 1554 (s), 1526 (s), 1517 (s), 1238 (s), 1172 (s), 1099 (s), 1058 (s), 1022 (s), 891 (s), 793 (s).

[CH{(CH$_3$)CN-2,6-*i*Pr$_2$C$_6$H$_3$}$_2$SnOC(NC$_6$H$_5$)C{(CH$_3$)CN-2,6-*i*Pr$_2$C$_6$H$_3$}{(CH$_3$)CN(H)-2,6-*i*Pr$_2$C$_6$H$_3$}], 10. Phenyl isocyanate (38.0 μL, 0.351 mmol) was added to a solution of β-

diketiminate tin diisopropylanilide (0.25 g, 0.35 mmol) in toluene (5mL), and the mixture was stirred for 4 days at room temperature, wrapped in foil. The solution was filtered and the solvent was concentrated under reduced pressure and stored at -27°C for 7 days yielding [Sn(L) OC(NC_6H_5)C{($(CH_3)_2$CN-2,6-*i*$Pr_2C_6H_3$}$_2$], (0.15 g, 40%) as colourless crystals. ^{1}H NMR (C_6D_6, 293 K): δ 13.67 (s, 1 H, *H*NAr), 7.18-7.00 (m, 14 H, Ar*H*), 6.82 (t, 1 H, *J* = 7.3 Hz Ar*H*), 6.32 (d, 2 H, *J* = 7.8 Hz, Ar*H*), 4.72 (s, 1 H, middle CH), 3.78 (septet, 2 H, *J* = 6.8 Hz, C*H*Me$_2$), 3.26 (septet, 2 H, *J* = 6.8 Hz, C*H*Me$_2$), 3.17 (septet, 2 H, *J* = 6.8 Hz, C*H*Me$_2$), 2.74 (septet, 2 H, *J* = 6.8 Hz), 1.58 (s, 6 H, NC*Me*), 1.50 (d, 6 H, *J* = 6.6 Hz, CH*Me$_2$*), 1.38 (s, 6 H, NC*Me*) 1.33 (d, 6 H, *J* = 6.8 Hz, CH*Me$_2$*), 1.27 (d, 6 H, *J* = 6.8 Hz, CH*Me$_2$*), 1.19 (d, 6 H, *J* = 6.9 Hz, CH*Me$_2$*), 1.16 (d, 12 H, *J* = 6.7 Hz, CH*Me$_2$*), 0.99 (d, 6 H, *J* = 7.2 Hz, CH*Me$_2$*), 0.96 (d, 6 H, *J* = 6.8 Hz, CH*Me$_2$*). ^{13}C{^{1}H} NMR (C_6D_6, 293 K): δ 172.7 (O*C*NPh), 165.5 (N*C*Me), 162.1 (N*C*Me), 147.8, 144.2 and 143.5 (*ipso*-C), 143.0, 142.7, 142.6, 140.7 and 138.9 (*ortho*-C), 127.7, 126.2, 125.8, 125.4, 124.6, 124.5, 123.7, 123.5 and 122.6 (*para*- or *meta*-C of Ar), 102.2 and 96.3 (middle C), 28.8, 28.8, 28.6 and 28.1 (*C*HMe$_2$), 26.5, 25.2, 24.8, 24.6, 24.4, 24.3 and 23.7 (CH*Me$_2$*), 23.6 and 19.9 (NC*Me*). ^{119}Sn{^{1}H} NMR (C_6D_6, 293K): δ -373. IR (Nujol, cm^{-1}) 2024 (s), 1946 (s), 1916 (s), 1599 (s), 1535 (s), 1319 (s), 1261 (s), 1099 (s), 1019 (s). Anal. Calc. for $C_{65}H_{87}N_5OSn$: C, 72.75; H, 8.17; N, 6.53. Found: C, 73.41; H, 7.56; N, 6.45%

[CH{(CH_3)CN-2,6-*i*$Pr_2C_6H_3$}$_2$SnMe], XXIX. Zinc dimethyl (2 M, 23.7 µL, 0.0474 mmol) or aluminium trimethyl (2 M, 25.1 µL, 0.0502 mmol) was added to a solution of the β-diketiminate tin phenyl isocyanate complex **10** (0.05 g, 0.05 mmol) in C_6D_6, and the mixture was stirred for 1 hour (aluminium trimethyl) or 6 hours (zinc dimethyl) at room temperature. ^{1}H NMR (C_6D_6, 293 K): δ 7.11–7.15 (m, 6 H, Ar*H*), 4.87 (s, 1 H, middle CH), 3.60 (septet, 2 H, C*H*Me$_2$), 3.37 (septet, 2 H, C*H*Me$_2$), 1.62 (s, 6 H, NC*Me*), 1.36 (d, 6 H, CH*Me$_2$*), 1.22 (d, 6 H, CH*Me$_2$*), 1.19 (d, 12 H, CH*Me$_2$*), 0.60 (t, 3 H, *Me*). Literature ^{1}H NMR

(C_6D_6): δ 7.10–7.15 (m, 6 H, Ar*H*), 4.86 (s, 1 H, middle CH), 3.59 (septet, 2 H, C*H*Me_2), 3.37 (septet, 2 H, C*H*Me_2), 1.60 (s, 6 H, NC*Me*), 1.35 (d, 6 H, CH*Me*$_2$), 1.22 (d, 6 H, CH*Me*$_2$), 1.19 (d, 12 H, CH*Me*$_2$), 0.59 (t, 3 H, *Me*).[85]

[CH{(CH$_3$)CN-2,6-*i*Pr$_2$C$_6$H$_3$}$_2$SnCC(C$_6$H$_5$)], 12. Phenyl acetylene (43 μL, 0.39 mmol) was added to a solution of β-diketiminate tin diisopropylamide (0.25 g, 0.39 mmol) in toluene (5 mL), and the mixture was stirred for 6 days at 70°C. The solution was filtered and the solvent was concentrated under reduced pressure and stored at -27°C yielding [Sn(L)CC(C_6H_5)], (0.24 g, 96%) as colourless crystals. ^{1}H NMR (C_6D_6, 293 K): δ 7.58-7.55 (m, 2 H, *o*-C), 717-6.94 (m, 9 H, Ar*H*), 5.04 (s, 1 H, middle CH), 4.08 (septet, 2 H, *J* = 6.8 Hz, C*H*Me_2), 3.39 (septet, 2 H, *J* = 6.8 Hz, C*H*Me_2), 1.65 (s, 6 H, NC*Me*), 1.45 (d, 6 H, *J* = 6.7 Hz, CH*Me*$_2$), 1.30 (d, 6 H, *J* = 7.0 Hz, CH*Me*$_2$), 1.28 (d, 6 H, *J* = 7.0 Hz, CH*Me*$_2$) 1.16 (d, 6 H, *J* = 6.8 Hz, CH*Me*$_2$). ^{13}C{^{1}H} NMR (C_6D_6, 293 K): δ 166.7 (N*C*Me), 146.1, 143.0, 142.9, 132.1, 128.4, 127.1, 126.5, 125.0, 124.4 and 124.1 (Ar-*C*), 106.5 (C*C*), 100.4 (middle CH), 29.2 and 28.3 (*C*HMe_2), 28.2, 24.9, 24.6 and 24.2 (CH*Me*$_2$), 24.0 (NC*Me*). ^{119}Sn{^{1}H} NMR (C_6D_6, 293K): δ -206. IR (Nujol, cm^{-1}) 1523 (s), 1316 (s), 1203 (s), 1171 (s), 1100 (s), 934 (s). Anal. calc. for $C_{37}H_{46}N_2Sn$: C, 69.71; H, 7.27; N, 4.39. Found: C, 69.99; H, 7.32; N, 4.33%

[CH{(CH$_3$)CN-2,6-*i*Pr$_2$C$_6$H$_3$}$_2$PbOSO$_2$CF$_3$], XXXIII. Methyl triflate (7.1 μL, 0.062 mmol) was added to a solution of β-diketiminate lead diisopropylanilide (0.05 g, 0.06 mmol) in C_6D_6, and the mixture was stirred for 1 hour at room temperature. ^{1}H NMR (C_6D_6, 293 K): δ 7.08–7.14 (m, 6 H, Ar*H*), 4.90 (s, 1 H, middle CH), 3.29 (septet, 2 H, C*H*Me_2), 1.61 (s, 6 H, NC*Me*), 1.27 (d, 12 H, CH*Me*$_2$), 1.20 (d, 12 H, CH*Me*$_2$). Literature ^{1}H NMR (C_6D_6): δ 6.99–7.12 (m, 6 H, Ar*H*), 4.88 (s, 1 H, middle CH), 3.26 (septet, 4 H, C*H*Me_2), 1.60 (s, 6 H, NC*Me*), 1.26 (d, 12 H, CH*Me*$_2$), 1.19 (d, 12 H, CH*Me*$_2$).[79]

[CH{(CH$_3$)CN-2,6-*i*Pr$_2$C$_6$H$_3$}$_2$PbI], XCV. Methyl iodide (4.3 μL, 0.069 mmol) was added to a solution of β-diketiminate lead diisopropylamide (0.05 g, 0.07 mmol) in C_6D_6, and the mixture was stirred for 3 hours at room temperature. ^{1}H NMR (C_6D_6, 293 K): δ 7.10-7.04 (m, 6 H, Ar*H*), 4.94 (s, 1 H, middle CH), 3.97 (septet, 2 H, C*H*Me$_2$), 3.02 (septet, 2 H, C*H*Me$_2$), 1.68 (s, 6 H, NC*Me*), 1.52 (d, 6 H, CH*Me$_2$*), 1.24 (d, 6 H, CH*Me$_2$*), 1.18 (d, 6 H, CH*Me$_2$*), 1.15 (d, 6 H, CH*Me$_2$*). Literature ^{1}H NMR (C_6D_6): δ 7.11 (d, 2 H, *m*-H), 7.09 (t, 2 H, *p*-H), 7.06 (d, 2 H, *m*-H), 4.93 (s, 1 H, middle CH), 4.00 (septet, 2 H, C*H*Me$_2$), 3.07 (septet, 2 H, C*H*Me$_2$), 1.70 (s, 6 H, NC*Me*), 1.53 (d, 6 H, CH*Me$_2$*), 1.28 (d, 6 H, CH*Me$_2$*), 1.21 (d, 6 H, CH*Me$_2$*), 1.10 (d, 6 H, CH*Me$_2$*).[72]

[{(HN-2,6-*i*Pr$_2$C$_6$H$_3$)PbI}$_2$], 13. Methyl iodide (4.3 μL, 0.069 mmol) was added to a solution of β-diketiminate lead diisopropylamide (0.05 g, 0.07 mmol) in C_6D_6, and the mixture was stirred at room temperature. The solution was filtered, the solvent was evaporated under reduced pressure and toluene was added to the solid. The solution was stored at -27°C yielding [Pb{HN-2,6-*i*Pr$_2$C$_6$H$_3$}$_2$I], as yellow crystals.

[CH{(CH$_3$)CN-2,6-*i*Pr$_2$C$_6$H$_3$}$_2$PbOC(NC$_6$H$_5$)C{(CH$_3$)CN-2,6-*i*Pr$_2$C$_6$H$_3$}{(CH$_3$)CN(H)-2,6-*i*Pr$_2$C$_6$H$_3$}], 14. Phenyl isocyanate (34 μL, 0.31 mmol) was added to a solution of β-diketiminate lead diisopropylanilide (0.25 g, 0.31 mmol) in toluene (5 mL), and the mixture was stirred for 24 hours at room temperature, wrapped in foil. The solution was filtered and the solvent was concentrated under reduced pressure and stored at -27°C for 7 days yielding [Pb(L)OC(NC$_6$H$_5$)C{(CH$_3$)$_2$CN-2,6-*i*Pr$_2$C$_6$H$_3$}$_2$], (0.14 g, 38%) as colourless crystals. ^{1}H NMR (C_6D_6, 293 K): δ 13.53 (s, 1 H, *H*NAr), 7.13-7.01 (m, 10 H, Ar*H*), 6.86 (t, 2 H, *J* = 7.6 Hz, *p*-H), 6.78 (t, 2 H, *J* = 7.3 Hz, *p*-H), 6.32 (d, 2 H, *J* = 7.4 Hz, *m*-H) 4.60 (s, 1 H, middle CH), 3.28 (septet, 4 H, *J* = 6.8 Hz, C*H*Me$_2$), 2.78 (septet, 2 H, *J* = 6.8 Hz, C*H*Me$_2$), 2.62 (septet, 2 H, *J* = 6.8 Hz, C*H*Me$_2$), 1.63 (s, 6 H, NC*Me*), 1.39 (s, 6 H, NC*Me*), 1.30 (d, 6 H, *J* = 6.9

Hz, CH*Me*$_2$), 1.24-1.18 (m, 12 H, CH*Me*$_2$), 1.13 (d, 6 H, *J* = 6.8 Hz, CH*Me*$_2$), 1.12 (d, 12 H, *J* = 6.8 Hz, CH*Me*$_2$), 0.99 (d, 6 H, *J* = 6.8 Hz, CH*Me*$_2$), 0.97 (d, 6 H, *J* = 6.8 Hz, CH*Me*$_2$). ^{207}Pb{^{1}H} NMR (C_6D_6, 293K): δ 981. IR (Nujol, cm^{-1}) 2024 (s), 1946 (s), 1916 (s), 1602 (s), 1535 (s), 1170 (s), 1101 (s), 1021 (s), 966 (s), 935 (s), 891 (s), 844 (s), 791 (s), 722 (s). Anal. calc. for $C_{65}H_{87}N_5OPb$: C, 67.21; H, 7.55; N, 6.03. Found: C, 67.59; H, 6.97; N, 6.25%

[CH{(CH$_3$)CN-2,6-*i*Pr$_2$C$_6$H$_3$}$_2$PbMe], XXIX. Zinc dimethyl (23.3 μL, 0.0474 mmol) or aluminium trimethyl (22.8 μL, 0.0456 mmol) was added to a solution of the β-diketiminate lead phenyl isocyanate complex **14** (0.05 g, 0.05 mmol) in C_6D_6, and the mixture was stirred for 1 hour at room temperature. ^{1}H NMR (C_6D_6, 293 K): δ 7.09–7.15 (m, 6 H, Ar*H*), 4.77 (s, 1 H, middle CH), 3.54 (septet, 2 H, C*H*Me$_2$), 3.44 (septet, 2 H, C*H*Me$_2$), 1.70 (s, 6 H, NC*Me*), 1.31 (d, 6 H, CH*Me*$_2$), 1.20 (d, 12 H, CH*Me*$_2$), 1.19 (d, 6 H, CH*Me*$_2$), 0.54 (t, 3 H, *Me*). Literature ^{1}H NMR (C_6D_6): δ 7.12–7.15 (m, 6 H, Ar*H*), 4.77 (s, 1 H, middle CH), 3.54 (septet, 2 H, C*H*Me$_2$), 3.43 (septet, 2 H, C*H*Me$_2$), 1.70 (s, 6 H, NC*Me*), 1.31 (d, 6 H, CH*Me*$_2$), 1.21 (d, 6 H, CH*Me*$_2$), 1.20 (d, 6 H, CH*Me*$_2$), 1.19 (d, 6 H, CH*Me*$_2$), 0.55 (t, 3 H, *Me*).[79]

[CH{(CH$_3$)CN-2,6-*i*Pr$_2$C$_6$H$_3$}$_2$PbOC(N*t*Bu)NH(2,6-*i*Pr$_2$C$_6$H$_3$)], 15. *Tert*-butyl isocyanate (32 μL, 0.28 mmol) was added to a solution of β-diketiminate lead diisopropylanilide (0.25 g, 0.28 mmol) in toluene (5 mL), and the mixture was stirred for 6 hours at room temperature. The solution was filtered and the solvent was concentrated under reduced pressure and stored at -27°C for 7 days yielding [Pb(L)OC(NC(CH$_3$)$_3$)NH(2,6-*i*Pr$_2$C$_6$H$_3$)], as yellow crystals. ^{1}H NMR (Tol-d$_8$, 293 K): δ 7.10-6.95 (m, 8 H, Ar*H*), 6.85 (t, 1 H, *J* = 7.8 Hz, *p*-H), 4.62 (s, 1 H, middle CH), 3.17 (s, 1 H, *H*NAr'), 2.51 (septet, 2 H, *J* = 6.8 Hz, C*H*Me$_2$), 1.59 (s, 6 H, NC*Me*), 1.24 (d, 12 H, *J* = 6.4 Hz, CH*Me*$_2$), 1.08 (d, 6 H, *J* = 6.8 Hz, CH*Me*$_2$), 1.00 (d, 6 H, *J* = 7.2 Hz, CH*Me*$_2$), 0.80 (s, 9 H, C*Me*$_3$). ^{13}C{^{1}H} NMR (Tol-d$_8$, 293 K): δ 164.5 (O*C*N), 160.9 (N*C*Me), 144.8 and 143.6 (*ipso*-C), 142.5, 129.3 and 128.5 (*ortho*-C), 125.9 (*meta*-C),

125.6, 123.8, 123.7 and 123.0 (*para*- or *meta*-C of Ar), 96.9 (middle CH), 49.9 (*C*Me_3), 29.8 (C*Me*$_3$), 28.4 and 27.6 (*C*HMe_2), 25.1, 24.6, 24.6 and 24.3 (CH*Me*$_2$), 21.3 (NC*Me*). ^{207}Pb{^{1}H} NMR (Tol-d_8, 293K): δ 881. IR (Nujol, cm^{-1}) 1685 (s), 1675 (s), 1653 (s), 1560 (s), 1549 (s), 1507 (s), 1051 (br), 722 (s). Anal. calc. for $C_{46}H_{68}N_4OPb$: C, 61.37; H, 7.61; N, 6.22. Found: C, 61.54; H, 7.15; N, 6.39%.

[CH{(CH$_3$)CN-2,6-*i*Pr$_2$C$_6$H$_3$}$_2$PbCC(C$_6$H$_5$)], XXIX. Phenyl acetylene (7.6μL, 0.069 mmol) was added to a solution of β-diketiminate lead diisopropylamide (0.05 g, 0.07 mmol) in C_6D_6, and the mixture was stirred for 1 hour at room temperature. ^{1}H NMR (C_6D_6, 293 K): δ 7.60 (d, 2 H, *o*-H), 7.04 (t, 2 H, *m*-H), 7.03-7.20 (m, 6 H, Ar*H*), 6.97 (tt, 1 H, *p*-H), 4.89 (s, 1 H, middle CH), 4.89 (septet, 2 H, C*H*Me_2), 4.09 (septet, 2 H, C*H*Me_2), 1.73 (s, 6 H, NC*Me*), 1.47 (d, 6 H, CH*Me*$_2$), 1.31 (d, 6 H, CH*Me*$_2$), 1.23 (d, 6 H, CH*Me*$_2$), 1.18 (d, 6 H, CH*Me*$_2$). Literature ^{1}H NMR (C_6D_6): δ 7.59 (d, 2 H, *o*-H), 7.05 (t, 2 H, *m*-H), 7.03–7.17 (m, 6 H, Ar*H*), 6.96 (tt, 1 H, *p*-H), 4.87 (s, 1 H, middle CH), 4.08 (septet, 2 H, C*H*Me_2), 3.22 (septet, 2 H, C*H*Me_2), 1.71 (s, 6 H, NC*Me*), 1.47 (d, 6 H, CH*Me*$_2$), 1.30 (d, 6 H, CH*Me*$_2$), 1.22 (d, 6 H, CH*Me*$_2$), 1.16 (d, 6 H, CH*Me*$_2$).[79]

[CH{(CH$_3$)CN-2,6-*i*Pr$_2$C$_6$H$_3$}$_2$GeSeP(C$_6$H$_{11}$)$_2$], 16. A slurry of selenium (0.03 g, 0.4 mmol), finely suspended in toluene, was added dropwise to a solution of β-diketiminate germanium dicyclohexylphosphide (0.25 g, 0.36 mmol) in toluene (5 mL), and the mixture was stirred for 24 hours at room temperature resulting in the colour changing from purple to orange. The solution was filtered, concentrated under reduced pressure and stored at -27°C for 1 day yielding [Ge(L)SeP(C_6H_{11})$_2$], (0.06 g, 21%) as orange crystals. ^{1}H NMR (C_6D_6, 293 K): δ 7.13 (dd, 2 H, *J* = 7.6 Hz, *m*-H), 7.08 (t, 2 H, *J* = 7.6 Hz, *p*-H), 7.01 (dd, 2 H, *J* = 7.6 Hz, *m*-H), 4.65 (s, 1 H, middle CH), 3.64 (septet, 2 H, *J* = 6.8 Hz, C*H*Me_2), 3.28 (septet, 2 H, *J* = 6.8 Hz, C*H*Me_2), 1.61 (d, 6 H, *J* = 6.8 Hz, CH*Me*$_2$), 1.57-1.54 (br, 4 H, P*Cy*), 1.50 (s, 6 H,

NC*Me*), 1.44-1.40 (br, 6 H, P*Cy*), 1.37 (d, 6 H, *J* = 6.8 Hz, CH*Me*$_2$), 1.15 (d, 6 H, *J* = 6.8 Hz, CH*Me*$_2$), 1.10 (d, 6 H, *J* = 6.8 Hz, CH*Me*$_2$), 1.08-0.96 (br, 10 H, P*Cy*), 0.67 (br, 2 H, PC*H*). ^{13}C{^{1}H} NMR (C_6D_6, 293 K): δ 165.7 (N*C*Me), 145.4, 144.3 and 140.5 (*ipso*- or *ortho*-C), 126.9 (*para*-C), 124.7 and 124.2 (*meta*-C), 96.3 (middle CH), 35.2 (d, *J* = 28 Hz, P*C*H), 30.2 (*J* = 18 Hz, *C*HMe$_2$), 29.7 (d, *J* = 7, *C*HMe$_2$), 29.5, 28.9, 27.8, 27.7, 27.6 and 27.6 (P*Cy*), 27.1 (*J* = 2 Hz, CH*Me*$_2$), 27.0 (P*Cy*), 25.3, 24.9 and 24.6 (CH*Me*$_2$), 23.2 (NC*Me*). ^{31}P{^{1}H} NMR (C_6D_6, 293 K): δ 41.9 ($J_{P\text{-}Se}$ = 198 Hz). ^{77}Se{^{1}H} NMR (C_6D_6, 293 K): -19.3 (d, $J_{Se\text{-}P}$ = 198 Hz). IR (Nujol, cm^{-1}) 1556 (s), 1317 (s), 1172 (s), 1099 (s), 1016 (s), 848 (s), 798 (s), 722 (s), 518 (s). Anal. calc. for $C_{41}H_{63}N_2PSeGe$: C, 64.24; H, 8.28; N, 3.65. Found: C, 65.46; H, 8.00; N, 3.18%

[CH{(CH$_3$)CN-2,6-*i*Pr$_2$C$_6$H$_3$}$_2$GeSeP(C$_6$H$_5$)$_2$], 17. A slurry of selenium (0.03 g, 0.4 mmol), finely suspended in toluene, was added dropwise to a solution of β-diketiminate germanium diphenylphosphide (0.25 g, 0.37 mmol) in toluene (5 mL), and the mixture was stirred for 10 days at room temperature resulting in the colour changing from purple to orange. The solution was filtered, the solvent evaporated under reduced pressure and ether was added to the residue. The solution was stored at -27°C for 1 day yielding [Ge(L)SeP(C$_6$H$_5$)$_2$], as orange crystals, interspersed with traces of diphenyl phosphine **19**. ^{1}H NMR (C_6D_6, 293 K): δ 7.33-6.93 (m, 16 H, Ar*H*), 4.80 (s, 1 H, middle CH), 3.67 (septet, 2 H, *J* = 6.8 Hz, C*H*Me$_2$), 3.35 (septet, 2 H, *J* = 6.8 Hz, C*H*Me$_2$), 1.53 (s, 6 H, NC*Me*), 1.42 (d, 6 H, *J* = 6.8 Hz, C*H*Me$_2$), 1.33 (d, 6 H, *J* = 6.8 Hz, C*H*Me$_2$), 1.16 (d, 6 H, *J* = 8.0 Hz, C*H*Me$_2$), 1.14 (d, 6 H, *J* = 7.2 Hz, C*H*Me$_2$). ^{31}P{^{1}H} NMR (C_6D_6, 293 K): δ 11.1 ($J_{P\text{-}Se}$ = 219 Hz). ^{77}Se{^{1}H} NMR (C_6D_6, 293 K): 136.5 (d, $J_{Se\text{-}P}$ = 217 Hz). Anal. calc. for $C_{41}H_{51}N_2PSeGe$: C, 65.27; H, 6.81; N, 3.71. Found: C, 66.88; H, 5.48; N, 2.53%

[CH{(CH$_3$)CN-2,6-*i*Pr$_2$C$_6$H$_3$}$_2$GeTeP(C$_6$H$_{11}$)$_2$], 18. A slurry of tellurium (0.05 g, 0.4 mmol), finely suspended in toluene, was added dropwise to a solution of β-diketiminate germanium dicyclohexylphosphide (0.25 g, 0.36 mmol) in toluene (5 mL), and the mixture was stirred for 24 hours at room temperature resulting in the colour changing from purple to red. The solution was filtered, concentrated under reduced pressure and stored at -27°C for 1 day yielding [Ge(L)TeP(C$_6$H$_{11}$)$_2$], as red crystals. ^{1}H NMR (C$_6$D$_6$, 293 K): δ 7.10-7.06 (m, 4 H, Ar*H*), 7.03 (dd, 2 H, *J* = 7.2 Hz, *m*-H), 4.70 (s, 1 H, middle CH), 3.62 (septet, 2 H, *J* = 6.8 Hz, C*H*Me$_2$), 3.28 (septet, 2 H, *J* = 6.8 Hz, C*H*Me$_2$), 1.68-1.66 (br, 4 H, P*Cy*), 1.61 (d, 6 H, *J* = 6.8 Hz, CH*Me$_2$*), 1.57-1.51 (m, 6 H, P*Cy*), 1.48 (s, 6 H, NC*Me*), 1.42 (d, 6 H, *J* = 6.8 *Hz*, CH*Me$_2$*), 1.15 (d, 6 H, *J* = 6.8 Hz, CH*Me$_2$*), 1.12 (d, 6 H, *J* = 6.8 Hz, CH*Me$_2$*), 1.08-1.04 (br, 10H, P*Cy*), 0.86-0.82 (br, 2 H, PC*H*). ^{13}C{^{1}H} NMR (C$_6$D$_6$, 293 K): δ 166.4 (N*C*Me), 146.0, 143.2 and 141.5 (*ipso*- or *ortho*-C), 127.1 (*para*-C), 124.7 and 124.5 (*meta*-C), 96.8 (middle CH), 33.6 and 33.4 (P*Cy*), 32.5 (d, *J* = 8 Hz, *C*HMe$_2$), 31.3 (d, *J* = 17 Hz, P*C*H), 29.6 (CH*Me$_2$*), 28.8, 27.8, 27.7, 27.7 and 27.7 (P*Cy*), 27.2 (d, *J* = 3 Hz, CH*Me$_2$*), 27.0 (P*Cy*), 25.2, 24.9 and 24.8 (CH*Me$_2$*), 23.4 (NC*Me*). ^{31}P{^{1}H} NMR (C$_6$D$_6$, 293 K): δ 26.1 ($J_{P\text{-}Te}$ = 407 Hz). ^{125}Te {^{1}H} NMR (C$_6$D$_6$, 293 K): -296.8 (d, $J_{Te\text{-}P}$ = 406 Hz). IR (Nujol, cm^{-1}) 1558 (s), 1317 (s), 1260 (s), 1169 (s), 1100 (s), 1017 (s), 933 (s), 887 (s), 847 (s), 824 (s), 722 (s).

[P$_2$(C$_6$H$_5$)$_4$], 19. A finely suspended slurry of selenium (0.03 g, 0.4 mmol) in toluene was added dropwise to a solution of β-diketiminate germanium diphenylphosphide (0.25 g, 0.37 mmol) in toluene (5 mL). The mixture was stirred at room temperature for 10 days resulting in the colour changing from purple to orange. The solution was filtered and the solvent evaporated under reduced pressure then ether was added to the residue. The solution was stored at -27°C for 1 day yielding [P$_2$(C$_6$H$_5$)$_4$], as yellow crystals, interspersed with traces of germanium diphenyl-selenophosphinite **17**. ^{1}H NMR (C$_6$D$_6$, 293 K): δ 7.55 (s, 8 H, Ar*H*), 6.96 (s, 12 H, Ar*H*), 4.80 (s, middle CH), 3.67 (septet, C*H*Me$_2$), 3.35 (septet,

C*H*Me$_2$), 1.67-1.05 (m, NC*Me* and C*H*Me$_2$). ^{31}P{^{1}H} NMR (C_6D_6, 293 K): δ -14.9. Literature ^{1}H NMR (C_6D_6): δ 7.51-7.57 (m, 8 H, Ar*H*), 6.92-6.97 (m, 12 H, Ar*H*). ^{31}P{^{1}H} NMR (C_6D_6): δ -13.6.[177]

[CH{(CH$_3$)CN-2,6-*i*Pr$_2$C$_6$H$_3$}$_2$Ge(Se)SeP(C$_6$H$_5$)$_2$], 20. Excess selenium (0.15 g, 1.9 mmol), finely suspended in toluene, was added dropwise to a solution of β-diketiminate germanium diphenylphosphide (0.25 g, 0.37 mmol) in toluene (5 mL), and the mixture was stirred vigorously for 24 hours at room temperature resulting in the colour changing from purple to yellow. The solution was filtered, the solvent evaporated under reduced pressure and ether was added to the residue. The solution was stored at -27°C for 1 day yielding [Ge(L)(Se)SeP(C_6H_5)$_2$], as yellow crystals and residual traces of an unknown. ^{1}H NMR (C_6D_6, 293 K): δ 7.83-7.77 (m), 7.46 (t, 2 H, *J* = 7.3 Hz, *m*-H), 7.46 (t, 2 H, *J* = 7.3 Hz, *m*-H), 7.16-7.09 (m, 6 H, Ar*H*), 7.02 (d, 1 H, *J* = 7.6 Hz, *m*-H), 7.00 (d, 1 H, *J* = 7.6 Hz, *m*-H), 6.97-6.82 (m, Ar*H*), 5.00 (s, 1 H, middle CH), 4.76 (s), 3.90 (septet, 2 H, *J* = 6.8 Hz, C*H*Me$_2$), 3.45 (septet, 2 H, *J* = 6.8 Hz, C*H*Me$_2$), 3.23 (m, *J* = 6.9 Hz), 1.55 (d, 6 H, *J* = 6.4 Hz, CH*Me$_2$*), 1.51 (s, 6 H, NC*Me*), 1.48 (s), 1.34 (d, *J* = 6.8 Hz), 1.26 (d, 6 H, *J* = 6.8 Hz, CH*Me$_2$*), 1.09 (d, 6 H, *J* = 6.8 Hz, CH*Me$_2$*), 1.06 (d, *J* = 7.2 Hz) 0.90 (d, 6 H, *J* = 6.8 Hz, CH*Me$_2$*). ^{13}C{^{1}H} NMR (C_6D_6, 293 K): δ 166.9 (N*C*Me), 146.7, 145.9, 139.9 and 139.6 (unknown), 137.9, 133.9 and 133.7 (*ipso*- or *ortho*-C), 132.0 (*J* = 32 Hz, P*Ph*), 129.9 (*J* = 8 Hz, P*Ph*), 128.8 (*J* = 4 Hz, P*Ph*), 128.4 (*para*- or *meta*-C), 128.4 and 127.8 (P*Ph* or unknown), 125.5 and 125.0 (*para*- or *meta*-C), 98.4 (middle CH), 29.6 (unknown), 29.3 (*J* = 3 Hz, *C*HMe$_2$), 26.9 (*C*HMe$_2$), 26.1, 25.9 and 25.2 (CH*Me$_2$*), 24.8 (*J* = 2 Hz, CH*Me$_2$*), 24.3 (unknown), 23.6 (NCMe), 15.6 (unknown). ^{31}P{^{1}H} NMR (C_6D_6, 293 K): δ 19.1 ($J_{P\text{-}Se}$ = 201 Hz), 26.3 ($J_{P\text{-}Se}$ = 579 Hz). Anal. calc. for $C_{41}H_{51}N_2PSe_2Ge$: C, 59.09; H, 6.17; N, 3.36. Found: C, 59.15; H, 6.23; N, 3.19%

5.4. Materials chemistry

The TGA data were compiled by Dr M. S. Hill at the University of Bath using a TGA 4000 (PerkinElmer Inc., UK). The thermal decomposition of [(BDI)GePCy$_2$] **CXXVI**, [(BDI)GeTePCy$_2$] **18**, [(BDI)SnSeP(Se)Cy$_2$] **CXXXII**[115] and [(BDI)PbSeP(Se)Cy$_2$] **CXXXIII**[115] was carried out using the method outlined by Gedanken.[190] This involved a sample of the precursor complex (masses stated in Table 16) which was introduced into a Swagelock cell at room temperature. The cell was tightly closed by two plugs and inserted into an iron pipe in the middle of a tube furnace. The temperature was elevated at a rate of 5°C per minute to 600°C, under a N_2 atmosphere with a purge rate of 20 mL per minute. The Swagelok fitting was steadily cooled by 1°C per minute to room temperature (25°C). Black powders were collected (masses stated in Table 16).

The aerosol assisted chemical vapour deposition data (AACVD) were collected by Dr M. S. Hill at the University of Bath. Thin steel grey films of SnSe material were deposited onto a Pyrex glass or silicon wafer substrate (the latter of which was stored in a dessicator prior to use) using a modified coldwalled CVD system (Electro-gas Systems Ltd, UK). This system was composed of a tubular quartz reactor containing a silicon carbide coated graphite susceptor. The temperature of the susceptor was monitored with a k-type thermocouple combined with a proportional-integral-derivative controller (PID controller), with the heating controlled via a water cooled IR lamp mounted externally beneath the reaction tube. The nebulizer consisted of an ultrasonic humidifier (Pifco Health). The ultrasonic transducer transmitted ultrasound through a water reservoir and the glass of the flask into the solution to be nebulized. A typical run used a solution of [(L)GeTePCy$_2$] **18**, [(L)SnSeP(Se)Cy$_2$] **CXXXII**[115] or [(L)PbSeP(Se)Cy$_2$] **CXXXIII** (25 mg) in THF (20 mL) with a substrate temperature of 200°C and an argon carrier gas flow rate of 160 sccm over 1 hour.

The SEM and EDS data were collected by Dr Q. Chen at the University of Sussex. SEM analysis of the films and powders were carried out on a Jeol JSM-820 scanning electron microscope with LinkISIS EDS for composition analysis, and an electron beam energy of 30 KV.

5.5. NMR parameters

Table 18 Nuclear spin properties.[191]

Isotope	^{1}H	^{13}C	^{31}P	^{77}Se	^{125}Te	^{119}Sn	^{207}Pb
Natural abundance, χ (%)	99.9885	1.07	100	7.63	7.07	8.59	22.1
Spin, I	½	½	½	½	½	½	½
Relative receptivity, D^p	1.000	0.000170	0.0665	0.000537	0.00228	0.00453	0.00201
Relative receptivity, D^c	5870	1.00	391	3.15	13.4	26.6	11.8
Magnetogyric ratio, γ (10^7 rad s^{-1} T^{-1})	26.7522128	6.728284	10.8394	5.1253857	-8.5108404	-10.0317	5.58046
Magnetic moment, μ (μ_N)	4.837353570	1.216613	1.95999	0.92677577	-1.5389360	-1.81394	1.00906
Frequency ratio, Ξ (%)	100.000000	25.145020	40.480742	19.071513	31.549769	37.290632	20.920599

5.6. Crystallographic data

Table 19 For Chapter: 2.5.1. β-diketiminate stannylene amide and anilide synthesis and characterisation.

Complex	**[(BDI)SnN(CH{CH_3}$_2$)$_2$], 1**	**[(BDI)SnNH(*i*Pr$_2$C$_6$H$_3$)], 2**	**[(BDI)SnNH(*i*PrC$_6$H$_4$)], 3**
Formula	$C_{35}H_{55}N_3Sn$	$C_{41}H_{59}N_3Sn$	$C_{38}H_{52}N_3Sn$
fw	636.51	712.60	669.54
Crystal system	Monoclinic	Triclinic	Triclinic
Space group	P 2_1/n (No. 14)	$P\bar{1}$ (No. 2)	$P\bar{1}$ (No. 2)
a/Å	10.3140(2)	9.2335(2)	8.6759(2)
b/Å	20.2436(4)	11.4606(2)	10.7217(2)
c/Å	17.9140(3)	19.1522(4)	21.0763(5)
α/°	90	100.622(1)	83.8270(10)

β/°	114.056(1)	102.355(1)	85.4080(10)
γ/°	90	99.208(1)	85.1970(10)
V/Å^3	3415.44(11)	1903.40(7)	1937.31(7)
Z/Å	4	2	2
μ(Mo-Kα)/mm^{-1}	0.77	0.70	0.685
Total no. reflns.	37640	30546	24860
No. unique reflns.	6909	8358	8744
R_{int}	0.065	0.055	0.057
No. of parameters	366	412	379
$R1$ [$I_o > 2\sigma(I_o)$]	0.036	0.031	0.038
$wR2$ [$I_o > 2\sigma(I_o)$]	0.080	0.064	0.105

*R*1 [all data]	0.048	0.039	0.047
*wR*2 [all data]	0.085	0.066	0.110

Table 20 For Chapter: 2.5.2. β-diketiminate plumbylene amide and anilide synthesis and characterisation.

Complex	**[(BDI)PbN(CH{CH_3}$_2$)$_2$], 4**	**[(BDI)PbNH(*i*$Pr_2C_6H_3$)], 5**	**[(BDI)PbNH(*i*PrC_6H_4)], 6**	**[(BDI)PbNH(C_6H_5)], 7**
Formula	$C_{35}H_{55}N_3Pb$	$C_{41}H_{59}N_3Pb$	$C_{38}H_{53}N_3Pb$	$C_{35}H_{47}N_3Pb$
fw	725.01	801.10	759.02	716.95
Crystal system	Monoclinic	Triclinic	Monoclinic	Monoclinic
Space group	P 2_1/c (No. 14)	$P\bar{1}$ (No. 2)	P 2_1/c (No. 14)	P 2_1/c (No. 14)
a/Å	10.4524(1)	9.2238(1)	27.135(1)	12.3216(2)
b/Å	20.3151(2)	11.4878(2)	9.337(1)	29.2568(6)

c/Å	17.9079(3)	19.2046(3)	34.163(4)	9.2746(2)
α/°	90	100.743(1)	90	90
β/°	114.358(1)	102.609(1)	123.535(6)	103.849(1)
γ/°	90	99.018(1)	90	90
V/Å^3	3464.11(8)	1909.24(5)	7214.8(12)	3246.21(11)
Z/Å	4	2	8	4
μ(Mo-Kα)/mm^{-1}	4.90	4.45	4.705	5.223
Total no. reflns.	53818	34650	92098	34216
No. unique reflns.	7664	8691	15257	7427
R_{int}	0.063	0.052	0.110	0.044
No. of parameters	367	412	816	358

$R1$ [$I_o > 2\sigma(I_o)$][a]	0.025	0.025	0.047	0.025
$wR2$ [$I_o > 2\sigma(I_o)$][b]	0.053	0.048	0.076	0.051
$R1$[a] [all data]	0.035	0.030	0.084	0.031
$wR2$[b] [all data]	0.056	0.049	0.087	0.053

Table 21 For Chapter: **2.6. Reactivity studies on β-diketiminate Sn(II) and Pb(II) amide and anilide complexes** (stannylene complexes).

Complex	**[(BDI)SnOCON(CH{CH_3}$_2$)$_2$], 8**	**[(BDI)SnOC(NC_6H_5)C{(CH_3)CN-2,6-*i*$Pr_2C_6H_3$}$_2$]·0.5(C_7H_8), 10**	**[(BDI)SnCC(C_6H_3)]·(C_7H_8), 12**
Formula	$C_{36}H_{55}N_3O_2Sn$	$C_{65}H_{87}N_5OSn$, 0.5 C_7H_8	$C_{37}H_{46}N_2Sn$, C_7H_8
fw	680.54	1119.15	729.58
Crystal system	Triclinic	Triclinic	Tetragonal
Space group	$P\bar{1}$ (No. 2)	$P\bar{1}$ (No. 2)	I 4/m (No.87)

a/Å	11.4858(3)	10.8899(2)	18.4398(4)
b/Å	13.1637(4)	11.7384(2)	18.4398(4)
c/Å	13.4152(4)	25.2778(3)	21.2276(6)
α/°	91.601(2)	93.961(1)	90
β/°	107.273(2)	99.556(1)	90
γ/°	114.822(4)	103.239(1)	90
V/Å^3	1730.45(11)	3082.37(9)	7217.9(3)
Z/Å	4	2	8
μ(Mo-Kα)/mm^{-1}	0.772	0.46	0.74
Total no. reflns.	25911	51415	11847
No. unique reflns.	7847	13304	3941

R_{int}	0.044	0.058	0.036
No. of parameters	381	664	173
$R1$ [$I_o > 2\sigma(I_o)$][a]	0.032	0.040	0.038
$wR2$ [$I_o > 2\sigma(I_o)$][b]	0.078	0.096	0.104
$R1$[a] [all data]	0.037	0.050	0.048
$wR2$[b] [all data]	0.081	0.100	0.108

Table 22 For Chapter: **2.6. Reactivity studies on β-diketiminate Sn(II) and Pb(II) amide and anilide complexes** (plumbylene complexes).

Complex	**[{(HN-2,6-*i*Pr$_2$C$_6$H$_3$)PbI}$_2$]·1.5(C$_7$H$_8$), 13**	**[(BDI)PbOC(N*t*Bu)NH(2,6-*i*Pr$_2$C$_6$H$_3$)], 15**
Formula	C24H$_{36}$I$_2$N$_3$Pb$_2$, 1.5 C$_7$H$_8$	C$_{46}$H$_{68}$N$_4$OPb , C$_7$H$_8$
fw	1158.93	900.24

Crystal system	Monoclinic	Orthorhombic
Space group	P $2_1/c$	P c $2_1/n$ (No. 33)
a/Å	13.2058(2)	9.30580(10)
b/Å	14.6460(2)	19.5694(3)
c/Å	19.7011(2)	27.4022(4)
α/°	90	90
β/°	99.4910(10)	90
γ/°	90	90
V/Å^3	3758.27(9)	4990.19(12)
Z/Å	4	4
μ(Mo-Kα)/mm^{-1}	0.772	3.413

Total no. reflns.	60206	11368
No. unique reflns.	8545	9274
R_{int}	0.062	0.065
No. of parameters	320	470
$R1$ [$I_o > 2\sigma(I_o)$][a]	0.039	0.044
$wR2$ [$I_o > 2\sigma(I_o)$][b]	0.072	0.116
$R1$[a] [all data]	0.046	0.062
$wR2$[b] [all data]	0.076	0.125

Table 23 For Chapter: 3.3.2. The reactivity of β-diketiminate group 14 metal phosphides with chalcogens.

Complex	**[(BDI)GeSeP(C_6H_{11})$_2$], 16**	**[(BDI)GeSeP(C_6H_5)$_2$], 17**	**[(BDI)GeTeP(C_6H_{11})$_2$], 18**	**[{P(C_6H_5)$_2$}$_2$], 19**
Formula	$C_{41}H_{63}GeN_2PSe$	$C_{41}H_{51}GeN_2PSe$	$C_{41}H_{63}GeN_2PTe$	$C_{24}H_{20}P_2$
fw	766.45	754.36	815.09	370.34
Crystal system	Triclinic	Triclinic	Monoclinic	Monoclinic
Space group	$P\bar{1}$ (No. 2)	$P\bar{1}$ (No. 2)	$P\,2_1$ (No. 4)	$P\,2_1/c$ (No. 14)
a/Å	12.1142(3)	11.8510(4)	12.3851(2)	6.1617(3)
b/Å	12.4636(5)	12.6357(5)	13.2583(4)	7.3499(4)
c/Å	14.2500(6)	14.2256(5)	12.4461(3)	21.8665(8)
α/°	90.687(2)	98.703(2)	90	90
β/°	98.514(2)	94.437(2)	94.331(2)	105.948(3)

γ/°	109.920(2)	113.262(2)	90	90
V/Å^3	1996.02(13)	1912.34(12)	2037.88(9)	952.17(8)
Z/Å	2	2	2	2
μ(Mo-Kα)/mm^{-1}	1.748	1.824	1.521	0.233
Total no. reflns.	27815	24584	29874	11493
No. unique reflns.	8431	8081	8791	2102
R_{int}	0.093	0.054	0.071	0.069
No. of parameters	417	417	417	158
$R1$ [$I_o > 2\sigma(I_o)$][a]	0.046	0.035	0.0446	0.038
$wR2$ [$I_o > 2\sigma(I_o)$][b]	0.091	0.081	0.092	0.084
$R1$[a] [all data]	0.079	0.052	0.055	0.052

*wR*2[b] [all data]	0.102	0.089	0.105	0.090

Table 24 For Chapter: 3.3.3. The reactivity of β-diketiminate group 14 metal phosphides with excess chalcogen.

Complex	**[(BDI)Ge(Se)SeP(C_6H_5)$_2$]·0.5((C_2H_5)$_2$O) , 20**
Formula	$C_{86}H_{112}Ge_2N_4OP_2Se_4$
fw	1740.768
Crystal system	Triclinic
Space group	$P\bar{1}$ (No. 2)
a/Å	10.8309(4)
b/Å	12.7855(4)
c/Å	16.7183(7)

$\alpha/°$	81.251(2)
$\beta/°$	78.847(2)
$\gamma/°$	66.679(2)
$V/Å^3$	2078.49(13)
$Z/Å$	1
μ(Mo-Kα)/mm^{-1}	2.559
Total no. reflns.	26100
No. unique reflns.	8776
R_{int}	0.067
No. of parameters	471
$R1$ [$I_o > 2\sigma(I_o)$][a]	0.045

$wR2$ [$I_o > 2\sigma(I_o)$][b]	0.076
$R1$[a] [all data]	0.079
$wR2$[b] [all data]	0.086

6. References

(1) J. Emsley. *Nature's Building Blocks,* Oxford University Press: New York, 2003.

(2) E. S. Claudio; H. A. Godwin; J. S. Magyar. *Fundamental Coordination Chemistry, Environmental Chemistry and Biochemistry of Lead(II),* Vol. 51. John Wiley and Sons, Inc.: New York, 2002.

(3) A. G. Massey. *Main Group Chemistry*; 1st ed. Ellis Horwood Limited: Chichester, 1990.

(4) P. J. Davidson; D. H. Harris; M. F. Lappert. *J. Chem. Soc., Chem. Commun.* **1976**, 261.

(5) D. H. Harris; M. F. Lappert. *J. Chem. Soc., Chem. Commun.* **1974**, 895.

(6) E. Krause; G. G. Reissaus. *Chem. Ber.* **1922**, *55*, 888.

(7) S. Hino; M. Brynda; A. D. Phillips; P. P. Power. *Angew. Chem. Int. Ed.* **2004**, *43*, 2655.

(8) L. Pu; M. M. Olmstead; P. P. Power. *Organometallics* **1998**, *17*, 5602.

(9) R. S. Simons; L. Pu; M. M. Olmstead; P. P. Power. *Organometallics* **1997**, *16*, 1920.

(10) B. E. Eichler; P. P. Power. *Inorg. Chem.* **2000**, *39*, 5444.

(11) C. Stanciu; S. S. Hino; M. Stender; A. F. Richards; M. M. Olmstead; P. P. Power. *Inorg. Chem.* **2005**, *44*, 2774.

(12) B. E. Eichler; L. Pu; M. Stender; P. P. Power. *Polyhedron* **2001**, *20*, 551.

(13) W. A. Merrill; E. Rivard; J. S. DeRopp; X. Wang; B. D. Ellis; J. C. Fettinger; B. Wrackmeyer; P. P. Power. *Inorg. Chem.* **2010**, *49*, 8481.

(14) P. P. Power. *Organometallics* **2007**, *26*, 4362.

(15) W. A. Merrill; J. Steiner; A. Betzer; I. Nowick; R. Herber; P. P. Power. *Dalton Trans.* **2008**, 5905.

(16) A. Schäfer; M. Weidenbruch; W. Saak; S. Pohl. *J. Chem. Soc., Chem. Commun.* **1995**, 1158.

(17) F. Stabenow; W. Saak; M. Weidenbruch. *Chem. Commun.* **1999**, 1131.

(18) P. A. Rupar; M. C. Jennings; K. A. Baines. *Organometallics* **2008**, *27*, 5043.

(19) P. A. Rupar; V. N. Staroverov; P. J. Ragogna; K. M. Baines. *J. Am. Chem. Soc.* **2007**, *129*, 15138.

(20) A. J. Arduengo III; H. V .R. Dias; J. C. Calabrese; F. Davidson. *Inorg. Chem.* **1993**, *32*, 1541.

(21) B. Gerhrus; P. B. Hitchcock; M. F. Lappert. *J. Chem. Soc., Dalton Trans.* **2000**, 3094.

(22) K. Izod; C. Wills; W. Clegg; R. W. Harrington. *Organometallics* **2009**, *28*, 2211.

(23) M. Assay; C. Jones; M. Driess. *Chem. Rev.* **2011**, *111*, 354.

(24) J. P. H. Charmant; M. F. Haddow; F. E. Hahn; D. Deitmann; R. Froehlick; S. M. Mansell; C. A. Russell; D. F. Wass. *Dalton Trans.* **2008**, 6055.

(25) F. E. Hahn; D. Heitmann; T. Pape. *Eur. J. Inorg. Chem.* **2008**, 1039.

(26) J. Heinicke; A. Oprea; M. K. Kindermann; T. Karpati; L. Nyulaszi; T. Veszpremi. *Chem.-Eur. J.* **1998**, *4*, 541.

(27) J. Pfeiffer; M. Noltemeyer; A. Z. Meller. *Anorg. Allg. Chem.* **1989**, *572*, 145.

(28) J. Pfeiffer; M. Noltemeyer; A. Z. Meller. *Chem. Ber.* **1989**, *122*, 245.

(29) J. Heinicke; A. Operea. *Heteroat. Chem.* **1998**, *9*, 439.

(30) W. A. Herrmann; M. Denk; J. Behm; W. Scherer; F. -R. Klingan; H. Bock; B. Solouki; M. Wagner. *Angew. Chem. Int. Ed.* **1992**, *31*, 1485.

(31) O. Kuehl; P. Loennecke; J. Heinicke. *Polyhedron* **2001**, *20*, 2215.

(32) A. C. Tomasik; N. J. Hill; R. J. West. *Organomet. Chem.* **2009**, *694*, 2122.

(33) S. M. Mansell; C. A. Russell; D. F. Wass. *Inorg. Chem.* **2008**, *47*, 11367.

(34) T. Gans-Eichler; D. Gudat; K. Maettinen; M. Mieger. *Chem.-Eur. J.* **2006**, *12*, 1162.

(35) T. Gans-Eichler; D. Gudat; M. Nieger. *Angew. Chem. Int. Ed.* **2002**, *41*, 1888.

(36) H. Braunschweig; B. Gehrhus; P. B. Hitchcock; M. F. Lappert. *Z. Anorg. Allg. Chem.* **1995**, *621*, 1922.

(37) F. E. Hahn; L. Wittenbecher; M. Huehn; T. Luegger; F. J. Froehlick. *J. Organomet. Chem.* **2001**, *617*, 629.

(38) F. E. Hahn; L. Wittenbecher; D. L. Van; A. V. Zabula. *Inorg. Chem.* **2007**, *46*, 7662.

(39) F. Ullah; O. Kuehl; W. Rehman; P. G. Jones; J. Heinicke. *Polyhedron* **2010**, *29*, 1041.

(40) A. V. Zabula; T. Pape; A. Hepp; F. M. Schappacher; U. C. Rodewald; R. Pöttgen; F. E Hahn. *J. Am. Chem. Soc.* **2008**, *130*, 5648.

(41) D. J. Eisler; R. J. Less; V. Naseri; J. M. Rawson; D. S. Wright. *Dalton Trans.* **2008**, 2382.

(42) K. Izod; J. Stewart; W. Clegg; R. W. Harrington. *Organometallics* **2010**, *29*, 108.

(43) K. Izod; J. Stewart; E. R. Clark; W. Clegg; R. W. Harrington. *Inorg. Chem.* **2010**, *49*, 4698.

(44) C. Jones; R. P. Rose; A. Stasch. *Dalton Trans.* **2008**, 2871.

(45) H. H. Karsch; P. A. Schlueter; M. Reisky. *Eur. J. Inorg. Chem.* **1998**, 433.

(46) Y. Xiong; S. Yao; R. Mueller; M. Kaupp; M. Driess. *Nat. Chem.* **2010**, *2*, 577.

(47) H. W. Roesky; B. Meller; M. Noltemeyer; H. -G. Schmidt; U. Scholz; G. M. Sheldrick. *Chem. Ber.* **1988**, *121*, 1403.

(48) U. Kilimann; M. Noltemeyer; F. T. Edelmann. *J. Organomet. Chem.* **1993**, *443*, 35.

(49) Y. Zhou; D. S. Richeson. *J. Am. Chem. Soc.* **1996**, *118*, 10850.

(50) K. B. Aubrecht; M. A. Hillmyer; W. B. Tolman. *Macromolecules* **2002**, *35*, 644.

(51) F. Antolini; P. B. Hitchcock; A. V. Khvostov; M. F. Lappert. *Can. J. Chem.* **2006**, *84*, 269.

(52) S. R. Foley; C. Bensimon; D. S. Richeson. *J. Am. Chem. Soc.* **1997**, *119*, 10359.

(53) N. Nimitsiriwat; V. C. Gibson; E. L. Marshall; A. J. P. White; S. H. Dale; M. R. J. Elsegood. *Dalton Trans.* **2007**, 4464.

(54) P. B. Hitchcock; M. F. Lappert; M. Layh. *J. Chem. Soc., Dalton Trans.* **1998**, 3113.

(55) A. P. Dove; V. C. Gibson; E. L. Marshall; H. S. Rzepa; A. J. P. White; D. J. Williams. *J. Am. Chem. Soc.* **2006**, *128*, 9834.

(56) A. Stasch; C. M. Forsyth; C. Jones; P. C. Junk. *New. J. Chem.* **2008**, *32*, 829.

(57) S. M. I. Al-Rafia; P. A. Lummis; M. J. Ferguson; R. McDonald; E. Rivard. *Inorg. Chem.* **2010**, *49*, 9709.

(58) D. Yang; J. Guo; H. Wu; Y. Ding; W. Zheng. *Dalton Trans.* **2012**, 2187.

(59) L. C. Dorman. *Tetrahedron Lett.* **1966**, *4*, 459.

(60) J. E. Parks; R. H. Holm. *Inorg. Chem.* **1968**, *7*, 1408.

(61) M. S. Hill; P. B. Hitchcock; R. Pongtavornpinyo. *Science* **2006**, *311*, 1904.

(62) L. Bourget-Merle; M. F. Lappert; J. R. Severn. *Chem. Rev.* **2002**, *102*, 3031.

(63) S. P. Green; C. Jones; A. Stasch. *Science* **2007**, *318*, 1754.

(64) C. Cui; H. W. Roesky; H. G. Schmidt; M. Noltemeyer; H. Hao; F. Cimpoesu. *Angew. Chem. Int. Ed.* **2000**, *39*, 4274.

(65) N. J. Hardman; B. E. Eichler; P. P. Power. *Chem. Commun.* **2000**, 1991.

(66) Y. C. Tsai; P. Y. Wang; K. M. Lin; S. A. Chen; J. M. Chen. *Chem. Commun.* **2008**, 205.

(67) Y. C. Tsai; P. Y. Wang; S. A. Chen; J. M. Chen. *J. Am. Chem. Soc.* **2007**, *129*, 8066.

(68) O. Eisenstein; P. B. Hitchcock; A. V Khvostov; M. F. Lappert; L. Maron; L. Perrin; A. V. Protchenko. *J. Am. Chem. Soc.* **2003**, *125*, 10790.

(69) A. Akkari; J. J. Byrne; I. Saur; G. Rima; H. Gornitzka; J. Barrau. *J. Organomet. Chem.* **2001**, *20*, 1190.

(70) A. Ayers; T. M. Klapotke; H. V. R. Dias. *Inorg. Chem.* **2001**, *40*, 1000.

(71) Y. Ding; H. W. Roesky; M. Noltmeyer; H.-G. Schmidt; P. P. Power. *Organometallics* **2001**, *20*, 1190.

(72) M. Chen; J. R. Fulton; P. B. Hitchcock; N. C. Johnstone; M. F. Lappert; A. V. Protchenko. *Dalton Trans.* **2007**, 2770.

(73) A. P. Dove; V. C. Gibson; E. L. Marshall; A. J. P. White; D. J. Williams. *J. Chem. Commun.* **2001**, 283.

(74) P. B. Hitchcock; J. Hu; M. F. Lappert; J. R. Severn. *Dalton Trans.* **2004**, 4193.

(75) P. D. Dove; V. C. Gibson; E. L. Marshall; H. S. Rzepa; A. J. P. White; D. J. Williams. *J. Am. Chem. Soc.* **2006**, *128*, 9834.

(76) J. R. Fulton; P. B. Hitchcock; N. C. Johnstone; E. C. Y. Tam. *Dalton Trans.* **2007**, 3360.

(77) A. Jana; H. W. Roesky; C. Schulzke; A. Döring; T. Beck; A. Pal; R. Herbst-Irmer. *Inorg. Chem.* **2009**, *48*, 193.

(78) E. C. Y. Tam; N. C. Johnstone; L. Ferro; P. B. Hitchcock; J. R. Fulton. *Inorg. Chem.* **2009**, *48*, 8971.

(79) A. Jana; S. P. Sarish; H. W. Roesky; C. Schulze; A. Döring; M. John. *Organometallics* **2009**, *28*, 2563.

(80) L. A. M. Harris; M. P. Coles; J. R. Fulton. *Inorg. Chim. Acta.* **2011**, *369*, 97.

(81) S. Yao; S. Block; M. Brym; K. Mertz; M. Driess. *Organometallics* **2008**, *27*, 3601.

(82) S. Yao; S. Block; M. Brym; M. Driess. *Chem. Commun.* **2007**, 3844.

(83) M. J. Taylor; A. J. Saunders; M. P. Coles; J. R. Fulton. *Organometallics* **2011**, *30*, 1334.

(84) L. W. Pineda; V. Jancik; K. Starke; R. B. Oswald; H. W. Roesky. *Angew. Chem. Int. Ed.* **2006**, *45*, 2602.

(85) A. Jana; H. W. Roesky; C. Schulzke; A. Doring; T. Back; A. Pal; R. Herbst-Irmer. *Inorg. Chem.* **2009**, *48*, 193.

(86) A. Jana; H. W. Roesky; C. Schulzke; A. Doring. *Angew. Chem. Int. Ed.* **2009**, *48*, 1106.

(87) A. Jana; I. Objartel; H. W. Roesky; D. Stalke. *Dalton Trans.* **2010**, 4647.

(88) A. Jana; H. W. Roesky; C. Schulzke; P. P. Samuel; A. Döring. *Inorg. Chem.* **2010**, *49*, 10208.

(89) A. Jana; S. P. Sarish; H. W. Roesky; D. Leusser; I. Objartel; D. Stalke. *Chem. Commun.* **2011**, 5434.

(90) S. K. Mandal; H. W. Roesky. *Acc. Chem. Res.* **2012**, *45*, 298.

(91) K. G. Caulton. *New. J. Chem.* **1994**, *18*, 25.

(92) H. E. Bryndza; W. C. Fultz; W. Tam. *Organometallics* **1985**, *4*, 939.

(93) D. S. Glueck; L. J. N. Winslow; R. G. Bergman. *Organometallics* **1991**, *10*, 1462.

(94) J. R. Fulton; A. W. Holland; D. J. Fox; R. G. Bergman. *Acc. Chem. Res.* **2002**, *35*, 44.

(95) A. W. Kaplan; J. C. M. Ritter; R. G. Bergman. *J. Am. Chem. Soc.* **1998**, *120*, 6828.

(96) J. Zhao; A. S. Goldman; J. F. Hartwig. *Science* **2005**, *307*, 1080.

(97) J. Cámpora; I. Matas; P. Palma; E. Álvarez; C. Graiff; A. Tiripicchio. *Organometallics* **2007**, *26*, 3840.

(98) J. Zhang; T. B. Gunnoe; J. L. Petersen. *Inorg. Chem.* **2005**, *44*, 2895.

(99) D. Rais; R. G. Bergman. *Chem.-Eur. J.* **2004**, *10*, 3970.

(100) D. J. Fox; R. G. Bergman. *J. Am. Chem. Soc.* **2003**, *125*, 8984.

(101) D. J. Fox; R. G. Bergman. *Organometallics* **2004**, *23*, 1656.

(102) Y. Liu; D. Zhang; S. Bi; C. Liu. *Organometallics* **2012**, *31*, 365.

(103) J. R. Fulton; S. Sklenak; M. W. Bouwkamp; R. G. Bergman. *J. Am. Chem. Soc.* **2002**, *124*, 4722.

(104) D. Connor; K. N. Jayaprakash; M. B. Wells; S. Manzer; T. B. Gunnoe; P. D. Boyle. *Inorg. Chem.* **2003**, *42*, 4759.

(105) J. R. Fulton; M. W. Bouwkamp; R. G. Bergman. *J. Am. Chem. Soc.* **2000**, *122*, 8799.

(106) S. R. Foley; G. P. A. Yap; D. S. Richeson. *Organometallics* **1999**, *18*, 4700.

(107) S. R. Foley; G. P. A. Yap; D. S. Richeson. *J. Chem. Soc., Dalton Trans.* **2000**, 1663.

(108) H. W. R. Y. Ding, M. Noltmeyer, H.-G. Schmidt, P.P Power. *Organometallics* **2001**, *20*, 1190.

(109) J. Clayden; N. Greeves; S. Warren; P. Wothers. *Organic Chemistry,* Oxford University Press: New York, 2001.

(110) L. Shimoni-Livny; J. P. Glusker; C. W. Bock. *Inorg. Chem.* **1998**, *37*, 1853.

(111) R. E. Allan; M. A. Beswick; M. K. Davies; P. R. Raithby; A. Steiner; D. S. Wright. *J. Organomet. Chem.* **1998**, *550*, 71.

(112) J. A. Dean. *Lange's Handbook of Chemistry*; 11th ed. McGraw-Hill Book Company: New York, 1973.

(113) W. A. Merrill; R. J. Wright; C. S. Stanciu; M. M. Olmstead; J. C. Fettinger; P. P. Power. *Inorg. Chem.* **2010**, *49*, 7097.

(114) H. E. Bryndza; W. Tam. *Chem. Rev.* **1988**, *88*, 1163.

(115) E. C. Y. Tam. PhD. Dissertation, Sussex University, 2012.

(116) F. Basuli; J. C. Huffman; D. J. Mindiola. *Inorg. Chem.* **2003**, *42*, 8003.

(117) M. M. Khusinyarov; E. Bill; T. Weyhermüller; E. Bothe; K. Wieghardt. *Angew. Chem. Int. Ed.* **2011**, *50*, 1652.

(118) D. W. Smith. *J. Organomet. Chem.* **1999**, *585*, 150.

(119) M. C. Kuchta; G. Parkin. *Coord. Chem. Rev.* **1998**, *176*, 323.

(120) W. Kutzelnigg. *Angew. Chem. Int. Ed.* **1984**, *23*, 272.

(121) I. Schranz; L. Grocholl; C. K. Carrow; L. Stahl. *J. Organomet. Chem.* **2008**, *693*, 1081.

(122) J. Escudie; C. Couret; H. Ranaivonjatovo; G. Anselme; G. Delpon-Lacaze; M.-A. Chaubon; K. A. Rodi; J. Satgé. *Main Group Met. Chem.* **1994**, *17*, 33.

(123) J. Satgé. *Adv. Organomet. Chem.* **1982**, *21*, 241.

(124) J. Satgé. *Pure Appl. Chem.* **1984**, *56*, 137.

(125) M. P. Egorov; P. P. Gaspar. *Encyclopedia of Inorganic Chemistry,* Wiley: New York, 1994.

(126) J. Escudie; C. Couret; H. Ranaivonjatovo; J. Satgé. *Coord. Chem. Rev.* **1994**, *130*, 427.

(127) N. Tokitoh; R. Okazaki. *Main Group Chemistry News* **1995**, *3*, 4.

(128) R. Okazaki; N. Tokitoh; A. Ishii; N. Ishii; Y. Matsuhasi; T. Matsumoto; H. Suzuki. *Phosphorus, Sulfur, Silicon* **1992**, *67*, 49.

(129) G. Trinquier; M. Pelissier; B. Saint-Roch; H. Lavayssiere. *J. Organomet. Chem.* **1981**, *214*, 169.

(130) T. Tsumuraya; S. A. Batcheller; S. Masamune. *Angew. Chem. Int. Ed.* **1991**, *30*, 902.

(131) J. Satgé. *J. Organomet. Chem.* **1990**, *400*, 121.

(132) D. P. Thompson; P. Boudjouk. *J. Chem. Soc., Chem. Commun.* **1987**, 1466.

(133) M. F. Lappert. *Main Group Met. Chem.* **1994**, *17*, 183.

(134) P. Arya; J. Boyer; F. Carré; R. Corriu; G. Lanneau; J. Lapasset; M. Perrot; C. Priou. *Angew. Chem. Int. Ed.* **1989**, *28*, 1016.

(135) P. Jutzi; A. Möhrke; A. Müller; H. Bögge. *Angew. Chem. Int. Ed.* **1989**, *28*, 1518.

(136) W. W. Harper; E. A. Ferrall; R. K. Hilliard; S. M. Stogner; R. S. Grev; D. J. Clouthier. *J. Am. Chem. Soc.* **1997**, *119*, 8361.

(137) M. Veith; S. Becker; V. Huch. *Angew. Chem. Int. Ed.* **1989**, *28*, 1237.

(138) N. Tokitoh; R. Okazaki. *Adv. Organomet. Chem.* **2001**, *47*, 121.

(139) R. Okazaki; N. Tokitoh. *Acc. Chem. Res.* **2000**, *33*, 625.

(140) N. Tokitoh; T. Matsumoto; R. J. Okazaki. *Chem. Soc. Jpn.* **1999**, *72*, 1665.

(141) N. Tokitoh; T. Sadahiro; K. Hatano; T. Sasaki; N. Takeda; R. Okazaki. *Chem. Lett.* **2002**, *31*, 34.

(142) N. Tokitoh; T. Matsumoto; R. J. Okazaki. *J. Am. Chem. Soc.* **1997**, *119*, 2337.

(143) N. Tokitoh; R. Okazaki. *Coord. Chem. Rev.* **2000**, *210*, 251.

(144) Y. Mizuhata; T. Sasamori; N. Tokitoh. *Chem. Rev.* **2009**, *109*, 3479.

(145) R. C. Fischer; P. P. Power. *Chem. Rev.* **2010**, *110*, 3877.

(146) M. Saito; N. Tokitoh; R. J Okazaki. *J. Am. Chem. Soc.* **2004**, *126*, 15572.

(147) N. Kano; K. Shibata; M. Tokitoh; R. Okazaki. *Organometallics* **1999**, *18*, 2999.

(148) M. C. Kuchta; G. Parkin. *J. Am. Chem. Soc.* **1994**, *116*, 8372.

(149) M. C. Kuchta; G. Parkin. *J. Chem. Soc., Chem. Commun.* **1994**, 1351.

(150) L. M. Berreau; L. K. Woo. *J. Am. Chem. Soc.* **1995**, *117*, 1314.

(151) W .-P. Leung; W. -H. Kwok; L. T. C. Law; Z. -Y. Zhou; T. C. W. Mak. *Chem. Commun.* **1996**, 505.

(152) W.-P. Leung; W.-H. Kwok; Z.-Y. Zhou; T. C. W. Mak. *Organometallics* **2000**, *19*, 296.

(153) T. Chivers; G. Schatte. *Chem. Commun.* **2001**, 2264.

(154) T. Chivers; T. J. Clark; M. Krahn; M. Parvez; G. Schatte. *Eur. J. Inorg. Chem.* **2003**, 1857.

(155) T. Chivers; D. J. Eisler; J. S. Ritch. *Z. Anorg. Allg. Chem.* **2004**, *630*, 1941.

(156) M. Veith; M. -L. Sommer; D. Jäger. *Chem. Ber.* **1979**, *112*, 2581.

(157) E. C. Y. Tam; N. A. Maynard; D. C. Apperley; J. D. Smith; M. P. Coles; J. R. Fulton. *Inorg. Chem.* **2012**, *51*, 9403.

(158) S. D. Reid; A. L. Hector; W. Levason; G. Reid; B. J. Waller; M. Webster. *Dalton Trans.* **2007**, 4769.

(159) J. S. Ritch; T. Chivers; M. Afzaalb; P. O'Brien. *Chem. Soc. Rev.* **2007**, *36*, 1622.

(160) D. Fan; M. Afzaal; M. A. Mallik; C. Q. Nguyen; P. O'Brien; P. J. Thomas. *Coord. Chem. Rev.* **2007**, *251*, 1878.

(161) T. Chen; W. Hunks; P. S. Chen; G. T. Stauf; T. M. Cameron; C. Xu; A. G. DiPasquale; A. L. Rheingold. *Eur. J. Inorg. Chem.* **2009**, 2047.

(162) B. P. Bade; S. S. Garje; Y. S. Niwate; M. Afzaal; P. O'Brien. *Chem. Vap. Deposition* **2008**, *14*, 292.

(163) I. P. Parkin; L. S. Price; T. G. Hibbert; K. C. Molloy. *J. Mater. Chem.* **2001**, *11*, 1486.

(164) M. A. Malik; M. Afzaal; P. O'Brien. *Chem. Rev.* **2010**, *110*, 4417.

(165) I. S. Chuprakov; K. -H. Dahmen; J. J. Schneider; J. Hagen. *Chem. Mater.* **1998**, *10*, 3467.

(166) I. S. Chuprakov; K.-H. Dahmen. *J. Phys. IV* **1999**, *9*, 313.

(167) P. Boudjouk; M. P. Remington; D. G. Grier; W. Triebold; B. R. Jarabek. *Organometallics* **1999**, *18*, 4534.

(168) A. L. Seligson; J. Arnold. *J. Am. Chem. Soc.* **1993**, *115*, 8214.

(169) M. Afzaal; K. Ellwood; N. L. Pickett; P. O'Brien; J. Raftery; J. Waters. *J. Mater. Chem.* **2004**, *14*, 1310.

(170) J. Akhtar; M. A. Malik; P. O'Brien; M. Helliwell. *J. Mater. Chem.* **2010**, *20*, 6116.

(171) J. S. Ritch; K. Ahmad; M. Afzaal; T. Chivers; P. O'Brien. *Inorg. Chem.* **2010**, *49*, 1158.

(172) K. Ahmad; M. Afzaal; P. O'Brien; G. Hua; J. D. Woollins. *Chem. Mater.* **2010**, *22*, 4619.

(173) J. Akhtar; M. Afzaal; M. A. Vincent; N. A. Burton; I. H. Hillierc; P. O'Brien. *Chem. Commun.* **2011**, 1991.

(174) Y. Yang; N. Zhao; H. Zhu; H. W. Roesky. *Inorg. Chem.* **2012**, *51*, 2425.

(175) H. Westermann; M. Nieger; E. Niecke. *Chem. Ber.* **1991**, *124*, 13.

(176) C. W. Liu; T. S. Lobana; J.-L. Xiao; H.-Y. Liu; B.-J. Liaw; C.-M. Hung; Z. Lin. *Organometallics* **2005**, *24*, 4072.

(177) V. P. W. Böhm; M. Brookhart. *Angew. Chem. Int. Ed.* **2001**, *40*, 4694.

(178) A. Dashti-Mommertz; B. Neumüller. *Z. Anorg. Allg. Chem.* **1999**, *625*, 954.

(179) M. Andrianarison; C. Couret; J.-P. Declercq; A. Dubourg; J. Escudie; H. Ranaivonjatovo; J. Satget. *Organometallics* **1988**, *7*, 1545.

(180) M. Stender; A. D. Phillips; P. P. Power. *Inorg. Chem.* **2001**, *40*, 551.

(181) H. Suzuki; N. Tokitoh; R. Okazaki; S. Nagase; M. Goto. *J. Am. Chem. Soc.* **1998**, *120*, 11096.

(182) *CRC Handbook of Chemistry and Physics*; 92nd ed. CRC Press: London, 2011.

(183) C. E. Check; T. O. Faust; J. M. Bailey; B. J. Wright; T. M. Gilbert; L. S. Sunderlin. *J. Phys. Chem. A* **2001**, *105*, 8111.

(184) W. R. Wadt; P. J. Hay. *J. Chem. Phys.* **1985**, *82*, 284.

(185) C. R. Landis; F. Weinhold. Tutorial Example for Methylamine. http://www.chem.wisc.edu/~nbo5/tutorial.html, (accessed 27/09/12)

(186) M. Stender; R. J. Wright; B. E. Eichler; J. Prust; M. M. Olmstead; H. W. Roesky; P. P. Power. *J. Chem. Soc., Dalton Trans.* **2001**, 3465.

(187) E. C. Y. Tam; N. A. Maynard; D. C. Apperley; J. D. Smith; M. P. Coles; J. R. Fulton. *Inorg. Chem.* **2012**, *51*, 9403.

(188) G. M. Sheldrick. *Acta Crystallographica Section A* **2008**, *64*, 112.

(189) Gaussian 03, Revision E.01., M. J. Frisch; G. W. Trucks; H. B. Schlegel; G. E. Scuseria; M. A. Robb; J. R. Cheeseman; J. A. Montgomery; T. Vreven; K. N. Kudin; J. C. Burant; J. M. Millam; S. S. Iyengar; J. Tomasi; V. Barone; B. Mennucci; M. Cossi; G. Scalmani; N. Rega; G. A. Petersson; H. Nakasuji; M. Hada; M. Ehara; K. Toyota; R. Fukuda; J. Hasegawa; M. Ishida; T. Nakajima; Y. Honda; O. Kitao; H. Nakai; M. Klene; X. Li; J. E. Knox; H. P. Hratchian; J. B. Cross; V. Bakken; C. Adamo; J. Jaramillo; R. Gomperts; R. E. Stratmann; O. Yazyev; A. J. Austin; R. Cammi; C. Pomelli; J. W. Ochterski; P. Y. Ayala; K. Morokuma; G. A. Voth; P.

Salvador; J. J. Dannenberg; V. G. Zakrzewski; S. Dapprich; A. D. Daniels; M. C. Strain; O. Farkas; D. K. Malick; A. D. Rabuck; K. Raghavachari; J. B. Foresman; J. V. Ortiz; Q. Cui; A. G. Baboul; S. Clifford; J. Cioslowski; B. B. Stefanov; G. Liu; A. Liashenko; P. Piskorz; I. Komaromi; R. L. Martin; D. J. Fox; T. Keith; A. Laham; C. Y. Peng; A. Nanayakkara; M. Challacombe; P. M. W. Gill; B. Johnson; W. Chen; M. W. Wong; C. Gonzalez; J. A. Pople. Gaussian, Inc., Wallingford CT, 2004.

(190) S. V. Pol; V. G. Pol; L. Gedanken. *Chem.-Eur. J.* **2004**, *10*, 4467.

(191) R. K. Harris; E. D. Becker; S. M. Cabral de Menezes; R. Goodfellow; P. Granger. *Magn. Reson. Chem.* **2002**, *40*, 489.